MICHELE TUCCILLO

Extending the Aircraft Conceptual Design Workflow

A Methodology for the Architecture Exploration and Optimization of Next Generation Multi-Role Seaplanes

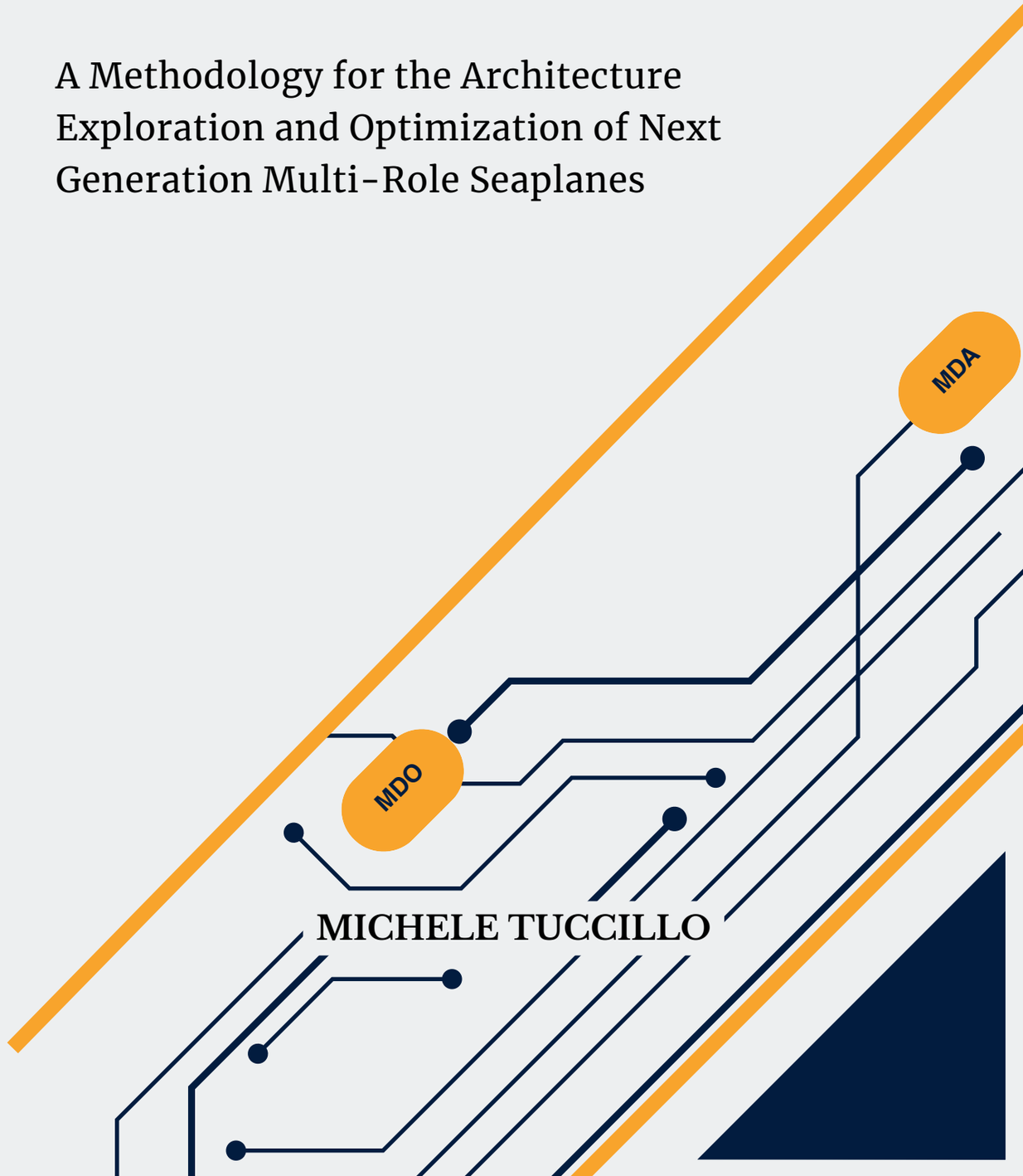

Extending the Aircraft Conceptual Design Workflow

Extending the Aircraft Conceptual Design Workflow

A Methodology for the Architecture Exploration and Optimization of Next Generation Multi-Role Seaplanes

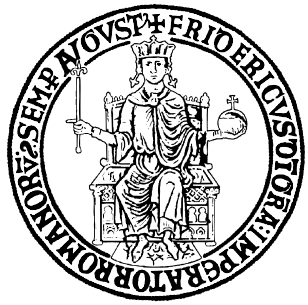

Doctoral Thesis

Industrial Engineering - Aerospace Division
University of Naples Federico II

by

Michele Tuccillo

Master of Science in Aerospace Engineering
University of Naples Federico II, Italy

Supervisors:
Prof. Fabrizio Nicolosi
Prof. Pierluigi Della Vecchia

Coordinator:
Prof. Michele Grassi

Declaration of Authorship

I, Michele Tuccillo, declare that this thesis, titled "Extending the Aircraft Conceptual Design Workflow: A Methodology for the Architecture Exploration and Optimization of Next Generation Multi-Role Seaplanes" is a product of my original research. I confirm that:

- The research and writing for this thesis were wholly or mainly conducted during my candidacy for a research degree at this University.
- In instances where any part of this thesis was previously submitted for a degree or any other qualification at this or any other institution, I have explicitly indicated so.
- Whenever I have consulted the published works of others, this was always clearly attributed.
- Any quotations from the works of others were properly cited, and except for these quotations, this thesis is entirely the result of my own efforts.
- I have acknowledged and cited all main sources of help.
- In cases where the thesis includes collaborative work, I have explicitly clarified the contributions made by others and those that are my own.

Date: 31st October 2025

Sign: 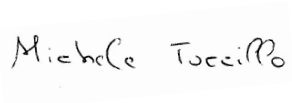

Abstract

The early stages of the aircraft design process, namely, the conceptual and preliminary phases, are characterized by the strong interdependence of analytical and numerical methodologies aimed at determining overall vehicle performance. These include low- and high-speed aerodynamics, in-flight and on-ground performance, flying qualities, stability and control characteristics, and economic efficiency. The inherently multidisciplinary nature of this process requires careful problem formulation, beginning with the identification of design requirements, objectives, variables, and parameters to ensure consistency across all analyses.

In recent years, increasing environmental awareness has driven the development of disruptive aircraft architectures and the retrofitting of existing platforms with eco-friendly propulsion systems, advanced materials, and improved aerodynamic designs. Consequently, multidisciplinary design and optimization frameworks have evolved to incorporate additional constraints, objectives, and design variables across both vehicle-level and subsystem-level analyses. The architecture of a multidisciplinary design process has thus become strongly dependent on the aircraft configuration and the performance metrics to be optimized. Preliminary investigations are often required to define appropriate optimization strategies and prioritize objectives, which can significantly increase the time and complexity of conceptual design studies.

The growing complexity of multidisciplinary design and analysis problems, combined with the need to reduce uncertainty from the earliest design stages, has encouraged the integration of higher-fidelity analytical and numerical methodologies. These include computational fluid dynamics, finite element models, six-degree-of-freedom dynamic simulations, and experimental data. To maintain the fast-response characteristics required during early design while leveraging such high-fidelity models, surrogate modelling and machine learning techniques have been increasingly adopted. These data-driven methods replace computationally expensive analyses within the design framework, enabling predictive and adaptive modelling capabilities. However, their application often requires extensive data generation through large-scale design of experiments campaigns to train accurate metamodels capable of capturing complex dependencies among design variables and performance metrics.

Seaplanes have recently re-emerged as promising platforms for passenger and cargo transport in remote regions, as well as valuable assets for emergency operations such as aerial firefighting. Despite their potential, their adoption has been limited by inherent drawbacks relative to land-based aircraft, including, weight penalties and aerodynamic inefficiencies associated with their unique configurations. The introduction of multi-role design strategies and hybrid-electric propulsion systems offers new opportunities to enhance the market viability and environmental sustainability of seaplanes. To explore these opportunities, this research proposes the use of non-conventional, operations-oriented MDO frameworks during the conceptual and preliminary design phases, addressing the overarching research question:

In what ways can conceptual and preliminary design workflows be extended and restructured to support architecture exploration and optimization of innovative amphibious aircraft, while enhancing the operational attractiveness in achieving an optimal balance between performance and cost-effectiveness ?

The exploration of seaplane architectures within the conceptual design phase represents only the initial step in evaluating the long-term potential of this aircraft category. Achieving true market competitiveness requires fully exploiting the inherent versatility of seaplanes, enabling efficient operation across multiple mission profiles and mitigating the limitations traditionally associated with such configurations. Once a suitable configuration is identified through the conceptual exploration of alternative architectures, the subsequent preliminary design phase must incorporate discipline-specific models to refine and enhance overall product performance. This phase involves the simultaneous consideration of multiple performance objectives and operational constraints, derived not only from stakeholder requirements and system specifications, as is typical in conventional aircraft design, but also from the conditions and mission profiles characteristic of the intended operational scenarios.

Contents

List of Figures

List of Tables

List of Abbreviations

Abbreviation	Description
AAA	Advanced Aircraft Design
ADAM	Adaptive Moment Estimation
AEA	Association of European Airlines
AFM	Aircraft Flight Manual
AL	Active Learning
ANN	Artificial Neural Network
AOPA	Aircraft Owners and Pilots Association
ASM	Available Seat Mile
ATA	Air Transport Association of America
AVGAS	Aviation Gasoline
BoP	Balance-of-Plant
CAD	Computer-Aided Design
CAPEX	Capital Expenditures
CASM	Cost per Available Seat Mile
CDF	Cumulative Distribution Function
CFD	Computational Fluid Dynamics
CG	Center-of-Gravity
COLOSSUS	Collaborative SoS Exploration of Aviation Products, Services and Business Models
CPACS	Common Parametric Aircraft Configuration Schema
CPI	Consumer Price Index
CS	Certification Specification
DAF	Design of Aircraft and Flight Technologies
DNN	Deep Neural Network
DOC	Direct Operating Costs
DOE	Design of Experiments
DSM	Design Structure Matrix
EASA	European Union Aviation Safety Agency
EIS	Entry Into Service
EM	Electric Motor
EMO	Evolutionary Many-Objective
ESAR	Energy Specific Air Range
EU	European Union

Abbreviation	Description
eVTOL	electric Vertical Take-Off and Landing
EW	Empty Weight
FAA	Federal Aviation Administration
FADEC	Full Authority Digital Engine Control
FAR	Federal Aviation Regulation
FEA	Finite Element Analysis
FEM	Finite Element Model
FRL	Fuselage Reference Line
FUSETRA	FUture SEaplane TRAffic
GP	Gaussian Process
GUI	Graphical User Interface
HEA	Hybrid-Electric Aircraft
ICAS	International Council of the Aeronautical Sciences
IDF	Individual Discipline Feasible
KCAS	Knots-Calibrated Air Speed
KIAS	Knots-Indicated Air Speed
KPI	Key Performance Indicator
KTAS	Knots-True Air Speed
LCA	Life-Cycle Assessment
LFL	Landing Field Length
LHS	Latin Hypercube Sampling
Li-ion	Lithium-ion
MAC	Mean Aerodynamic Chord
MCD	Monte Carlo Dropout
MCDA	Multi-Criteria Decision Analysis
MDA	Multidisciplinary Desing and Analysis
MDAO	Multidisciplinary Design Analysis and Optimization
MDF	Multidisciplinary Feasible
MDO	Multidisciplinary Design and Optimization
MEREC	MEthod based on the Removal Effects of Criteria
MICADO	Multidisciplinary Integrated Conceptual Aircraft Design and Optimization
ML	Machine Learning
MLP	Multi-Layer Perceptron
MSE	Mean Squared Error
MTOM	Maximum Take-Off Mass
NMC	Nickel-Manganese-Cobalt
OBS	On-Board Systems
ODE	Ordinary Differential Equation
OEM	Operating Empty Mass
OPEX	Operational Expenditures
PEM	Proton Exchange Membrane
PMSM	Permanent Magnet Synchronous Machines
POH	Pilot Operating Handbook
PrADO	Preliminary Aircraft Design and Optimization

Abbreviation	Description
PREE	Payload-Range Energy Efficiency
RCE	Remote Component Environment
SaR	Search and Rescue
SAR	Specific Air Range
SBO	Surrogate-Based Optimization
SFC	Specific Fuel Consumption
SGD	Stochastic Gradient Descent
SL	Sea Level
SMT	Surrogate Modeling Toolbox
SOFC	Solid Oxide Fuel Cell
SoS	Systems of Systems
SoTA	State-of-the-Art
SPOTIS	Stable Preference Ordering Towards Ideal Solution
SSM	Static Stability Margin
STOL	Short Take-Off and Landing
SUAVE	Stanford University Aerospace Vehicle Environment
TCDS	Type Certificate Data Sheet
TDC	Transformative Digital Collaborative
TLAR	Top-Level Aircraft Requirement
TOC	Total Operating Costs
TOPSIS	Technique for Order Preference by Similarity to an Ideal Solution
TRL	Technological Readiness Level
TSFC	Thrust Specific Fuel Consumption
VIKOR	VlseKriterijumska Optimizacija I Kompromisno Resenje
WP	Work Package
WSM	Weighted Sum Method
XDSM	eXtended Design Structure Matrix

List of Symbols

Symbol	Unit(s)	Description
α_B	deg, rad	Body Angle of Attack
AC_{price}	USD million	Acquisition Price
AR_w	-	Wing Aspect Ratio
B	ft, m	Maximum Hull Beam
β_1	deg, rad	Forebody Deadrise Angle
β_2	deg, rad	Afterbody Deadrise Angle
BT	min	Mission Block Time
$\overline{c}$	ft, m	Mean Aerodynamic Chord
C_{2025}	USD	Cost in year 2025
$C_{\text{Reference Year}}$	USD	Cost in year "Reference Year"
$C_{L,0}$	-	3D Lift Coefficient at zero angle of attack
$C_{L,\alpha}$	1/rad	3D Lift Curve Slope
C_{L,δ_e}	1/rad	3D Lift Longitudinal Control Power Derivative
$C_{\mathcal{M},0}$	-	3D Pitching Moment Coefficient at zero angle of attack
$C_{\mathcal{M},\alpha}$	1/rad	3D Pitching Moment Derivative
$C_{\mathcal{M},\delta_e}$	1/rad	3D Pitching Moment Longitudinal Control Power Derivative
c_e/c_{htp}	-	Elevator Chord Ratio
c_f/c_w	-	Flap Chord Ratio
c_r/c_{vtp}	-	Rudder Chord Ratio
c_p	lb/hp hr	Specific Fuel Consumption
$CM_{\text{firefight}}$	%	Commonality Level with respect to the aerial firefight baseline
$CM_{\text{pax transport}}$	%	Commonality Level with respect to the passenger transport baseline
C_R	-	Hydrodynamic Resistance Coefficient
C_V	-	Speed Coefficient
D	N	Aerodyanmic Drag
δ_e	deg, rad	Elevator Deflection
$\Delta(C_V)$	N	Displacement as function of the speed coefficient
DOC_m	USD/hr	Aircraft Maintenance DOC
$DOC_{m,\text{ AF}}$	USD/hr	Airframe Maintenance DOC
$DOC_{m,EM_{line}}$	USD/hr	Electric Motor Line Maintenance DOC
$DOC_{m,EM_{base}}$	USD/hr	Electric Motor Base Maintenance DOC
$DOC_{m,\text{ ICE}}$	USD/hr	Internal Combustion Engine Maintenance DOC

Symbol	Unit(s)	Description
DP	yr	Depreciation Period
d_{LND}	ft	Landing Distance
d_{TO}	ft	Take-Off Distance
d_{scoop}	ft	Scooping Distance
$E_{0,tot}$	J	Initial Total Energy
E_{bat}	kWh	Rated Battery Energy
e_{bat}	J/kg	Battery Specific Energy
e_f	J/kg	Fuel Specific Energy
En	hr	Endurance
En_{factor}	-	Endurance Factor
E_{trip}	kWh	Battery Energy Consumed in one trip
$\mathbf{f}\left(\mathbf{x}_j^{train}\right)$	-	MLP Model Training Labels
φ	deg, rad	Sternpost Angle
Φ	-	Supplied Power Ratio
Φ_{CL}	-	Supplied Power Ratio in Climb
Φ_{CR}	-	Supplied Power Ratio in Cruise
Φ_{DS}	-	Supplied Power Ratio in Descent
Φ_{TO}	-	Supplied Power Ratio in Take-Off
Fr_B	-	Beam Froude Number
g	m/s^2	Gravitational Acceleration
$h_{\%B}$	%	Step Height as percentage of the maximum beam
$h_{Ceil,\ AEO}$	ft	Absolute Ceiling
h_{fire}	ft	Fire Pressure Altitude
h_{water}	ft	Water Pressure Altitude
i_H	deg	Horizontal Tail Incidence
i_w	deg	Wing Incidence
I_y	$kg\,m^2$	Moment of Inertia
L	N, lb_f	3D Aircraft Lift Curve
L_a	m, ft	Afterbody Length
Λ_H	deg	Horizontal Tail Sweep Angle
Λ_V	deg	Vertical Tail Sweep Angle
λ_w	-	Wing Taper Ratio
Λ_w	deg	Wing Sweep Angle
L/D	-	Lift-to-Drag Ratio
$\mathcal{M}_{aero}$	Nm, lb_f-ft	3D Aerodynamic Pitching Moment
$\mathcal{M}_{hydro}$	Nm, lb_f-ft	Hydrodynamic Pitching Moment
M_{CR}	-	Cruise Mach Number
$M_{CR,max}$	-	Maximum Cruise Mach Number
M_{drop}	-	Mach Number (Drop Phase)
$\hat{\mu}(\mathbf{x}_j)$	-	Predictive Mean
N_1	N	Forebody Contribution to the hydrodynamic Lift
N_2	N	Afterbody Contribution to the hydrodynamic Lift
ND	-	Negative Ideal Solution in the VIKOR MCDA Method
N_{drop}	-	Number of Drops
P_0	hp	Rated Power Turboprop Engine
PD	-	Positive Ideal Solution in the VIKOR MCDA Method
P_{EE}	USD/kWh	Electric Energy Unit Price
P_{EM}	kW	Rated Power Electric Motor
P_{fuel}	USD/kg, USD/US Gal.	Jet-A1 Unit Price
P/W	hp/lb	Power-to-Weight Ratio
$p(Y\|\mathbf{x}_j)$	-	Posterior Predictiive Probability Distribution

Symbol	Unit(s)	Description
q	Pa	Dynamic Pressure
q	rad/s	Pitch Rate
R	N	Friction Component of the Hydrodynamic Resistance
R	nm	Range
R_{factor}	-	Range Factor
R_{hydro}	N	Total Hydrodynamic Resistance
RV	-	Aircraft Residual Value
ρ_w	kg/m^3	Water Density
S	-	Score of the VIKOR MCDA Method
$\hat{\sigma}^2(\mathbf{x}_j)$	-	Prediction Uncertainty
T	N	Propeller Thrust
t/c	-	Airfoil Mean Thickness Ratio
$(t/c)_H$	-	Horizontal Tail Thickness Ratio
$(t/c)_V$	-	Vertical Tail Thickness Ratio
θ	rad	Pitch Attiude
TI	USD	Total Investment
V_{CL}	KCAS	Climb Speed
$\mathcal{V}_H$	-	Horizontal Tail Volumetric Coefficient
$\mathcal{V}_V$	-	Vertical Tail Volumetric Coefficient
W_f	lb$_f$	Final Weight
W_i	lb$_f$	Initial Weight
W_F	lb	Fuel Mass Consumption
$W_{F,\text{max}}$	lb	Max Fuel Mass
W_{OE}	N, lb$_f$	Operating Empty Weight
W_{PL}	N, lb$_f$	Payload Weight
W/S	lb/ft^2	Wing Loading
$\mathbf{x}_j^{\text{train}}$	-	MLP Model Training Features
$\mathbf{x}_j$	-	MLP Model Unlabelled Features
$X_{LE,w}$	ft	Wing Apex
X_T	N	Horizontal Component of the Thrust in the Body Reference Frame
Y	-	Set of outputs of the MLP model for T stochastic passes
$y^{(t)}$	-	MLP output at the t-th stochastic pass
Z_T	N	Vertical Component of the Thrust in the Body Reference Frame
η_1	-	Transmission Efficiency Branch 1
η_2	-	Transmission Efficiency Branch 2
η_3	-	Transmission Efficiency Branch 3
η_{ops}	lt/min, US Gal./min	Operational Efficiency
η_P	-	Propeller Efficiency

Chapter 1

Introduction

Contents

1.1 Research Motivation

THE design process of aerial vehicles has always represented a highly multidisciplinary and iterative problem [1]. The multidisciplinary nature of this process primarily stems from the inherent complexity of aircraft architectures and their configuration layouts. When considering conventional utility functions, such as passenger or freight transport, the most common configurations, even in recent years, are based on well-established tube-and-wing layouts. In such architectures, each component is designed to fulfil a specific role in achieving the primary mission objective, whether transporting passengers or carrying cargo [2].

The distinct functional purposes assigned to each aircraft component therefore act as the main drivers in their respective design processes [2]. For instance, in traditional tube-and-wing configurations, the principal function of the wing is to generate the majority, if not the entirety, of the lift required to sustain the aircraft throughout its mission profile. Consequently, aerodynamic and structural sizing become the dominant disciplines to be integrated into the design of the wing. Similarly, the fuselage is primarily intended to accommodate the payload and provide structural support for the other aircraft components. Hence, its design requires not only structural sizing capabilities but also disciplinary models capable of defining the internal arrangement and systems layout necessary to meet payload and operational

requirements.

The coupling between the various disciplines represents the primary factor driving the iterative nature of the aircraft design process. Classical software architectures and Multidisciplinary Design and Analysis (MDA) frameworks, discussed later in this chapter, are developed, particularly for the early design stages, to achieve a consistent and converged design solution. Such consistency, however, depends on the interdependencies among the involved disciplines. For instance, statistical Class-I and semi-empirical Class-II weight estimation methods require knowledge of the aircraft layout and geometry, as well as the normal operating conditions and performance limits [3]. Consequently, appropriate geometry modelling and performance analysis modules must be integrated within the design framework to supply the necessary input data [4]. The exchange of information among these disciplines is typically performed iteratively until no significant modifications in the aircraft configuration are observed, indicating convergence of the design solution.

The continuous pursuit of improved flight performance has driven designers to incorporate high-fidelity methodologies and tools, such as Computational Fluid Dynamics (CFD) and Finite Element Analysis (FEA), already in the early stages of the aircraft design process [5], both for conventional and unconventional vehicle and system architectures. However, this trend introduces potential incompatibilities between the large number of design variables required by high-fidelity tools and the comparatively smaller set of parameters typically employed in low-fidelity analyses characteristic of early design phases. Furthermore, the significant computational costs associated with such detailed models pose additional challenges. To address these issues, state-of-the-art MDA practices advocate the use of surrogate models to approximate computationally expensive disciplinary analyses [6]. This approach enables the formal definition of surrogate-based optimization (SBO) problems and their effective integration within multidisciplinary design optimization (MDO) frameworks.

The growing demand for more sustainable aviation solutions has driven the development of novel and often disruptive design concepts aimed at meeting stringent environmental targets, most notably those outlined in the European Commission's "Flightpath 2050" initiative, which aspires to achieve net-zero emissions within the aviation sector by 2050 [7]. Among the various technological pathways explored, all-electric and hybrid-electric powertrain architectures have demonstrated the greatest potential to contribute to these environmental objectives, both in the short term and in the pursuit of long-term sustainability goals [8, 9]. The introduction of such technologies has necessitated the evolution of existing aircraft design tools and MDO frameworks to accommodate new disciplinary capabilities required for the sizing and performance assessment of advanced powertrain systems [10, 11]. Furthermore, these frameworks must be adapted to effectively manage the additional design degrees of freedom introduced by such architectures, as well as to model their interactions with conventional methodologies that constitute the current state of the art in conceptual and preliminary aircraft design.

Lastly, additional complexities in the formulation of the aircraft design problem may arise from the nature of the intended mission profile, and more specifically, from the operational role of the aircraft. In contemporary civil fixed-wing aircraft, three principal classes of operations can generally be identified: (1) passenger transport, (2) freight and cargo transport, and (3) emergency response missions, which typically encompass Search and Rescue (SaR) activities and aerial firefighting operations.

Conceptual and preliminary design frameworks are traditionally developed to guide the design process toward fulfilling a predefined set of architecture- and performance-based requirements, often derived from an existing reference platform [12]. Consequently, these frameworks tend to focus on a single operational role, which inherently limits the ability of current early-stage design methods to fully exploit the potential for rapid, multi-role capability assessment and adaptation.

However, the primary purpose of the conceptual and preliminary design stages is to enable the exploration of a wide range of aircraft configurations and capabilities starting not from an existing product, but rather from a notional or "sketch" baseline [13]. This flexibility allows the investigation of multiple operational roles during the design process, thereby promoting enhanced versatility, responsiveness, and overall market attractiveness of the resulting aircraft architecture.

Seaplanes represent a compelling case study for investigating how conceptual and preliminary design frameworks can be extended and refined to meet emerging requirements in the development of next-generation aerial systems. These aircraft exhibit a wide variety of configurations and have historically been employed across multiple mission profiles, from early passenger transport services in the 1930s, exemplified by platforms such as the Martin JRM Mars and the Boeing 314, to subsequent designs like the Grumman G-73 Mallard and its military evolution, the HU-16 Albatross [14]. More recent developments include modern adaptations such as the amphibious conversion of the Cessna Caravan, the ShinMaywa US-2, and the Dornier Seastar.

Seaplanes have also played a critical role in specialized mission domains, most notably aerial firefighting, with iconic examples including the Canadair CL-215, its successor the CL-415, and the future DHC-515. Despite their operational versatility, the seaplane market has historically experienced periods of stagnation, primarily due to inherent performance limitations associated with this class of aircraft. These include aerodynamic penalties resulting from increased drag, structural weight increments required to ensure buoyancy, and elevated operational costs linked to specialized pilot training and maintenance requirements [15].

In recent years, both established aerospace manufacturers and emerging startups have begun to reconsider the potential of seaplanes as viable solutions for future air mobility. Increasing congestion at major airports, combined with the advent of advanced composite materials, electric and hybrid-electric propulsion systems, and innovative design methodologies, has renewed interest in this class of aircraft [16]. These technological advancements offer the prospect of overcoming many of the

traditional limitations associated with seaplane operations, including aerodynamic inefficiencies, structural penalties, and elevated operational costs.

This context provides the foundation and motivation for the main research question guiding the present work:

In what ways can conceptual and preliminary design workflows be extended and restructured to support architecture exploration and optimization of innovative amphibious aircraft, while enhancing the operational attractiveness in achieving an optimal balance between performance and cost-effectiveness ?

The exploration of seaplane architectures with respect to their typical utility functions represents only the initial step in assessing the future potential of such aerial platforms. Achieving true market attractiveness, particularly within a segment currently dominated by small general aviation aircraft in the 18-passenger class, requires fully leveraging the versatility of seaplanes to operate effectively across multiple mission scenarios. Consequently, once a suitable configuration has been identified through the conceptual exploration of multiple vehicle architectures, the subsequent preliminary design phase should employ more refined and targeted disciplinary models to enhance the overall attractiveness of the product. This involves simultaneously addressing multiple performance objectives and operational constraints.

1.2 The European International Context

This section provides an overview of the international context underpinning the research work, with particular emphasis on the integration of advanced conceptual and preliminary design strategies for the development of non-conventional aircraft architectures. The objective is to highlight the main goals of the COLOSSUS project, the knowledge gained, and the contributions made toward the advancement of multidisciplinary design analysis and optimization (MDAO) strategies for the conceptual and preliminary aircraft design phases. The focus is placed on conventional and hybrid-electric multi-role seaplane configurations, addressing the inherent complexities and limitations that typically characterize such platforms, and proposing approaches to mitigate these challenges in order to enhance the attractiveness of this market niche.

1.2.1 The COLOSSUS Project

Systems of Systems (SoS) can be defined as collections of constituent systems whose objective is to cooperate in order to achieve benefits that would not be attainable by the individual systems if operating independently [17]. The EU-funded COLOSSUS project (Collaborative SoS Exploration of Aviation Products, Services and Business

Models) adopts this framework to investigate innovative approaches for product and service development in aviation. Designing within a SoS environment introduces challenges not typically encountered in the technical design of isolated constituent systems, including: (i) the need to explore additional design and analysis domains to assess the capabilities and impacts of SoS approaches, and (ii) the integration of multi-level and non-technical design variables and constraints [18].

Within COLOSSUS, a multi-level approach is applied to identify needs, capabilities, and system requirements to support a holistic product development process. The hierarchical breakdown structure encompasses: (I) needs and business models, (II) the system-of-systems design space, (III) the constituent systems design space, and (IV) the subsystem design space, the latter extending down to the level of individual components. The consortium comprises 14 partners from academia, research institutes, and industry, collaborating within six work packages (WPs). Two WPs address administrative and management tasks, while four technical WPs focus respectively on scenario and business model analysis, the design and assessment of novel aerial products, SoS engineering and optimization, and the integration of outcomes into a collaborative digital framework that supports the multi-level process structure, as illustrated in Figure 1.1.

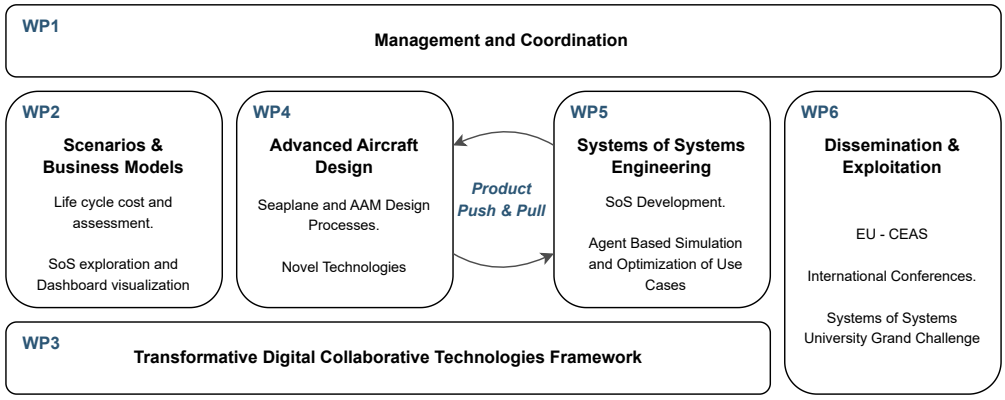

Figure 1.1: COLOSSUS Work Packages Structure

Objectives And Motivation

The COLOSSUS project is aligned with the current research priorities of the Climate, Energy and Mobility cluster promoted under the Horizon Europe Programme. It addresses two major challenges: (i) accelerating the reduction of aviation-related impacts and emissions through a comprehensive strategy to support the European Union's objective of climate neutrality by 2050 [7], and (ii) contributing to the preservation of the European aviation industry's global leadership by fostering digital transformation, disruptive technologies, innovative business models, and new opportunities enabled by digitalisation.

Within this context, COLOSSUS aims to develop and validate new products and services through a holistic System-of-Systems methodology, thereby contributing to the digital transformation of the European air transport system while strengthening competitiveness across relevant industrial sectors. These high-level ambitions are translated into three specific technical objectives:

1. Development of a Transformative Digital Collaborative (TDC) Framework capable of supporting research, technology development and innovation through a holistic SoS approach. The framework will enable modelling, analysis, optimisation, and evaluation of complex aviation products and services under realistic operational scenarios.

2. Expansion and validation of the TDC framework through two use cases:

    - *Use Case 1*: Creation of a business model for sustainable multi-modal mobility, evaluating the concept for performance, competitiveness, environmental impact and life cycle footprint.
    - *Use Case 2*: Development of an integrated, fast-response wildfire-fighting approach that combines advances in aircraft design and technology with agent-based modelling, artificial intelligence, and digitalisation tools.

3. Execution of conceptual design studies for two aerial products identified as transversal technology enablers for sustainable mobility and aviation decarbonisation: (i) a multi-role seaplane equipped with hybrid-electric propulsion, and (ii) an all-electric advanced air mobility vehicle with vertical take-off and landing (eVTOL) capabilities, designed for both passenger and cargo transport.

Lesson Learnt

The COLOSSUS project provided the author with the opportunity to develop and integrate advanced MDAO workflows aimed at enhancing the overall competitiveness of niche aerial products, specifically seaplanes. Collaboration with experts in System-of-Systems engineering and industrial partners facilitated the incorporation of design variables, constraints, and objectives from multiple stakeholder perspectives. This approach contributed to the establishment of an aircraft design methodology that extends beyond conventional performance metrics, explicitly addressing scenario-specific operational requirements.

Beyond the activities directly conducted within COLOSSUS, the author's research further incorporated machine learning and surrogate-based optimisation techniques in the early design stages to systematically explore families of seaplane architectures, tailored to given set of requirements. These methods were subsequently applied in the preliminary design phase to improve operational flexibility and efficiency, thereby strengthening the robustness of the overall design process.

Author's Contributions

The author's primary contribution to the project consisted of conducting the conceptual and preliminary design of the multi-role seaplane—developed in both passenger transport and aerial firefighting configurations—within the scope of WP4, that foster the development of next-generation aerial platforms, specifically within the seaplane category, with a planned entry into service year in 2035. The project targets a 30% reduction in fuel consumption compared to 2020 benchmark aircraft in the same category and certification class.

This process relied on the analysis of operating scenarios defined in WP2, which, together with industrial constraints, informed the derivation of a consistent and feasible set of design requirements. The ambition to extend beyond the current State-of-the-Art (SoTA) in conventional aircraft design methodologies necessitated the integration of multiple disciplinary analyses within a collaborative MDAO environment, specifically, the Remote Component Environment (RCE), developed by the German Aerospace Center (DLR). These analyses encompassed low-fidelity aerodynamic modelling, the design and assessment of alternative propulsion system architectures, evaluation of performance across payload–range envelopes, determination of mass properties and stability characteristics, and the economic assessment of the aircraft.

Within WP4, multiple design and analysis workflows were established to support both early-phase configuration exploration and later-stage multi-objective optimisation, addressing in-flight performance as well as economic viability. The outcomes of these design exploration and optimisation activities were incorporated into the TDC framework, enabling performance assessment in both the multi-modal mobility and wildfire-fighting scenarios. This iterative process facilitated the refinement of design requirements and ultimately supported the implementation of a SoS-driven aircraft design methodology.

Related Publications

One journal publication describe the SoS-driven aircraft design methodology:

> [19] **Tuccillo, M.**; Ruocco, M. *Aircraft Design Capabilities for a System-of-Systems Approach (eVTOL and Seaplane Design)*. Eng. Proc. 2025, 90, 21. https://doi.org/10.3390/engproc2025090021.
>
> Presented at the 14th EASN International Conference on "Innovation in Aviation & Space towards sustainability today & tomorrow", Thessaloniki, Greece, 8–11 October 2024. The journal article describes the aircraft design space exploration process, leveraging the analysis of relevant stakeholders, and associated Key Performance Indicators (KPIs), to derive an informed MDA design workflow, targeting the most impacting design variables and constraints towards stakeholders metrics and interests.

1.3 Thesis Objectives and Outline

This thesis aims to address the research needs identified in the preceding sections by presenting the author's work in developing dedicated surrogate-based conceptual exploration workflows and in restructuring the preliminary design process to enhance the efficiency and competitiveness of future seaplane architectures.

The remainder of this document is organized as follows:

- **Chapter 2** presents a comprehensive review of the current state of the art in conceptual and preliminary aircraft design processes, identifying key trends, methodologies, and research gaps. The chapter examines both closed software architectures and multidisciplinary design and analysis, and multidisciplinary design and optimization, frameworks applied to early-stage aircraft development. Particular attention is devoted to recent advancements involving the integration of high-fidelity disciplinary models, the application of machine learning techniques to support component design and optimization, and the emerging limitations introduced by these methodologies.

- **Chapter 3** introduces the case study underpinning this research. It describes the derivation of Top-Level Aircraft Requirements from the operational context motivating this work, complemented by a concise market analysis of existing seaplane competitors in both the passenger transport and emergency response sectors, particularly those adapted for aerial firefighting operations. The main outcome of this chapter is a comprehensive set of design requirements aimed at enhancing the attractiveness and operational versatility of the

proposed seaplane concept while maintaining competitiveness with respect to existing platforms.

- **Chapter 4** presents the surrogate-based conceptual exploration process developed to investigate potential seaplane architectures exhibiting optimal performance with respect to selected figures of merit and key performance indicators. The chapter addresses the initial part of the main research question, by tackling the need of improving the efficiency and flexibility of the conceptual design problem for innovative seaplanes. It provides a comprehensive description of the surrogate-based conceptual design methodology, beginning with the identification of appropriate performance metrics and objective functions, followed by the selection of design variables exerting the greatest influence on these metrics, thereby guiding the exploration process. The discussion then details the architecture of the design workflow, including the generation of a configurations' pool, the development of surrogate models serving as the computational core of the conceptual design problem, and the formulation and solution of the architecture-based optimization problem aimed at identifying the family of seaplane concepts that best satisfy the prescribed requirements and design objectives. Appendix A and Appendix B complement this chapter by, respectively, illustrating the classical statistical sizing procedure employed to define the baseline configuration used as input for the concept exploration campaign, and by presenting the analysis of multiple aerial firefighting scenarios aimed at deriving a design table to support the optimization process of the aerial firefighting variant.

- **Chapter 5** focuses on the second component of the research question, by presenting a dedicated preliminary design strategy to improve the attractiveness of innovative seaplanes during multi-role operations, highlighting the necessary trade-off between flight performance and economic performance. It therefore outlines the application of multi-criteria decision-making techniques to filter the family of candidate architectures derived in Chapter 4, ultimately identifying a reference configuration to guide the subsequent preliminary design process. Particular emphasis is placed on disciplinary methodologies, such as cost modelling and hydrodynamic performance analysis, which play a pivotal role at this stage for this class of air vehicles. The chapter concludes by presenting the optimal multi-role seaplane architecture, demonstrating the trade-off achieved between performance penalties and the level of commonality across multiple operational scenarios. Appendix C completes the chapter by providing complete economic assumptions to drive the operating costs analysis.

Finally, the Conclusions summarize the main findings of the research and discuss the broader implications of the proposed methodologies, along with recommendations and perspectives for future developments.

Chapter 2

Aircraft Conceptual Design: Trends and Gaps

Contents

2.1 State-of-the-Art of Aircraft Design Frameworks

THE aircraft design process can seldom be regarded as a straightforward task. Since the early years of the aviation industry, best practices and accumulated industrial experience have guided the development of aerial products, as well as the numerical processes supporting their continuous evolution [2]. Over time, these industrial best practices have fostered the formalization of the aircraft design process. The strong influence of manufacturers on this formalization is evident from the general consensus among various authors regarding the typical steps required to conduct the design process effectively.

According to many authors like Gudmundsson [20], Torenbeek [21], Raymer [22], Roskam [23], and Jenkinson [13], the aircraft design process can be structured into multiple phases, each characterized by a progressive increase in the knowledge of aircraft performance and behaviour, as well as in the associated design and analysis costs (including man hours and economic expenses). Specifically, all authors converge on the identification of three fundamental stages of the design process: the

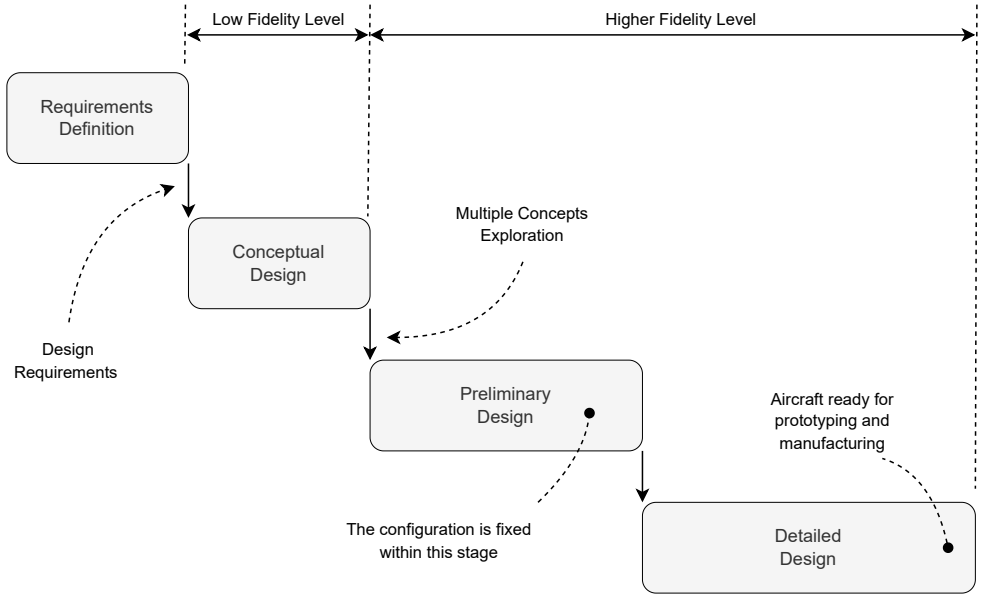

Figure 2.1: The three steps composing the aircraft design process. The process begins with the identification of design requirements. Adapted from Gudmundsson [20] and Jenkinson [13].

conceptual design, the preliminary design, and the detailed design phases, which are summarised in Figure 2.1.

According to the proposed diagram, the process begins with the identification of the design requirements, whose purpose is to define the target objectives for the platform under development and to ensure a competitive position relative to existing and potential future solutions. The first stage, namely the conceptual design phase, focuses on exploring both conventional and innovative configurations to identify layouts that are technically feasible and commercially viable [13]. At this stage, a broad range of options is examined, requiring the definition of the overall geometry, engine type, number and placement, level of technological innovation, and key operational parameters. The main outcome of this phase is an assessment of the technical feasibility of the candidate concepts and an approximate estimation of the size and characteristics of the most promising configurations [24].

Unlike the conceptual design phase, the preliminary design stage lacks a universally accepted definition, as well as a clear consensus on its starting point. For instance, Raymer defines the preliminary design phase as beginning once a single promising configuration has been identified from the conceptual design stage, thereby allowing more detailed analyses to be conducted on a fixed configuration. In contrast, Torenbeek and Jenkinson describe the preliminary design as a phase of continuous modification, with the configuration being considered “frozen” only at its conclusion, prior to entering detailed design. Similarly, both Gudmundsson and Sgueglia [24] interpret the preliminary design phase as an intermediate step aimed

at refining and validating the outcomes of the conceptual design stage, resolving any inconsistencies or non-conformities to achieve a prototype-ready configuration for detailed design.

In the context of this research, the definition proposed by Nicolai [25] is adopted. According to Nicolai, the preliminary design phase involves a fine-tuning process applied to the most promising configuration, previously selected based on cost and performance criteria. This stage encompasses detailed aerodynamic analyses, stability and control assessments through rigid-body motion studies, and structural stress evaluations. Modifications to the configuration are permissible during this process, provided they do not substantially alter the overall aircraft architecture.

Finally, the detailed design phase begins toward the end of the aircraft development process. During this stage, the configuration is refined to a higher level of detail, typically relying on high-fidelity numerical methodologies and experimental validation through prototype testing. With the external geometry fixed, the structural framework and subsystem integration are defined. At this point, major configuration changes are generally avoided, as they could invalidate analyses and design efforts carried out during the conceptual and preliminary stages. Upon completion of this phase, the aircraft design is finalized and formally "released for production" [13].

Over the past two decades, numerous tools and software systems have been developed to support the aircraft design process, particularly during the conceptual and preliminary phases. These stages can be highly automated, thereby reducing the effort required to progress toward a configuration ready for the detailed design stage. Concurrently, the increasing computational capabilities of modern hardware have enabled the implementation of complex design frameworks that support Multidisciplinary Design Analysis and Optimization (MDAO) workflows, which today constitute the core structure of many advanced aircraft design environments.

These tools can generally be classified into two main categories: *closed-structure tools* and *collaborative frameworks*. Closed-structure tools comprise software systems in which the design workflow, whether for conceptual or preliminary design, follows a predefined structure with a fixed sequence of disciplinary analyses. In such systems, the user cannot modify the underlying workflow but can control input parameters and select the type of analysis to be conducted, such as aircraft design from scratch, performance assessment of an existing platform, or configuration optimization.

In contrast, *collaborative design frameworks* offer a more flexible and modular design process. Typically built upon open-source MDAO frameworks, these tools treat each disciplinary module as an independent component that can be integrated into the design workflow as needed. Although they require a deeper understanding of both the disciplinary models and the underlying MDAO architecture, their flexibility enables users to perform a broader range of analyses and to tailor workflows to specific research needs.

2.1.1 Closed-Structure Design Tools

The development of computer aided "closed-structure" aircraft design tools began as early as the 1980s, with several systems emerging as foundational examples of automated design environments. Among the first were the Preliminary Aircraft Design and Optimization (PrADO) [26] tool, developed by the Institute of Aircraft Design and Lightweight Structures (IFL) at the Technical University of Braunschweig; Piano [27], a professional software developed by the UK-based company Lissys in the early 1990s; and the Advanced Aircraft Analysis (AAA) [28] program, created by DARcorporation.

These tools share several conceptual and structural similarities. For instance, PrADO consists of multiple design submodules, each dedicated to specific analytical tasks, which can be flexibly organized to implement various design, analysis, and optimization workflows. The tool supports a wide range of aircraft configurations, including unconventional architectures such as blended wing body (BWB) designs [26, 29]. Similarly, Piano integrates all the fundamental modules required for a comprehensive multidisciplinary aircraft analysis, enabling the user to perform preliminary sizing, aerodynamic and performance assessments, and cost estimation. The software can evaluate key aspects such as weight and balance, aerodynamic characteristics, static stability, performance metrics, emissions, and operating costs.

The AAA software, on the other hand, is primarily based on the design methodology developed by Roskam and Lan [30], while also incorporating a variety of empirical and semi-empirical methods derived from NACA/NASA studies and from DARcorporation's internal research. This allows AAA to address both conventional and unconventional aircraft configurations, including tiltrotor and tiltwing concepts.

Among the most recent developments in this class of design tools are the Multidisciplinary Integrated Conceptual Aircraft Design and Optimization (MICADO) [31] environment, the Stanford University Aerospace Vehicle Environment (SUAVE) [32], and the Java-based Preliminary Aircraft Design (JPAD) [33] framework.

MICADO, developed since 2008 at the Institute of Aerospace Systems (ILR) of RWTH Aachen University, is a conceptual and preliminary design tool that enables rapid and comprehensive assessment and optimization of new aircraft concepts. A key feature of MICADO is its capability to perform fast preliminary sizing of new aircraft configurations starting from a limited set of Top-Level Aircraft Requirements (TLARs) and design specifications. This sizing process is executed in an automated manner through a structured workflow that iteratively evaluates the convergence toward a consistent and feasible design, ensuring compliance with key requirements such as maximum take-off weight and operating empty mass.

Similarly, SUAVE is an open-source, Python-based framework developed to support design and analysis of both conventional and unconventional aircraft configurations [34]. It enables users to perform diverse analyses by modifying only a few lines in the input definition file, thereby offering high flexibility in configuration man-

agement. One of SUAVE's most notable features is its ability to integrate both low-fidelity and high-fidelity analysis methodologies within the same environment [34], like Euler CFD analysis for lift drag calculation through the multiphysics simulation and design software SU2 [35], facilitating scalable fidelity in multidisciplinary aircraft design studies.

JPAD is a framework developed in-house at the University of Naples Federico II by the DAF research group in collaboration with the university spin-off SmartUp Engineering. The framework enables multidisciplinary analysis and optimization of civil transport aircraft. JPAD represents the culmination of the DAF group's extensive experience acquired through participation in numerous European research projects, which have contributed to the development of advanced methodologies and tools supporting the aircraft design process.

The framework is organized as an integrated ecosystem of software modules, each dedicated to a specific design task. These include Computer-Aided Design (CAD) modelling of aircraft configurations, design exploration through sensitivity analyses across multiple architectures, and single- and multi-objective optimization using evolutionary algorithms. This modular and extensible structure makes JPAD a flexible and powerful environment for supporting both conceptual and preliminary aircraft design studies.

A typical advantage of such frameworks lies in their automated nature, meaning that the design process is governed by underlying algorithms and predefined workflows. This structure prevents the user from introducing errors during the configuration generation process and ensures that unfeasible aircraft layouts are automatically identified. In cases where inconsistencies or infeasible configurations arise, the software typically alerts the user and provides guidance or suggestions for corrective modifications.

As previously discussed, another defining characteristic of these aircraft design tools is the fixed nature of their embedded design and analysis workflows. Even when equipped with a Graphical User Interface (GUI), users are generally limited to selecting the type of analysis to perform, without the ability to modify the underlying MDA and MDO sequences required to achieve a consistent solution. This constraint represents a significant limitation in terms of flexibility, as it restricts the capability of the framework to adapt to unconventional configurations or novel mission profiles. For example, when investigating an aerial firefighting aircraft, the framework must already include the disciplinary modules required to size firefighting-specific systems and to assess the associated flight performance and fuel consumption across representative mission profiles.

2.1.2 Collaborative Design Frameworks

Collaborative aircraft conceptual or preliminary design tools are typically built upon MDAO frameworks, which enable the various disciplinary modules to exchange data

and information through a centralized data schema and standardized input/output interfaces. Among the most widely adopted frameworks are RCE [36], developed by the German Aerospace Center (DLR); GEMSEO [37], created by the Multidisciplinary Design Optimization Competence Center of IRT Saint Exupéry; and OpenMDAO [38], developed through a collaboration between the NASA Glenn Research Center, the University of California, and the Department of Aerospace Engineering at the University of Michigan.

The strong multidisciplinary nature of the aircraft design process has encouraged the extensive application of these frameworks, not only for traditional design tasks but also for optimization processes conducted at both the aircraft and subsystem levels. Examples include aerodynamic shape optimization at the aircraft level [39], as well as subsystem level, such as the optimization of the thermal management system for innovative aircraft architectures [40], particularly for hybrid-electric transport aircraft integrating conventional turbofan engines coupled with propulsive battery packs powering electric motors. The primary advantage of these frameworks lies in their ability to enable designers to structure and execute a wide range of design and optimization processes, provided that the disciplinary models, typically referred to as *components*, are implemented and executed using the framework's built-in classes.

To support the comprehension of generic MDA and MDO problems that can be constructed using such frameworks, Martins and Lambe introduced the eXtended Design Structure Matrix (XDSM) [41]. This standardized diagram extends the classical Design Structure Matrix (DSM) by allowing not only the visualization of dependencies among different disciplines, or components, but also a clear representation of the data exchanged between them, thereby simplifying the development of modules based on a common data schema.

An example of a centralized data schema is the XML-based Common Parametric Aircraft Configuration Schema (CPACS). CPACS is an open-source format that provides a standardized framework for exchanging aircraft and fleet data. It enables the storage of parametric definitions of aircraft geometries, subsystem characteristics, structural masses, mission profiles, and aerodynamic data (e.g., drag polars and lift curves) within a structured dictionary. This centralized schema ensures consistent data exchange across various levels of design fidelity [42, 43]. In practice, CPACS provides a comprehensive predefined data dictionary encompassing the typical input and output parameters used by tools in conceptual and preliminary aircraft design. Within a MDAO framework, each disciplinary module reads a CPACS file instance as input and writes its results to an output CPACS file which is an updated version of the input one [2]. This schema is typically adopted by frameworks such as RCE, while others, such as OpenMDAO, rely on different, often decentralized data structures.

Frameworks like OpenMDAO can also operate using decentralized data schemas, as described by van Gent [2]. In this approach, each component maintains its own set of input and output specifications, and the process integrator is responsible for

manually mapping the interconnections between components. Although this approach offers greater flexibility in the development of individual disciplinary models, it introduces significant challenges for the management of interfaces among components. In a decentralized schema, if n represents the number of components, then $n(n-1)$ interfaces must be defined, causing the number of connections to grow quadratically with the number of disciplines. Conversely, a centralized schema such as CPACS requires only $2n$ interfaces, each discipline reads from and writes to a common file, resulting in a linear scaling of the number of interfaces [43].

Among the aircraft design tools that leverage collaborative MDAO frameworks are NASA's recently developed "Aviary" and FAST-OAD, the latter developed through a collaboration between the French aerospace research center, ONERA, and the *Institut supérieur de l'aéronautique et de l'espace* ISAE-SUPAERO. Both tools are built upon the OpenMDAO framework and support the conceptual and preliminary design of both conventional and unconventional aircraft architectures. A key feature of these frameworks is the capability to modify the core design workflow, not only by adding custom-defined components, but also by altering the workflow structure itself.

Figure 2.2 illustrates how Aviary conducts the design of an aircraft configuration and performs performance analyses over representative mission profiles. Notably, the tool allows users to modify existing core components or integrate new ones, thereby demonstrating the flexibility of the underlying framework. An additional advantage of both Aviary and FAST-OAD lies in their ability to incorporate high-fidelity disciplinary components within the overall design process. This is made possible by the OpenMDAO core, which enables derivative computation for gradient-based optimization. In the current implementation, these gradients are computed numerically, as most of the integrated models, in FAST-OAD especially, do not provide analytical gradient definitions [44].

2.2 Uncertainty Reduction in Early Design

The need to reduce uncertainty during the early stages of aircraft design has become increasingly critical in modern aerospace development. Industrial stakeholders are progressively urging design departments to enhance the level of knowledge and predictive capability already within the preliminary design phases [46]. CFD and structural Finite Element Analysis (FEA) have emerged as promising high-fidelity methodologies to address these challenges also in the conceptual design stage [47, 48]. These tools are employed not only for performance assessment but also to support and guide MDO campaigns aimed at improving overall aircraft performance and design quality [49].

Aerodynamic shape optimization, in particular, has been extensively utilized to minimize aerodynamic drag during critical flight conditions such as climb and cruise, thereby enabling the development of more efficient aircraft configurations. Such

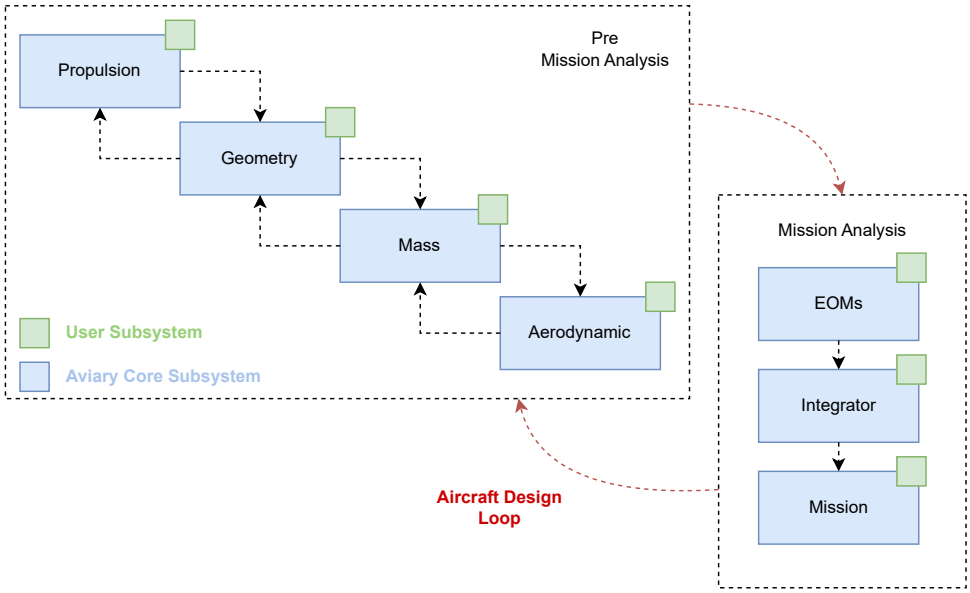

Figure 2.2: Baseline aircraft design process according to the Aviary framework. Adapted from Ref. [45]. Both the integrated components and the design process can be modified by the user leveraging capabilities of OpenMDAO.

studies commonly exploit CFD-based analyses on baseline configurations to optimize specific components of the aircraft architecture, most notably the wing, or the coupling between wing and tailplanes, in order to account for aerodynamic interaction effects within the optimization process [50].

It is worth noting that CFD-based aerodynamic shape optimization is typically applied to individual aircraft components rather than to the entire configuration, primarily due to several inherent challenges [49]. In the context of preliminary design, the most critical among these challenges include the robustness of the numerical solver, the scalability of the optimization process with respect to the number of design variables, and the geometric parametrization strategy. Solver robustness is essential because optimization algorithms generally lack the qualitative sensitivity of a human designer. As a result, they may select design variables defining geometries that lead to unfeasible or physically meaningless configurations. The likelihood of obtaining credible and convergent architectures decreases as the number of components involved increases, which also amplifies the probability of converging to local optima, a well-known issue in aerodynamic shape optimization design spaces [51].

Furthermore, the number of design variables required in CFD-based aerodynamic shape optimization scales rapidly with the number of components considered. For instance, optimizing a single wing may involve several hundred design variables, whereas a full-aircraft optimization can require thousands. In parallel, CAD tools are necessary to parameterize the geometry, typically through independent and modular approaches to prevent meshing inconsistencies. These factors collectively limit

the applicability of high-fidelity methodologies in the preliminary design phase of a new aircraft. At this stage, the available knowledge of the configuration is still limited, constraining CAD usage primarily to the definition of external surfaces. Consequently, design constraints associated with other disciplines are often neglected, as the parameters describing systems' behaviour are characterized by a level of abstraction that does not yet allow for a fully detailed geometric definition of each subcomponent [4].

Similarly, FEA exhibits comparable limitations. Structural sizing of aircraft components, such as the wing, is typically divided into two or three major stages, with the level of complexity increasing alongside the sophistication of the aircraft's MDAO framework [52]. At the conceptual design stage, the Finite Element Model (FEM) is generally constructed using simplified and constant elements, for instance, beam elements representing the entire wing. During the preliminary design phase, this model is progressively refined to achieve a more realistic representation of the wing box [52]. As with the aircraft-level MDA process, these structural analyses are typically iterative by nature.

For FEM-based solvers, the loads acting on the structure of the primary lifting surfaces must be known in order to perform their structural sizing. Such loads are usually derived from a representative set of flight conditions, typically the most critical cases and those required by certification authorities [53]. Consequently, the computational cost associated with performing a structural MDO problem within a broader aircraft-level MDO framework becomes evident. In this context, the aircraft configuration evolves continuously throughout the optimization, leading to corresponding variations in aerodynamic loads and structural constraints, thereby further increasing the computational burden of FEM-based optimization.

The increasing complexity of modern aircraft architectures, particularly with the emergence of hybrid-electric configurations, has introduced an additional source of uncertainty in the early design stages: the accurate representation of the powertrain system. As with other high-fidelity methodologies, the integration of hybrid-electric or fully electric powertrains necessitates the inclusion of dedicated design variables beyond those typically employed in conventional aircraft design frameworks.

For example, Palladino et al. [54] optimized a hybrid-electric powertrain for a regional aircraft, implementing a parallel-hybrid configuration composed of a turboprop engine and a fuel cell. In their work, the non-conventional portion of the powertrain was modelled not as an isolated fuel cell but as a complete Balance-of-Plant (BoP) system. The BoP components were sized using statistical and semi-empirical correlations, complemented by a set of technological assumptions defining the maturity levels of each subsystem. Despite these simplifying assumptions, the optimization process incorporated four additional design variables related to the management of electrical power supplied by the fuel cells and electric motors across different flight segments.

Grazioso et al. [55] further demonstrated that the complexity of managing power

distribution within a hybrid-electric propulsion system escalates with the number of alternative energy sources. By enforcing energy conservation across the powertrain [56], the authors showed that system complexity scales not only with the number of components but also with the architectural configuration itself. This leads to an increased number of degrees of freedom (identified as the throttle setting parameters for each powertrain component as a function of mission time) and to a higher number of design and analysis constraints. These constraints are required to prevent non-physical system behaviours, achieved through the definition of distinct "operating modes" that characterize the feasible power and energy flows within the powertrain [55, 57, 58].

2.2.1 Machine Learning Approach

During the conceptual design phase, the systematic exploration of families of configurations represents a critical activity. Such exploration may be conducted through broad investigations of the design space using MDA workflows initiated from multiple starting points, often defined as perturbations of an initial statistically derived sizing point, or through the analysis of Pareto fronts obtained from multi-objective MDO campaigns. This process ensures that all configurations, or at least those equivalently feasible, are rigorously evaluated in the identification of a suitable baseline concept to guide subsequent, more detailed design stages.

Nevertheless, the scalability of this approach remains a significant limitation. Extensive Design of Experiments (DOE) campaigns can result in prohibitive runtimes, particularly when coupled with the computational demands associated with increasingly complex MDO-based aircraft design problems. Such complexity often arises from the integration of high-fidelity disciplinary models and the additional degrees of freedom introduced by non-conventional system architectures. These inefficiencies conflict with the primary objective of the conceptual design phase, which is to deliver timely and cost-effective insights that support informed early-stage decision-making.

To address these challenges, recent research has emphasized the potential of surrogate modeling, reduced-order methods, and machine learning (ML)–based approaches to accelerate design space exploration while maintaining sufficient accuracy to support configuration trade-offs and baseline selection [59]. These methods provide approximations of the original high-fidelity models that can be executed significantly faster while retaining an acceptable level of accuracy, provided that adequate training data are available. Surrogate modeling can be defined as the non-linear inverse process of determining a continuous function of a given set of variables, from a limited amount of numerical or experimental data, potentially including noisy observations [60]. The advantage of surrogate models stems from the ability of such approaches, often referred to as metamodels, to derive predictive relationships directly from data, without explicitly relying on the underlying physical models, which are often computationally expensive [61].

For instance, Li et al. [62] investigated the benefits and challenges associated with integrating ML techniques into a two-dimensional aerodynamic shape optimization problem. Their study demonstrated how ML can automate geometric parameterization while incorporating historical design trends to avoid unfeasible configurations. Moreover, ML algorithms can predict flow behaviour not only by learning from existing training datasets but also by leveraging a limited number of representative high-fidelity solutions to accelerate the training process.

In the broader context of aircraft design, ML approaches have been employed to replace or augment traditional sizing methodologies. For example, Tong [63] used ML models to predict turbofan engine size, thrust, and Thrust Specific Fuel Consumption (TSFC) by training algorithms on a database of 144 existing engines. Similarly, other studies have applied ML to predict time-dependent fuel flow rates, enabling the integration of predictive models into Full Authority Digital Engine Control (FADEC) systems for use in dynamic aircraft simulations [64].

Additional applications of ML methodologies span various aerospace domains, including flight control systems [65, 66], autonomous operations, and flight performance enhancement. In particular, ML and deep learning (DL) techniques have demonstrated the potential to improve fuel efficiency and optimize flight trajectories during the design process of aerial vehicles, thereby facilitating the development of more efficient and innovative configurations [67].

ML methods, particularly multilayer Artificial Neural Networks (ANNs), have been employed as alternatives to conventional surrogate models for predicting aircraft performance metrics, including aerodynamic characteristics, in-flight performance, structural weight, and propulsion efficiency [68]. Unlike traditional surrogate or response surface models, neural networks are capable of efficiently handling large and highly nonlinear design spaces. Once trained, these networks can be integrated within optimization frameworks, where the aircraft configuration parameters (e.g., geometric variables) serve as the inputs, and the overall vehicle performance constitutes the output. The resulting surrogate-based model can then be optimized using established optimization algorithms to enhance the overall design performance [68, 69].

The application of surrogate models, and, more generally, ML models, during the early design stages has enabled the execution of design and optimization studies with significantly reduced computational costs by coupling these models with optimization algorithms. An optimization problem that relies on surrogate models is commonly referred to as a surrogate-based optimization (SBO) problem [70]. Within a MDO framework, the surrogate model may represent the entire optimization problem, receiving as input the full set of design variables and returning the corresponding objective functions and constraints, as illustrated in Figure 2.3, or it may constitute a single component within a broader MDO architecture.

The primary advantages of employing metamodels include their inherent capability to smooth noisy data, which often arise from high-fidelity numerical simulations,

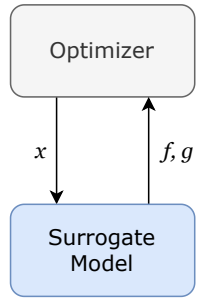

Figure 2.3: Surrogate-Based Optimization. Adapted from Ref. [70]

and their ability to provide analytically differentiable output functions. This property facilitates the efficient use of gradient-based optimization algorithms, which, together with the latest evolutionary algorithms, have demonstrated superior performance compared to traditional gradient-free approaches, particularly when addressing large-scale MDO problems characterized by extensive design spaces [70, 71].

It is, however, important to note that SBO approaches are typically not applied to the entire aircraft conceptual design process but are instead limited to the optimization of specific subsystems or component groups. For instance, Nikolaou et al. [72] integrated conceptual design methodologies for wing design within an SBO framework employing mixed-fidelity analyses, with the objective of simultaneously determining the optimal wing geometry and airfoil shapes to maximize the lift-to-drag ratio.

Similarly, metamodels, specifically Kriging surrogate models [73] trained on CFD and FEM analyses, have been incorporated into aircraft MDO processes to evaluate the aerodynamic and structural performance of canard-based configurations. In this context, the objective was to identify the optimal geometry, for the lifting surfaces, that maximizes aircraft range according to standard formulations, such as the Breguet range equation [74].

More recently, surrogate-based optimization techniques have also been employed to assess the techno-economic and environmental feasibility of hybrid-electric aircraft architectures within multi-mission frameworks. These studies aimed to integrate operational considerations directly into the design of non-conventional aircraft configurations [75], although the focus has generally remained on a limited set of disciplinary models (the powertrain, costs and flight profile data) rather than on a fully integrated design process.

Chapter 3

Use Cases Introduction

Contents

3.1 Purpose of Multi-Role Seaplanes

THE aviation transport sector recorded, in 2023, a 19.3% increase in total flight demand compared to 2021, with national and intra-EU flights accounting for 15.0% and 35.9% of total passenger volumes, respectively[1], with the additional 4.5% increase in 2024, with respect 2023, contributing to the reach of pre-Covid CO_2 emission levels (-0.4% with respect to 2019) [76]. The ongoing drive toward a more sustainable aviation industry, particularly for routes within the 300–499 km range, which have experienced the most significant decline in demand, has encouraged the exploration of novel products and services aimed at reducing environmental impact while maintaining competitive, cost-efficient performance.

The seaplane sector represents a niche market in Europe, and the development of a new aircraft in this category poses significant technical, operational and commer-

[1] https://ec.europa.eu/eurostat/statistics-explained/index.php?title=Air_passenger_transport_statistics

cial challenges. Characteristic architectural features, such as pontoons and hull-shaped fuselages, confer operational flexibility by enabling operations from conventional airports as well as seaports, commercial harbours, and waterways, providing therefore unique transportation solutions in regions surrounded by significant water bodies [77]. Conversely, these features impose significant hydrodynamic and aerodynamic penalties. For example, the integration of floats or stepped hulls results in increased parasite drag and structural weight, adversely affecting both take-off/landing performance and cruise efficiency.

The capability of operating from multiple types of runways requires seaplanes to comply with a broad spectrum of regional and international regulations issued by different authorities. Specifically, a seaplane is classified as a vessel when operating on water, such as during taxiing, take-off, or landing within a commercial port, while it is treated as an aircraft once airborne [78]. This dual regulatory framework poses significant safety challenges, as seaplanes must satisfy both maritime and aeronautical safety standards. In addition, substantial economic complexities arise from the development of new seaplane transport networks, particularly due to the higher investments required to design and certify environmentally sustainable seaplane architectures. These factors, combined with the stringent requirements for continued airworthiness, render maintenance costs and scheduling critical factors of the overall economic viability of seaplane operations [79].

The efficiency of a new aircraft program, when constrained by techno-economic challenges, can be significantly enhanced through the introduction of multi-role operational capabilities [80]. According to the Joint Research Centre of the European Commission, by early 2025 wildfires had affected more than one million hectares of land, with over 1 800 individual events releasing approximately 38.68 million tonnes of CO_2 into the atmosphere[2]. In this context, the capability of seaplanes to operate from water surfaces constitutes a key technological advantage for supporting emergency response operations, particularly aerial firefighting missions, where the ability to perform repeated water scooping cycles directly from lakes, rivers, or coastal areas significantly enhances mission efficiency.

This dual-use, passenger transport and wildfire fighter, potential strengthens the economic viability of such platforms, while also improving fleet adaptability to fluctuating market demands or seasonal emergency needs.

3.2 Top-Level Aircraft Requirements: Classes and Definition

For the conceptual design of the seaplane, the definition of a specific set of Top-Level Aircraft Requirements (TLARs), together with a systematic analysis of existing

[2] https://joint-research-centre.ec.europa.eu/projects-and-activities/natural-and-man-made-hazards/fires/current-wildfire-situation-europe_en

competitors within the same market segment, is essential to ensure an efficient and streamlined design process. Benchmarking activities provide valuable insights into product performance across multiple dimensions. The metrics collected and compared may encompass technical parameters, architectural characteristics and features, and, in some cases, qualitative assessments of operational behaviour in normal operating conditions. Such analyses are commonly conducted by current or future competitors to evaluate the relative strengths and weaknesses of their products within a given market segment, with the ultimate goal of enhancing performance and maximizing revenue potential.

The outcome of these activities is typically a set of TLARs, which can be broadly classified into two categories. Performance-based requirements, addressing key environmental, economic, and operational metrics (e.g., cruise Mach number, emissions reduction, or take-off distance), while architecture-based requirements constrain the design space by narrowing the range of viable configurations. The latter specify fundamental architectural features, such as wing–body positioning, tailplane configuration, seating layout, and powerplant characteristics, including technological attributes [19].

According to Mattmann [81], requirements can be formulated in different ways to indicate whether a parameter must satisfy a minimum or maximum threshold, adhere to a fixed value, or fall within a specified interval. A minimum requirement implies that a design solution is acceptable if the parameter value is greater than or equal to the stated threshold. Conversely, a maximum requirement is fulfilled when the parameter value does not exceed the specified limit. A fixed requirement dictates that the parameter must exactly match the prescribed value. Finally, an interval requirement defines an acceptable range bounded by minimum and maximum values within which the parameter must lie. A summary and schematic representation of requirement types is proposed in Table 3.1.

3.3 Requirements Analysis: Passenger Transport Seaplanes

3.3.1 Market Analysis

In the seaplane market, the principal competitors are identified among fixed-wing seaplanes certified under the European Union Aviation Safety Agency (EASA) Certification Specifications for Normal, Utility, Aerobatic, and Commuter Aeroplanes (CS-23), or, equivalently, under the Federal Aviation Regulations (FAR) Part 23 – Airworthiness Standards: Normal, Utility, Acrobatic, and Commuter Airplanes. Analysis presented in [77] indicates that airlines with the largest fleet, in size, of seaplanes are operated in Asia (e.g., Maldives, Indonesia, Japan, and Thailand), as well as in the United States and Canada, as summarised in Table 3.2. For each operator

Table 3.1: Definition and visualization of requirement types.

Graph. View	Requirement Type
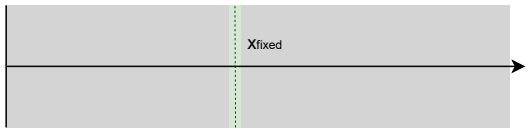	Fixed
	Minimum
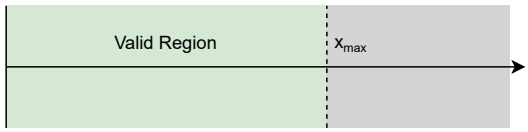	Maximum
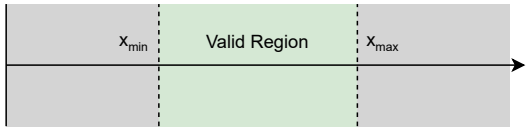	Interval

typical one-way routes range between 280 km and 395 km and are predominantly serviced by floatplanes certified under the EASA CS-23 regulation, which limits the maximum passenger capacity to 19. On average, a small proportion of the fleet consists of nine-seat commuter aircraft, whereas scheduled daily services are generally operated with aircraft configured for 14 or more passengers. Versatility of such aircraft category allows operators to provide also round trips and scenic tours for small groups of passengers; their fleet therefore accounts also for small two- and six-seater seaplanes.

Table 3.2: List of largest seaplane operators (adapted from [77]).

Airline	**Country**	**# Aircraft**	**Fleet Composition (Seaplane)**
Trans Maldivian Airways	Maldives	65	DHC-6 Twin Otter
Harbour Air Seaplanes	Canada	28	DHC-2 Beaver, DHC-3 Otter, DHC-6 Twin Otter, Cessna Grand Caravan
Kenmore Air	United States	20+	DHC-2 Beaver, De Havilland Turbine Beaver, DHC-3 Otter, DHC-6 Twin Otter, Cessna Grand Caravan EX, Cessna 208 Caravan, Piper PA-18 Super Cub
Maldivian	Maldives	11	DHC-6 Twin Otter

A preliminary analysis of Table 3.2 shows that, despite differences in geographic sce-

narios, the most operated seaplanes are the De Havilland DHC-6 Twin Otter, the Cessna 208 Caravan and the Grand Caravan EX, both in their floatplane configuration.

In 2023, the DHC-6 Twin Otter entered its fifth generation with the introduction of the "Classic 300-G," manufactured by De Havilland Canada, following the earlier Series 100 to 300 models. The fourth generation, designated as Series 400, was produced by Viking Air between 2008 and 2023. As of August 2024, the global in-service fleet comprises more than 440 DHC-6 Twin Otters, with an additional reserve of approximately 156 aircraft [82]. According to Conklin & De Decker, market prices vary depending on the series and the aircraft's age, ranging from approximately USD 1.9 million for a 1985 DHC-6 Series 300 to USD 6.29 million for a new DHC-6 Series 400 [83]. Furthermore, Conklin & De Decker estimate the average direct operating cost of the Series 400 at USD 972.4 per flight hour [83], excluding ownership-related expenses such as depreciation, insurance, and interest. The Aircraft Owners and Pilots Association (AOPA) estimates, for the DHC-6 Twin Otter 400, USD 968.40 per flight hour [84].

Introduced in 1982, the Cessna 208 Caravan has become one of the most successful turboprop aircraft in the 9–14 seat class, with more than 2 600 units currently in service [85]. Acquisition costs range from approximately USD 1.86 million for preowned models to USD 3.10 million for newly manufactured aircraft in 2022. According to the AOPA, variable operating costs for the 208 Caravan range between USD 508.73 and USD 512.80 per flight hour, the higher value accounting for the installation of a cargo pod [84]. Jet Advisors provides a more detailed cost breakdown, including fuel, maintenance (parts and labor), and route-dependent miscellaneous expenses. Excluding the latter, the estimated direct operating cost amounts to approximately USD 859.0 per flight hour.

The first deliveries of the Cessna Grand Caravan EX commenced in 2013 [86], and by October 2019 Textron Aviation had already reported the sale of 500 units [87]. According to the AOPA, variable operating costs for this model range from USD 545.31 to USD 551.37 per flight hour [84], with the upper value corresponding to the configuration equipped with a cargo pod. Conversely, Jet Advisors provides a more detailed cost breakdown—including fuel, maintenance (parts and labor), and miscellaneous route-dependent elements—but consistently reports higher estimates, with operating costs for the Grand Caravan EX reaching approximately USD 914.0 per flight hour[3]. This systematic overestimation with respect to AOPA values mirrors the discrepancy already observed for the Cessna 208 Caravan.

It is important to note that no official data are publicly available regarding acquisition prices or direct operating costs for the aircraft considered in this benchmarking activity. Consequently, information has been retrieved from multiple independent references, such as the AOPA, Jet Advisors, and other industry reports. While AOPA provides indicative estimates of variable operating costs, Jet Advisors offers more de-

[3] `https://jetadvisors.com/jet/caravan-208b-ex-specifications/operating_costs/`

tailed breakdowns. Moreover, AOPA's available estimates refer to the year 2016 and therefore require adjustment to reflect 2025 economic conditions, ensuring consistency in the comparison. An inflation correction factor, the Consumer Price Index (CPI), is hence applied to each collected value, expressing all costs in equivalent USD for the year 2025. The applied correction is outlined in Eq. (3.1), while Table 3.3 summarises variable Direct Operating Costs (DOC) for each benchmarked aircraft.

$$C_{2025} = C_{\text{Reference Year}} \frac{\text{CPI}_{2025}}{\text{CPI}_{\text{Reference Year}}} \tag{3.1}$$

Table 3.3: Operating costs comparison for benchmarked aircraft.

Aircraft	**Min DOC [USD/h]**	**Max DOC [USD/h]**	**Sources**
DHC-6 Twin Otter	972.4	1 303.5[a]	Conklin & DeDecker, AOPA
Cessna 208 Caravan	648.7[a]	859.0	AOPA, Jet Advisors
Cessna Grand Caravan EX	734.0[a]	914.0	AOPA, Jet Advisors

[a] The ratio between the CPI in 2025 and 2016 is 1.35, indicating that 1 USD in 2016 equals 1.35 USD in 2025 [88].

3.3.2 Technical Benchmark and TLAR

Sources of information for technical benchmarks can be classified in primary, or official documents, and on secondary data sources. Official sources typically include: aicraft Type Certificate Data Sheet (TCDS), Aircraft Flight Manual (AFM), Pilot Operating Handbook (POH) and Manufacturer statements (brochure).

TCDSs are available for all aircraft certificated by the Federal Aviation Administration (FAA) and by EASA and contain information about the general aircraft layout, engines main characteristics and limits as well as basic weight breakdown (gross weight, empty weight, usable fuel weight) and performance limitations (airspeed limits). Manufacturers statements are available on their websites and on brochures, however stated performance could be limited and not sufficiently detailed. The most complete sources are AFMs and POHs, but unfortunately those documents are not freely available. Secondary sources of information can be found in scientific journals, professional websites and on annual publication books. Those sources provide a large amount of data, but in some cases, it is difficult to verify the reliability.

Table 3.4 provides an overview of the principal technical indicators derived from manufacturers official data, including external dimensions, certified masses, and typical in-flight and ground performance parameters. Clear differences are observed in both geometric characteristics and certified masses. The DHC-6 Twin Otter, in its 2023 300-G configuration, exhibits a larger wingspan and wing area compared to the Cessna 208 Caravan and Grand Caravan EX, while maintaining a comparable aspect

Table 3.4: Technical benchmarks of most operated seaplanes from primary sources.

	Twin Otter	**208 Caravan**	**Grand Caravan EX**
Dimensions			
Wingspan	65.0 ft[a]	52.0 ft[b]	52.0 ft[b]
Wing Area	420.0 ft^2 [a]	279.4 ft^2 [c]	279.4 ft^2 [c]
Length	51.75 ft[a]	38.0 ft[b]	41.58 ft[b]
Height	22.66 ft[a]	17.58 ft[b]	17.50 ft[b]
Engine			
Manufacturer	Pratt & Whitney[a]	Pratt & Whitney[b]	Pratt & Whitney[b]
Model	PT6A-27[a]	PT6A-114A[b]	PT6A-140[b]
Output Power	680 shp[a]	675 shp[b]	867 shp[b]
Number of Units	2	1	1
Weights			
Max Take-Off Weight	12 500 lb[a]	8 750 lb[b]	9 062 lb[b]
Max Landing Weight	12 300 lb[a]	7 300 lb[c]	8 500 lb[c]
Empty Weight	8 573 lb[a]	5 585 lb[b]	5 975 lb[b]
Fuel Capacity	2 576 lb[a]	2 224 lb[c]	2 246 lb[c]
Performance			
Take-Off Ground Roll	1 843 ft[a]	1 431 ft[b]	1 826 ft[b]
Take-Off Water Run	1 965 ft[a]	2 341 ft[b]	2 000 ft[b]
Landing Distance	1 450 ft[a]	-	-
Max Cruise Speed	162 KTAS[a]	159 KTAS[b]	164 KTAS[b]
Max Range	705 nm[a]	875 nm[b]	813 nm[b]

[a] Data from Ref. [89].

[b] `https://cessna.txtav.com/-/media/cessna/files/product-cards/turboprop/caravan_amphibian_productcard.pdf`

[c] `https://www.easa.europa.eu/en/document-library/type-certificates/aircraft-cs-25-cs-22-cs-23-cs-vla-cs-lsa/easaima226-cessna-208`

ratio. The increased wing area enables the Twin Otter to achieve superior take-off and landing performance, despite a Maximum Take-Off Mass (MTOM) that is 38.0% greater than that of the Grand Caravan EX and 42.8% greater than that of the 208 Caravan. This higher MTOM is primarily attributable to payload capacity, as the Twin Otter accommodates up to 19 passengers, whereas both the 208 Caravan and the Grand Caravan EX are certified to carry a maximum of 14 passengers.

Wing loading (MTOM to wing area ratio) and power loading (MTOM-to-installed engine brake horsepower ratio) represent key performance benchmarks, as they govern both low-speed characteristics (take-off and landing distances) and high-speed performance (typical and maximum cruise speeds). In general, higher wing loading is associated with smaller wing areas, which reduce the parasite drag coefficient and thus improve high-speed characteristics. However, reduced wing area negatively affects low-speed performance: stall speed increases, and consequently, more powerful engines capable of delivering greater thrust and acceleration are required

to maintain acceptable ground performance. The collected data show that all aircraft in the sample exhibit similar wing loading values. Among them, the Cessna 208 Caravan displays the highest power loading, which corresponds to the lowest maximum cruise speed and a water take-off run distance approximately 20% longer than that of the STOL-certified DHC-6 Twin Otter. Moreover, the Twin Otter's short take-off and landing (STOL) capabilities make it the most competitive aircraft in terms of take-off performance. Nevertheless, despite its comparatively low power loading—reflecting the highest installed total engine power—its cruise speed remains similar to, or in some cases lower than, that of the lighter competitors.

The operational flexibility of a passenger transport aircraft is commonly assessed through its payload–range diagram [90], which illustrates, for a given range, the maximum payload that can be transported and the corresponding fuel mass required to complete the mission. The primary drivers of high operational flexibility are the maximum payload capacity, the maximum fuel capacity, and the ratio between the aircraft's Empty Weight (EW)—defined as the sum of airframe, propulsion system, on-board systems, and fixed equipment—and its certified MTOM.

For any commercial transport aircraft, payload capacity affects revenue potential, since higher payloads allow for greater transport capability. For instance a high Available Seat Miles (ASM) enable a distribution of operating costs across passengers and over longer distances, therefore reducing normalized operating costs indices, such as the Cost per Available Seat Mile (CASM), under otherwise similar conditions [91, 92]. Adequate fuel capacity further enhances operational flexibility by enabling operation across a broader spectrum of mission profiles. However, this is constrained by safety regulations, as certification authorities prohibit operation at masses exceeding the certified MTOM. Consequently, for extended missions, payload may need to be reduced in order to accommodate the additional fuel mass required.

A lower EW-to-MTOM ratio mitigates this trade-off by allowing a greater fraction of the MTOM to be allocated to useful load, thereby improving operational flexibility. In the general aviation segment, this ratio typically falls between 0.58 and 0.63 [93, 94] but tends to be slightly higher for seaplanes due to the additional structures required to ensure static and dynamic buoyancy. For instance, the DHC-6 Twin Otter exhibits an EW-to-MTOM ratio of 0.68 and also demonstrates the shortest maximum range, whereas the Cessna 208 Caravan and Grand Caravan EX exhibit values of 0.64 and 0.66, respectively. These figures highlight the critical importance of minimising the EW-to-MTOM ratio in the conceptual design of future seaplanes, as doing so directly enhances payload capability, extends operational range, and ultimately improves competitiveness in the short-haul transport market.

In a multimodal transportation environment multiple transport modes and coordinated infrastructure networks jointly facilitate point-to-point connectivity. While payload capacity and typical range requirements determine operational flexibility of an aircraft, travel time, dictated by the aircraft's speed and altitude profiles, serves

as a key performance metric for assessing competitiveness relative to alternative modes of transport, as well as with respect to potential competitors in the aviation industry [95, 96]. During the conceptual design phase, travel time is predominantly determined by the block speed, and consequently by an appropriate cruise speed. The latter is typically chosen to balance fuel-related operating costs with time-related operating costs, thereby achieving an optimal trade-off between efficiency and economic performance. In a multimodal context, an additional consideration is the manner in which different modes of transport collectively facilitate connectivity between origin and destination points. In a competitive transport environment, the cruise speed is selected to ensure that the aircraft remains both cost- and time-competitive relative to other available modes within the network. Conversely, in a cooperative transport framework, flight scheduling may instead be optimised to maximise the overall network efficiency, whether in terms of total travel time, operational costs, or minimisation of the cumulative environmental footprint of the journey. Providing passengers with alternative itineraries that prioritise different criteria, such as time, cost, or environmental impact, and quantifying the associated environmental footprint (e.g., estimated CO_2 emissions saved, as implemented in platforms such as Google Flights) enables informed decision-making and supports the adoption of more sustainable travel behaviours. However, during such early design phase, comprehensive data describing the multimodal transport network are often unavailable. This limitation necessitates the adoption of simplified estimation methods to determine an appropriate design cruise speed for a given range and payload specification, usually referring to benchmarked aircraft and therefore enabling the choice of a minimum requirement on the typical, or maximum, cruise speed that allows performing comparisons with existing competitors.

Take-off performance of small commuter and regional aircraft is often disregarded, as these vehicles are typically operated from large airports with runways designed for jet- and turboprop-powered aircraft certified under EASA CS-25 or the equivalent FAR Part 25 regulations. As already highlighted, seaplanes possess unique operational features that enable take-off and landing from water surfaces, thereby allowing access to locations where conventional airport infrastructure is absent. However, water-based operations are inherently constrained by environmental factors, particularly the aircraft's ability to safely operate under varying wave and wind conditions, typically quantified by the so-called *sea state*.

To mitigate operational limitations, seaplanes are frequently designed in amphibious configurations, incorporating either fixed or retractable conventional landing gear. This dual capability enables operations from paved runways, thereby increasing operational flexibility and minimizing downtime due to adverse sea conditions. In this context, take-off and landing performance from conventional airports becomes a key factor in assessing the overall attractiveness of seaplane operations. An analysis of global airport infrastructure indicates that, in order to ensure competitiveness with benchmarked aircraft and guarantee accessibility to at least 85% of the world's airports, the total take-off and landing distances should not exceed 1 850.0 ft.

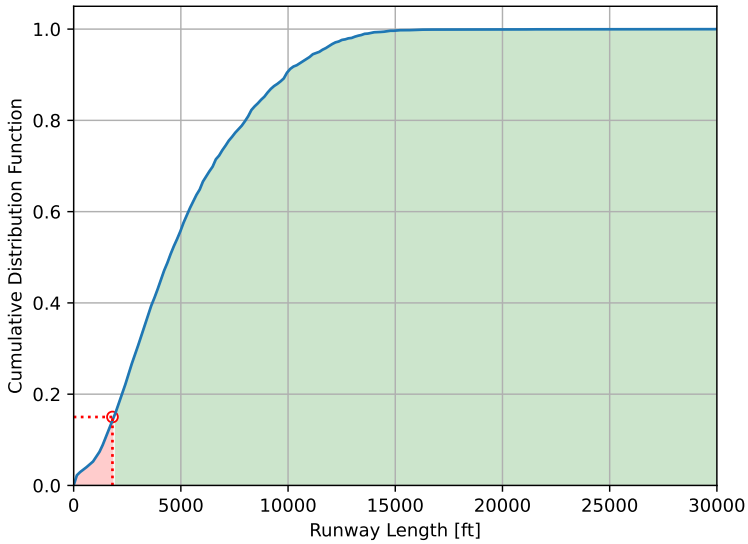

Figure 3.1: Cumulative distribution function of global runways length. Source: `https://ourairports.com/` (visted on 09/01/2025).

Figure 3.1 illustrates the Cumulative Distribution Function (CDF) of global runways length, with the green region highlighting all airports having a runway longer than the select requirement.

Table 3.5 summarizes the main TLARs defined for a new generation passenger transport seaplane. These requirements have been derived from the comparative analysis of benchmarked aircraft, complemented by needs and specifications identified within the international context of the COLOSSUS project, as well as by rules established by regulatory authorities.

3.4 Requirements Analysis: Aerial Firefight Seaplanes

3.4.1 Market Analysis

The development of aerial firefighting assets began in the early 1950s with the conversion of fixed-wing military aircraft into air tankers. This process continued over the following decades, with significant milestones, including the introduction in the 1960s, of dedicated on-board systems designed to accommodate various types of fire retardants. Between 1970 and 1995, a substantial number of firefighting aircraft, both landplanes and seaplanes, were produced, among which the most notable platforms are the Canadair CL-215 and its successor, the CL-415 [98].

Historically, legacy aircraft were primarily manufactured in the United States, with a focus on landplanes adapted for use as air tankers, whereas Canada emerged as a pi-

Table 3.5: Passenger Transport Seaplane - Reference set of TLAR

Parameter	**Value**	**Req. Type**	**Source**	**Note(s)**
MTOM	19 000 lb	Maximum	CS-23	Certification limit.
Payload	3 510 lb	Maximum	Benchmark	18 Pax. at 175 lb per pax plus 20.0 lb luggage.
Take-Off Distance	1 850 ft	Maximum	-	At MTOM, ISA Sea Level. From complete stop to 35 ft obstacle.
Landing Distance	1 850 ft	Maximum	-	ISA Sea Level. From 50.0 ft obstacle to complete stop.
Max. Cruise Speed	160 KTAS	Minimum	Benchmark	At 10 000 ft (FL100).
Cruise Altitude	10 000 ft	Fixed	Benchmark	Typical for the Caravan series [97].
Absolute Ceiling	25 000 ft	Minimum	Benchmark	-
Block Range	189 nm	Fixed	Benchmark	Design Point. At maximum payload. FL100.
Wingspan	78.74 ft	Maximum	Benchmark	ICAO B category.
Entry Into Service	2035	Fixed	COLOSSUS	-
Fuel Saving	-30.0%	Minimum	COLOSSUS	With respect to existing seaplanes operating in the same certification category.

oneer in the development of amphibious seaplanes. These latter platforms offered the operational advantage of scooping water directly from natural sources such as coastal areas, lakes, and rivers, provided that their dimensions were sufficient to allow safe operations. An overview of aircraft employed as air tankers and scoopers, including their manufacturers, entry into service (EIS) year, and payload capacities, is briefly presented in Table 3.6.

Table 3.6 does not present an exhaustive inventory of all fixed-wing air tankers but rather illustrates the diversity in payload capacity, expressed as the maximum volume of fire suppressant or water carried onboard, and the age distribution of the listed aircraft. Nowadays, many of these platforms are no longer in active service due to age-related limitations, with only a few exceptions, such as the DC-10, which remain in operation owing to their capability to transport very large quantities of fire suppressant. The limited pace of innovation in the aerial firefighting sector has resulted in a strong reliance on a small number of proven platforms. In particular, the CL-415, now manufactured by Viking Air, and the AT-802 have emerged as the most widely adopted solutions, operated globally by national firefighting agencies as well as by private contractors delivering specialized services for emergency response operations, including aerial firefighting and search-and-rescue missions.

In 2023, Air Tractor delivered its 1000th AT-802, of which 208 units correspond to the "Fireboss" configuration, specifically converted for aerial firefighting operations. The base acquisition cost of an AT-802 is approximately USD 2.8 million, with an additional USD 1.5 million required for the conversion to the Fireboss configuration [99], resulting in a total investment of roughly USD 4.3 million. The primary

Table 3.6: Overview of in-service and dismissed aircraft serving aerial firefight operations.

Manufacturer	Model	EIS	Max Capacity
Air Tractor	AT-802	1990	3 100 litres
Boeing	Stearman 75[a]	1955	640 litres
Boeing	B-17[a]	1938	6 000 litres
Boeing	747[b]	2009	74 000 litres
Canadair	CL-215[b]	1969	5 450 litres
Canadair	CL-415[b]	1994	6 137 litres
Glenn L. Martin Company	Mars[b]	1943	27 250 litres
Grumman	S-2T[b]	1954	4 540 litres
Grumman	F7F-3[a]	1944	6 800 litres
Lockheed Martin	C-130 Hercules[b]	1956	15 141 litres
Lockheed Martin	P-3 Orion[b]	1962	11 350 litres
McDonnell Douglas	DC-10[b]	1971	35 583 litres
North America Aviation	AJ-1[a]	1950	9 100 litres

[a] https://www.fs.usda.gov/sites/default/files/fs_media/fs_document/aviation-history.pdf

[b] https://gacc.nifc.gov/swcc/dc/azpdc/operations/documents/aircraft/links/Aircraft%20Recognition%20Guide.pdf

payload for this class of aircraft consists of water and fire suppressants. Given the inherently cyclic mission profile, characterized by multiple drops and subsequent refills, economic performance metrics are typically not expressed in terms of cost per flight hour or CASM, but rather as cost per unit volume of suppressant delivered, usually in USD per gallon or litre. An assessment of manufacturer data and published studies indicates variable operating costs in the range of USD 0.64[4] to USD 0.95 per gallon [98] of suppressant delivered.

The CL-415, initially produced by Canadair in 1994 and subsequently manufactured by Viking Air (as part of De Havilland Canada) from 2016 onwards, is widely considered as the first aircraft specifically designed for aerial firefighting missions. Its primary operators are located in the United States, Canada, and Europe. A 2013 economic assessment reported an acquisition cost of approximately USD 35.0 million, with an expected service life of around 30 years, similar to that of cargo aircraft and longer than that of a typical regional turboprop passenger aircraft [100, 101], and direct operating costs, including fuel, crew salaries, and maintenance, of approximately USD 1.5 million per year [102]. To update these values to the 2025 economic context, the ratio CPI in 2025 and 2013 has been applied, yielding an estimated acquisition cost of approximately USD 48.5 million. As with the AT-802, operating costs are also reported in terms of suppressant delivered, ranging between USD 1.50 [98] and USD 2.04[4] per gallon. Despite its substantially higher acquisition cost compared to the AT-802, the CL-415 achieves competitive performance in terms of cost per gallon delivered.

It is important to note that, as previously highlighted for passenger transport sea-

[4] https://firebossllc.com/cost-comparison/

planes, the absence of official data on the economic performance of aerial firefighting platforms necessitates the use of multiple independent sources and reports. This approach enables the construction of an interval of estimated operating costs, reflecting the inherent uncertainty in the available information. Table 3.7 summarises the principal economic indicators for the two aircraft currently leading the amphibious aerial firefighting market.

Table 3.7: Summary of economic performance of the AT-802 and CL-415.

Aircraft	**MTOM [lb]**	**Price [USD million]**	**Min DOC [USD/US Gal.]**	**Max DOC [USD/US Gal.]**
AT-802	16 000	4.3	0.64	0.95
CL-415	41 000	48.5	1.50	2.04

3.4.2 Technical Benchmark and TLAR

The overview of the aerial firefighting market indicates that the two leading competitors, the Air Tractor AT-802 and the Viking Air CL-415, belong to distinct aircraft classes. The smaller AT-802 has been certified under the EASA CS-23 and FAR Part 23 certification standards, whereas the CL-415 demonstrates compliance with the EASA CS-25 and FAR Part 25 regulation basis. Table 3.8 summarises the principal technical performance parameters, derived from primary information sources.

To enhance the overall efficiency of the development process and to mitigate penalties associated with substantial performance and architectural differences, a certain degree of commonality between the two seaplane variants is required.

Table 3.8 highlights the distinctions between the certification classes of the benchmarked aircraft, which generally preclude direct comparison, except when relying on non-dimensional performance indicators. The AT-802 exhibits a higher wing loading compared to the CL-415, which is advantageous for both low-speed and high-speed performance. However, the superior power loading of the CL-415 compensates for this difference, enabling shorter take-off distances from both land and water surfaces, as well as a higher maximum cruise speed. The AT-802 marginally outperforms the CL-415 only during the landing phase, where the influence of power loading, and consequently of the total installed power, becomes negligible.

It is worth noting the non-linear relationship between the increase in maximum water capacity and the corresponding increase in the maximum take-off mass of the aircraft. Specifically, while the CL-415 has a water capacity approximately twice that of the Fireboss, its MTOM is 2.56 times higher. To preserve a certain level of commonality with the certification class of the passenger transport variant, the Fireboss is therefore considered the primary reference for deriving the Top-Level Aircraft Requirements. These include the minimum required water capacity, the maximum achievable capacity, and the number of drops to be performed during the reference

design mission. Operational studies conducted by the Department of Sustainability and Environment of the Forest Fire Management Victoria indicate that the payload released during an AT-802 Fireboss mission is neither constant over time nor equal to the aircraft's maximum certified payload capacity [103]. This behaviour arises from procedural and performance limitations that constrain the aircraft mass during critical operational phases such as take-off, climb, and manoeuvring, where prescribed design masses and structural limit load factors must not be exceeded. In practice, the Fireboss typically operates with an initial water payload of approximately 540 US gallons (2 100 L) to ensure that the MTOM is not surpassed. Once sufficient fuel has been consumed, the water payload can be increased to the aircraft's maximum capacity. Depending on the distance between the fire location and the nearest accessible water source, the average payload delivered varies: approximately 540 US gallons when the distance is below 8.6 nautical miles, and up to 660 US gallons (2 500 L) for distances between 8.6 and 17.27 nautical miles. As a result, the average payload corresponds to approximately 65–80% of the maximum certified capacity.

Operational efficiency during a wildfire-fighting mission, expressed as the volume of suppressant delivered per unit of time, is strongly influenced by the distance between the wildfire location and the nearest accessible water source. Landplanes must return to their base or origin airport to refill both the suppressant and fuel tanks, whereas seaplanes are frequently equipped with water-scooping systems that enable them to refill directly from natural bodies of water. This capability significantly reduces the turnaround time and thereby increases overall operational efficiency. Table 3.9 reports turnaround times for both aircraft as a function of distance. A linear regression applied to the datasets, as illustrated in Figure 3.2, indicates that the CL-415 consistently exhibits longer turnaround times, with the difference reduced to less than one minute only for distances shorter than 4.25 statute miles (3.7 nautical miles).

Finally, Table 3.10 presents the design requirements established for the wildfire fighting variant of the seaplane. Several requirements associated with the typical mission profile have been inherited from the passenger transport configuration, primarily to ensure certification commonality, reduce development risks, and streamline the overall design process through component and system commonality. This approach enables a conservative design basis. Conversely, firefighting-specific requirements have been derived from the benchmarking analysis, ensuring that the aircraft is appropriately tailored to the operational and performance demands of aerial firefighting missions.

Table 3.8: Technical benchmarks of the AT-802 Fireboss and CL-415 from primary sources.

	AT-802 Fireboss	**CL-415**
Dimensions		
Wingspan	59.25 ft[a]	93.8 ft[b]
Wing Area	401.0 ft^{2}[a]	1 080.0 ft^{2}[b]
Length	35.69 ft[a]	65.0 ft[b]
Height	16.17 ft[a]	29.5 ft[b]
Engine		
Manufacturer	Pratt & Whitney	Pratt & Whitney
Model	PT6-67F[a]	PW123AF[b]
Output Power	1 600 shp	2 380 shp
Number of Units	1	2
Weights		
Max Take-Off Weight (Land)	16 000 lb[a]	41 000 lb[b]
Max Take-Off Weight (Water)	11 500 lb[a]	37 850 lb[b]
Max Landing Weight (Land)	12 300 lb[a]	37 000 lb[b]
Max Landing Weight (Water)	11 500 lb[a]	37 000 lb[b]
Empty Weight	8 600 lb[a]	28 650 lb[b]
Max Water Capacity	820 US Gal.[a]	1 621 US Gal.[b]
Max Foam Capacity	74 US Gal.[a]	180 US Gal.[b]
Fuel Capacity	2 500 lb[a]	10 200 lb[b]
Performance		
Take-Off Distance (Land)	3 299 ft[a]	2 570 ft[b]
Take-Off Distance (Water)	5 600 ft[a]	2 670 ft[b]
Landing Distance (Land)	1 970 ft[a]	2 210 ft[b]
Scooping Run	2 200 ft[a]	1 350 ft[c]
Max Cruise Speed	150 KIAS[a]	187 KIAS[b]

[a] `https://www.firebossllc.com/specifications-and-performance/#specifications`

[b] `https://dehavilland.com/wp-content/uploads/2025/01/DHC-515_Spec_Sheet_v14_DIGITAL.pdf`

[c] `https://www.fs.usda.gov/sites/default/files/media_wysiwyg/amphibious_water_scooper_aircraft_operations_plan_final_2016-_041316.pdf`

Table 3.9: Turnaround times for the CL-415 and the AT-802 Fireboss as function of distance between fire location and water source.

Distance		**CL-415 Turnaround Time**[a]	**Fireboss Turnaround Time**
1 mile	(0.87 nmi)	3.0 min	3.0 min
3 mile	(2.60 nmi)	4.0 min	-
5 mile	(4.34 nmi)	-	4.0 min
6 mile	(5.21 nmi)	6.0 min	-
10 mile	(8.69 nmi)	9.0 min	6.0 min
15 mile	(13.03 nmi)	12.0 min	9.0 min
20 mile	(17.38 nmi)	-	11.0 min

[a] `https://www.fs.usda.gov/sites/default/files/media_wysiwyg/amphibious_water_scooper_aircraft_operations_plan_final_2016-_041316.pdf`

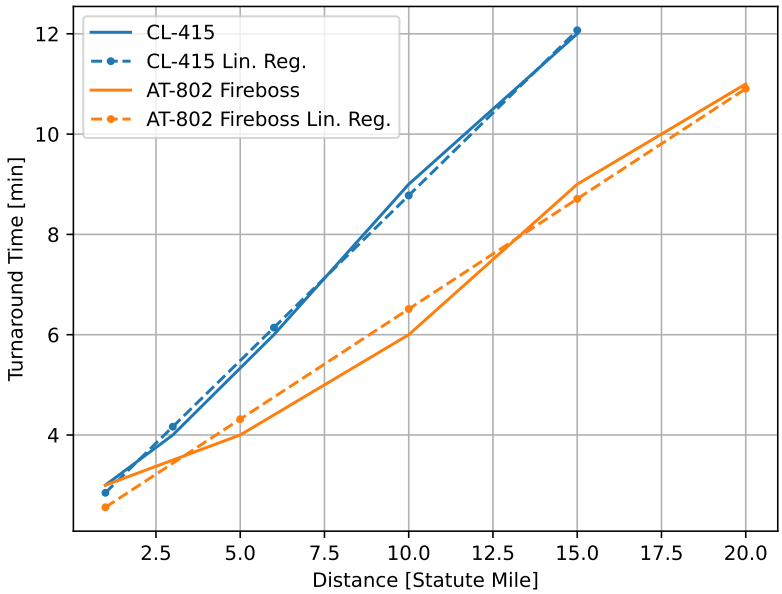

Figure 3.2: Linear regression of turnaround times for the AT-802 Fireboss and the CL-415.

Table 3.10: Wildfire Fighting Seaplane - Reference set of TLAR

Parameter	**Value**	**Req. Type**	**Source**	**Note(s)**
MTOM	19 000 lb	Maximum	CS-23	Certification limit.
Take-Off Distance	1 850 ft	Maximum	Pax Transport TLAR	-
Landing Distance	1 850 ft	Maximum	Pax Transport TLAR	-
Max. Cruise Speed	160 KTAS	Minimum	Pax Transport TLAR	-
Cruise Altitude	10 000 ft	Fixed	Pax Transport TLAR	-
Absolute Ceiling	25 000 ft	Minimum	Pax Transport TLAR	-
Wingspan	78.74 ft	Maximum	Pax Transport TLAR	ICAO B category.
Block Range	189 nm	Fixed	Pax Transport TLAR	Design Point. At design payload. FL100.
Design Payload	540 US Gal.	Fixed	Benchmark	73.5% of Max. Payload
Max. Payload	735 US Gal.	Fixed	Benchmark	-
Distance Ops.	3.7 nmi	Fixed	Benchmark	Sizing Point
Entry Into Service	2035	Fixed	COLOSSUS	-
Fuel Saving	-30.0%	Minimum	COLOSSUS	-

3.5 Architecture Analysis: Technological Enablers and Assumptions

When addressing the conceptual and preliminary design of innovative aircraft, it is essential to assess the technological enablers that can support the development of promising and competitive solutions. In the specific case of seaplanes, the technologies under consideration must directly influence the target objectives and constraints, namely, the TLARs.

For this class of aircraft, and particularly when accounting for the dual nature of the mission profile, encompassing both passenger transport and aerial firefighting variants, the relevant enabling technologies can be broadly categorized into two primary classes: aircraft-layout-dependent enablers and subsystem-related technologies.

The primary objective of this analysis is to facilitate the identification of aircraft features and subsystem specifications required to define, during the conceptual design stage, a configuration that satisfies the assigned design requirements and mission-specific objectives. Consequently, strong emphasis is placed on the physical architecture of the seaplanes under investigation, which will be simply referred to as the "architecture", or "configuration", throughout this thesis.

Aircraft Layout Enablers

According to Gudmundsson [104], the term seaplane refers to an aircraft specifically designed to operate from water surfaces. Seaplanes can be categorized into three distinct classes: floatplanes, flying boats, and amphibians.

A floatplane is derived from a conventional landplane through the removal of its landing gear, which is replaced by pontoons, floats that when are submerged support the aircraft while keeping the fuselage elevated above the water surface. In the passenger transport category, this configuration is typically employed for small seaplanes with seating capacities of up to approximately 18 passengers. Common examples include the De Havilland DHC series, the Cessna Caravan, and, in the aerial firefight class, the Air Tractor AT-802 Fireboss.

A flying boat, on the other hand, is a seaplane in which the fuselage itself is designed to act as a hydrodynamic hull, allowing the aircraft to take off from and land on water while carrying passengers or cargo within the hull structure.

An amphibian represents a hybrid configuration that combines a hull-type fuselage suitable for water operations with retractable landing gear, enabling takeoff and landing on both water and conventional paved runways. These latter two architectures are employed across a wide range of aircraft categories, from small general aviation and CS-VLA-certified models to large transport and emergency response aircraft. Representative examples include the Beriev Be-103, Beriev Be-200, Dornier

Seastar, Grumman Albatross, Grumman G-73 Mallard, Lake LA-4, ShinMaywa US-2, and the Canadair CL-415.

A primary factor influencing the selection of the seaplane class to be designed concerns the aircraft's capability to withstand wave and wind conditions during water operations. This capability is typically quantified through the maximum sea-state level that the seaplane can safely operate in. Such a factor is particularly critical for passenger transport aircraft, as it constrains operational scheduling in accordance with prevailing weather and sea conditions, thereby reducing the vehicle's availability and potential revenue. In the framework of the EU-funded FUture SEaplane TRAffic (FUSETRA) project, Kalogeri et al. [105] applied the Thurston equation [106] to estimate the significant wave height that a seaplane can withstand as a function of its weight and hull length. Their analysis demonstrated that heavier seaplanes with longer hulls exhibit enhanced capability to operate in higher sea states, achieving operability percentages exceeding 60%, in the reference scenario, equal for all analysed seaplanes.

In the present research, the seaplane design is constrained by the CS-23 certification category, consistent with existing platforms in the same class. Consequently, to enhance operability while maintaining compliance with this weight limitation, an amphibious configuration is considered a suitable compromise, as it allows the exploitation of the full fuselage length for hydrodynamic support during waterborne operations.

To accurately characterize a hull-shaped fuselage, it is essential to define the functional requirements it must satisfy and the geometric features influencing these functions. In an amphibious seaplane, the fuselage serves a dual purpose: it acts as the primary payload carrier, as in conventional aircraft, and simultaneously functions as the main hull enabling take-off and landing operations on water surfaces.

According to Morabito [107], the key parameters to be considered during the early design stage include the length of the planing surfaces, both for the forebody flat section and the afterbody, the geometry of the step (particularly its height), the deadrise angle at the step location and its variation along the hull length, as well as the sternpost angle. A detailed description of these parameters is provided in Table 3.11.

The step is typically positioned at a distance corresponding to 0.2 to 0.4 times the beam aft of the center of gravity [107], while its height generally ranges between 5% and 8% of the maximum beam [104]. The step geometry significantly influences both the stability of the hull and its total hydrodynamic resistance, often in an inverse relationship; consequently, a design trade-off is usually required.

The deadrise angle affects the hydrodynamic lift capability of the hull. Larger angles tend to reduce lift and necessitate greater wetted areas to sustain the seaplane on the water. However, an increased deadrise angle can be advantageous during landing operations, as it helps mitigate impact loads [109]. The sternpost angle represents one of the most complex parameters to define, as it influences both stability characteristics and total hydrodynamic resistance. Unlike the step geometry, there

Table 3.11: Description of the main geometric features of a hull-shaped fuselage according to Gudmundsson [104] and Chicken S. H. [108].

Feature	Description
Beam	The width of the seaplane hull. Usually indicated as its maximum value.
Step	Geometric discontinuity in the lowest part of the hull-shaped fuselage. Its objective i to help the aircraft rotate during take-off and reduce the wetted area.
Forebody	Portion of the fuselage that's forward with respect to the step. It encompasses the fuselage portion between the nose and the step.
Afterbody	Portion of the hull-shaped fuselage that's aft of the step, econpassing the trunk between the tail and the step.
Forebody Flat	Portion of the forebody that has zero gradient in the keel line. Suggested to be at least 1.5 times the beam.
Sternpost	The aft end of the atfterbody.
Sternpost Angle	The angle between the line tangent to the forebody keel at the step and the line between the step and the sternpost.
Deadrise Angle	Angle measured between the tangent to the planing bottom at the keel (at any station along the fuselage) and a horizontal transverse line.

are no universally accepted design guidelines for this parameter, since it simultaneously induces both beneficial and adverse effects, for instance an increased sternpost angle increase the upper stability limit but also increase the spray generated during water runs, also it can help the seaplane to rotate but causes high impact accelerations [109]. Therefore, it is commonly determined based on manufacturer experience, typically ranging between 7 deg and 9 deg [107].

It is therefore evident that an appropriate selection of this parameter, potentially supported by parametric hull modeling techniques, can significantly enhance the operational attractiveness of the aircraft during the preliminary design stage, as it directly influences take-off and landing performance as well as the operability percentage under given environmental conditions.

Powertrain and Subsystems Enablers

A primary objective for seaplanes, and aircraft in general, developed within the current context of increasing demand for sustainable products and operations is the reduction of emissions during standard mission profiles, with particular emphasis on CO_2 emissions. These sustainability-driven trends have, in recent years, fostered significant research efforts, particularly within the academic community, aimed at exploring the integration of non-conventional powertrain architectures. Among these, hybrid-electric propulsion systems have received particular attention, with studies spanning a wide range of aircraft categories, from large jet-powered transport aircraft [40, 110] to regional [111, 112], commuter, and general aviation segments [58].

Despite technological limits, electric-based propulsion architectures showed great potential to fulfil these new environmental objectives [8, 9]. Among existing solutions, energy carriers such as batteries and pressurized, or liquid, hydrogen-based propulsive systems [113, 114] have been largely investigated as promising enablers of the energy transition in the near-term future, since substantial developments are required to improve propulsive batteries specific energy and hydrogen storing systems design to enable all-electric aircraft to operate on a large scale [115, 116].

Among the possible energy carriers that can be integrated into a hybrid-electric powertrain, the most common alternatives include propulsive batteries, hydrogen, and, for the conventional segment of the powertrain, traditional fuels such as Jet A-1 and Aviation Gasoline (AVGAS, for reciprocating engines), as well as alternative fuels such as biodiesel, which may become, despite a small increase in the engine specific fuel consumption, viable options for reducing CO_2-based emissions in future general aviation reciprocating engines [117]. Power generation within these architectures is typically provided by batteries, fuel cells, and conventional turboprop or reciprocating engines.

The analysis of existing passenger transport and aerial firefight seaplanes revealed that turboprop engines represent the most widely adopted class of internal combustion engines. Specifically, for seaplanes certified under the EASA CS-23 regulatory framework, the Pratt & Whitney Canada PT6A engine family appears to be the preferred choice. This engine series is capable of delivering shaft power outputs ranging from approximately 500 to 1 900 horsepower [118], with a specific fuel consumption (SFC) between 0.47 and 0.70 lb/hp hr [119]. The necessity to reduce fuel consumption and associated emissions, combined with the potential to integrate electric generators to support the most power-intensive flight phases, has enabled the introduction of more fuel-efficient piston engines in 18-passenger class aircraft. A representative example is the Ampaire Eco Caravan, a retrofitted variant of the conventional Cessna Caravan, equipped with a parallel hybrid-electric powertrain supported by a reciprocating engine rated at approximately 500 hp [120, 121]. This configuration has demonstrated fuel consumption reductions of up to 40%, while maintaining total operating costs comparable to the conventional version, thereby confirming the economic viability of such hybrid architectures. This result was also achieved considering the effect of the retrofitting costs for the powertrain systems. A new PT6A engine, as the one considered in the study, can cost up to 571 000.0 USD [122], if a customer trade its old engine, while a brand new RED engine can cost up to 232 900.0 USD [123], adjusted from the 2012 to the 2024 economic scenario, realizing therefore a 60% saving in the acquisition cost of the thermal engine.

Currently, the most widely adopted battery technology for electrified propulsion systems corresponds to third-generation lithium-ion (Li-ion) batteries. Considering the expected EIS year of 2035 for the target seaplane, this battery generation can be reasonably assumed to represent a viable near-term technological solution for powering electric propulsion systems. In the context of this research, Li-ion batteries

employing Nickel-Manganese-Cobalt (NMC) oxide cathodes and graphite-silicon anodes are assumed [124]. Specifically, the NMC811/Si–C chemistry, characterized by a composition of 80% nickel, 10% manganese, and 10% cobalt, is selected due to its favourable balance between specific energy and cycle life.

In the pursuit of net-zero emissions, fuel cells have emerged as a promising technological enabler for the energy transition in the aviation sector. Their primary advantage lies in the absence of carbon-based by-products during operation [125]. Currently, the state-of-the-art in aviation-oriented fuel cell technology is represented by low-temperature Proton Exchange Membrane Fuel Cells (PEMFCs) [126], which operate using hydrogen as the fuel and oxygen from ambient air as the oxidant, with a maximum operating temperature typically below 100 °C. Alternatively, Solid Oxide Fuel Cells (SOFCs) offer the potential for higher conversion efficiencies compared to PEMFCs [127]; however, their high operating temperatures and limited technological maturity currently restrict their application to research and experimental studies, making them unsuitable candidates for short-term EIS scenarios.

The integration of fuel cells as part of a feasible hybrid-electric powertrain architecture necessitates the inclusion of hydrogen storage systems, while the required oxygen can be obtained directly from ambient air through dedicated air intakes. A major challenge associated with hydrogen storage lies in its low energy density, which under standard atmospheric conditions is approximately 8.5 MJ/lt. For comparison, Jet-A1 fuel exhibits a density of approximately 34.9 MJ/lt under the same conditions [125]. To overcome this limitation, modern storage systems employ either high-pressure gaseous storage or cryogenic liquid storage solutions. When compressed to pressures of about 700 bar, hydrogen can achieve an ideal density of about 42 kg/m^3 [128]. Despite this, its density remains considerably lower than that of conventional aviation fuels. However, hydrogen offers a significantly higher specific energy content, with an approximate value of 33 kWh/kg, compared to the 12 kWh/kg of Jet-A1, thereby partially compensating for its lower volumetric density [125, 129, 130].

Hydrogen storage tanks that currently exhibit a sufficiently high Technological Readiness Level (TRL) for integration into aerospace applications, and are capable of withstanding repeated pressurization and depressurization cycles, are Type IV pressurized tanks. These tanks employ a polymer liner reinforced with composite overwraps and fitted with metallic bosses to ensure structural integrity at the connection interfaces. Owing to the lower density of polymers compared to metals, Type IV tanks offer superior mass efficiency relative to earlier generations, Type I, Type II, and even Type III tanks. Nevertheless, these legacy technologies, particularly Type III tanks, which use metallic materials only for the pressure-bearing liner, continue to coexist in certain applications, primarily due to cost considerations [125].

To effectively integrate non-conventional energy carriers and power generation systems within the aircraft architecture during the conceptual design phase, it is necessary to convert the electrical power produced by batteries or fuel cells into mechan-

Table 3.12: Technological assumptions for the powertrain subsystems to investigate during the aircraft conceptual design phase.

Item	**Value**	**Unit**
Battery		
Type	Li-ion	-
System Specific Energy	280.0	Wh/kg
Nominal C-Rate	2.0	1/h
Fuel Cell		
Gravimetric Power Density	0.5	kW/kg
Volumetric Density	0.3	kW/lt
Hydrogen Tank Type	Pressurized	-
Hydrogen Tank Pressure	500	bar
Electric Machines		
Specific Power	6.0	kW/kg
Efficiency	96.0	%

ical power to drive the propellers. This conversion is typically achieved by coupling the aforementioned power sources with an electric machine. Meindl et al. [131] identified six main classes of electric machines suitable for aerospace applications and concluded that Permanent Magnet Synchronous Machines (PMSMs) generally provide the best overall performance, albeit at a higher cost. The use of permanent magnets enables significant weight reduction and improved power density, though it increases manufacturing expenses. However, in the context of hybrid-electric or all-electric aircraft, efficiency and power density are prioritized over cost considerations, as they directly influence aircraft weight and consequently the overall energy demand. Table 3.12 summarises the main technological assumptions for the electric components that will be integrated, as detailed in the following chapters, in the configurations exploration process at conceptual level.

Chapter 4

Machine Learning Support to Configuration Exploration

Contents

4.1 Introduction

THE review of the literature describing the conventional aircraft design process in a structured and procedural manner reveals a general consensus among authors on a hierarchical framework consisting of three main phases: *Conceptual Design*, *Preliminary Design*, and *Detailed Design* [20, 21, 93]. The earliest stage in the development of a new aeronautical product begins with the identification of a problem to be solved or the recognition of potential market opportunities, together with the associated operational and functional needs [132]. As discussed in Chapter 3, this initial step is exemplified by the analysis of the potential benefits of multi-role

seaplanes and by the derivation of TLARs, formulated to ensure that such platforms achieve competitiveness within the targeted market segment.

The derived top-level aircraft requirements constitute the primary input to the conceptual design phase. During this stage, a wide range of both conventional and innovative configurations is examined to assess their technical feasibility and commercial viability. At the beginning of the process, the design space remains intentionally broad, encompassing variations in overall geometrical layout, engine type, number and placement, as well as the degree of advanced technology to integrate [13]. Consequently, configuration exploration and trade-off analyses form the fundamental activities of the conceptual design process, serving as essential tools for evaluating the potential success of a new aircraft program. To balance accuracy with computational efficiency, this phase typically relies on low- to medium-fidelity sizing and analysis models, as high-fidelity simulations are not yet required for preliminary performance assessments.

One of the most effective approaches for conducting trade-off studies and exploring the aircraft design space is represented by MDO methodologies. These techniques enable the simultaneous integration of all relevant design and analysis disciplines to identify solutions that satisfy imposed constraints while optimizing selected figures of merit, or objective functions. The conceptual design stage is typically characterized by a large number of degrees of freedom, encompassing architectural features (e.g., engine type, installation position, and wing–fuselage configuration), geometrical parameters (e.g., fuselage diameters, wing area, aspect ratio, empennage dimensions), and mission-related variables (e.g., climb schedule, cruise Mach number, and altitude profile).

It follows that both the formulation of a well-posed optimization problem by the designer and the computational effort required by the optimization algorithm scale with the size of the design space, i.e., with the number of degrees of freedom. Moreover, the design of a hybrid-electric aircraft, whether a retrofit of an existing platform or a clean-sheet configuration, driven by the growing interest in non-conventional powertrain architectures, requires the integration of dedicated methodologies for sizing the electric components of the powertrain. In addition, the identification of appropriate power-management strategies aimed at achieving use-case-specific objectives, such as the minimization of fuel consumption over the mission profile and of pollutant emissions during on-ground operations [133, 134], further increases the complexity of disciplinary couplings by introducing additional degrees of freedom that must be controlled within the MDO process. These added complexities therefore influence also conventional disciplines, including mass breakdown analysis, centre-of-gravity estimation, and the assessment of both in-flight and on-ground performance.

This poses significant challenges in the context of MDO-based aircraft conceptual design. While the use of low-fidelity, or zero-order, models is typically adopted to reduce computational time, the increasing complexity of the MDO problem nonethe-

less leads to a substantial computational burden. This, in turn, necessitates the adoption of alternative numerical strategies capable of maintaining the conceptual design phase both computationally affordable and sufficiently robust to generate meaningful insights that can guide subsequent configuration developments. In Chapter 1, these considerations were formalized into the presented research question, from which the following sub-question can be derived and addressed in this chapter:

In what ways can conceptual design workflows be extended to support architecture exploration and optimization of innovative amphibious aircraft ?

4.2 Surrogate-Based Concepts Exploration

The exploration of design solutions and families of configurations, enabled by conceptual design methodologies and supported by the use of metamodels, such as reduced-order models, surrogate models, response surfaces, or machine-learning-based models, can be broadly referred to as surrogate-based concept exploration. This approach shares many similarities with well-established frameworks of SBO. Typically, surrogate-based optimization consists of three main stages: (1) the design of experiments, (2) surrogate model construction, and (3) model infilling [135]. DOE methods are employed to generate a set of uniformly distributed sample points, which are then used as training data for the initial surrogate model. The infilling step improves model accuracy by iteratively adding new sample points to the training set. These additional points may be selected, for example, from regions along the predicted Pareto front [136], determined through trust region strategies [137], or simply by selecting the predicted optimum in successive iterations.

In surrogate-based concept exploration, the need to mitigate computational burden necessitates a reformulation of the third step of the process. Instead of improving model accuracy by infilling the training set with points derived from MDO results, active learning techniques are employed. Active learning is particularly valuable in scenarios where the generation of new data is computationally expensive. In this context, sample selection is typically guided by uncertainty estimation, whereby the most uncertain predictions are identified and added to the training set. The process assumes the existence of a finite set of unlabelled data, referred to as the pool. A ranking function, commonly known as an acquisition function or query function, is then applied to quantify prediction uncertainty and select new training points. The objective is to strategically include a relatively small number of additional samples in order to significantly improve the predictive performance of the model.

Figure 4.1 illustrates the application of surrogate-based concept exploration to aircraft conceptual design studies. The process begins with the identification of the degrees of freedom (design variables) and the performance metrics to be used in assessing the quality of candidate configurations, both in terms of performance and

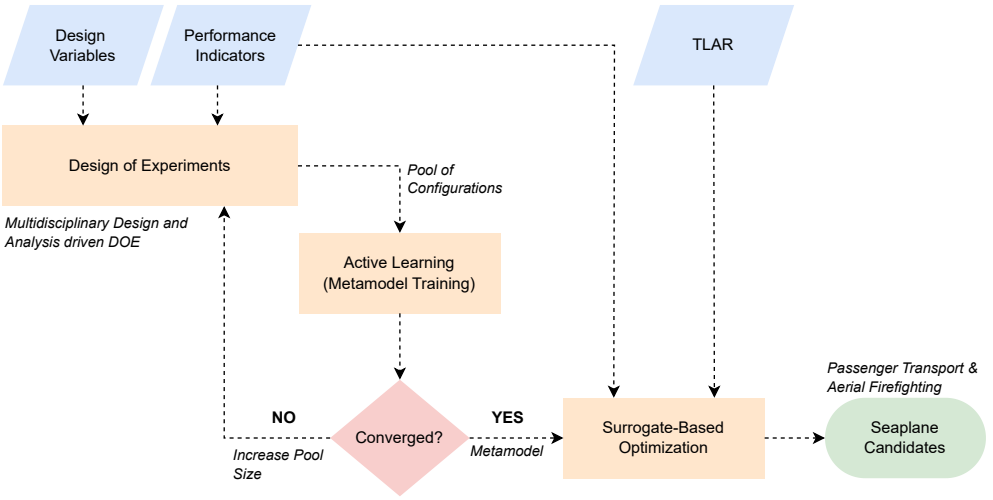

Figure 4.1: Aircraft conceptual design process supported by surrogate-based concepts exploration.

feasibility with respect to design constraints and requirements. In parallel, an MDA workflow is established to perform the sizing of the aircraft and evaluate its overall performance for each population of design variables. A DOE strategy is then employed to sample a sufficiently large set of design variables, thereby generating a pool of candidate configurations, which may include both feasible and infeasible solutions (e.g., those that do not satisfy the TLARs). Subsequently, active learning methods are employed to construct and iteratively refine a multi-input, multi-output metamodel, designed to surrogate the computationally expensive MDA workflow. Finally, a SBO problem is formulated and solved, enabling the identification of the promising design candidates across both passenger transport and aerial firefighting seaplane categories.

4.3 The Vehicle Design Space Exploration

The first step in a surrogate-based concept exploration process involves the creation of an initial design pool to support the subsequent active learning phase. This stage is characterized by three main tasks: (i) the selection of design variables and performance metrics, (ii) the definition of a suitable MDA or MDO workflow, and (iii) the choice of a suitable sampling strategy. It is important to note that the first two tasks are not fully independent. The inclusion of a larger number of design variables typically reflects the designer's intention to capture detailed coupling effects between independent degrees of freedom and dependent performance metrics, even when analyses are limited to low-order methods. For example, engine parameters such as the overall pressure ratio or bypass ratio in turbofan configurations simultaneously affect thrust generation and specific fuel consumption, which in turn influ-

Table 4.1: The "Basic Six" variables for the aircraft conceptual design and optimization problem (adapted from [139]).

Variable	**Symbol**
Power-to-Weight Ratio[a]	P/W
Wing Loading	W/S
Wing Aspect Ratio	AR_w
Wing Taper Ratio	λ_w
Wing Sweep Angle	Λ_w
Airfoil Mean Thickness Ratio	t/c

[a] For jet-driven aircraft the Thrust-to-Weight ratio is used.

ence mission fuel burn, in-flight performance metrics (e.g., maximum rate of climb, maximum cruise speed), manufacturing costs, direct operating costs and certification characteristics, like the induced loads on the airframe and the necessary wing ground clearance or landing gear leg length [138]. Similarly, geometric parameters such as the planform characteristics of the vertical and horizontal tail surfaces impact lateral–directional and longitudinal stability and controllability, respectively. Capturing such coupled effects requires the integration of dedicated disciplinary models into the design framework, extending beyond simple scaling relations or redesign laws to ensure consistency in the overall aircraft configuration.

The selection of design variables for exploring the aircraft design space, as well as the definition of the performance indicators to be assessed, depends both on the intended scope of the aircraft and on the degree of coupling effects that the designer aims to capture. To simplify this process, a general rule of thumb proposed by Raymer [139] can be applied. Specifically, for conceptual design problems, Raymer identified six fundamental design variables that are broadly applicable across a wide range of aircraft categories. These “basic six” variables, summarized in Table 4.1, provide a systematic basis for extending the analysis towards scope-specific variables and performance indicators. Their effectiveness in influencing key figures of merit—including weight, cost, stability and controllability constraints, as well as geometric limitations—has led to their successful application for more than 50 years in aircraft configuration development and optimization [139].

Similarly, the design workflow architecture must be structured to incorporate all relevant coupling effects while simultaneously minimizing the number of feedback variables, thereby improving the computational efficiency of each execution. To effectively address a heterogeneous set of design objectives and constraints, the workflow must retain a sufficient degree of flexibility. In this context, the use of independent disciplinary methodologies, integrated within a properly structured MDA or MDO workflow, is often more advantageous than relying on a monolithic, “packed” aircraft conceptual design software. The latter is typically constrained by a fixed set of performance metrics, feasibility criteria, and predefined design procedures, which are applied uniformly regardless of the aircraft category, design variables, or

intended application.

The final step in setting up a vehicle design space exploration involves the selection of an appropriate sampling strategy, which includes defining both the number of samples and the sampling algorithm. The primary objective is to enable subsequent machine learning (ML) models to capture the variability of the underlying true model while minimizing the number of required samples. To maintain a certain level of independence between the exploration process and the metamodel training phase, space-filling criteria are often employed to generate the initial pool of design configurations [140]. Commonly adopted algorithms include Latin Hypercube Sampling (LHS), Sobol sequences, and Halton sequences. In these approaches, the initial sample size is typically chosen as a multiple of the number of input design variables. For relatively simple or static problems, the sample size is generally set between 5 and 10 times the dimensionality of the design space, whereas for problems exhibiting strong nonlinearities in the output variables, the scaling factor may increase to 10–20 times the number of design variables.

4.3.1 Passenger Transport Seaplanes

The primary objective of passenger transport aircraft, including seaplanes, is to generate revenue by providing air transport services, which typically encompass scheduled flights, as well as touristic and scenic routes. Consequently, design variables must be selected to influence performance indicators that directly contribute to enhancing the aircraft's attractiveness to its key stakeholders, namely, operators and passengers. The development of a DOE campaign therefore begins with the identification of these indicators, together with relevant constraints, as they define both the potential and competitiveness of the aircraft. A review of the literature on the design of conventional and innovative aircraft configurations, including hybrid-electric concepts, highlights a wide set of key performance indicators (KPIs). In particular, Brelje et al. [9] and Abu Salem et al. [141] provide comprehensive summaries of the most commonly adopted KPIs across both aircraft classes, encompassing flight performance, economic performance, weight-based and utility-based metrics.

Utility-based indicators are highly dependent on the intended operational role of the aircraft. For passenger transport vehicles, these typically include range-related capabilities, often expressed in normalized forms such as the Specific Air Range (SAR) for conventional architectures, or the Energy Specific Air Range (ESAR) in the case of hybrid-electric configurations leveraging multiple energy carriers [142]. Another relevant metric is the Payload-Range Energy Efficiency (PREE), which quantifies the amount of payload transported per unit range and per unit of energy consumed.

Among weight-based indicators, the mass of fuel burned is the most common metric, as it directly affects both operating costs and CO_2-related emissions. The Operating Empty Mass (OEM) also plays a critical role, as it is strongly correlated with production and acquisition costs.

Table 4.2: Performance indicators of the passenger transport variant of the seaplane.

Performance Indicator	**Symbol**	**Unit**	**Category**
Take-Off Distance	d_{TO}	ft	Performance
Landing Distance	d_{LND}	ft	Performance
Absolute Ceiling	$h_{Ceil,\,AEO}$	ft	Performance
Max Cruise Mach Number	M_{max}	-	Performance
Mission Block Time	BT	min	Performance
Energy Consumption	E	kWh	Utility
Fuel Mass Consumption	W_F	lb	Weight
Operating Empty Mass	W_{OE}	lb	Weight
Maximum Take-Off Mass	MTOM	lb	Weight
Acquisition Price	AC_{price}	USD million	Economic
Direct Operating Costs	DOC	USD/flight	Economic

From an economic perspective, DOCs are a central metric, encompassing costs associated with aircraft ownership and utilization, including leasing, insurance, depreciation, fuel, electricity, maintenance, navigation and airport fees, and crew wages. These are often normalized by the number of available passenger seats and the mission range, leading to the well-known metric CASM.

Finally, flight performance indicators are typically included as design constraints within an aircraft MDO problem. State-of-the-art conceptual design methodologies list these parameters in the TLARs table for the specific aircraft category under investigation. As outlined in Chapter 3, their primary role is to ensure competitiveness of the new aircraft concept against existing and potential future competitors; consequently, they will not be further discussed here. Table 4.2 provides an overview of the performance indicators and metrics selected to evaluate the suitability of the passenger transport variant of the seaplane, together with an indication of the corresponding classification category.

Design variables can now be selected from those most influencing the performance indicators and metrics listed in Table 4.2. Five of the “Basic Six” variables will constitute the foundation of the design space, while sweep angle effects are neglected, since maximum operating Mach numbers for general aviation seaplanes do not approach the operational limits imposed by the buffet barrier. The design space is further completed by including the wing longitudinal placement along the fuselage, the volumetric coefficients of the horizontal and vertical tails, as well as their thickness ratio and sweep angle, operational flight conditions, related to the typical operating cruise Mach number and climb speed, and the architecture of the propulsion system. Owing to the simulation-based nature of the aircraft design problem, the design space comprises a heterogeneous set of input variable types, including continuous, categorical, and integer parameters, in addition to variables subjected to hierarchical dependencies.

The design of non-conventional aircraft, particularly those integrating novel technologies that remain insufficiently addressed by current certification frameworks,

significantly expands the degrees of freedom in the early design phases. When environmental objectives and constraints are considered, all-electric and hybrid-electric propulsion systems exhibit the greatest potential for addressing both near-term and long-term sustainability goals, albeit at the cost of increased complexity in the MDA process. In conventional configurations, the propulsion system architecture is typically not treated as a design variable, since each aircraft category is generally associated with a single, well-established solution. For instance, large transport aircraft predominantly employ turbofan engines, CS-23 and CS-25 regional aircraft rely on turboprops, while small commuter and utility aircraft are powered by reciprocating engines. This paradigm, however, no longer applies to hybrid-electric architectures, where multiple energy sources can contribute to delivering shaft power or generating thrust, thereby introducing a fundamentally new degree of freedom in the conceptual design stage.

In this context, the powertrain architecture can be modeled as a set of mixed-discrete design variables, where the architecture itself is represented by a discrete variable, while the associated architecture-specific parameters can be either continuous or discrete [143]. Such variables often exhibit strong interdependencies, thereby necessitating the introduction of hierarchical relationships within the design framework.

For instance, in a propeller-driven aircraft, the primary function of the powertrain system is to deliver the required power to the propeller shaft. This requirement can be satisfied by four different powertrain architectures suitable for the considered aircraft category: a conventional turboprop, a reciprocating engine, a hybrid-electric system, or an all-electric system. Each of these architectures is characterized by its own set of specific parameters. For example, the rated power of the turboprop or reciprocating engine, the rated power of the electric motors (EM) in hybrid-electric and all-electric configurations, as well as the type and capacity of the onboard energy storage system, such as a propulsion battery or hydrogen fuel cell.

Table 4.3 summarizes the cumulative set of design variables and parameters necessary to represent and manage the powertrain system within the conceptual design framework. These variables collectively define the architecture-dependent design space, which is then integrated into the complete list of design variables reported in Table 4.4, leading to a total of 23 design parameters.

To conduct the exploration campaign, it is first necessary to identify and integrate an appropriate MDA or MDO disciplinary workflow. When computational performance plays a critical role in the design process, monolithic MDAO architectures generally demonstrate superior efficiency compared to distributed ones, with the Multidisciplinary Feasible (MDF) and Individual Discipline Feasible (IDF) formulations being the most commonly adopted in practical applications [2]. To minimize both the number of variables and the overall computational cost, an MDF architecture is selected, as it eliminates the need for an external optimizer to ensure consistency. While a common limitation of MDF lies in the requirement to perform a full MDA at each iteration, this drawback is not significant in the present context,

Table 4.3: Powertrain architectures and specific design parameters for L0 and L1 methods in the aircraft conceptual design process.

Powertrain	Variable	Type	Options
Turboprop	Rated Power	Continuous	-
Reciprocating	Rated Power	Continuous	-
	Fuel Type	Categorical	Jet-A1, Diesel
Hybrid-Electric	Energy Carrier	Categorical	Battery, Hydrogen
	Energy Supplier	Categorical	Battery, Fuel-Cell
	Thermal Engine	Categorical	Reciprocating, Turboprop
	Take-Off Hybrid Ratio	Continuous	-
	Climb Hybrid Ratio	Continuous	-
	Cruise Hybrid Ratio	Continuous	-
	Descent Hybrid Ratio	Continuous	-

Table 4.4: Design variables table for the conceptual design of the passenger transport variant of the seaplane.

Variable	Symbol	Type
Power-to-Weight Ratio	P/W	Continuous
Wing Loading	W/S	Continuous
Wing Aspect Ratio	AR_w	Continuous
Wing Taper Ratio	λ_w	Continuous
Airfoil Mean Thickness Ratio	t/c	Continuous
Wing Apex	$X_{LE,w}$	Continuous
Horizontal Tail Volumetric Coef.	$\mathcal{V}_H$	Continuous
Horizontal Tail Thickness Ratio	$(t/c)_H$	Continuous
Horizontal Tail Sweep Angle	Λ_H	Continuous
Vertical Tail Volumetric Coef.	$\mathcal{V}_V$	Continuous
Vertical Tail Thickness Ratio	$(t/c)_V$	Continuous
Vertical Tail Sweep Angle	Λ_V	Continuous
Cruise Mach Number	M_{CR}	Continuous
Climb Speed	V_{CL}	Continuous
Powertrain Architecture	-	Mixed-Discrete

Table 4.5: DHC-6 Twin Otter: design weights and performance metrics (public data from Ref. [89]).

Item	**Public data**	**MDA framework**	**Error (%)**
Maximum take-off mass	12 500 lb	12 510 lb	+0.08
Maximum landing weight	12 300.0 lb	12 295.6 lb	–0.04
Equipped empty weight	8 573.0 lb	7 980.0 lb	–6.9
Standard fuel weight	2 576.0 lb	2 559.0 lb	–0.7
FAR 23 take-off distance[a]	1 965.0 ft	1 804.5 ft	–8.2
FAR 23 landing distance[b]	1 851.0 ft	1 955.0 ft	+5.6
Maximum cruise speed[c]	162 KTAS	173 KTAS	+6.8

[a] At maximum take-off weight, to a 35 ft obstacle.
[b] At maximum landing weight, from a 50 ft obstacle.
[b] At FL 100.

since the workflow is primarily driven by a DOE. Consequently, there is no need to return coupling variables to the optimizer for the computation of objectives and constraints.

Figure 4.2 illustrates the XDSM diagram of the DOE campaign and shows how the MDA workflow, implemented through a Gauss–Seidel sequential procedure, is integrated into the exploration process (further remarks on illustrated disciplines are presented later in this chapter). It is worth noting that some disciplines, such as “Geometry”, “Powertrain Design”, and “Weight Class I”, require not only their respective input variables but also an initial design point. This is due to the presence of a full MDA, which, at the beginning of each DOE iteration, demands an initial estimate of state variables provided by disciplines appearing later in the workflow. These state variables are subsequently employed to check the convergence of the MDA. The initial design point, corresponding to a reference seaplane configuration used to drive the DOE campaign, has been derived in Appendix A.

To validate the fidelity of our multidisciplinary design methodology, a benchmarking activity was first conducted on the DHC-6 Twin Otter, a widely recognised commuter seaplane in the passenger transport category. By accurately reproducing its design weights and principal in-flight and on-ground performance characteristics, the design process was verified to faithfully capture real-world behaviour. Table 4.5 presents a comparison between publicly available data and the results obtained from the MDA framework, highlighting the percentage error for each metric.

The large number of design variables to consider makes the use of a full-factorial design space impractical. For instance, assuming only two levels for each of the 23 variables, and disregarding any hierarchical dependencies, the resulting design space would contain 2^{23} samples, corresponding to more than 8 million design points to be evaluated. To enhance both performance and computational efficiency of the underlying MDF design process, LHS strategies, as implemented in the Python-based Surrogate Modeling Toolbox (SMT) [144], are employed. This framework enables the treatment of mixed-discrete variables with hierarchical dependencies while ensur-

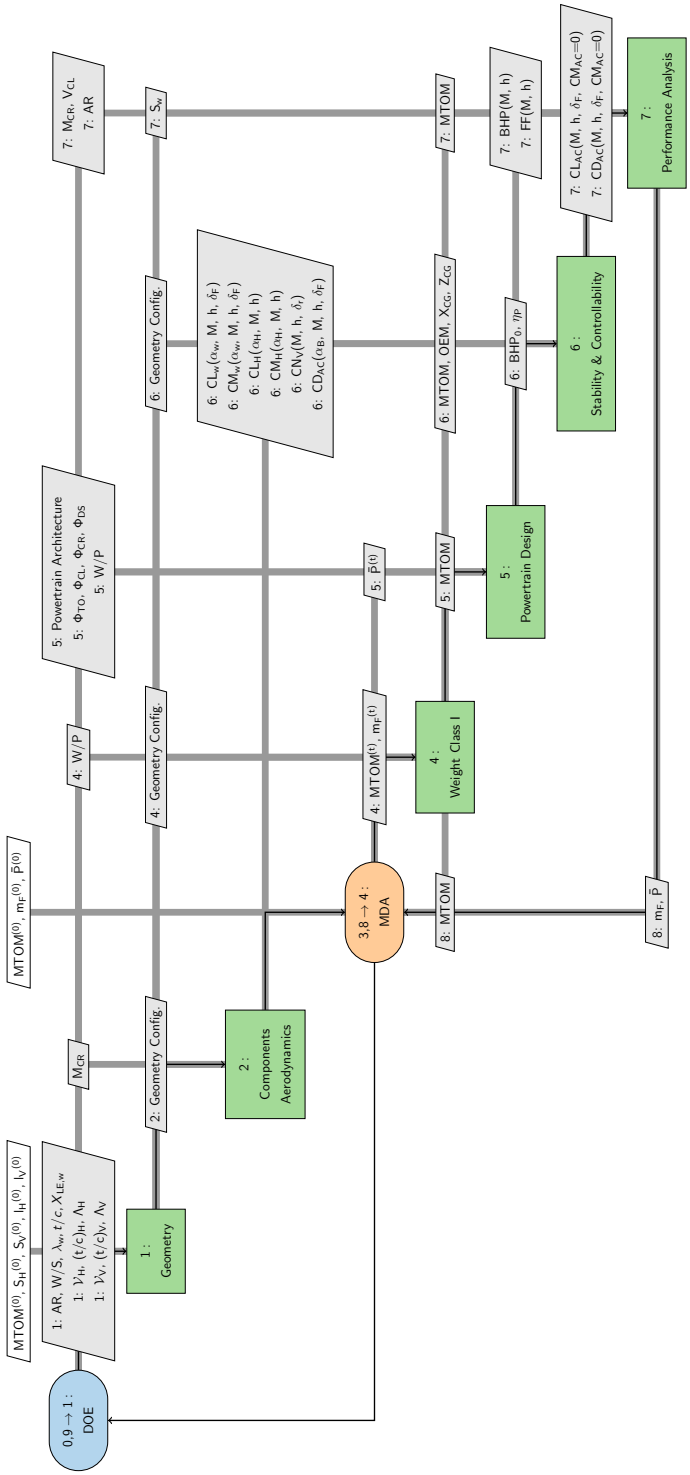

Figure 4.2: XDSM diagram of the conceptual MDA chain for the passenger transport variant of the seaplane.

ing appropriate coverage of the design space. Considering the inherent non-linear behaviour of aerodynamic methods and their impact on stability and controllability characteristics, as well as the needs for the subsequent training process of dedicated machine learning models, the sample size has been set to 50 times the number of design variables, resulting in 1300 initial design points included in the configurations pool. This choice represents a trade-off between computational feasibility and sufficient exploration of the design space, ensuring that relevant trends and coupling effects can be effectively captured during subsequent analyses.

4.3.2 Aerial Firefight Seaplanes

Seaplanes employed in aerial firefighting operations belong to the broader class of vehicles dedicated to emergency response activities. The performance metrics and figures of merit optimized for this category typically differ, even if partially, from those that characterize passenger transport aircraft or freighters, primarily due to the operational nature and mission profiles these platforms are required to perform on a daily basis. Environmental considerations, which have increasingly influenced the civil aviation sector and driven both industry and academia toward more efficient and adaptable solutions, also play a critical role in the domain of emergency operations. However, what differentiates aerial firefighting aircraft from passenger transport counterparts is the manner in which these environmental requirements are interpreted and incorporated during the conceptual design stage, with the objective of enhancing both the operational effectiveness and the overall attractiveness of this aircraft category.

Carbon-based emissions generated during wildfires can generally be attributed to two principal sources: (i) the combustion of vegetation, infrastructure, and vehicles within the affected area, and (ii) the emissions produced by firefighting operations, including those from air tankers, helicopters, and other supporting vehicles. Analyses of total CO_2 release during wildfire events indicate that the contribution from the first source typically exceeds that of the second, with its magnitude being strongly dependent on both the fire duration and the extent of its spatial spread. According to [145], wildfires in Europe emitted approximately 579.6 million tonnes of CO_2 in 2024. In comparison, aviation emissions (from both domestic and international flights) were estimated at 182.29 million tonnes in the same year [146], corresponding to nearly 24% of total CO_2 output. These figures highlight that meaningful reductions in wildfire-induced emissions can only be achieved by improving the effectiveness of suppression operations to minimize fire spread. In this context, the enhancement of aerial firefighting seaplane performance represents a promising strategy to strengthen operational efficiency and environmental impact mitigation.

In parallel with passenger transport aircraft, the KPIs for aerial firefighting seaplanes can be grouped into performance-based, economic, weight-based, and utility-based metrics. This classification highlights the significant overlap between firefighting and passenger transport aircraft in terms of design indicators.

The primary distinction, however, lies in the utility-based metrics and their role in the design process. While passenger transport aircraft are generally optimized to provide extended payload–range capabilities, aerial firefighting aircraft are designed with a strong emphasis on minimizing the frequency of refuelling operations during normal mission conditions, thereby reducing turnaround times at the base of operations. As a result, endurance becomes a dominant utility-driven metric, with design choices generally aimed at maximizing loiter time and operational autonomy during fire suppression missions. This consideration is particularly relevant for flying boat and amphibious configurations, where the capability to scoop water from nearby sources significantly reduces the need to return to the base airport, thereby enhancing overall operational efficiency.

While several numerical and theoretical approaches have been proposed to evaluate the efficiency of fire-retardant agents in reducing wildfire spread rates [147], a standardized definition of aircraft operational effectiveness has not yet been widely established. In this research, the definition introduced by Strumińska and Filippone [98] is adopted, as it integrates mission specifications, aircraft flight performance, and architectural features. A slightly modified version of their formulation is employed in order to address some of the limitations inherent in the original definition.

According to Strumińska and Filippone [98], the operational effectiveness of an aerial firefighting aircraft can be quantified as the ratio between the total amount of water or fire-retardant released on the fire and the corresponding mission duration. The quantity of suppressant delivered is defined as the product of the aircraft tank capacity and the number of drops performed, under the assumption that the aircraft is fully loaded for each passage over the fire. Furthermore, the authors assumed that all drops occur at the end of the descent phase over the fire. The principal advantage of this formulation lies in its suitability for application during the conceptual design phase, when detailed operational procedures are typically unavailable and performance evaluation models cannot yet incorporate specific mission parameters. Conversely, in later stages—such as preliminary performance assessment, usually carried out at the conclusion of the concept development phase—more advanced simulation models can be employed. These enable the integration of refined mission profile parameters, such as variable water loads per sortie or the possibility of performing drops not only at the end of the descent phase but also during levelled flight conditions.

Therefore, within the scope of this research, aircraft effectiveness is initially quantified using the proposed ratio, providing a practical measure at the conceptual design stage. Nevertheless, in subsequent preliminary performance assessment stages, the assumptions will be progressively relaxed. Specifically, the hypothesis that water or fire-retardant is always dropped during a fixed flight segment, such as the end of the descent phase, will be reconsidered to include alternative mission profiles, for example level flight releases. Likewise, the assumption that the aircraft tank is always filled to its maximum capacity prior to each sortie will be removed, allowing

Table 4.6: Summary of limitations and advantages of aerial firefight operational effectiveness definitions.

Definition	**Advantages**	**Limitations**
Strumińska & Filippone (original)	- Conceptual Design Level - No Operational Dependencies	- Constant Payload - Constant Drop Phase
Strumińska & Filippone (modified)	- Variable Payload - Mission Adaptable - Generalized	- Simulation Required - Preliminary Design Level

the consideration of variable payload conditions dictated by mission requirements and operational constraints. These refinements aim to support the identification and evaluation of operational procedures capable of improving overall effectiveness, thereby bridging the gap between numerical performance estimations and realistic mission operations. Table 4.6 proposes a summary of limitations and advantages of both definitions.

The market analysis of aerial firefighting aircraft indicates that manufacturers and operators are increasingly directing development efforts toward more economically viable solutions. The focus is not only on maximizing operational efficiency but also on reducing total operating costs through adaptive tactics and optimized mission planning. Despite substantial operational differences, aerial firefighting seaplanes, and more broadly, fixed-wing air tankers, exhibit an operating cost structure that closely parallels that of conventional passenger transport aircraft. This similarity becomes even more pronounced in cases where wildfire suppression services are provided by private operators, realising a perfect overlap also in the structure of indirect operating costs. The main distinction arises from the normalization metrics employed to evaluate and compare operating costs across platforms. In passenger transport aviation, costs are typically normalized with respect to the number of passengers and distance travelled, leading to the widely used CASM metric. Conversely, in aerial firefighting operations, operating costs are commonly normalized with respect to the total quantity of fire suppressant delivered during a mission, typically expressed in terms of USD per litre or USD per U.S. gallon of water or retardant dropped.

Table 4.7 provides an overview of the principal performance indicators considered during the conceptual design stage of air tanker aircraft. It is noteworthy that this category shares many indicators with passenger transport aircraft, particularly during the early phases of concept development. As mentioned, substantial differences emerge in utility-based and economic-based metrics, reflecting the unique operational requirements of firefighting missions. Additionally, minor differences are also observed in weight-based indicators, most notably the inclusion of the maximum storable fuel mass, $m_{F,\,max}$. This parameter is critical to ensuring that the aircraft remains operable only within feasible mission profiles and is therefore typically incorporated as a design constraint in the conceptual design process.

Table 4.7: KPIs for aerial firefighting aircraft at the conceptual design stage. While many indicators are shared with passenger transport aircraft, distinct differences emerge in utility-based and economic-based metrics, reflecting the operational focus on suppression effectiveness, endurance, and mission turnaround time.

Performance Indicator	**Symbol**	**Unit**	**Category**
Take-Off Distance	d_{TO}	ft	Performance
Landing Distance	d_{LND}	ft	Performance
Absolute Ceiling	$h_{Ceil,\,AEO}$	ft	Performance
Max Cruise Mach Number	M_{max}	-	Performance
Scooping Distance	d_{scoop}	ft	Performance
Operational Efficiency	η_{ops}	US Gal/min	Utility
Endurance	En	hr	Utility
Fuel Mass Consumption	W_F	lb	Weight
Max Fuel Mass	$W_{F,\,max}$	lb	Weight
Operating Empty Mass	W_{OE}	lb	Weight
Maximum Take-Off Mass	MTOM	lb	Weight
Acquisition Price	AC_{price}	USD million	Economic
Direct Operating Costs	DOC	USD/US Gal	Economic

The discussed similarities and differences are also reflected in the selection of design variables that govern the exploration of the design space. Raymer's "Basic Six" design variables, reduced to five in the case of small CS-23 air tankers, again constitute the foundation of the parameter set. These are further complemented by additional geometrical and architectural variables, analogous to those considered for the passenger transport variant. Furthermore, the set is expanded with flight-related parameters specifically introduced to capture the distinctive characteristics of the "active phases" that define the mission profile of aerial firefighting aircraft. A complete summary of these design variables is reported in Table 4.8.

Several simplifying assumptions have been adopted in the selection of the design variables. The analysis of the SoTA in hybrid-electric powertrain architectures generally highlights reductions in payload–range capability and endurance compared to conventional turboprop configurations. Furthermore, recent environmental assessments indicate that the overall impact of wildfires on carbon emissions is significantly greater than the direct emissions generated by aircraft operations. This consideration justifies focusing on conventional, widely adopted turboprop engines and, consequently, excluding the investigation of alternative propulsion solutions at the conceptual design stage. Additional operational factors influencing turnaround time and overall efficiency, such as the distance between the base airport and the fire location or between the fire location and the nearest accessible water source, are not explicitly accounted for in Table 4.8. Nonetheless, it is important to emphasize that the primary objective of the conceptual design phase remains the sizing of the vehicle under representative operating conditions, defined as the design conditions, which are specified in Table 3.10.

A significant advantage arising from the high degree of similarity between the two

Table 4.8: Design variables considered in the conceptual design of the aerial firefighting seaplane variant, including firefighting-specific parameters.

Variable	**Symbol**	**Type**
Power-to-Weight Ratio	P/W	Continuous
Wing Loading	W/S	Continuous
Wing Aspect Ratio	AR_w	Continuous
Wing Taper Ratio	λ_w	Continuous
Airfoil Mean Thickness Ratio	t/c	Continuous
Wing Apex	$X_{LE,w}$	Continuous
Horizontal Tail Volumetric Coef.	$\mathcal{V}_H$	Continuous
Horizontal Tail Thickness Ratio	$(t/c)_H$	Continuous
Horizontal Tail Sweep Angle	Λ_H	Continuous
Vertical Tail Volumetric Coef.	$\mathcal{V}_V$	Continuous
Vertical Tail Thickness Ratio	$(t/c)_V$	Continuous
Vertical Tail Sweep Angle	Λ_V	Continuous
Cruise Mach Number	M_{CR}	Continuous
Climb Speed	V_{CL}	Continuous
Number of Drops	N_{drop}	Integer
Mach Number (Drop Phase)	M_{drop}	Continuous
Fire Pressure Altitude	h_{fire}	Continuous
Water Pressure Altitude	h_{water}	Continuous

seaplane variants lies in the possibility of readily adapting the design workflow from one application domain to another. The MDF architecture presented in Figure 4.2 can be straightforwardly modified and applied to the exploration of the aerial firefighting variant. The principal differences concern the integration of an additional discipline dedicated to the sizing of the additional on-board systems required for firefighting operations, including water tanks, actuators, probes, and release doors, according to the methodology developed by partners in the context of the COLOSSUS project [148]. This methodology, suitable for the conceptual stage, requires only the vehicle geometry and the prescribed water payload, the former being a variable controlled by the DOE driver and the latter a constant defined in the TLARs. As a result, this module can be placed outside the MDA loop shown in Figure 4.2.

This integration also enables the estimation of the scooping distance performance for amphibious configurations, which represents a critical parameter in evaluating the accessibility of available water sources. The adapted workflow is illustrated in Figure 4.3, which reports the XDSM diagram for the conceptual design and design space exploration of the aerial firefighting seaplane variant (further remarks on illustrated disciplines are presented later in this chapter). A LHS composed of roughly 50 times the number of design parameters, 900 samples, complete the DOE setup process.

Remark Figure 4.2 & Figure 4.3

The disciplinary models integrated in Figures 4.2 and 4.3, supporting the conceptual design of the seaplanes in both passenger transport and aerial firefighting variants, were derived from those developed by the Design of Aircraft and Flight Technologies (DAF) research group at the University of Naples Federico II. These models encompass low-fidelity aerodynamic analyses (within the "Components Aerodynamics" discipline), statistical and semi-empirical weight estimation methods, evaluations of longitudinal and directional stability and controllability (through the "Stability & Controllability" discipline), as well as conceptual-level assessments of aircraft performance over assigned mission profiles (in the "Performance Analysis" discipline) and the sizing of non-conventional powertrain architectures (managed within the "Powertrain Design" discipline) integrating multiple energy sources [58, 149, 150, 151, 152, 153, 154, 155].

The models were further enhanced to account for the specific characteristics of the aircraft class under investigation. In particular, the geometric module is based on a Python class developed by the author within a collaborative framework that supports the centralized CPACS data schema and leverages the TiGL parametric geometry library [156], developed by the German Aerospace Center (DLR), in combination with the CPACSCreator plug-in. This integration enables automated updates of the seaplane geometry for each set of design variables.

The statistical weight breakdown, encompassing the mass of the on-board systems typically installed on passenger transport and freight aircraft, while excluding firefighting-specific subsystems, and produced through the “Weight Class I” discipline for the hull-type fuselage, was derived from the methodologies of Roskam [157] and Chicken [108]. These references provide, for different seaplane classes (floatplanes, flying boats, and amphibians), comprehensive mass databases and regression models for weight estimation. Finally, the performance analysis module was extended to account for both the conventional passenger transport mission and a representative aerial firefighting mission. The model incorporates an “active firefighting phase,” as described in Appendix A, along with the corresponding payload and mission parameters defined in the design variable table. Owing to its modular structure, the numerical framework can employ existing submodules to compute climb, cruise, and descent performance throughout the firefighting mission phases.

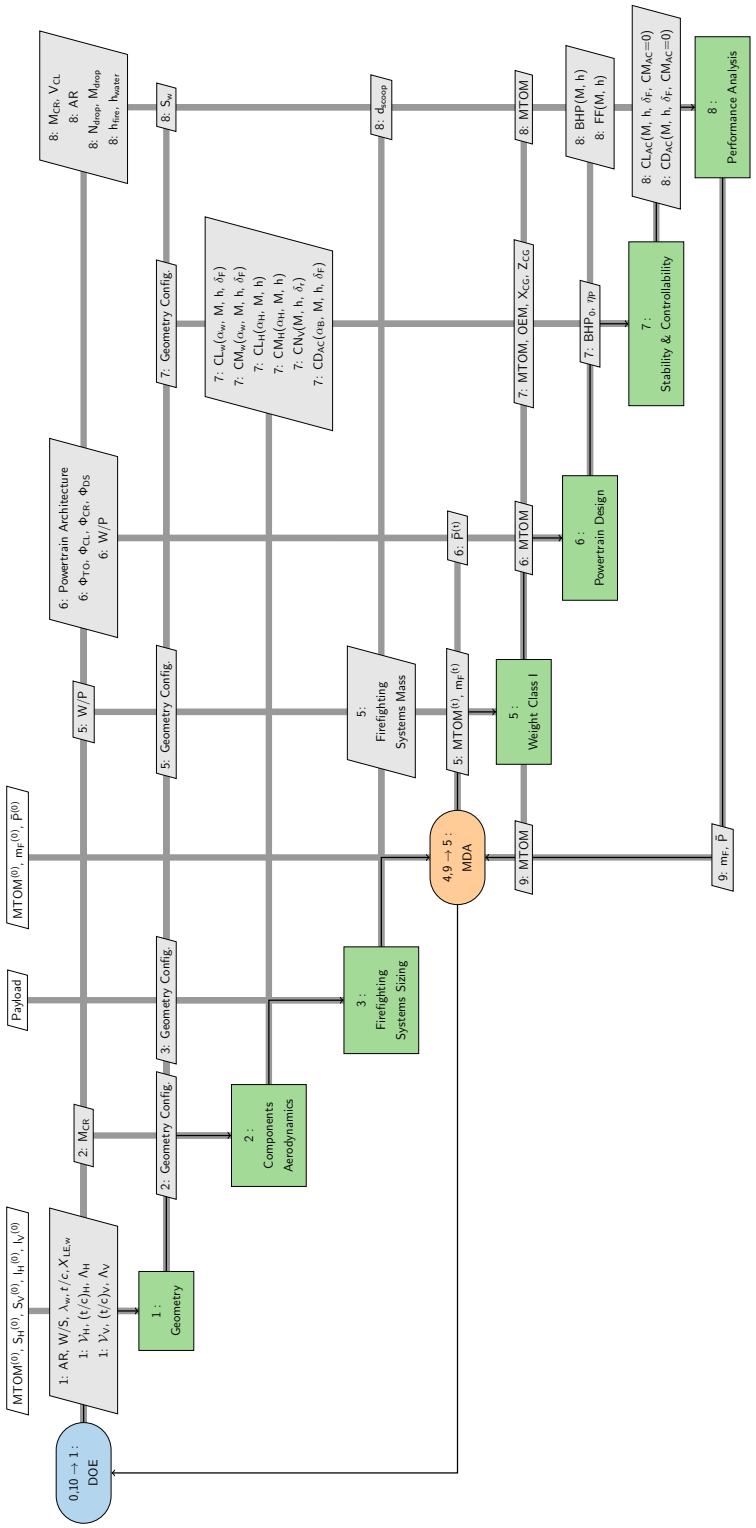

Figure 4.3: XDSM diagram of the conceptual MDA chain for the aerial firefight variant of the seaplane.

Related Publications

One conference publication presents preliminary results on the design space exploration of non-conventional seaplane solutions:

> [15] **Tuccillo, M.**; Della Vecchia, P. (2024). *Multidisciplinary preliminary design process of hybrid-electric seaplane*. Paper presented at the 34th Congress of the International Council of the Aeronautical Sciences (ICAS 2024), Florence, Italy. Paper `ICAS2024_0470`. ISSN 2958-4647. Published 08-10-2024.
>
> Presented at the 34th Congress of the International Council of the Aeronautical Sciences (ICAS 2024), Florence, Italy. The conference paper discuss the trend and potential benefits of non-conventional seaplane configurations. Addressing the vehicle design space exploration, at conceptual level, through a collaborative MDA framework that drive the conceptual design of a passenger transport seaplane, operating on a representative mission and for which the most promising hybridization strategy has to be found across multiple alternatives.

4.4 ML Models for the Conceptual Design

ML models, or more generally metamodels, are increasingly regarded as key enablers of surrogate-based concepts exploration and SBO processes. Their primary function, regardless of whether their underlying mathematical formulation is deterministic or stochastic, is to provide accurate predictions of systems' behaviour without directly relying on the original, low-fidelity or high-fidelity, physical models and their associated constraints.

In the context of ML-assisted aircraft conceptual design, here referred to as surrogate-based concept exploration, the central objective of ML models is to extract meaningful patterns from data generated during design space exploration campaigns. These models are then employed to design and predict, with sufficient accuracy, the performance of seaplane configurations under investigation, given a prescribed set of input parameters encompassing both performance-related and architecture-dependent variables.

In the current state of the art of SBO, two principal strategies for integrating metamodels into the optimization process can be identified: (i) the use of multiple ML models, each replacing a specific disciplinary capability individually, and (ii) the use of a single ML model that represents the MDA framework in its entirety. The selection of one strategy over the other depends primarily on the characteristics of the MDA process to be emulated. Replacing each discipline individually provides greater flexibility, as it allows the rearrangement of disciplinary modules within the

design framework to satisfy different requirements and constraints. However, the effectiveness of this approach is strongly influenced by the number and nature of coupling variables. A limited ability of metamodels to accurately capture coupling effects may compromise the feasibility of the resulting designs. Conversely, replacing the entire MDA workflow with a single metamodel eliminates consistency issues, since inter-disciplinary constraint checks become unnecessary. Nevertheless, this approach presents non-trivial challenges, as the construction of such a model requires managing a potentially large and complex input–output space, as well as handling heterogeneous variables and performance indicators, including mixed-discrete variables.

It is important to remember that the conceptual design of non-conventional aircraft configurations can pose significant computational challenges, not necessarily driven by the fidelity level of the disciplinary models themselves, but rather by the consistency checks and the large number of constraints that must be satisfied. In this context, the second strategy—employing a single metamodel to represent the entire MDA framework—then emerges as a more convenient approach.

ANNs, and in particular Multi-Layer Perceptron (MLP) models, have demonstrated strong potential in handling both multi-input and multi-output problems, making them attractive candidates for approximating the MDA workflow [140]. However, their capability to address mixed-discrete variables remains relatively underexplored, thereby requiring the development and application of dedicated strategies to effectively incorporate this class of variables.

Recent advancements in Gaussian Processes (GPs), such as those implemented in the latest releases of the SMT toolbox, have extended their applicability to problems involving mixed-discrete variables and parameters [144], enabling the construction of complex multi-input models. Nonetheless, a key limitation persists, as these methods are generally restricted to single-output predictions. In multi-output applications, this limitation is typically addressed by constructing multiple independent GP models, each corresponding to one of the outputs of interest.

A similar strategy was applied to the MLP models employed in this study to address mixed-discrete variables. These variables are particularly relevant in the management and selection of alternative powertrain architectures, which can be treated as categorical inputs. To accommodate this, the collected dataset was partitioned into a number of independent subsets, each corresponding to a specific powertrain architecture. Consequently, for the two seaplane classes, with three distinct powertrain architectures considered for the passenger transport variant, four independent MLP models were trained, each replicating the aircraft conceptual MDA problem under the corresponding architectural configuration.

4.4.1 The MLP Models Architecture

A fundamental step in the development of a neural network is the definition of its architecture, which includes the selection of the network depth (i.e., the number of hidden layers), the distribution of perceptrons within each layer, and the choice of non-linear activation functions, usually referred to as the network hyperparameters.

The complexity of a neural network is typically characterized by its depth. Shallow networks, consisting of only a single hidden layer, have limited capability in modelling highly non-linear behaviours across large design spaces. Nevertheless, their simplicity enables training even with small datasets, making them suitable for problems with restricted data availability. By contrast, Deep Neural Networks (DNNs) may incorporate several to hundreds, or even thousands, of hidden layers, depending on the complexity of the target problem. However, the increase in depth significantly raises the number of trainable parameters, thereby demanding larger training datasets to ensure adequate model generalization.

In the present study, the strong non-linear relationships linking aircraft performance to both operational and architectural features, as well as the inherent non-linearities in the MDA framework, necessitate the use of a DNN. Nevertheless, the limited number of available training samples constrains the feasible network depth, leading to the adoption of relatively compact architectures consisting of four to five hidden layers.

Early approaches to determining the number of perceptrons per hidden layer often relied on a "mirrored pyramid" strategy. In this approach, the number of perceptrons is progressively increased in successive hidden layers, starting from a value comparable to the number of input features, until a central layer is reached. Beyond this point, the number of perceptrons is symmetrically reduced, approaching the number of output variables in the final layer, as illustrated in Figure 4.4 for a network with three hidden layers. With the advent of more advanced training techniques, such as regularization functions and early stopping criteria, designed to mitigate overfitting issues, no universally accepted rule currently exists for defining the distribution of perceptrons across layers. Although several empirical guidelines are available, they lack a rigorous mathematical justification, as they generally assume that model generalization will be ensured through appropriate regularization or early stopping mechanisms. In this study a uniform distribution of 64 perceptrons has been chosen to balance accuracy in predicting complex non-linear behaviours and computational efficiency, since the use of a number of units that is a power of two represents a common practice on many hardware architectures [158].

An essential component of the training process of an MLP model is the selection of appropriate activation functions, which play a critical role in both classification and regression tasks, the latter including applications such as aircraft design and performance analysis. To enhance the predictive capability of the network, it is common practice to employ a combination of linear and bounded non-linear activation functions in the hidden layers, while the use of activation functions in the output layer is

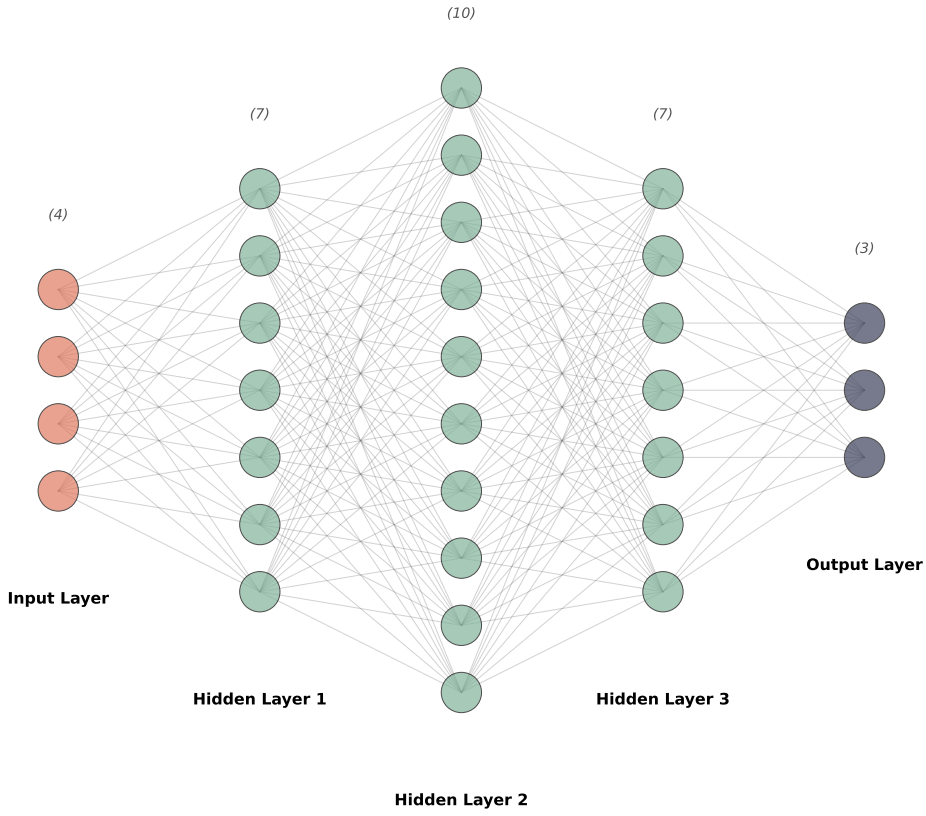

Figure 4.4: Example of "mirrored pyramid" strategy for distributing perceptrons among hidden layers.

generally optional [159]. In this study, Rectified Linear Unit (ReLU) and hyperbolic tangent (Tanh) functions were selected for the hidden layers, owing to their well-documented ability to capture non-linear relationships, whereas a linear (identity) function was employed in the output layer to ensure unbiased predictions for continuous target variables.

To complete the definition of the neural network architecture, it is necessary to specify the optimization algorithm used to minimize a suitable loss function. In this regression study, the Mean Squared Error (MSE) was selected as the loss function, given its effectiveness in quantifying prediction accuracy for continuous outputs. The Adaptive Moment Estimation (ADAM) optimizer was employed to guide the training process. ADAM implements a stochastic gradient descent (SGD) approach with adaptive learning rates for each parameter, thereby enhancing convergence stability and efficiency [160]. This method combines the advantages of AdaGrad, which adapts learning rates for infrequently updated parameters [161], and RM-

Table 4.9: MLP Model Architecture Summary

Item	Value	Note(s)
Hidden Layers	3	-
Perceptrons Distribution	[64, 64, 64]	Uniform Distribution
Activation Functions	[ReLU, Tanh, ReLU]	-
Optimizer	ADAM	SGD Approach
Initial Learning Rate	0.001	-

SProp, which maintains efficiency in non-stationary settings through exponentially decaying averages of past gradients [162]. The final adopted architecture of the MLP model, trained on data generated during the conceptual design space exploration campaign, is presented in Table 4.9.

4.4.2 The Active Learning Process

Active Learning (AL) is a supervised ML strategy designed to maximize model performance in scenarios where the acquisition of additional data points is computationally or experimentally expensive [163]. The methodology relies on iteratively selecting the most informative samples to refine the predictive capability of the model, thereby reducing the overall number of training points required. The main components of the AL framework applied in this study include: (1) an initial database, or pool, specific to each powertrain architecture under consideration, (2) a subset of this pool defined as the initial training set for each independent model, (3) a set of MLP models trained to approximate the conceptual design problem, and (4) a selection criterion that exploits intrinsic model features to identify which candidate configurations should be added to the training dataset in subsequent iterations.

No structural differences were introduced between the MLP models; thus, for both the passenger transport and aerial firefighting variants, the architecture reported in Table 4.9 serves as the baseline representation. For each model, the training process begins with the division of the database into two subsets: (i) a training set, $\mathcal{D}_{\text{train}} = \left\{\mathbf{x}_j^{\text{train}}, \mathbf{f}\left(\mathbf{x}_j^{\text{train}}\right), \quad j = 1, \ldots, \text{N}_{\text{train}}\right\}$, employed to perform SGD optimization of the network weights and biases, in which $\mathbf{x}_j^{\text{train}}$ represents the array of design variables and $\mathbf{f}\left(\mathbf{x}_j^{\text{train}}\right)$ the array of performance metrics and indicators identified for each use case; and (ii) an unlabelled dataset, $\mathcal{D}_{\text{unlabelled}} = \{\mathbf{x}_j, \quad j = 1, \ldots, \text{N}_{\text{unlabelled}}\}$, comprising approximately 80% of the total configuration pool, $\mathcal{P}$, that is $\mathcal{D}_{\text{unlabelled}} \subset \mathcal{P}$ and extracted randomly from the latter. After the initial training phase, model performance is assessed on the unlabelled set to conduct uncertainty quantification and identify the samples for which the predictions exhibit the largest errors. These results are subsequently passed to an acquisition function, whose objective is to select a finite number of configurations with the highest prediction uncertainty for inclusion in the training set. The procedure is iteratively repeated until convergence is achieved, specifically when the maximum uncertainty between two consecutive

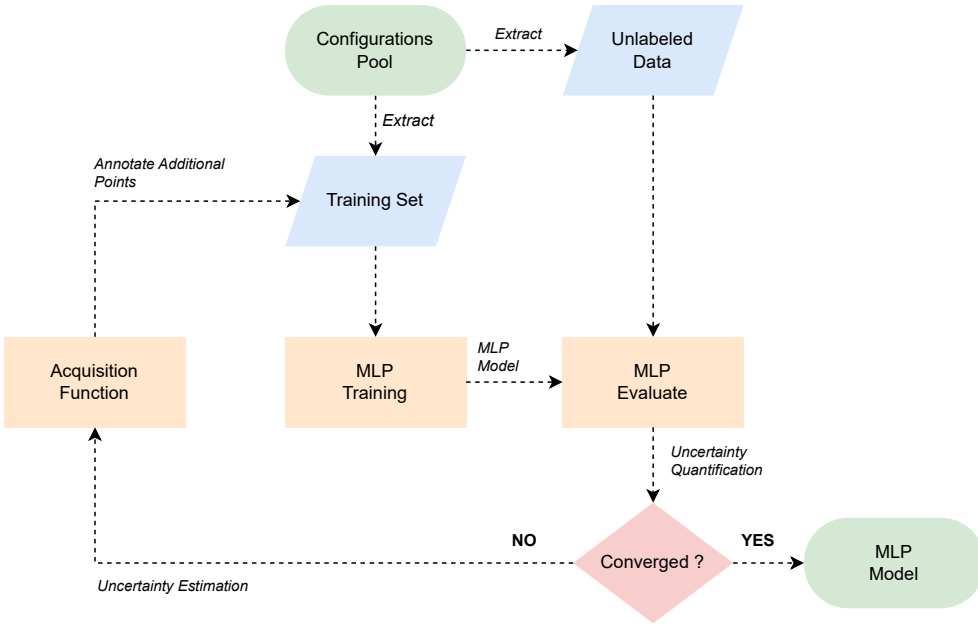

Figure 4.5: Active Learning Flowchart.

iterations becomes stationary. The overall AL workflow is illustrated in Figure 4.5, while its integration within the broader conceptual design framework is indicated in Figure 4.1 as “Active Learning”.

It is worth noting that, for both use cases, the initial pool of configurations corresponds to the results of the exploration campaigns, which were deliberately limited to reduce computational effort. However, the convergence process illustrated in Figure 4.5 inherently produces an iterative increase in the size of the training dataset, accompanied by a progressive reduction of the unlabelled dataset, since uncertainty quantification cannot be performed on data already used to train the MLP model. At the onset of the AL procedure, it is not possible to predict the number of iterations required to achieve convergence, as this strongly depends on both the neural network architecture and the underlying data distribution. Consequently, it may occur that the iterative process exhausts the unlabelled dataset, leading to an early termination with an unsatisfactory convergence residual. To mitigate this issue, an auxiliary convergence mechanism has been integrated into the global surrogate-based concept exploration framework, as shown in Figure 4.1. This mechanism aims to expand the configuration pool by adding five additional configurations whenever an early termination condition is detected, based on the size of the unlabelled dataset at the final inner iteration.

The core activity of an AL process lies in the application of a selection criterion to identify the data points that, if added to the training dataset, would yield the greatest improvement in the predictive performance of the neural network without the need of extensively large training datasets. In Figure 4.5, this criterion is represented

by the model's predictive uncertainty on previously unseen data, commonly referred to as uncertainty quantification. A major challenge associated with neural network architectures typically employed for regression tasks is that they do not inherently provide an output distribution. For any given input sample $\mathbf{x}_j$, the output is deterministic, consistently returning the same prediction regardless of repeated evaluations. This characteristic prevents a direct assessment of predictive uncertainty. Gal et al. [164] addressed this limitation by demonstrating that a neural network with dropout applied before every layer with trainable parameters (weights and biases) can be interpreted as a Bayesian approximation to a probabilistic Gaussian Process, thereby enabling uncertainty estimation within standard neural network frameworks. This technique is often identified as Monte Carlo Dropout (MCD).

In this study, three dropout layers were introduced before each trainable layer of the network. The dropout probability was fixed at 0.15 for all layers, consistent with the average value suggested by Gal et al. [164]. This implies that, at each forward pass, 15% of the perceptrons in a given layer are randomly deactivated, effectively yielding a different model realization every time an input sample is propagated through the network. Uncertainty quantification is performed by executing multiple stochastic forward passes (500 in this work) with MCD enabled also during the evaluation phase. Each pass produces a distinct prediction due to the stochastic nature of dropout.

Let $Y = \left\{y^{(1)}, y^{(2)}, \ldots, y^{(T)}\right\}$ denote the set of outputs obtained from T stochastic forward passes ($T = 500$) corresponding to a given input $\mathbf{x}_j$. Due to the probabilistic nature of the MCD technique, this ensemble of predictions provides an approximation of the posterior predictive distribution $p(Y|\mathbf{x}_j)$.

The predictive mean is estimated as the average of the T stochastic predictions, as shown in Eq. (4.1), where $y^{(t)}(\mathbf{x}_j)$ represents the prediction obtained at the t-th stochastic forward pass.

$$\hat{\mu}(\mathbf{x}_j) = \frac{1}{T}\sum_{t=1}^{T} y^{(t)}(\mathbf{x}_j) \tag{4.1}$$

In this study, the prediction uncertainty is quantified using the standard deviation of the stochastic outputs as in Eq. (4.2).

$$\hat{\sigma}^2(\mathbf{x}_j) = \frac{1}{T-1}\sum_{t=1}^{T}\left(y^{(t)}(\mathbf{x}_j) - \hat{\mu}(\mathbf{x}_j)\right)^2 \tag{4.2}$$

Thus, the MCD approach yields both an estimate of the expected model response and a statistically grounded measure of predictive confidence, enabling the integration of uncertainty quantification into the conceptual design and performance evaluation process of the conventional and innovative seaplane configurations.

Figures 4.6 to 4.9 illustrate the iterative evolution of the predictive standard deviation

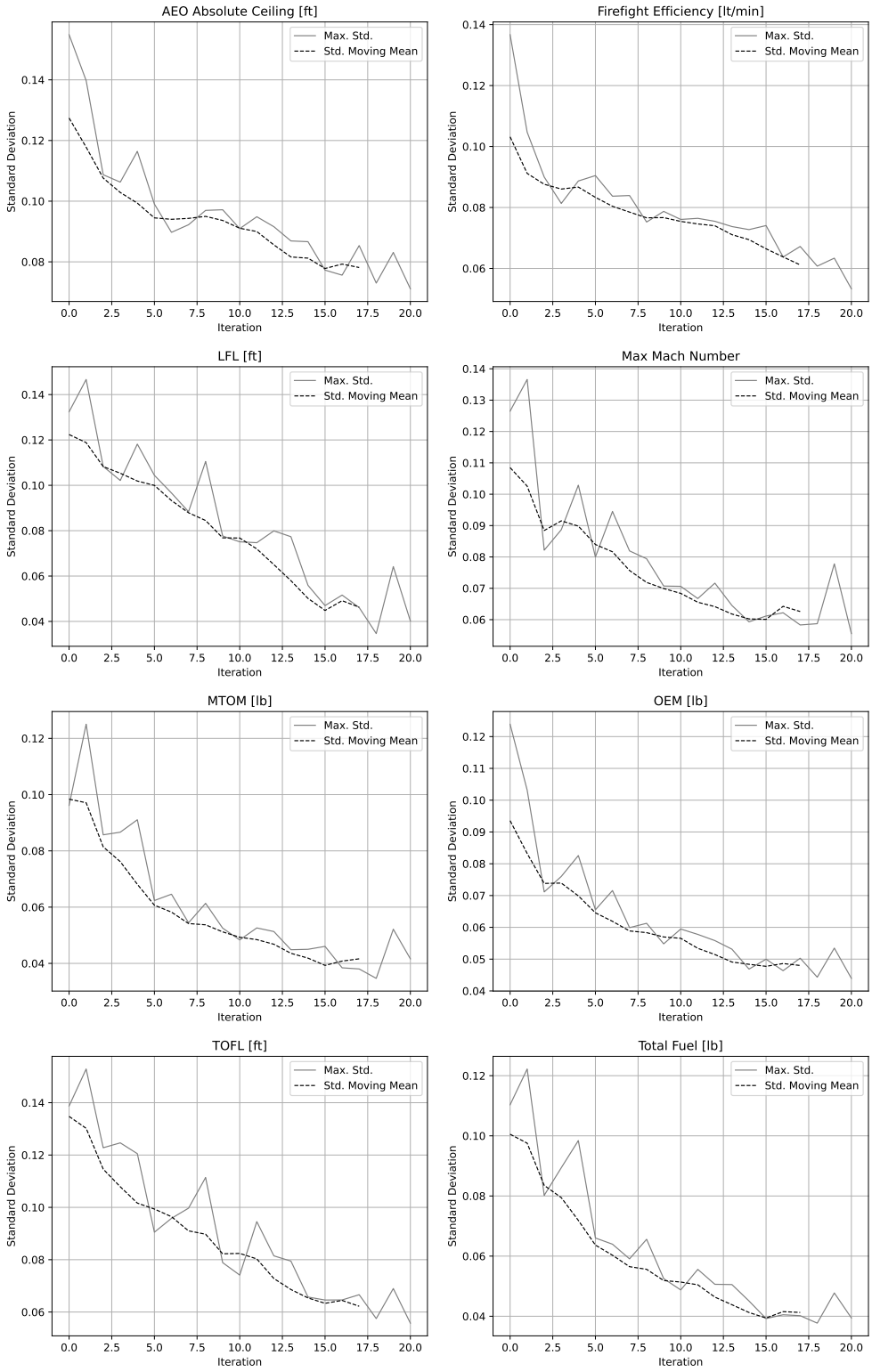

Figure 4.6: Standard deviation for the aerial firefight variant. The solid line represents the maximum standard deviation for each iteration, the dashed line represents the moving mean.

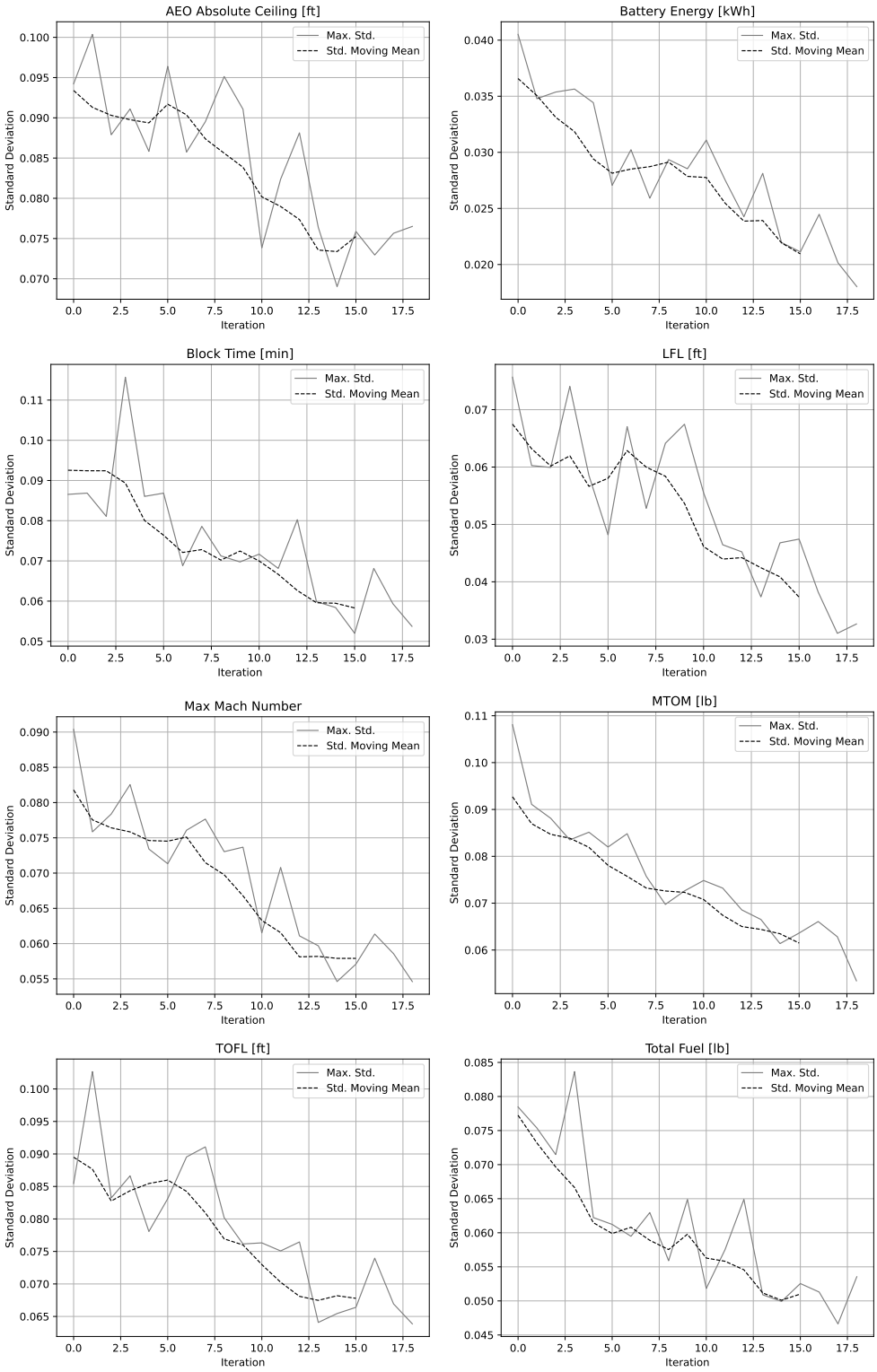

Figure 4.7: Standard deviation for the passenger transport variant (Hybrid-Electric-Reciprocating). The solid line represents the maximum standard deviation for each iteration, the dashed line represents the moving mean.

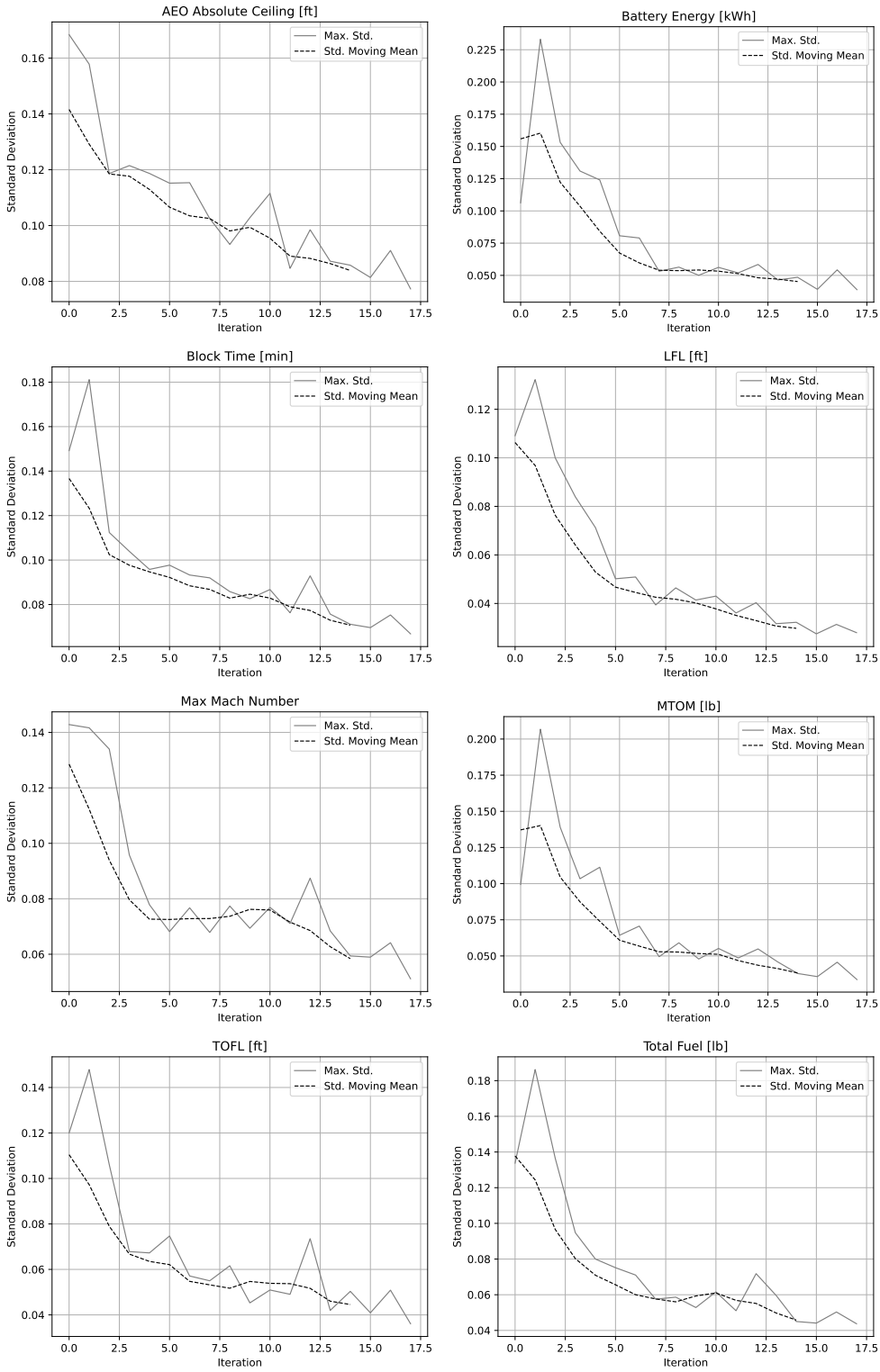

Figure 4.8: Standard deviation for the passenger transport variant (Hybrid-Electric-Turboprop). The solid line represents the maximum standard deviation for each iteration, the dashed line represents the moving mean.

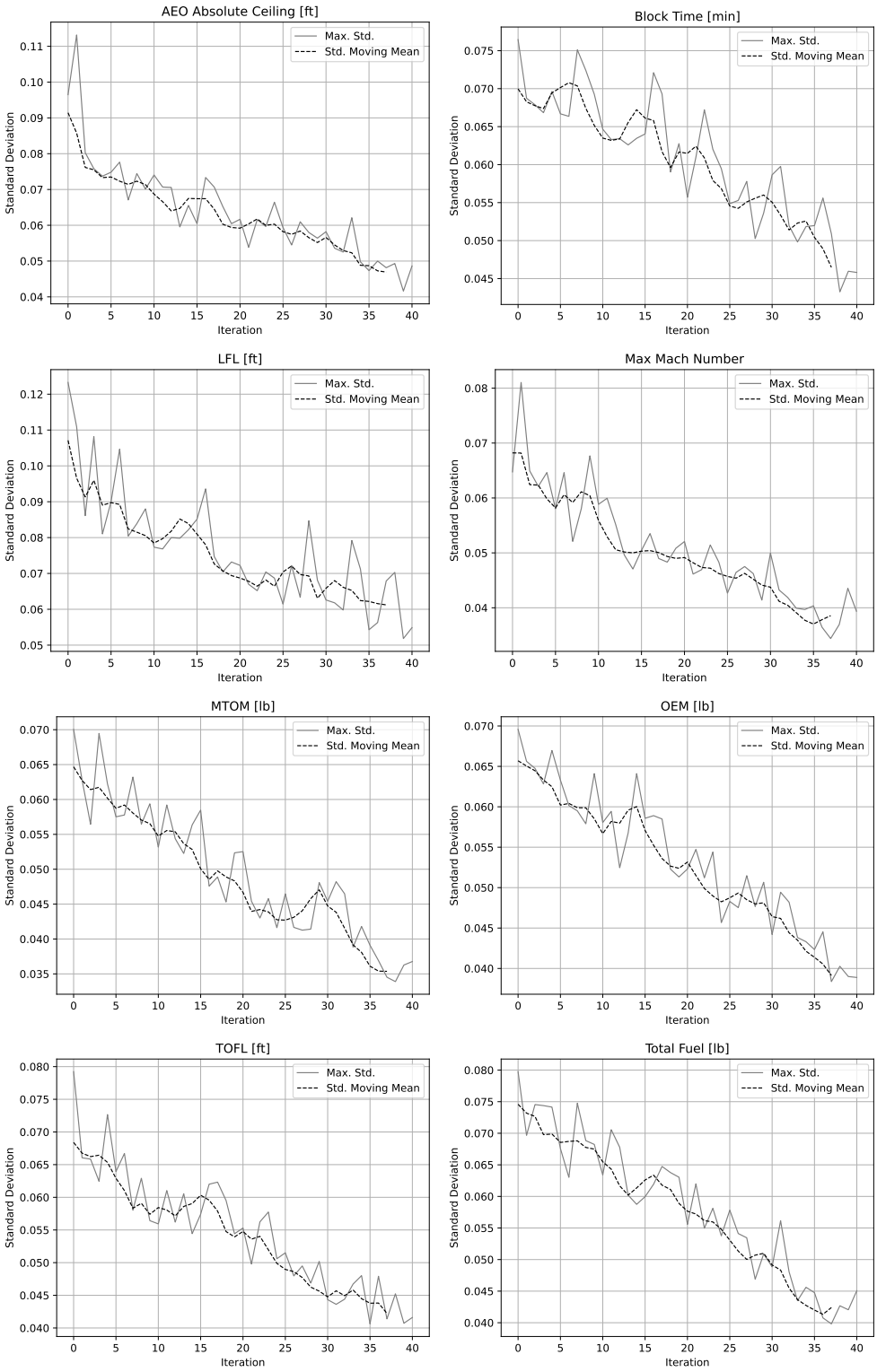

Figure 4.9: Standard deviation for the passenger transport variant (Turboprop). The solid line represents the maximum standard deviation for each iteration, the dashed line represents the moving mean.

Table 4.10: Active Learning summary with training set sizes and required iterations for convergence.

Use Case	Powertrain	Initial Size	Final Size	Iterations
Firefight	Turboprop	75	450	20
Pax Transport	Turboprop	54	401	40
	Hybrid-Electric (Reciprocating)	51	352	18
	Hybrid-Electric (Turboprop)	67	386	17

for each performance indicator during the AL process, for both use cases: the aerial firefighting variant and the passenger transport variant, the latter including results for each of the three investigated powertrain architectures.

In each figure, the solid line represents the maximum predictive standard deviation computed over the T stochastic forward passes at a given iteration, while the dashed line denotes the moving average of the maximum standard deviation, evaluated over a sliding window of four iterations. The latter provides a more robust and smoothed indicator for applying the convergence exit criterion. A monotonic decrease in both functions indicates that the iterative addition of samples characterized by the highest predictive uncertainty effectively enhances the model's performance, thereby reducing the need for excessively large training datasets.

For both use cases, the number of iterations required to achieve convergence ranged between 17 and 40, a small difference attributed to the different powertrain architectures and the high degree of similarity between the design variables and performance metrics of the two aircraft categories. Furthermore, no early termination of the AL process was observed, confirming that the initial configurations' pools were appropriately sized. Table 4.10 summarizes the AL procedure, reporting the size of the initial and final training datasets, together with the number of iterations required to reach convergence.

4.5 The SBO Problem

4.5.1 Problem Formulation

The primary objective of the aircraft conceptual design process is the exploration of alternative vehicle configurations and architectures capable of addressing the requirements of emerging market segments. Within the classical formulation of conceptual design, MDO methods represent the most effective framework for analysing and comparing multiple configurations. These approaches enable the simultaneous satisfaction of a given set of TLARs while supporting trade-off analyses among optimal solutions with respect to KPIs and objective functions that reflect the potential

competitiveness of the vehicle in its target market.

Within a surrogate-based concept exploration framework, design and optimization techniques maintain their central role in supporting design and trade-off analyses. The main distinction, however, lies in the fact that the underlying disciplinary analyses, or, in some cases, the complete MDA and MDO processes, are replaced by surrogate models or ML models. This substitution is expected to enable a substantial reduction in computational cost, while preserving the ability to capture system-level interactions and to support the evaluation of multiple candidate architectures in the early design stages.

The integration of the exploratory nature of the aircraft conceptual design process into an SBO framework requires the designer to carefully define two fundamental elements of any optimization problem: the optimization algorithm and the objective function space. In the context of aircraft design, the objective function space is typically multidimensional, as multiple, often competing, objectives are incorporated into the optimization framework. As a result, the process generally yields a "family" of feasible designs rather than a single optimal solution, as would be the case in single-objective optimization problems. This multi-objective approach enables the explicit quantification of trade-offs among conflicting objectives, which is essential for comparing alternative vehicle architectures that equally satisfy the set of design requirements.

As with the selection of design variables, the choice of objective functions to drive the SBO process strongly depends on the intended scope of the aircraft. In this context, the collection of identified performance indicators and metrics represents the most suitable source for extracting candidate objective functions. It is important to emphasize that the selection of objective functions is, in practice, an "extraction" process from relevant KPIs. This is motivated by two principal considerations: (1) the set of performance indicators characterizing an aircraft can be very large, which would lead to the formulation of a "many-objective" optimization problem. Such problems typically exhibit reduced performance due to the complexity of the objective space [165]. (2) Many of the identified KPIs are not independent but instead exhibit correlations, introducing biases in the optimization process. As a consequence, dependent KPIs may disproportionately influence the determination of the optimal solution, thereby reducing the overall effectiveness of the optimization algorithm.

For instance, in the passenger transport variant of the seaplane, minimizing the mission block time on a representative route, assuming operation at a constant cruise altitude, necessitates a parallel maximization of the cruise Mach number. This, in turn, requires a powertrain system capable of delivering higher shaft power, thereby enabling a higher maximum achievable Mach number. However, the simultaneous inclusion of both block time and maximum Mach number as objective functions within the optimization space reduces the overall effectiveness of the algorithm, as the two metrics are inherently correlated and introduce redundancy into the objective function space. To address the aforementioned challenges, the number of

objective functions is deliberately reduced, for both use cases, relative to the full set of identified KPIs. The selected objectives are required to be, even if potentially conflicting, mutually independent.

The optimization algorithm plays a pivotal role in SBO problems, as its primary objective is to identify all optimal candidate solutions belonging to the Pareto front while ensuring compliance with the imposed design constraints. More specifically, within a surrogate-based concept exploration framework, the optimization algorithm is also tasked with managing the exploration of the design space, addressing the multi-objective nature of the problem, and efficiently navigating the selected set of design variables.

In the present SBO formulation, the optimization algorithm must operate with a black-box evaluator, namely, the MLP model employed to represent the conceptual design framework of the seaplanes, and must additionally address discontinuities in the objective space arising from mixed-discrete variables, which govern the selection of alternative powertrain architectures. These considerations clearly indicate that gradient-free optimization algorithms represent the most suitable choice for this category of problems [70]. Such methods are capable of handling heterogeneous design spaces and surrogate models that do not provide analytical gradients, or for which numerical gradient estimation is unreliable due to the inherent approximation error of the metamodel.

Among gradient-free optimization methods, this study investigates the use of evolutionary algorithms, with a specific focus on genetic algorithms (GAs). These algorithms are extensively implemented in a wide range of open-source optimization frameworks and are available in multiple variants, making them suitable for addressing many-objective optimization problems. Furthermore, GAs have demonstrated strong applicability in problems that incorporate architecture-dependent parameters within the set of design variables [166].

Passenger Transport Seaplanes

In the case of passenger transport aircraft, a primary metric governing both operational strategies and market competitiveness is DOC, which therefore constitutes a natural first choice in defining the objective function space. Furthermore, the increasing demand for sustainable and environmentally responsible aviation necessitates the inclusion of performance metrics that capture the environmental impact of the aircraft. While a full Life-Cycle Assessment (LCA) is beyond the scope of disciplines typically integrated at the conceptual design stage, simplified models, often derived from international regulatory and monitoring agencies such as EUROCONTROL and IATA, can be employed. These approaches generally approximate environmental impact through indicators directly proportional to fuel consumption. Consequently, incorporating fuel consumption into the objective function space not only supports the improvement of environmental performance but also enhances

Table 4.11: List of Symbols for Eq. (4.3) and Eq. (4.4).

Description	**Symbol**	**Unit**	**Note(s)**
Propeller Efficiency	η_{P}	-	In cruise condition
Specific Fuel Consumption	c_{p}	lb/hp hr	In cruise condition
Lift-to-Drag Ratio	L/D	-	In cruise condition
Initial Weight	W_i	$\mathrm{lb_f}$	-
Final Weight	W_f	$\mathrm{lb_f}$	-
Transmission Efficiency Branch 1	η_1	-	Table 1 of [167]
Transmission Efficiency Branch 2	η_2	-	Table 1 of [167]
Transmission Efficiency Branch 3	η_3	-	Table 1 of [167]
Supplied Power Ratio	Φ	-	-
Gravitational Acceleration	g	$\mathrm{m/s^2}$	-
Battery Specific Energy	e_{bat}	J/kg	-
Fuel Specific Energy	e_{f}	J/kg	-
Operating Empty Weight	$\mathrm{W_{OE}}$	N	-
Payload Weight	$\mathrm{W_{PL}}$	N	-
Initial Total Energy	$\mathrm{E_{0,tot}}$	J	-

the attractiveness of the aircraft to potential operators.

An additional objective is incorporated to enhance the operational flexibility of the aircraft. It is important to note that low fuel consumption and reduced operating costs do not inherently guarantee the capability of the aircraft to adapt to diverse mission profiles. This flexibility is quantified through a mission "range factor", which, at the conceptual design stage, is derived from standard flight mechanics formulations. Specifically, for kerosene-based powertrain architectures, the metric is obtained from the classical Breguet range equation, while for hybrid-electric configurations, an equivalent formulation proposed by De Vries et al. [167] for battery-powered architectures is adopted. These formulations are reported in Eq. (4.3) and Eq. (4.4), respectively, with Table 4.11 describing the list of symbols used and the corresponding units of measure.

$$\mathrm{R} = \frac{\eta_{\mathrm{P}}}{c_{\mathrm{p}}} \left(\frac{\mathrm{L}}{\mathrm{D}}\right) \ln\left(\frac{\mathrm{W}_i}{\mathrm{W}_f}\right) \tag{4.3}$$

$$\begin{aligned} \mathrm{R} = {} & \eta_3 \frac{e_{\mathrm{f}}}{g} \left(\frac{\mathrm{L}}{\mathrm{D}}\right) \left(\eta_1 + \eta_2 \frac{\Phi}{1-\Phi}\right) \\ & \times \ln\left[\frac{\mathrm{W_{OE}} + \mathrm{W_{PL}} + (g/e_{\mathrm{bat}})\,\mathrm{E_{0,tot}}\,(\Phi + (e_{\mathrm{bat}}/e_{\mathrm{f}})\,(1-\Phi))}{\mathrm{W_{OE}} + \mathrm{W_{PL}} + (g/e_{\mathrm{bat}})\,\Phi \mathrm{E_{0,tot}}}\right] \end{aligned} \tag{4.4}$$

In both equations, three main functional groups can be identified: (i) the powertrain-related energy conversion and mechanical efficiencies, which include propeller efficiency, engine specific fuel consumption, battery and fuel specific energy, as well as the supplied power ratio (referred to in this study as hybridization ratios); (ii) the

aerodynamic efficiency of the aircraft, expressed through the lift-to-drag ratio at the reference flight condition; and (iii) the ratio between the aircraft weight at the beginning and at the end of the level-flight phase. The role of the "range factor," when included in the objective space, is not to directly optimize the aircraft range, which has been fixed by the design requirements, but rather to enhance the functional dependencies that contribute to the maximum achievable range.

The mathematical formulation of the adopted range factor is reported in Eq. (4.5). It is important to note that in this formulation, all terms related to powertrain operating efficiency have been neglected, since they act as equivalent scaling factors for both range equations. Furthermore, the contribution of the battery energy, and its associated mass, is integrated into the aircraft operating weight. This formulation compels the optimizer to select an appropriate hybridization ratio (supplied power ratios) that maximizes the ratio between the fully loaded aircraft weight and the operating empty weight, thereby achieving a balance between battery utilization and the maximum storable fuel mass.

$$R_{\text{factor}} = \left(\frac{L}{D}\right) \ln\left(\frac{W_{OE} + W_F}{W_{OE}}\right) \tag{4.5}$$

In order to fully define the aircraft conceptual design and optimization problem, it is necessary to introduce the optimization design variables together with the corresponding constraints. For the passenger transport variant, the design variables encompass all parameters required to generate and evaluate candidate configurations through the trained MLP models. These variables are consistent with those previously adopted during the surrogate-based concept exploration phase, specifically within the DOE campaign, and are summarized in Table 4.4.

On the other hand, the definition of design constraints is derived directly from the TLARs associated with this category of aircraft, as already introduced in Chapter 3. The integration of TLARs into the optimization framework ensures that the Pareto-optimal solutions obtained remain compliant with stakeholder requirements and competitive within the targeted market segment.

The evolutionary nature of the optimization algorithm inherently leads to the exploration of multiple generations of design variable populations, which include both conventional continuous variables and mixed-discrete variables associated with powertrain architecture alternatives. It is important to note that, in general, optimization algorithms treat each variable independently. As a result, within a given generation, the population may include unfeasible combinations. For instance, the algorithm might simultaneously select a conventional turboprop powertrain architecture while also assigning a rated power value to electric motors, thereby producing non-viable configurations.

To mitigate such inconsistencies, Bussemaker [143] proposed enhancements to optimization algorithms, in the context of System Architecture Optimization, by introducing the concepts of *activation relationships* and *value constraints*. Activation

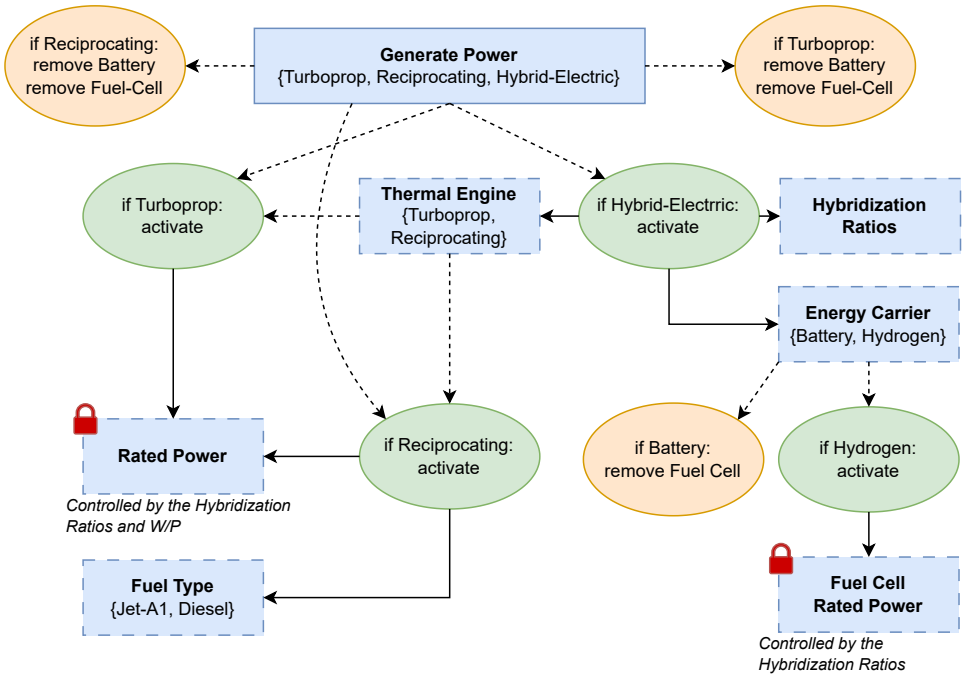

Figure 4.10: Illustration of design variable hierarchy for the powertrain system. Green ellipses represents activation relationships, orange represents value constraints (adapted from [143]).

relationships define the conditions under which lower-level design variables are enabled, based on the selection of higher-level variables. Value constraints, in turn, restrict the feasible options of active lower-level variables to ensure consistency with the overarching design architecture.

Figure 4.10 illustrates the hierarchical structure of the powertrain system design variables, explicitly highlighting the dependency relationships required to properly manage mixed-discrete design spaces. In the figure, green ellipses denote *activation relationships*: starting from either a required function or a design variable option, these relationships determine which dependent variables must be activated. Solid-line arrows indicate the activation of "second-order" variables, while dashed-line arrows connect the primary function, or design variable, to its associated set of activation relationships. Similarly, orange ellipses represent *value constraints*, used to restrict the admissible range of dependent variables according to architectural consistency.

It should be emphasized that the hierarchical framework depicted in Figure 4.10 is intended as a general representation and may not fully coincide with the specific optimization problem addressed in this study, since multiple strategies exist for managing and integrating energy sources in hybrid-electric architectures. Finally, the "locks" illustrated in the figure identify variables excluded from the conceptual design MDA workflow and, consequently, from the SBO problem, together with the indication of the controlling drivers responsible for their deactivation.

Finally, Table 4.12 consolidates the complete formulation of the optimization problem for the passenger transport seaplane, presenting the selected design variables, the imposed constraints, the objective functions to be optimized and a brief overview of the *activation relationships* among design variables. This formulation constitutes the core of the surrogate-based exploration framework applied in this research. The entire optimization framework has been implemented leveraging the Python programming language and its vast library of open-source optimization environments, specifically the "pymoo" package [168] for the formalisation of the constrained multi-objective optimization problem and the SBArchOPT package [169, 170] for integrating surrogate-based optimization capabilities, as well as architecture optimization functionalities.

Aerial Firefight Seaplanes

As highlighted in the market analysis, both national and international emergency response operators are increasingly seeking platforms that combine operational effectiveness with reduced operating costs, the latter emerging as a key performance metric also among manufacturers of aerial firefighting aircraft. Consequently, the integration of operating costs as a primary objective in the design of firefighting seaplanes is straightforward. The major distinction with respect to passenger transport applications lies in the normalization metric used to express these operating costs, as observed, for firefighting aircraft, DOC is normalized with respect to the total mass or volume of fire suppressant delivered during a mission. Furthermore, competitiveness in the aerial firefighting segment, as reflected by the analysed operational efficiency metric, has consistently been a decisive factor in the selection of one aircraft configuration over another. This makes operational efficiency a fundamental objective to be maximized in the optimization framework.

The operational flexibility of the passenger transport seaplane has been quantified through the “range factor” objective function. In parallel, a performance indicator more commonly associated with air-tactical aircraft than with air tankers is the flight endurance. Notably, this metric can significantly contribute to the overall efficiency of also air tankers, particularly in amphibious configurations. Indeed, by combining appropriate flight strategies with satisfactory endurance capabilities, operational efficiency can be enhanced through the reduction of turnaround times associated with refuelling operations. The Breguet endurance equation for conventional propeller-driven aircraft, assuming a flight at constant altitude and constant attitude, is reported in Eq. (4.6).

$$\mathrm{En} = \frac{\eta_\mathrm{P}}{c_\mathrm{p}} \frac{\mathrm{C_L}^{3/2}}{\mathrm{C_D}} \sqrt{2\rho \mathrm{S_w}} \left(\frac{1}{\sqrt{\mathrm{W}_f}} - \frac{1}{\sqrt{\mathrm{W}_i}} \right) \tag{4.6}$$

As in the case of the range equation, three principal functional groups can be identified: (i) the powertrain system efficiency group, (ii) the aerodynamic efficiency

Table 4.12: Formulation of the surrogate-based optimization problem for the design of the passenger transport seaplane.

	Function/Variable	**Nature**	**Quantity**	**Note(s)**
minimize	DOC	cont.	1	-
	$1/R_{factor}$	cont.	1	-
	W_F	cont.	1	-
			3	**Total Objectives**
with respect to	P/W	cont.	1	-
	W/S	cont.	1	-
	AR_w	cont.	1	-
	λ_w	cont.	1	-
	t/c	cont.	1	-
	$X_{LE,w}$	cont.	1	-
	$\mathcal{V}_H$	cont.	1	-
	$(t/c)_H$	cont.	1	-
	Λ_H	cont.	1	-
	$\mathcal{V}_V$	cont.	1	-
	$(t/c)_V$	cont.	1	-
	Λ_V	cont.	1	-
	M_{CR}	cont.	1	-
	V_{CL}	cont.	1	-
	Φ_{TO}‡	cont.	1	Take-Off Hybrid Ratio
	Φ_{CL}‡	cont.	1	Climb Hybrid Ratio
	Φ_{CR}‡	cont.	1	Cruise Hybrid Ratio
	Φ_{DS}‡	cont.	1	Descent Hybrid Ratio
	Powertrain Architecture	cat.	1	-
	Fuel Type†	cat.	1	-
	Energy Carrier‡	cat.	1	-
	Energy Supplier‡	cat.	1	-
	Thermal Engine‡	cat.	1	-
				‡ active only if powertrain architecture is hybrid-electric. † active only if thermal engine is reciprocating.
			18	**Total cont. variables**
			5	**Total cat. variables**
			23	**Total variables**
subject to	$d_{TO} \leq 1\,850.0$ ft	cont.	1	-
	$d_{LND} \leq 1\,850.0$ ft	cont.	1	-
	MTOM $\leq 19\,000.0$ lb	cont.	1	-
	$h_{Ceil,\,AEO} \geq 25\,000.0$ ft	cont.	1	-
	Wingspan ≤ 78.74 ft	cont.	1	ICAO B category
	BT ≤ 1.0 hr	cont.	1	From TLAR on max. cruise speed
			6	**Total constraints**

group, and (iii) the weight-dependent group. This classification enables the extraction of an "endurance factor," which preserves the fundamental dependencies of the full endurance formulation while providing a simplified objective function for the SBO problem of the firefighting variant. The functional dependencies retained in the definition of the "endurance factor" include those governing the selection of operational parameters, such as the Mach number during levelled flight and active firefighting segments, as well as architectural features that influence the trade-off between the maximum fuel capacity and the take-off mass of the aircraft. The resulting mathematical formulation of the adopted "endurance factor" is presented in Eq. (4.7).

$$\mathrm{En_{factor}} = \frac{\mathrm{C_L^{3/2}}}{\mathrm{C_D}} \sqrt{\mathrm{S_w}} \left(\frac{1}{\sqrt{\mathrm{W_{OE}} + \mathrm{W_{PL}}}} - \frac{1}{\sqrt{\mathrm{W_{OE}} + \mathrm{W_{PL}} + \mathrm{W_F}}} \right) \tag{4.7}$$

To fully define the optimization problem for the aerial firefighting seaplane, it is necessary to specify both the design variables and the optimization constraints. The choice of design variables follows the same rationale adopted for the passenger transport variant: they must include all parameters required to enable a complete configuration design and subsequent performance analysis within the trained surrogate models. Accordingly, the design variables are drawn directly from those employed in the DOE campaign, as summarized in Table 4.8. These encompass both architectural and performance-related parameters, as well as mission-specific variables that are unique to the firefighting role, such as the number of drops, the Mach number during the drop phase, and the fire and water pressure altitudes.

In parallel, the constraints of the optimization problem are derived from the TLARs introduced in Chapter 3. This formulation guarantees that all non-dominated solutions lying on the Pareto front represent viable aircraft configurations capable of addressing the practical demands of aerial firefighting operations, while simultaneously enabling trade-off analyses between competing objectives such as endurance, cost-effectiveness, and operational efficiency.

A fundamental distinction in the aerial firefighting use case lies in the role played by operational design variables, such as fire ground altitude, water ground altitude, and the number of water drops, within the optimization problem. These variables are inherently dependent on the specific mission scenario in which the aircraft is required to operate. Their inclusion among independent design variables, particularly in the absence of explicit constraints on operational behaviour, introduces a bias into the optimization process. In such a formulation, the optimization algorithm would not only adjust the vehicle configuration with respect to the defined objectives but would also implicitly optimize the operational scenario itself, thereby conflating two distinct problem domains.

Such an approach is fundamentally inappropriate. An air tanker aircraft, particularly within the seaplane class, must demonstrate the capability to adapt effectively across a wide range of operational environments. Optimization restricted to a single,

Table 4.13: Samples of aerial firefight scenarios.

Scenario ID	Number of Drops	Fire Ground Altitude	Water Ground Altitude
1	5	500 ft	SL
2	5	500 ft	400 ft
3	5	2 000 ft	1 500 ft
4	5	2 000 ft	1 900 ft
5	13	500 ft	SL
6	13	500 ft	400 ft
7	13	2 000 ft	1 500 ft
8	13	2 000 ft	1 900 ft

unconstrained design point risks undermining this adaptability, leading to solutions tailored to a non-representative operational scenario. Moreover, the optimizer could converge toward trivial or non-demanding scenarios that are misaligned with the true mission requirements. For instance, in an effort to reduce operating costs, the algorithm might minimize the number of drops, thereby lowering fuel consumption and mission block time, but at the expense of the aircraft's effectiveness in fulfilling its primary firefighting role.

To address such limitation, the conceptual sizing of the seaplane was performed across eight representative mission scenarios, parametrized in terms of the number of water drops per mission, the fire ground altitude, and the ground altitude of the nearest accessible water source. These scenarios are summarized in Table 4.13, which was constructed based on the analysis of real firefighting mission profiles obtained from Flightradar24 records of the Italian firefighting department. The methodology employed to construct this sampling table is detailed in Appendix B, where the actual operational scenarios are systematically collected and analysed to derive the representative mission set used for sizing.

An immediate consequence of this strategy is the generation of multiple families of configurations resulting from the SBO problem, whose formal definition, analogous to that of the passenger transport variant, is provided in Table 4.14, again supported by the "pymoo" multi-objective optimization framework, as well as by enhanced SBO capabilities of SBArchOPT. For each considered scenario, a family of seaplane configurations is obtained that satisfies the imposed design requirements while achieving optimal performance with respect to the selected objective functions. Consequently, the subsequent post-processing trade-off analysis becomes a critical step for identifying the most suitable baseline architecture to guide the preliminary design phase.

4.5.2 Results and Discussion

The high dimensionality of both the design space and the objective function space renders the post-processing and interpretation of the results obtained from the SBO

Table 4.14: Formulation of the surrogate-based optimization problem for the design of the aerial firefight seaplane.

	Function/Variable	**Nature**	**Quantity**	**Note(s)**
minimize	DOC	cont.	1	-
	$1/\mathrm{En}_{\mathrm{factor}}$	cont.	1	-
	$1/\eta_{\mathrm{ops}}$	cont.	1	-
			3	**Total Objectives**
with respect to	P/W	cont.	1	-
	W/S	cont.	1	-
	AR_{w}	cont.	1	-
	λ_{w}	cont.	1	-
	t/c	cont.	1	-
	$\mathrm{X}_{\mathrm{LE,w}}$	cont.	1	-
	$\mathcal{V}_{\mathrm{H}}$	cont.	1	-
	$(\mathrm{t/c})_{\mathrm{H}}$	cont.	1	-
	Λ_{H}	cont.	1	-
	$\mathcal{V}_{\mathrm{V}}$	cont.	1	-
	$(\mathrm{t/c})_{\mathrm{V}}$	cont.	1	-
	Λ_{V}	cont.	1	-
	M_{CR}	cont.	1	-
	V_{CL}	cont.	1	-
	$\mathrm{M}_{\mathrm{drop}}$	cont.	1	-
			15	**Total variables**
subject to	$\mathrm{d}_{\mathrm{TO}} \leq 1\,850.0$ ft	cont.	1	-
	$\mathrm{d}_{\mathrm{LND}} \leq 1\,850.0$ ft	cont.	1	-
	MTOM $\leq 19\,000.0$ lb	cont.	1	-
	$\mathrm{h}_{\mathrm{Ceil,\,AEO}} \geq 25\,000.0$ ft	cont.	1	-
	Wingspan ≤ 78.74 ft	cont.	1	ICAO B category
	Payload ≥ 540.0 US Gal.	cont.	1	-
	$\mathrm{W}_{\mathrm{F,\,max}} \geq \mathrm{W}_{\mathrm{F}}$	cont.	1	-
	$\mathrm{h}_{\mathrm{fire}} = \mathrm{h}_{\mathrm{fire,\,scenario}}$	cont.	1	Scenario constraint.
	$\mathrm{h}_{\mathrm{water}} = \mathrm{h}_{\mathrm{water,\,scenario}}$	cont.	1	Scenario constraint.
	$\mathrm{N}_{\mathrm{drop}} = \mathrm{N}_{\mathrm{drop,\,scenario}}$	int.	1	Scenario constraint.
			1	**Total int. constraints**
			9	**Total cont. constraints**
			10	**Total constraints**

Table 4.15: Overview of the SBO problem results. Number of generations for each use case, populations evaluated and total computational time.

Use Case	ID	Generations	N. Eval	Optimal Configs.	Elapsed Time
Pax. Transport	-	866	199 180	78	322 min
Aerial Firefight	1	591	88 650	22	112 min
	2	648	97 200	24	120 min
	3	697	104 550	31	129 min
	4	611	91 650	23	113 min
	5	732	109 800	35	140 min
	6	711	106 650	31	128 min
	7	751	112 650	35	145 min
	8	572	85 800	20	111 min

problems a non-trivial task. This complexity arises from the need to compare a large number of aircraft architectures simultaneously, not only in terms of their performance but also with respect to their architectural characteristics. In parallel, it is essential to critically assess the advantages and limitations of the surrogate-based design and optimization framework, particularly when compared against traditional conceptual design methodologies.

One immediate advantage of employing the SBO approach lies in the significant reduction of computational costs associated with the use of GA in large-scale design spaces. Table 4.15 provides an initial overview of the outcomes of the SBO problems, reporting, for each optimization case, the number of generations evaluated, the cumulative number of population samples processed, the number of optimal configurations identified by the optimizer and the total computational time required.

Both use cases are addressed using the NSGA-III algorithm [165, 171], as implemented in the “pymoo” package. NSGA-III belongs to the class of Evolutionary Many-Objective optimization (EMO) algorithms, and its initial population is generated through an LHS strategy, rather than conventional random initialization. This approach mitigates the risk of under-sampling and ensures a more uniform coverage of the design space. The main hyperparameters of the algorithm include the definition of reference directions, the population size, and the standard parameters common to any genetic algorithm, such as mutation and crossover operators.

The population size was determined by combining empirical tuning with conventional rules of thumb, which recommend selecting a population at least one order of magnitude larger than the number of design variables [70]. Following this guideline, a population size of 230 individuals was adopted for the passenger transport optimization problem, while 150 individuals were employed for the aerial firefighting optimization problem. The Simulated Binary Crossover (SBX) operator [172] was used as the crossover mechanism, owing to its ability to adaptively control the spread of offspring. Mutations were introduced through random bit-flip operations applied to offspring chromosomes, thereby ensuring diversity within the evolving

Table 4.16: Powertrain architecture distribution for the passenger transport seaplane. Labels consistent with those reported in Figure 4.11.

Powertrain Architecture	**Specification**
Turboprop	Conventional turboprop. Technological level consistent with assumptions outlined in § 3.5.
Hybrid-Turboprop	Parallel hybrid-electric architecture integrating a turboprop engine and electric machines powered by propulsive batteries. Technological level consistent with assumptions in § 3.5.
Hybrid-Piston	Parallel hybrid-electric architecture integrating a reciprocating diesel engine and electric machines powered by propulsive batteries. Technological level consistent with assumptions in § 3.5.

population. Finally, the Das-Dennis [173] approach is used to determine reference directions and obtain a more uniform distribution of solutions on the Pareto front.

Passenger Transport Seaplanes

According to Table 4.15, a total of 866 generations were analyzed for the passenger transport use case, resulting in nearly 200 000 evaluated seaplane configurations and 78 optimal solutions. The total computational effort amounted to more than five hours (322 minutes). Comparable outcomes were obtained for the aerial firefighting use case; however, due to the smaller dimensionality of its design space, fewer evaluations were required to identify the optimal solutions. The maximum computational time observed across the firefighting scenarios was 145 minutes (i.e., less than three hours).

A noteworthy aspect concerns the total number of evaluations required by the NSGA-III algorithm, which is inherently driven by the large size of the design space. A conventional optimization process, directly employing the original disciplinary models, would have required a comparable number of iterations. This stems from the fact that such disciplinary models are derived from the state of the art in aircraft design and performance analysis, which predominantly rely on procedural, rather than analytical, formulations, rendering the use of gradient-based algorithms impractical. Moreover, the computational effort associated with the evaluation of a single configuration was approximately 5.25 minutes[1] (induced by the necessity of integrating re-size laws and consistency constraints). Consequently, completing a single optimization problem without surrogate-based acceleration would demand more than six months of continuous analysis, a computational burden typically associated with high-fidelity optimization frameworks rather than with conceptual design stages.

A first approach to analyzing the outcomes of an SBO problem is to examine the distribution of solutions in the objective function space, with the aim of identify-

[1] Desktop PC with Intel Core i7 Processor (4x 3.6 GHz) and 32 GB DDR4 RAM.

Table 4.17: Mean value and standard deviation of the operating empty weight to maximum take-off mass ratio for each powertrain configuration of Figure 4.11.

Powertrain Architecture	**Mean Value**	**Standard Deviation**
Hybrid-Piston	0.732	0.015
Hybrid-Turboprop	0.668	0.020
Turboprop	0.626	0.007

ing performance trends. Figure 4.11 presents the pairwise scatter plots of the three objective functions optimized for the passenger transport design problem. In this representation, the economic performance is expressed in terms of Total Operating Costs (TOC), rather than DOC alone, to provide a more comprehensive assessment of the aircraft's economic competitiveness. Figure 4.11 also highlights the mixed-discrete nature of the design space. Specifically, the optimal configurations cluster into three distinct groups, corresponding to the different powertrain architectures explored by the optimization algorithm.

These powertrain architectures, summarized in Table 4.16, include: (i) conventional turboprop configurations, and (ii) battery-based hybrid-electric architectures coupled with either reciprocating diesel engines (operating on Diesel fuel) or turboprop engines (operating on Jet-A1). The adoption of Diesel fuel in the reciprocating engines, as opposed to conventional Jet-A1, is motivated by its lower specific fuel consumption, which substantially reduces mission fuel burn. Despite its higher unit cost, this translates into a net reduction in overall operating costs. Furthermore, reciprocating diesel engines offer an additional advantage in terms of acquisition costs, potentially reducing the cost of the powertrain system by up to 60%, as previously discussed in § 3.5.

A major drawback of reciprocating engines lies in their limited power output, which necessitates the use of multiple engines operating in parallel to achieve the required brake horsepower at the propeller shaft. Moreover, the inherently lower power-to-weight ratio of this engine class directly impacts the overall aircraft configuration, resulting in a higher ratio of operating empty weight to maximum take-off mass, $W_{OE}/MTOM$, compared to configurations employing turboprop engines. This trend is clearly illustrated in Table 4.17, which reports the average $W_{OE}/MTOM$ ratios and the corresponding population standard deviations for the optimal solutions. The penalty in structural efficiency subsequently translates into a significant reduction in range performance for reciprocating-engine variants, with range factors approximately 66% lower than those of hybrid-turboprop configurations and up to 81% lower compared to purely turboprop-powered alternatives. Such limitations, while partially offset by lower acquisition and operating costs, inevitably reduce the operational flexibility of reciprocating-engine aircraft and constrain their competitiveness in missions requiring extended range or high payload efficiency.

Table 4.17 also highlights the wider spread of the $W_{OE}/MTOM$ ratio observed in the hybrid-electric architectures, measured through the standard deviation, which

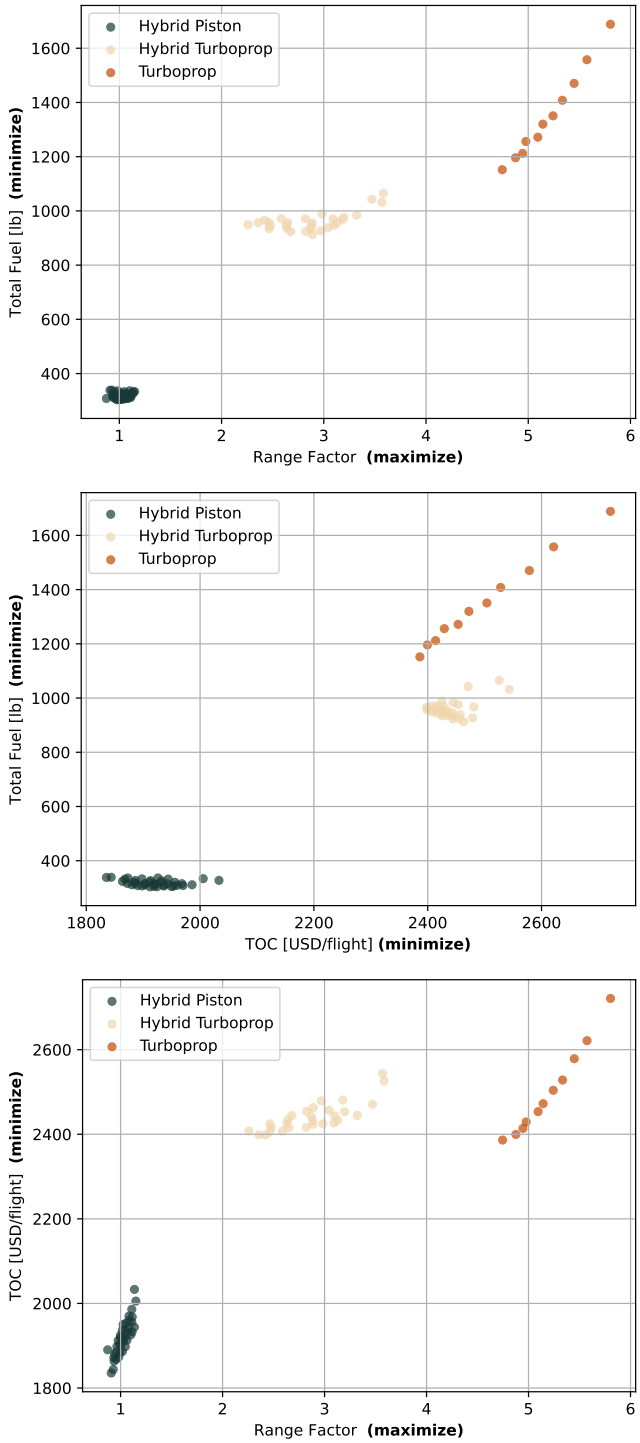

Figure 4.11: Solution space of the passenger transport SBO problem. The reference mission is specified in the TLAR table.

is approximately twice as large as that of the turboprop configurations. This increased variability is a direct consequence of the NSGA-III algorithm exploring multiple hybridization strategies. Such strategies significantly influence the sizing and weight of the electric powertrain components, particularly the batteries, which, being non-consumable, are included in the W_{OE}. Variations in hybridization levels strongly impact the trade-off between flight performance, fuel consumption, and aircraft weight, occasionally resulting in hybrid-electric configurations exhibiting even poorer environmental performance and higher consumption compared to their conventional counterparts. The root cause of this phenomenon can be traced to the snowball effect induced by the full MDA workflow in the DOE campaign, combined with the underlying sizing logic of the propulsive batteries. Specifically, the batteries must either be dimensioned to supply high power over short time intervals or designed with sufficient capacity to sustain extended cruise phases, both of which considerably affect in different ways the overall aircraft mass and performance.

Figure 4.12 illustrates the influence of the hybridization level, as defined in Eq. (4.8), on the fuel consumption of turboprop-based hybrid-electric configurations and on the rated power of the thermal engine. The data were extracted from the configurations pool generated during the DOE campaign and are intended to demonstrate that a given hybridization level, achievable through theoretically infinite combinations of hybridization factors, can yield both superior and inferior performance relative to conventional counterparts, also reported in Figure 4.12. This highlights the critical importance of employing a suitable optimization algorithm capable of managing hybridization ratios in order to fully exploit the potential of hybrid-electric architectures to enhance both environmental and economic performance. In particular, downsizing the thermal engine not only reduces kerosene consumption, making the engine operate close to its maximum efficiency point, but also decreases acquisition costs and, consequently, operating expenses. Consistently, among the optimal solutions, hybrid-turboprop configurations exhibit lower kerosene consumption and operating costs, positioning them at the lower end of the cost spectrum compared to conventional turboprop alternatives.

$$\text{Hybridization Level} = \frac{\Phi_{TO} + \Phi_{CL} + \Phi_{CR} + \Phi_{DS}}{4} \tag{4.8}$$

At the opposite end of the objective function space lie the configurations equipped with conventional turboprop engines. As shown in Figure 4.11, these architectures provide superior operational flexibility, primarily due to their higher range factor. However, this advantage comes at the expense of increased operating costs and higher fuel consumption, which in turn limits their potential to reduce the overall environmental footprint. By contrast, hybrid-electric turboprop configurations appear to offer a balanced trade-off, combining the high operational flexibility characteristic of conventional turboprops with improved economic performance and reduced fuel consumption, thereby representing an intermediate yet promising solution.

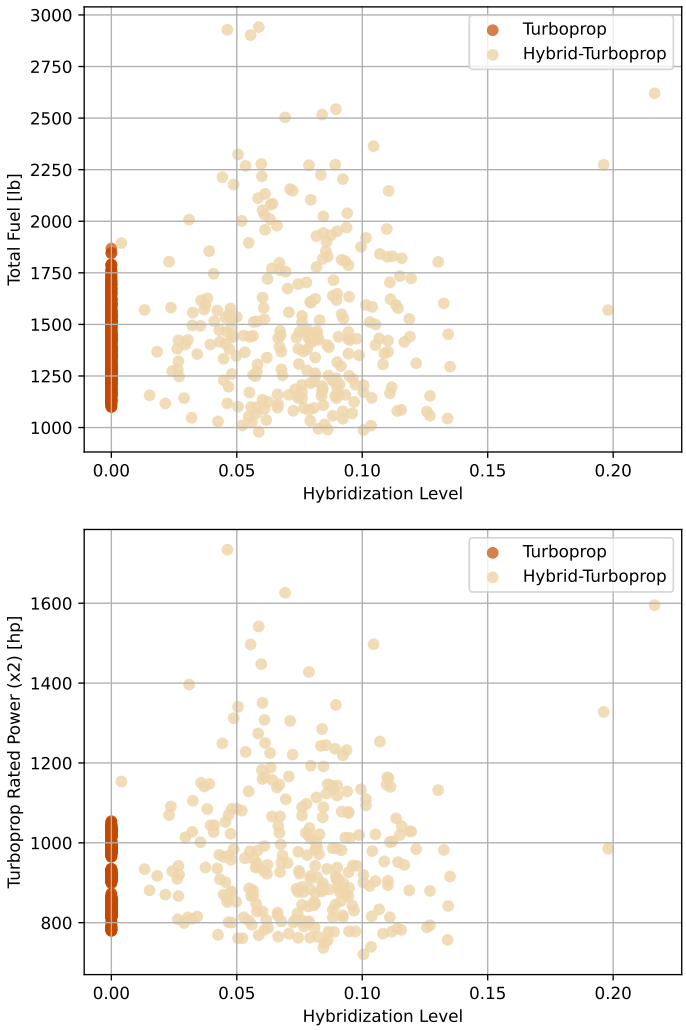

Figure 4.12: Effect of the hybridization levels on the fuel consumption and on the thermal engine rated power of hybrid-electric configurations integrating turboprop engines.

Table 4.18: Summary of the main architectural and operational features of the passenger transport optimal seaplanes.

Item	**Turboprop**		**Hybrid-Electric Reciprocating**		**Hybrid-Electric Turboprop**	
	min	max	min	max	min	max
S_w	33.0 m^2	35.0 m^2	37.5 m^2	42.0 m^2	34.5 m^2	37.7 m^2
AR_w	8.3	9.0	7.5	8.5	7.5	8.8
$(t/c)_{mean}$	0.12	0.12	0.14	0.18	0.15	0.16
λ_w	0.60	0.77	0.70	0.92	0.64	0.84
$\mathcal{V}_H$	0.60	0.81	0.90	1.15	0.76	0.92
Λ_H	7.0 deg	11.0 deg	13.6 deg	15.0 deg	0.0 deg	5.0 deg
λ_H	0.95	1.00	0.95	1.00	0.65	0.85
S_V	4.9 m^2	5.3 m^2	5.6 m^2	6.1 m^2	5.0 m^2	5.7 m^2
Λ_V	26.0 deg	27.0 deg	28.0 deg	32.0 deg	33.0 deg	38.0 deg
λ_V	0.65	0.70	0.49	0.66	0.63	0.70
P_0[a]	725.0 hp	975.0 hp	290.0 hp[b]	305 hp[b]	705.0 hp	785.0 hp
E_{bat}	-	-	185.0 kWh	305.0 kWh	109.0 kWh	224.0 kWh
M_{CR}	0.33	0.35	0.29	0.33	0.28	0.33
MTOM	13 340.0 lb	14 100.0 lb	15 000.0 lb	17 050.0 lb	13 490.0 lb	15 025.0 lb

[a] Single Engine.
[b] Four thermal engines are required in the piston-based hybrid-electric architectures.

One of the main limitations of evolutionary algorithms in exploring sets of optimal solutions lies in their limited ability to perform trade-offs among equally satisfactory architectures, as this task is inherently constrained by the definition of Pareto-optimality. Table 4.18 summarizes the key architectural and operational features of the solutions identified in Figure 4.11. To highlight the variability across the resulting powertrain architectures while preserving a concise representation, these features have been grouped in terms of their minimum and maximum values.

The trends reported in Table 4.18 do not reveal any anomalies, indicating that both the underlying MLP models and the optimization problem are correctly formulated. Pure turboprop configurations are generally characterized by relatively small wing surfaces and higher aspect ratios, aimed at minimizing total drag. In parallel, the operating cruise Mach number and thermal engine power are maximized to reduce the mission block time and, consequently, the mission DOC, which for these configurations are predominantly driven by time-related items. Conversely, hybrid-electric architectures rely on smaller thermal engines and lower cruise Mach numbers, typically close to the point of maximum lift-to-drag ratio, thereby prioritizing reductions in fuel consumption and consumable costs over time-dependent operating costs. These architectures also exhibit larger wing surfaces and lower aspect ratios compared to conventional turboprops, a configuration not typically associated with reduced fuel consumption since higher engine power would normally be required to ensure satisfactory flight performance and compliance with design constraints. However, this limitation is addressed by the optimization algorithm through the ex-

ploitation of hybridization strategies, whereby the electric machines are appropriately sized to provide the required excess power. This approach effectively counterbalances the associated increase in MTOM, ensuring that all solutions remain compliant with EASA CS-23 regulations.

Aerial Firefight Seaplanes

The eight scenarios defining the aerial firefighting use case render the representation of the SBO problem results non-trivial. An initial comparison of the resulting families of configurations, analogous to the passenger transport case, can be performed by evaluating their performance with respect to the adopted objective functions. Figure 4.13 provides an alternative visualization to the scatter plots employed in the previous analysis. In this case, box plots are adopted to capture the statistical distribution of performance within each family of solutions. This representation offers a more informative overview than scatter plots when comparing multiple families simultaneously, as it highlights central tendencies, variability, and the presence of outliers. By doing so, it enables a clearer understanding of how operational parameters and architectural features influence the overall performance across the different objective functions.

Figure 4.13 reveals a clear trend in the firefighting efficiency metric, with the average value increasing progressively from Scenario 1 to Scenario 8. This behavior is directly attributable to the scenario-dependent operating conditions. Specifically, as the number of drops per mission increases, the overall mission duration also rises, since a larger number of water releases must be performed. It is important to recall that firefighting efficiency, as defined in this study, accounts for both the total payload delivered, which, at the conceptual stage, is assumed to scale linearly with the number of drops given a constant payload per release, and the mission duration. The observed increase in efficiency arises because the rate of increase in mission time is lower than the rate of increase in payload delivered, leading to a growing ratio and, consequently, an improvement in firefighting efficiency.

In contrast, the analysis of operating costs reveals the formation of two distinct performance clusters. Shorter missions, characterized by a reduced number of drops, exhibit lower fuel consumption and shorter block times; however, the limited amount of payload delivered causes the cost per unit of suppressant to remain relatively high. Conversely, missions involving a higher number of drops (e.g., 13) incur greater absolute costs due to extended mission durations and increased fuel use, yet these costs are distributed over a substantially larger delivered payload, ultimately reducing the unit operating cost.

The influence of the altitude differential between the fire location and the water source manifests differently across the two considered metrics, depending on the mission scenario. Specifically, its effects are more pronounced in the firefighting efficiency metric for longer missions, whereas in the case of operating costs, the impact

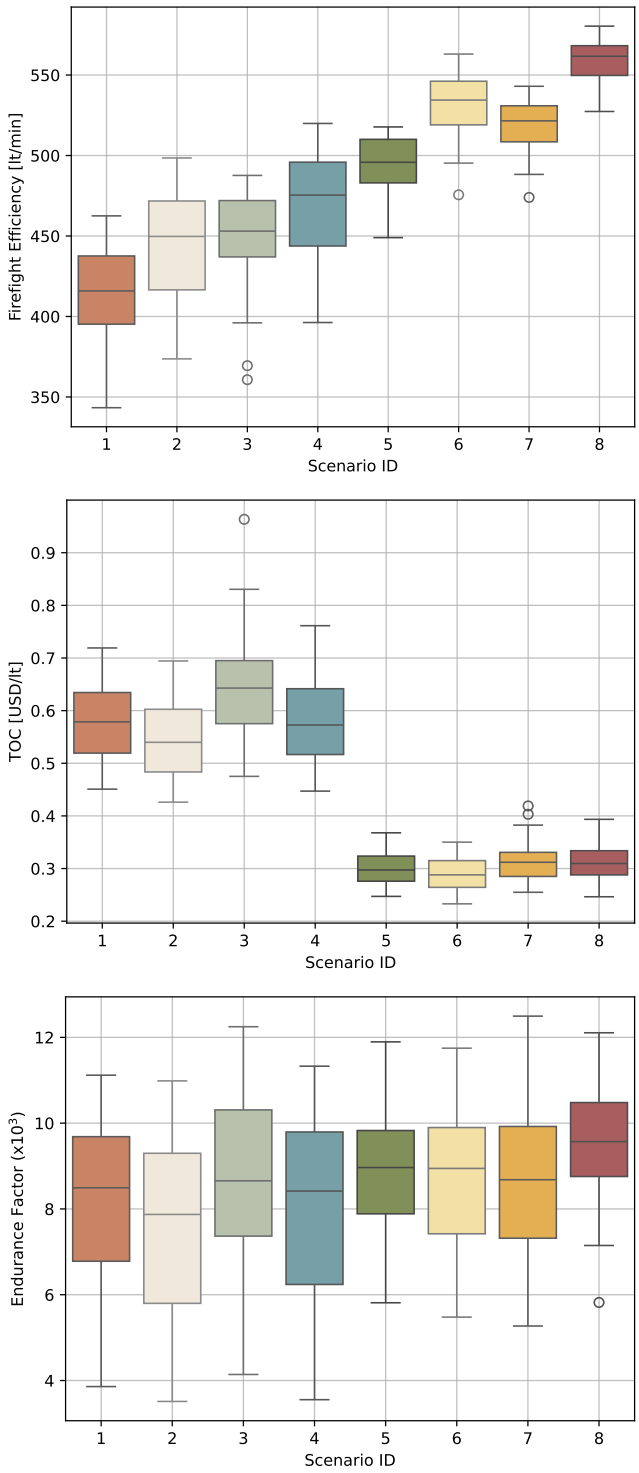

Figure 4.13: Performance of each family of configurations resulting from the 8 scenarios optimized in the SBO problem. The reference mission is specified in the TLAR table.

Table 4.19: Mission block time statistics.

Scenario ID	Median	$Q_{0.25}$	$Q_{0.75}$	Trend
1	56.2 min	54.4 min	59.3 min	↑
2	52.4 min	50.7 min	55.9 min	↓
3	61.2 min	58.6 min	68.3 min	↑
4	56.6 min	53.5 min	61.1 min	↓
5	90.1 min	87.8 min	91.7 min	↑
6	83.0 min	81.7 min	86.6 min	↓
7	94.2 min	92.5 min	99.5 min	↑
8	87.2 min	85.8 min	88.3 min	↓

is more evident in shorter missions characterized by a reduced number of drops. A larger altitude differential increases the climb and descent times required for each cycle, thereby extending the total mission block time, which average values and reference quantiles, across scenarios, are summarised in Table 4.19. This, in turn, negatively affects firefighting efficiency while simultaneously raising time-related operating costs. For longer missions, the repeated climbs and descents accumulate and significantly contribute to the overall duration, making the effect more evident in the efficiency metric. Conversely, in shorter missions, the relative increase in block time has a stronger impact on operating costs, which explains why scenarios with lower altitude differentials consistently exhibit reduced operational expenses.

Finally, no significant trend can be observed in the endurance factor. Each family of optimal configurations exhibits comparable performance, indicating a weak correlation between endurance performance and scenario-specific operating conditions. This weak correlation can also be quantified. By considering the median value of each family as a random variable, assumed to follow a Student's t-distribution (since only the population mean and variance can be estimated), it is possible to measure the confidence interval within which any given observation, x, can be considered statistically indistinguishable from the population mean. Using a two-tailed t-distribution with a 95% confidence level, the corresponding confidence interval can be determined through the Student's t-test, as expressed in Eq. (4.9).

$$\bar{x} - 2.365\frac{s}{\sqrt{n}} \leq x \leq \bar{x} + 2.365\frac{s}{\sqrt{n}} \tag{4.9}$$

According to the results reported in Table 4.20, only the second and last scenarios exhibit median values of the endurance factor that fall outside the boundaries of the calculated confidence interval, with values of 7.9 and 9.4, respectively. This indicates that only two scenarios display statistically significant deviations in performance relative to the average. Such findings suggest that the optimization algorithm consistently converges toward similar aircraft architectures across most scenarios, a trend that will be further discussed in the following sections.

The analysis of results also highlights an inherent limitation in the use of evolution-

Table 4.20: Results of the Student's t-test on the endurance Factor

Item	**Value**	**Note(s)**
$\bar{x}$	8.7	Endurance Factor ($\times 10^3$) mean.
s	0.49	Endurance Factor ($\times 10^3$) variance.
n	8	Number of repetitions (scenarios).
v	7	Degrees of freedom of the Student t-distribution.
$t_{0.95}$	2.365	95% confidence level observation.
$\bar{x} - 2.365\, s/\sqrt{n}$	8.2	-
$\bar{x} + 2.365\, s/\sqrt{n}$	9.1	-

ary optimization strategies for the exploration of vehicle architectures, particularly when combined with machine learning models and surrogate-based approaches. Any performance indicator that is not explicitly integrated into the MLP model, either as an output variable, a constraint, or part of the optimization objectives, remains a hidden factor that cannot be evaluated at the end of the process. Consequently, while the capability of exploring multiple families of vehicle architectures through optimization frameworks supported by machine learning offers clear advantages over conventional conceptual design methods, it also introduces additional requirements during the planning phase. Specifically, a careful and systematic identification of the most influential performance indicators, as well as the corresponding vehicle features that drive them, is essential to ensure that critical effects are neither neglected nor overlooked during the optimization process.

Chapter 5

The Preliminary Design and Perfomance Assessment

Contents

5.1 Introduction

UNLIKE the conceptual design stage, the definition of the aircraft preliminary design phase remains somewhat ambiguous, with different authors proposing varying interpretations of its onset and scope. For instance, Raymer defines the preliminary design phase as beginning once all major configuration changes have been completed [22]. Conversely, Torenbeek characterizes this phase as one in which substantial modifications are still possible, with the aircraft configuration becoming frozen only at the end of the process [21]. Nicolai offers an intermediate perspective, suggesting that while continuous modifications may occur during preliminary design, they should remain relatively minor and primarily serve to fine-tune aircraft performance without introducing major alterations to the overall configuration [25].

In this research work, the approach proposed by Nicolai is adopted as the foundation for guiding the preliminary design and assessment of the seaplane, with the broader objective of enhancing the overall attractiveness of this aircraft category. The conceptual design phase demonstrated the existence of distinct families of optimal configurations capable of independently serving both passenger transport and aerial firefighting missions. A promising pathway toward renewed interest in seaplanes lies in the development of multi-role platforms, capable of fulfilling passenger transport and aerial firefighting functions with minimal modifications and limited performance penalties [18]. Building on this rationale, an immediate consequence of the proposed research question reads:

How can preliminary design methodologies be restructured to enhance operational attractiveness by integrating multi-role capabilities, achieving an optimal balance between performance and cost-effectiveness in innovative seaplanes ?

The present chapter outlines a strategy to transition from the promising configurations identified during the conceptual stage toward preliminary design solutions that enable multi-role capabilities. To this end, a multi-criteria decision analysis is employed to reduce the dimensionality of the solution space and to identify two representative baseline configurations: one optimized for passenger transport and one for aerial firefighting. These baselines are then integrated into an optimization-based design framework aimed at enhancing commonality in architecture and operational strategies. The process leverages conventional figures of merit and design variables relevant to aircraft preliminary design, while also incorporating mission-specific performance indicators, design parameters, and operational procedures tailored to the unique requirements of seaplanes in both passenger transport and aerial firefighting roles.

5.2 Multi Criteria Decision Analysis

The outcome of the SBO problems consists of families of optimal solutions, distributed along a Pareto front, each providing equally satisfactory performance with respect to the defined objectives and constraints. In this context, Multi-Criteria Decision Analysis (MCDA) serves as a valuable tool for ranking multiple design alternatives according to the goals or preferences of the decision-maker. The ultimate aim is to identify a single passenger transport seaplane and a single aerial firefighting seaplane that can be adopted as baseline configurations to support the development of a multi-role seaplane solution.

The integration of MCDA into the selection process for unique seaplane configurations can be structured as a three-step procedure: (i) definition of the evaluation criteria, (ii) establishment of the weighting strategy, and (iii) selection of the decision-making algorithm. The criteria defining the decision-making objective can

be directly derived from the set of objective functions already embedded in the SBO campaign, thereby enabling MCDA to perform trade-offs among solutions that are otherwise equally optimal. While the selection of evaluation criteria is relatively straightforward, given that the objective remains the identification of promising configurations based on performance indicators that justify the development of a seaplane, the choice of an appropriate weighting strategy and decision-making method is considerably more challenging.

The relatively small number of criteria in each use case could, in principle, justify the adoption of subjective weighting methods, which are easier to interpret and directly reflect the preferences of the decision-maker. However, it is important to emphasize that the criteria employed in this study are selected from among the optimization objectives, all of which carry equal significance within the SBO framework. Consequently, the manual assignment of weights would introduce bias into the identification of suitable configurations, as it would reflect the decision-maker's subjective preference for one or more criteria. Such bias would undermine the neutrality of the SBO process and diminish the validity of its results. To overcome this limitation, objective weighting methods are adopted, even in the presence of a limited number of criteria, thereby eliminating non-quantifiable effects introduced by the decision-maker. In this study, the MEthod based on the Removal Effects of Criteria (MEREC) [174] has been implemented as the weighting strategy, as it determines the importance of each criterion by quantifying the impact of its removal on the overall performance of the alternatives.

At present, many, if not all, available MCDA methods satisfy the formal requirements for addressing decision-making problems and, in principle, can be applied independently of the specific problem to be solved. However, it must be acknowledged that despite the abundance of available methods and their apparent universal applicability, no single method can be considered universally correct [175]. The application of multiple methods to the same multi-criteria decision problem is therefore a common practice, offering both advantages and disadvantages. The primary advantage lies in the possibility of comparing results across different methods to assess the robustness of the evaluation. If several methods converge toward the same solution, which best reflects the preferences of the decision-maker, the decision can be considered reliable without the need for further validation. Conversely, the main drawback arises when different methods provide conflicting recommendations. In such cases, assessing the validity of each outcome becomes complex, and additional support mechanisms are required. These may include the integration of supplementary decision-support methods or the involvement of domain experts to critically evaluate each recommendation and determine which solution most closely aligns with the objectives of the decision-maker.

Four different MCDA methods were applied to both use cases: the Stable Preference Ordering Towards Ideal Solution (SPOTIS) method [176], the Technique for Order Preference by Similarity to an Ideal Solution (TOPSIS) method [177, 178], the VlseKriterijumska Optimizacija I Kompromisno Resenje (VIKOR) method [177, 178],

and the classical Weighted Sum Method (WSM). These methods are commonly employed in discrete MCDA problems, which is consistent with this study, as the task is to rank and score a finite set of alternatives represented by the candidate seaplane configurations.

The SPOTIS method evaluates each alternative by computing its distance from an ideal solution, which may correspond to the one that minimizes all criteria simultaneously, maximizes them, or reflects a general reference point chosen by the designer. The best alternative is then identified as the one with the minimum distance, i.e., the lowest score. By contrast, the TOPSIS method considers both a positive ideal solution (representing the direction of desired improvement) and a negative ideal solution (representing the direction of deterioration). Each alternative is evaluated by calculating its distance to both references, with the final score obtained as the ratio of the distance to the positive ideal solution to the sum of both distances, as expressed in Eq. (5.1). The optimal alternative is thus the one achieving the highest score, as it is simultaneously closest to the positive ideal and farthest from the negative ideal.

The VIKOR method, like the previous approaches, is also based on the distance from an ideal solution but is particularly suited for problems involving conflicting criteria, such as those addressed in this work. It identifies a compromise solution that balances trade-offs between competing objectives. Finally, the WSM constitutes the simplest MCDA approach, where the best alternative is defined as the one that maximizes the weighted sum of the selected criteria.

$$S = \frac{PD}{PD + ND} \tag{5.1}$$

The multi-criteria decision-making problems for both use cases were addressed using the capabilities integrated into the PyMCDM framework [179]. This framework enabled a consistent comparison of different MCDA algorithms as well as the evaluation of alternative weighting strategies, including the MEREC approach.

5.2.1 Passenger Transport Seaplane

The first step in performing an MCDA consists of constructing a decision matrix, i.e., a table in which each row represents an alternative and each column corresponds to a decision criterion. In the passenger transport use case, the SBO process yielded 78 seaplane configurations. Consequently, the decision matrix has a size of 78×3, as three criteria, coinciding with the optimization objectives, are considered.

Each criterion must then be assigned an appropriate weight. To avoid subjective biases introduced by the decision maker, the MEREC algorithm was employed to derive criteria weights. The resulting values are reported in Table 5.1, where they are also compared to the hypothetical case in which equal importance is assigned to all criteria.

Table 5.1: MEREC weights for the passenger transport use case, compared to the equal weights approach.

Criterion	**MEREC Weight**	**Equal Weight**	**Note(s)**
Total Fuel [lb]	0.158	0.333	-
Range Factor	0.776	0.333	-
TOC [USD/flight]	0.066	0.333	-
	1.00	**1.00**	**Sum**

According to the MEREC strategy, which is based on evaluating the effects of criterion removal, the range factor induces the largest variation in the performance of solutions when excluded from the set of criteria. Consequently, it receives the highest weight, followed by total fuel consumption, while operating costs exhibit the least influence. In parallel, Figure 5.1 presents the ranking of the seaplane configurations, reduced for brevity to the 26 best-performing alternatives out of the 78 total, ordered in ascending order from the most to the least suitable configuration. Based on this ranking, configuration A_{23} emerges as the most promising candidate, across all methods, with respect to the assigned criteria and weights and is therefore identified as the preferred baseline for guiding the preliminary design stage.

It is worth noting that the four implemented methods exhibit a high level of agreement in the evaluation of many alternatives. In particular, they show perfect consistency in identifying the four best-performing configurations, with discrepancies emerging only for a limited subset of alternatives. A quantitative way to assess the degree of agreement between methods is to compute the correlation between their respective rankings. Specifically, the ranking assigned to each alternative by each method is used to calculate the Pearson correlation coefficient, which is summarized in the heatmap presented in Figure 5.2. The results indicate a strong pairwise agreement across all methods, with the largest deviation observed for the TOPSIS method. Nevertheless, even in this case, the correlation remains very high, at 0.98.

5.2.2 Aerial Firefight Seaplane

Similarly to the procedure adopted in the SBO problem, the application of MCDA techniques requires an independent analysis of the configurations' performance across the eight operating scenarios. In both cases, the underlying rationale is to prevent the evaluation framework from favoring solutions that appear optimal under aggregated conditions but fail to account for scenario-dependent effects. Thus, the integration of MCDA ensures that the selected seaplane candidate is not only promising with respect to the chosen performance indicators but also robust across the range of operating conditions, eliminating the bias towards longer missions, characterized by reduced operating costs and high operational efficiency.

Eight independent MCDA analyses were therefore conducted; each aimed at iden-

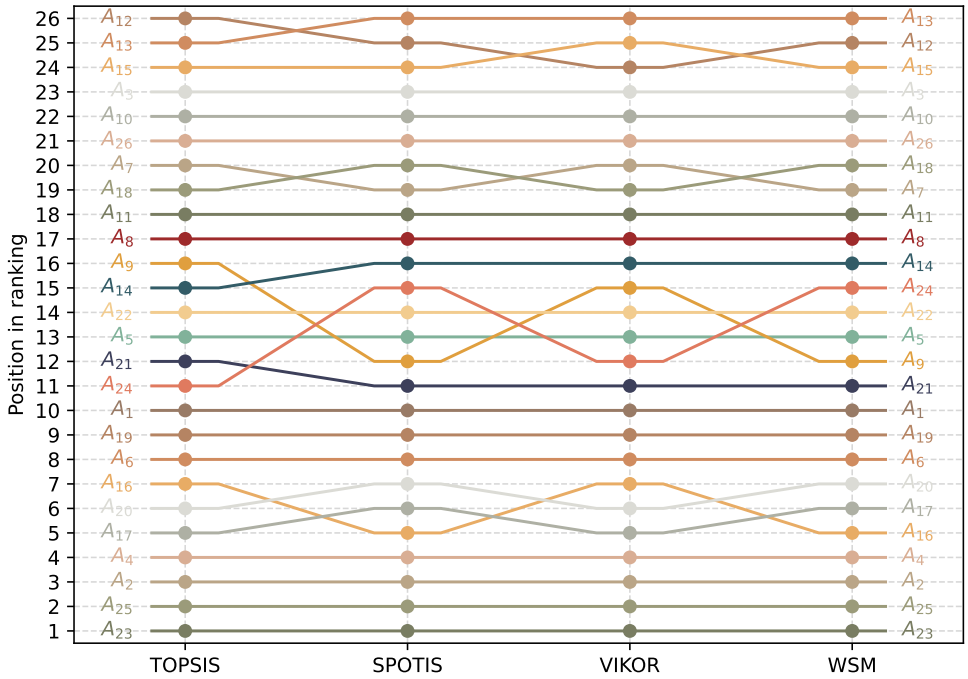

Figure 5.1: Passenger transport seaplane solutions ranking.

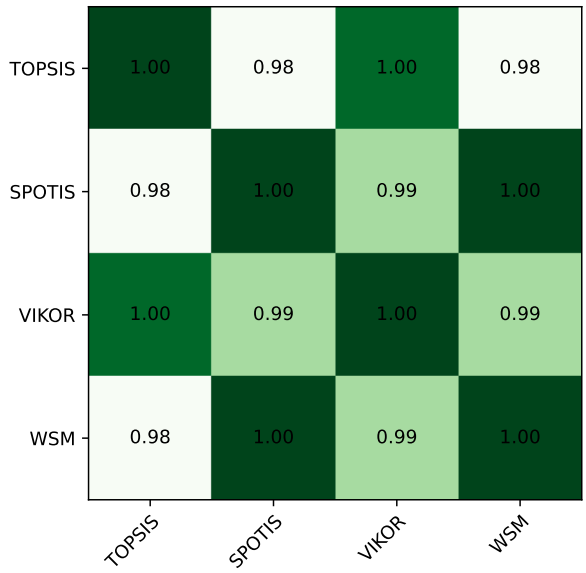

Figure 5.2: Heatmap of the Pearson's correlation coefficient among the rankings of the implemented MCDA methods for the passenger transport use case.

Table 5.2: MEREC weights for each scenario in the aerial firefight use case.

Scenario ID	Weight Endurance Factor	Weight TOC [USD/lt]	Weight η_{ops} [lt/min]
1	0.652	0.195	0.153
2	0.638	0.223	0.139
3	0.532	0.314	0.154
4	0.636	0.234	0.130
5	0.578	0.293	0.129
6	0.595	0.263	0.142
7	0.555	0.345	0.100
8	0.624	0.305	0.071

tifying a suitable seaplane candidate within the corresponding operating scenario. The weights assigned to the selected criteria are reported in Table 5.2. Notably, the endurance factor, contrary to its limited influence in the results of the SBO problem, plays a more significant role than both operating costs and operational efficiency. This increased importance is primarily driven by the variability (spread) of the endurance factor, rather than its mean value, which was higher compared to the other two criteria. Furthermore, two distinct clusters can be observed in the weight matrix: in scenarios characterized by a limited number of drops, the endurance factor assumes greater importance, whereas in longer missions, defined by a higher number of drops, its relative weight decreases in favour of total operating costs, which become the dominant driver of performance in such conditions.

The results obtained are consistent with those observed for the passenger transport case and are therefore not described in detail. In this section, only the ranking flows and the Pearson correlation coefficient heatmaps for two representative scenarios are reported, namely Scenario 5 and Scenario 7, which proved to be the most challenging for the MCDA methods. The ranking flows across the different methods, shown in Figure 5.3 and Figure 5.4 for Scenarios 5 and 7, respectively, reveal widespread discrepancies among almost all MCDA methods. These differences are evident even for the highest-performing configurations, which the methods struggled to consistently identify. Ultimately, configuration A_{21} was selected as the best alternative in both Scenario 5, where only the VIKOR method yielded a substantially different ranking, and Scenario 7, where the TOPSIS approach resulted in the major differences. It should be noted, however, that although the best-performing configurations share the same label (A_{21}), they correspond to different sets of vehicles. The limited agreement among methods is further confirmed in Figure 5.5, which presents the heatmaps of the pairwise correlation coefficients for both scenarios.

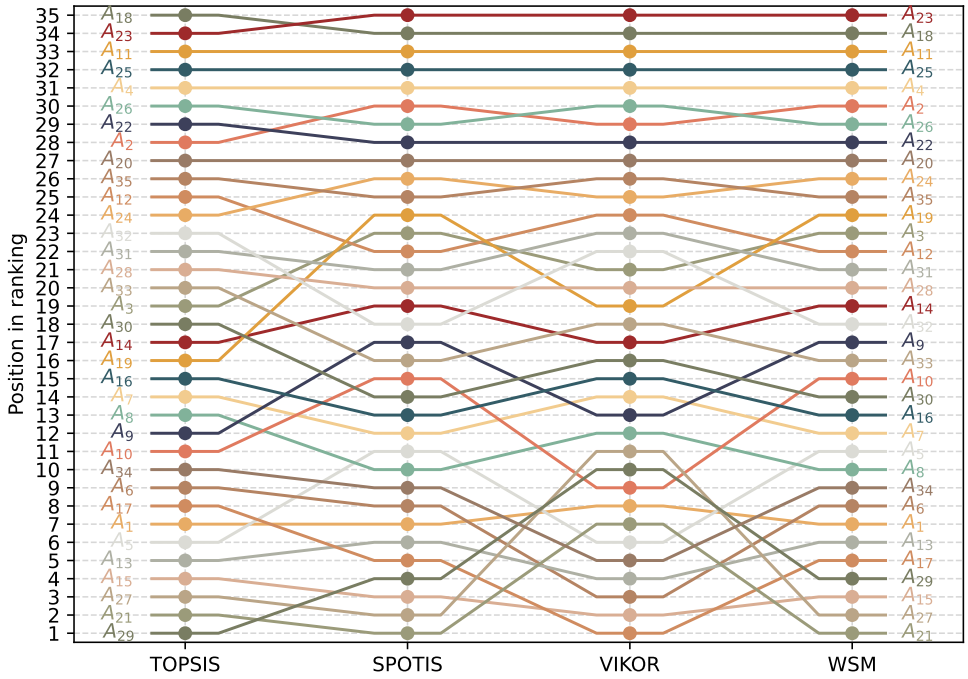

Figure 5.3: Aerial firefight Scenario 5 solutions ranking.

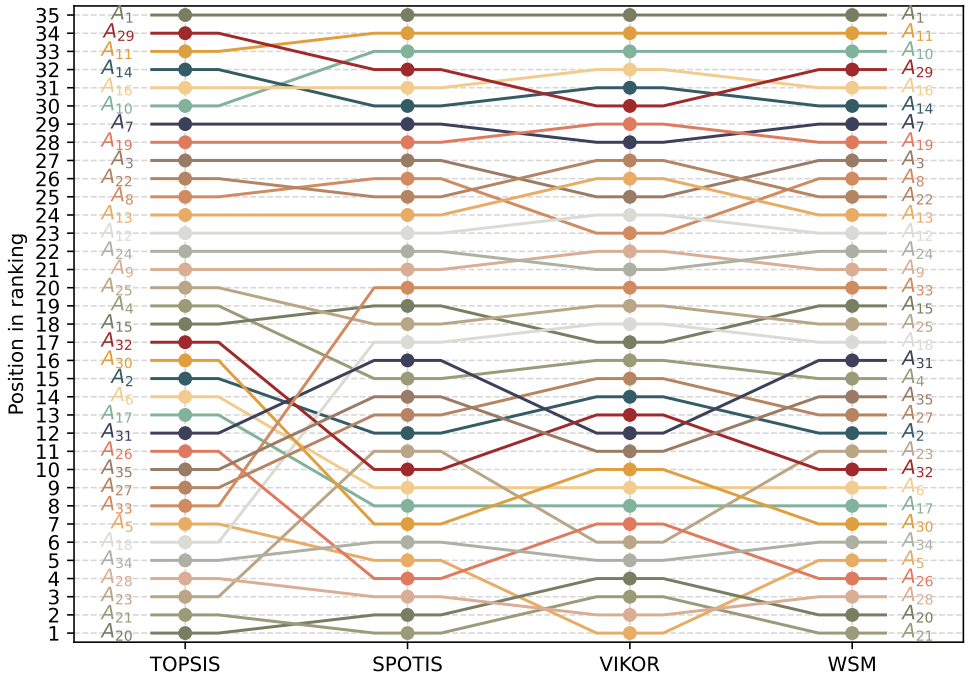

Figure 5.4: Aerial firefight Scenario 7 solutions ranking.

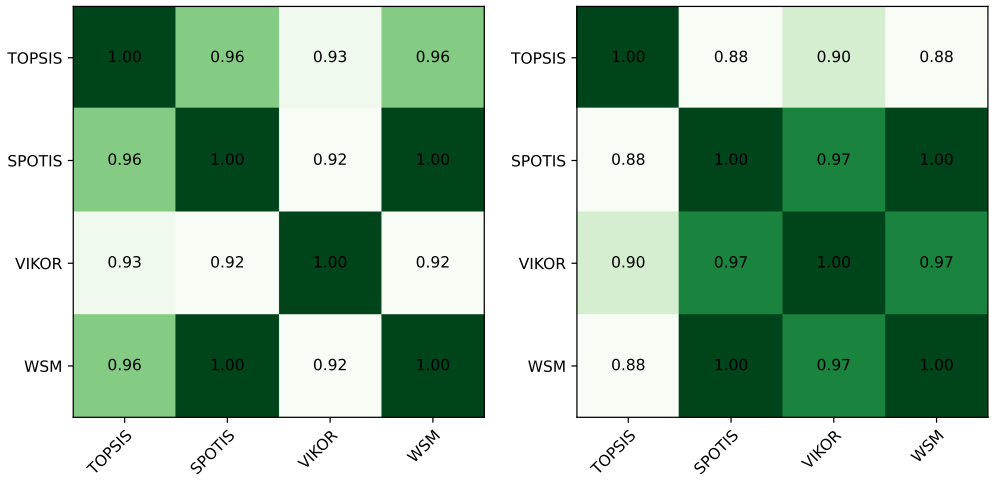

(a) Scenario 5 (b) Scenario 7

Figure 5.5: Pearson's correlation coefficient heatmaps for the Scenario 5 and Scenario 7 of the aerial firefight use case.

5.2.3 Baseline Seaplanes

The application of the MCDA enabled the identification of two promising seaplane configurations, one for each use case, which serve as the starting point for the preliminary design phase aimed at developing multi-role vehicle architectures. These baseline configurations are summarized in Table 5.3.

The comparison between the two configurations highlights substantial differences in both architectural features and operational parameters. The passenger transport variant is characterized by a wing area approximately 30% smaller than that of the firefighting variant. Similarly, the rated power of its thermal engine is about 40% lower, a reduction made possible by the additional excess power supplied by the electric machines, which are powered by two battery packs providing a total capacity of 261.28 kWh. Another relevant difference lies in the cruise Mach number, which is also lower in the passenger transport configuration. These distinctions directly reflect the optimization strategy applied during the conceptual design stage, where the passenger transport variant was tailored to maximize fuel efficiency and reduce operating costs. Conversely, the firefighting variant was optimized to prioritize operational efficiency and endurance, which necessitated more powerful propulsion systems capable of achieving higher operational speeds, thereby reducing turnaround times, as well as a larger wing area to accommodate increased fuel capacity. In both use cases, the climb speeds are nearly identical, corresponding to the velocity at which the maximum rate of climb is achieved. This choice minimizes the time required to reach cruise altitude and, under constant engine settings and fuel flow, also reduces fuel consumption during climb conditions.

Table 5.3: Baseline seaplanes configurations for the preliminary design phase.

Item	**Pax. Transport**	**Aerial Firefight**
S_w	35.17 m^2	49.73 m^2
AR_w	7.95	7.52
$(t/c)_{mean}$	0.155	0.130
λ_w	0.884	0.674
$\mathcal{V}_H$	1.13	0.835
Λ_H	8.5 deg	0.0 deg
λ_H	0.50	1.0
S_V	5.45 m^2	7.67 m^2
Λ_V	35.0 deg	30.0 deg
λ_V	0.68	0.48
Powertrain	Hybrid-Turboprop	Turboprop
P_0	720.5 hp	1 200.0 hp
E_{bat}	261.28 kWh	-
M_{CR}	0.28	0.33
V_{CL}	110.0 KTAS	112.5 KTAS
MTOM	15 396.8 lb	16 137.6 lb
Range factor	3.856	-
Total Fuel	1 107.3 lb	2 292.7 lb
TOC	2 580.0 USD	0.35 USD/lt
Endurance Factor	-	11×10^{-3}
η_{ops}	-	500.0 lt/min
d_{TO}	1 409.5 ft	1 109.0 ft
d_{LND}	1 760.0 ft	1 640.4 ft
$h_{Ceil,\ AEO}$	25 690.0 ft	27 700.0 ft

Minimal differences are observed in the size of the horizontal and vertical tailplanes, with both surfaces being slightly smaller in the passenger transport variant in order to minimize parasite drag contributions. The vertical tailplane exhibits a higher sweep angle, which shifts its aerodynamic centre rearward, thereby increasing the moment arm relative to the aircraft centre of gravity and enabling equivalent directional control authority with a reduced surface area. Similarly, the increased sweep angle allows for a rearward positioning of the tail-mounted horizontal tailplane. This effect is further enhanced by its 8.5 deg sweep angle, which increases the moment arm and consequently allows for a reduction in the exposed surface area without compromising longitudinal stability and control effectiveness.

5.3 Preliminary Design Towards Commonality

To ensure a preliminary design process consistent with Nicolai's definition, it is essential to allow for controlled modifications of the existing configurations, enabling a more rigorous technical assessment without introducing major architectural alterations. The objective of this phase is to achieve a finalized, or "frozen," configuration through refined geometric development, detailed component weight estima-

tion, and improved evaluations of performance, stability, and controllability. These refinements aim to enhance mission capabilities, improve certifiability, and provide a more accurate assessment of both operating and production costs.

When addressing the preliminary design of aircraft intended for multi-role operations, it becomes necessary to manage multiple baseline configurations derived from the conceptual design stage, each optimized for a specific single-role mission. In the context of this research, multi-role seaplane operations are pursued by combining passenger transport and aerial firefighting capabilities, thus requiring the integration and reconciliation of two distinct baseline configurations.

Since each baseline configuration is optimized exclusively for its respective reference operating scenario, it is evident that adapting a design to an entirely different mission profile without addressing operational limitations and performance penalties, for instance, converting the passenger transport variant to perform aerial firefighting missions solely by rearranging the internal layout and equipment, would result in impractical design solutions and degraded performance outside the bounds of the original role. A viable strategy to enable multi-role operations is to employ a preliminary design process focused on enhancing commonality characteristics while simultaneously optimizing performance metrics and satisfying the constraints associated with both operational roles.

Implementing such an approach requires:

- the identification of performance metrics and objectives inherited from the conceptual design phase, as well as those introduced in refined performance assessments;
- the integration of disciplinary models extending beyond statistical correlations between aircraft features and performance, incorporating low- and medium-fidelity physics-based and parametric analyses for subsystem design and performance evaluation;
- the definition of methodologies for incorporating commonality criteria within the design optimization framework; and
- the adaptation of conventional design workflows to manage commonality-driven optimizations and multi-role performance analyses effectively.

In the context of passenger transport and aerial firefighting seaplanes, the primary performance indicators to be improved can be derived from the conceptual design stage, specifically, operating costs, operational efficiency and and fuel consumption. Additionally, take-off performance from water surfaces represents a key operational parameter, directly influencing the aircraft's appeal to potential operators.

The disciplinary models supporting this stage can be derived from those implemented within the MDA framework of the conceptual phase and subsequently refined to capture more accurately the dependencies between detailed mission pro-

files and overall aircraft performance, for instance addressing Class-II weight estimation methodologies to better manage subsystems shared during commonality optimization. Particular attention should be given to the integration of tailored methodologies for estimating the operating costs of seaplanes in both passenger transport and aerial firefighting missions, especially considering the hybrid-electric nature of one of the configurations, as well as to methods linking aerodynamic and hydrodynamic analyses to evaluate take-off performance from water surfaces.

The adaptation of preliminary design workflows does not necessarily require the development of dedicated commonality-driven design and analysis methodologies. Instead, it should enable the formulation of an aircraft MDO problem that incorporates subproblems to ensure consistency in performance across multiple operational roles. These subproblems, commonly referred to as family-level workflows [180], are responsible for coupling the design processes of each platform involved in the commonality-driven optimization, thereby ensuring coherence and balanced performance among all configurations within the multi-role aircraft optimization problem.

5.3.1 Aircraft Cost Modelling

The operating cost estimation methodology is grounded in established practices in aircraft economic analysis and has been explicitly adapted for hybrid-electric aircraft (HEA). The DOC, a key factor in airline decision-making, encompasses all operationally dependent expenditures directly associated with aircraft characteristics. The proposed approach builds upon the methodology presented by [112], incorporating targeted modifications to account for the specific features of hybrid-electric propulsion systems. In particular, the enhanced framework systematically considers both capital and operational expenditures to provide a more comprehensive cost assessment.

Capital expenditures (CAPEX) primarily comprise the aircraft acquisition cost, representing the purchase price of the seaplane and constituting a major upfront investment. Financing mechanisms such as leases or loans can significantly affect the overall financial structure and long-term cost distribution. Although comparatively modest relative to the construction of conventional airport infrastructure, initial investments may still be required for water-based terminals, specialized docking facilities, and dedicated maintenance hangars at each operational base. These capital expenditures are decomposed into depreciation, interest, and insurance costs. The annual depreciation is expressed in Eq. (5.2), as a function of the total investment in aircraft procurement, TI, the residual value attributable to material recyclability RV, and the typical depreciation period, DP.

$$\mathrm{DOC}_{\mathrm{dep}} = \frac{TI}{DP} \cdot (1 - RV) \tag{5.2}$$

CAPEX items typically also include the annual hull insurance costs and the annual interests on the financial strategy selected to purchase the aircraft, these cost items are derived from benchmarked cost methodologies developed by the Air Transport Association of America (ATA) [181] and later adopted in Europe by the Association of European Airlines (AEA) [182].

Operational expenditures (OPEX), on the other hand, include crew salaries, energy costs, maintenance, and navigation and terminal charges. The introduction of a hybrid-electric propulsion system adds distinct cost components that are systematically integrated alongside conventional aviation expenses. In this framework, both aviation fuel (e.g., Jet A-1 or Diesel) and electricity costs are considered critical contributors to operational expenses, with the model incorporating realistic, market-based price assumptions for both. Owing to the inherently higher efficiency of electric propulsion, a substantial reduction in overall energy-related costs is anticipated when compared to conventional propulsion systems. Crew costs are estimated following standard industry assumptions. Energy costs, subdivided into fuel and electricity components, are formulated as shown in Eq. (5.3) and Eq. (5.4), in which P_{fuel} and P_{EE} represent unit cost of aviation fuel and electric energy, while m_{fuel} and E_{trip} represent the total fuel mass and energy consumed during the mission.

$$\text{DOC}_{\text{fuel}} = P_{\text{fuel}} \cdot m_{\text{fuel}} \tag{5.3}$$

$$\text{DOC}_{\text{EE}} = P_{\text{EE}} \cdot E_{\text{trip}} \tag{5.4}$$

A significant component of the overall operating costs is represented by maintenance expenses, which include both scheduled and unscheduled activities for the airframe, conventional engines (where applicable in hybrid configurations), and, critically, the electric propulsion system components, namely, the batteries, electric motors, and power electronics. The lifecycle maintenance costs of the batteries, including their expected replacement intervals, play a particularly important role and are estimated following the formulation proposed by Marciello et al. [112]. Maintenance of the airframe and internal combustion engine is assessed using the classical ATA methodology, while the maintenance of electric motors is further distinguished between line and base maintenance, as expressed in Eq. (5.5) and derived from Cusati et al. [121].

$$\text{DOC}_{\text{m}} = \text{DOC}_{\text{m, AF}} + \text{DOC}_{\text{m, ICE}} + \text{DOC}_{\text{m,EM}_{\text{line}}} + \text{DOC}_{\text{m,EM}_{\text{base}}} \tag{5.5}$$

Equation (5.5) summarizes the formulation for the total aircraft maintenance costs, where $\text{DOC}_{\text{m, AF}}$ and $\text{DOC}_{\text{m, ICE}}$ denote the airframe and thermal engine maintenance costs, respectively, as computed using the ATA method. Similarly, $\text{DOC}_{\text{m,EM}_{\text{line}}}$ and $\text{DOC}_{\text{m,EM}_{\text{base}}}$ correspond to the line and base maintenance costs of the electric machines, as proposed by Cusati et al. [121].

Table 5.4: Summary of DOC items methodologies implemented in the seaplane preliminary design problem. Economic assumptions in Appendix C.

DOC Item	**Ref. Method**
Depreciation	Eq. (5.2)
Interests	[182]
Insurance	[182]
Navigation Charges	[182]
Landing Fees	[182]
Carbon Permit Charges	[183, 184]
Cabin Crew	[182, 112]
Cockpit Crew	[182, 112]
Fuel Price	Eq. (5.3)
Electricity Price	Eq. (5.4)
Airframe Maintenance	[181]
Thermal Engine Maintenance	[181]
Battery Maintenance	[112]
Electric Machine Maintenance	[121]

Finally, navigation and airport service fees, which include terminal, en-route navigation, ground handling, and take-off and landing charges, are estimated following the established EUROCONTROL guidelines. In addition to conventional airport landing and parking fees, seaplane operations may incur specific charges related to seaport or waterbase usage. These fees are generally lower than those levied by major international airports, thereby contributing to reduced overall operating costs. EUROCONTROL en-route charges, which depend on both the aircraft's weight and the distance flown, remain applicable for flight segments within controlled airspace; however, optimized routing strategies can effectively mitigate these costs. Appendix C completes the analysis of aircraft operating costs models by providing a comprehensive analysis of the economic assumptions necessary to integrate discussed DOC methodologies.

This comprehensive cost estimation framework enables accurate financial modelling for both conventional and hybrid-electric seaplane configurations, ensuring that all relevant operational and economic dimensions are captured for informed decision-making. Table 5.4 summarizes the DOC components and the corresponding reference methodologies adopted in this study.

Related Publications

The author participated in one conference publication discussing operating costs and profitability of hybrid-electric seaplanes in the passenger transport use-case:

> (*Accepted*) Vincenzo Cusati; **Michele Tuccillo**; Fabrizio Nicolosi; Manuela Ruocco. *Economic and Environmental Assessment of Hybrid-Electric Commuter Aircraft: A Business Case for the Spanish Seaplane Market.* To be presented at the 2026 AIAA SciTech, Orlando, Florida.
>
> The study examines the economic viability of hybrid-electric commuter aircraft in the Spanish regional market. Building on a previously developed cost estimation methodology for hybrid-electric aircraft and incorporating recent advancements in hybrid-electric seaplane design, the analysis evaluates direct operating costs and profitability under realistic market conditions.

5.3.2 Commonality-Driven Aircraft Optimization

Conducting a preliminary design process aimed at enhancing aircraft attractiveness through multi-role operational capability presents two primary challenges. The first concerns the identification of which design features from both baseline configurations should be retained or integrated into a unified design solution. The second involves the adaptation of conventional MDO workflows to simultaneously address vehicle-level disciplinary analyses across multiple mission profiles and operating conditions and design constraints.

The selection and integration of features from the baseline architectures serve as the foundation for defining the maximum commonality level relative to a chosen reference configuration. For instance, by assuming the passenger transport variant as the reference configuration and initiating the preliminary design process from that point, the first iteration of the aircraft MDO problem corresponds to a 100% commonality level. Subsequent modifications that introduce variations from the reference design, such as incorporating subsystems or structural components from the firefighting variant, progressively decrease the degree of commonality with respect to the baseline.

It is evident that the commonality level with respect to the firefighting variant can be determined as shown in Eq. (5.6), where $CM_{\text{pax transport}}$ represents the percentage commonality level relative to the passenger transport variant, and $CM_{\text{firefight}}$ denotes the percentage commonality level relative to the firefighting variant. In the context of this research, only architectural features are shared among the configurations, in a discrete manner. Specifically, since the baseline configurations already share the same fuselage, given the similarity between the two payload categories,

Table 5.5: Architectural features shared among configurations during the preliminary design process.

Group Component	Parameter	Pax Transport	Aerial Firefight
Wing	$(t/c)_{mean}$	0.155	0.130
	S_w	35.17 m^2	49.73 m^2
	AR_w	7.95	7.52
	λ_w	0.884	0.674
	Λ_w	0.0 deg	5.0 deg
Horizontal Tail	$\mathcal{V}_H$	1.130	0.835
	Λ_H	8.5 deg	0.0 deg
	λ_H	0.5	1.0
Powertrain	Type	Hybrid-Turboprop	Turboprop
	P_0	720.5 hp	1 200.0 hp
	E_{bat}	261.28 kWh	-

the features selected for commonality include the wing architectural parameters, horizontal tailplane characteristics, and powertrain architectures derived during the conceptual design phase. Table 5.5 summarizes, for each component group (wing, horizontal tailplane, and powertrain), the corresponding defining parameters.

$$CM_{\text{firefight}} = 100.0 - CM_{\text{pax transport}} \tag{5.6}$$

It is important to note that, in Table 5.5, only the horizontal tailplane is considered as a component group to be shared, while the vertical tailplane is intentionally excluded. This decision stems from the necessity of ensuring aircraft certifiability. Specifically, the vertical tailplane is sized to satisfy regulatory requirements for minimum control speed and crosswind capability during landing operations. If the entire vertical tailplane architecture were to be shared between configurations, compliance with these requirements could not be guaranteed, as the minimum control speed is highly sensitive to the installed powertrain characteristics. Consequently, including the vertical tailplane as a shared component would introduce a dependency between two key design variables in the preliminary design phase, namely, the vertical tailplane size and the powertrain architecture. Such a dependency would bias the optimization process, as the MDA or MDO algorithm would tend to converge toward the single configuration that satisfies the minimum control speed requirement in both operating scenarios, effectively favouring either the passenger transport or the aerial firefighting variant depending on which exhibits the most critical conditions for minimum control speed compliance.

To address this issue, the vertical tailplane sizing parameters, although already considered during the conceptual design stage, are included among the design variables required for the analyses performed in the preliminary design phase. This inclusion ensures an accurate evaluation of aircraft performance and compliance with stability and controllability requirements. Consequently, from an architectural stand-

Table 5.6: Design variables for the commonality-driven preliminary design process.

Variable	**Symbol**	**Range/Options**
Wing Architecture	-	{ Pax Transport, Aerial Firefight }
Horizontal Tail Architecture	-	{ Pax Transport, Aerial Firefight }
Powertrain Architecture	-	{ Pax Transport, Aerial Firefight }
Airfoils	-	{ NACA23012, NACA23015, NACA23018, NACA43015, NACA43018 }
Vertical Tail Area	S_V	[5.0, 8.0][a] m^2
Vertical Tail Sweep	Λ_V	[30.0, 35.5][a] deg
Vertical Tail AR	AR_V	[1.5, 3.5][a]
Wing Incidence	i_w	[-1.5, 1.5][b] deg
Horizontal Tail Incidence	i_H	[-2.0, 2.0][b] deg
Elevator Chord Ratio	c_e/c_{htp}	[0.30, 0.60][b]
Rudder Chord Ratio	c_r/c_{vtp}	[0.25, 0.55][b]
Flap Chord Ratio	c_f/c_w	{ 0.25, 0.30 0.40 }[c]
Cruise Mach Number	M_{CR}	[0.28, 0.35][a]
Climb Speed	V_{CL}	[105.0, 120.0][a] KCAS

[a] Selected from the families of configurations developed in the conceptual design phase.
[b] Typical values suggested by Roskam [185] in the class of amphibian aircraft and flying boats.
[c] Limited by a 5% gap between the secondary wing spar and the flap structure suggested by Niu [186].

point, the maximum achievable commonality level with respect to either baseline configuration is limited to approximately 75%.

Additional parameters integrated to enable a more refined design process can be derived from the guidelines proposed by Raymer [139]. These include the wing and horizontal tail incidence angles, which are essential for improving stability characteristics. Along with the elevator and rudder chord ratios, they support the trade-off analysis between enhanced controllability and increased trim drag. Furthermore, the flap chord ratio and the airfoil distribution are incorporated to improve both low-speed performance, while maintaining adequate internal wing volume for fuel storage, and high speed performance. Table 5.6 summarises the design variables adopted in the preliminary design phase and their respective ranges of variation.

According to Bussemaker et al. [180], two hierarchical levels can be distinguished within the design process when incorporating commonality aspects. The first is the "aircraft" level, which encompasses the selected disciplinary capabilities required to perform the preliminary design process, as illustrated in the XDSM representation of Figure 5.6. The second is the "family" (or fleet) level, which ensures the consistency of design solutions across the two considered operational scenarios. The inclusion of this second level is essential to address two primary limitations inherent to procedural aircraft design processes: (i) the presence of hidden constraints, as defined by Bussemaker [143], which necessitate the use of rescaling laws or conditional statements to prevent computational failures; and (ii) the semi-empirical nature of conventional design methodologies, which are typically developed for single-mission

analyses. As a result, applying such methodologies to multi-role design problems may lead to inconsistencies, producing distinct aircraft configurations even when based on an identical set of design variables.

The design process, illustrated in Figure 5.6 for the aerial firefight use case, begins with the geometric update of the configuration based on the assigned vector of design variables. The aerodynamic characteristics of the isolated components and the sizing of the firefighting-specific on-board systems (OBS) are subsequently determined. The preliminary design workflow for the passenger transport use case follows the same general structure shown in Figure 5.6, but does not require the disciplinary modules dedicated to firefighting-specific systems. All subsystems typically installed on passenger transport seaplane, including those applicable to innovative hybrid-electric aircraft [187], are instead sized within the "Weight Class II" discipline, leveraging semi-empirical formulations rather than simple statistical relations. As in the conceptual design phase, a comprehensive MDA serves as the main mechanism to ensure consistency and to account for the snowball effect. The required initial estimates of take-off mass and fuel consumption are derived from the corresponding baseline configuration.

At this stage, the workflow no longer includes the disciplinary module responsible for powertrain sizing, as the powertrain architecture is treated as a categorical design variable. This variable is used to inform the sizing of the horizontal and vertical tailplanes, to verify longitudinal stability and controllability requirements, and to determine flight performance and fuel consumption along the relevant mission profiles, either those associated with aerial firefighting operations or with typical passenger transport missions, depending on the use case.

In the proposed design workflow, the operating scenario influences nearly all disciplinary analyses, ranging from the evaluation of longitudinal and lateral–directional trimmed characteristics, dependent on the centre of gravity (CG) position, which itself is a function of mass distribution and structural mass, to the sizing of the OBS. It is important to note that not all variations in aircraft performance result in design inconsistencies. For instance, the OBS required for aerial firefighting operations differ in both mass and installation position compared to those used in passenger transport configurations. Consequently, variations in subsystem masses and CG positions are permissible, as are performance differences arising from changes in take-off mass. However, discrepancies that lead to variations in the characteristics of components intended to remain common across configurations are not acceptable. For example, Class-II weight estimation methods depend on the aircraft's operating empty weight, W_{OE}, to size the wing structure; thus, any scenario-induced variation in W_{OE} (e.g., due to differences in OBS) would result in distinct wing designs. The family-level design process is therefore introduced to prevent such inconsistencies by ensuring that shared component groups are coherently maintained across both operational scenarios, while the resulting aircraft performance continues to satisfy all design constraints, including those related to certification and stability.

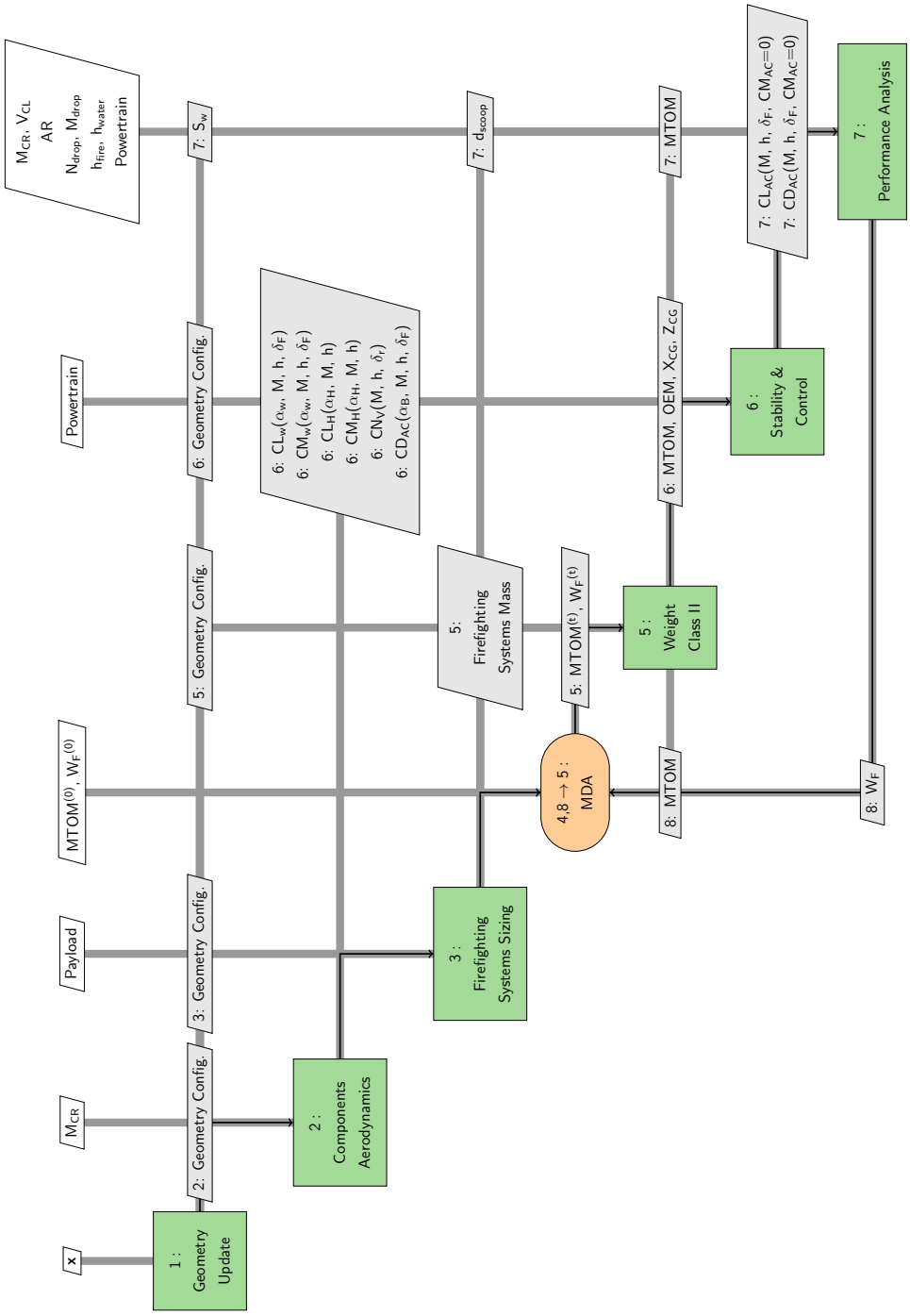

Figure 5.6: XDSM diagram for the preliminary design of the seaplane in the firefighting use case.

Figure 5.7 presents the XDSM diagram of the commonality-driven preliminary design framework, highlighting both the “aircraft” level, corresponding to the pseudo-disciplinary modules “Passenger Design” and “Firefighting Design,” and the “family” level, governed by the MDA block. As illustrated, the design process begins with the optimizer defining suitable values for the design variables, collected in the vector, $\mathbf{x}$. The aircraft level then performs the independent design and analysis of the two seaplane variants under equivalent conditions. The resulting configurations are passed to the family-level MDA, which extracts information regarding shared component groups and synthesizes a consistent mass breakdown. Class-II weight estimation methods are applied to the most demanding configuration, for instance, by considering the wing with the highest structural mass or evaluating the maximum fuel capacity based on the most fuel-demanding and energy-intensive mission, thus ensuring a coherent aircraft architecture. Subsequent analyses include the assessment of stability and controllability characteristics, followed by mission simulations to evaluate performance and energy consumption. These outputs are iteratively fed back to the MDA until convergence is achieved. Finally, the “Functions” block receives the converged vehicle configuration, associated properties, and performance metrics, and computes the objective functions and design constraints, denoted as "f" and "c" in the diagram for clarity of representation.

Remark Figure 5.7

In the preliminary design of individual vehicle architectures, certain performance parameters and characteristics remain independent of the operational scenario. Specifically, the overall geometrical configuration, defined by the vector of design variables, and the aerodynamic properties of isolated components, such as the wing, fuselage, horizontal tailplane, and vertical tailplane, depend solely on their geometry and relative positioning. These aerodynamic characteristics are subsequently supplied to the other disciplinary modules as functions of Mach number, altitude, and control surface deflections, ensuring their applicability to both operational scenarios. For this reason, quantities such as the “Geometry Config.” and the aerodynamic functions are extracted, in Figure 5.7, from either the passenger transport or the aerial firefighting variant, with the only purpose to facilitate the interpretation of the XDSM representation.

An MDO formulation once again serves as the primary driver of the aircraft design process. At the preliminary design stage, however, the objective is not to explore a wide range of feasible configurations, as in the conceptual phase, but rather to refine the vehicle specifications while incorporating the capability to perform multi-role operations. This process aims to achieve an optimal compromise between the two operational scenarios, minimizing the associated performance penalties and thereby enhancing overall vehicle attractiveness. Table 5.7 presents the formulation of the commonality-driven optimization problem, consistent with the workflow il-

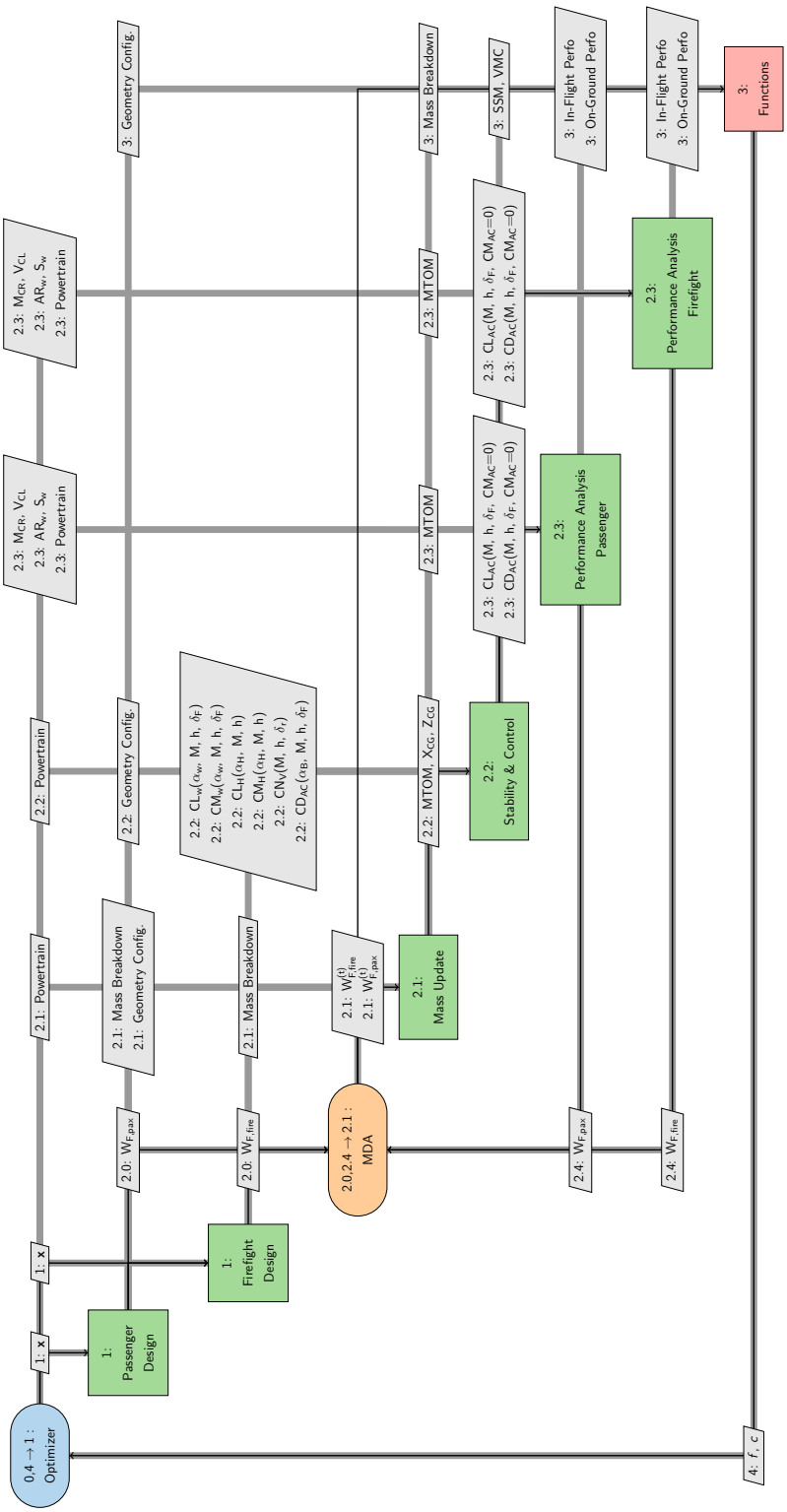

Figure 5.7: XDSM diagram of the commonality-driven preliminary design framework.

lustrated in Figure 5.7.

An interesting aspect emerging from Table 5.7 concerns the analysis of the selected design constraints. The multi-role nature of the targeted optimal seaplane necessitates the Boolean union of constraints applied independently to each operational use case. This approach inherently introduces redundancy when common constraints are shared between use cases, as functions or variables must be evaluated multiple times to determine the overall feasibility of a design solution.

Another notable distinction from the conceptual design stage lies in the introduction of "performance-consistency" constraints, such as the verification of the maximum achievable Mach number in level flight conditions, the assessment of the longitudinal Static Stability Margin (SSM), and the compliance check with minimum control speed requirements. These constraints are essential because the "family" level of the design workflow ensures only architectural consistency, without guaranteeing operational coherence. For instance, the absence of a dedicated disciplinary module for powertrain sizing, as highlighted in Figure 5.6, may lead the optimizer to select a cruise Mach number exceeding the physically attainable limit for the selected powertrain architecture (this limit is not known at priori because it depends also on the overall aircraft configuration). Similarly, unsuitable combinations of wing, horizontal tail, and vertical tail architectures could yield aerodynamically unstable configurations, underscoring the necessity of these additional performance-based constraints.

The "pymoo" and "SBArchOpt" frameworks can be effectively employed to structure this type of design problem, thanks to their combined capability to manage mixed-discrete variables. To prevent the generation of a family of distinct design solutions while still achieving a balanced compromise between the key performance metrics of the two operational use cases, a single-objective formulation is adopted. This is accomplished through a weighted-sum approach that combines all KPIs, mainly derived from the conceptual stage, into a single aggregate objective. As shown in Table 5.7, this objective is mathematically expressed, in normalized form, in Eq. (5.7) using normalized weights, w_i, which collectively sum to unity. Table 5.8 provides a detailed description of how discussed performance metrics contribute to the aggregated objective function.

$$\overline{f}_{\text{obj}}(\mathbf{x}) = \sum_{i=1}^{n_f} w_i \overline{f}_i(\mathbf{x}) \qquad \text{s.t.:} \quad \sum_{i=1}^{n_f} w_i = 1 \tag{5.7}$$

Table 5.9 summarizes the main architectural specifications of the optimal seaplane configuration designed for multi-role operations. Among the shared variables, it is noteworthy that the optimal solution adopts the same wing and powertrain architectures as the passenger transport variant, while the horizontal tailplane architecture is derived from the aerial firefighting configuration. This results in an overall commonality level of approximately 50% relative to the passenger transport variant. Such an outcome is consistent with the findings reported in Ref. [180], which

Table 5.7: Formulation of the commonality-driven optimization problem for the preliminary design problem.

	Function/Variable	**Nature**	**Quantity**	**Note(s)**
minimize	$\overline{f}_{\text{obj}}(\mathbf{x})$	cont.	1	-
			1	**Total Objectives**
with respect to	S_V	cont.	1	-
	Λ_V	cont.	1	-
	AR_V	cont.	1	-
	i_w	cont.	1	-
	i_H	cont.	1	-
	c_e/c_{htp}	cont.	1	-
	c_r/c_{vtp}	cont.	1	-
	M_{CR}	cont.	1	-
	V_{CL}	cont.	1	-
	c_f/c_w	cat.	1	-
	Wing Architecture	cat.	1	-
	Powertrain Architecture	cat.	1	-
	Horizontal Tail Architecture	cat.	1	-
	Wing Airfoils	cat.	1	-
			9	**Total cont. variables**
			5	**Total cat. variables**
			14	**Total variables**
subject to	$d_{TO} \leq 1\,850.0$ ft	cont.	2	-
	$d_{LND} \leq 1\,850.0$ ft	cont.	2	-
	MTOM $\leq 19\,000.0$ lb	cont.	2	-
	$h_{Ceil,\,AEO} \geq 25\,000.0$ ft	cont.	2	-
	Payload ≥ 540.0 US Gal.	cont.	1	Aerial Firefight Use Case.
	$W_{F,\,max} \geq W_F$	cont.	2	-
	$E_{bat} \geq E_{trip}$	cont.	2	-
	$M_{CR,max} \geq M_{CR}$	cont.	2	-
	$V_{MC} \geq 1.2\,V_{S,TO}$	cont.	2	-
	SSM ≤ 0.0	cont.	2	-
	BT ≤ 1.0 hr	cont.	1	Passenger Transport Use Case
	$h_{fire} = h_{fire,\,scenario}$	cont.	1	Scenario 5 Aerial Firefight Use Case.
	$h_{water} = h_{water,\,scenario}$	cont.	1	Scenario 5 Aerial Firefight Use Case.
	$N_{drop} = N_{drop,\,scenario}$	int.	1	Scenario 5 Aerial Firefight Use Case.
			1	**Total int. constraints**
			22	**Total cont. constraints**
			23	**Total constraints**

If not specified, design constraints apply to both use cases.

Table 5.8: Performance metrics contributing to the objective function for the commonality-driven preliminary design problem.

Function	Description
n_f	Number of performance metrics: 5
w_i	Performance metric weight. $w_i = 0.20 \, \forall i$
$f_1(\mathbf{x})$	Total Fuel Passenger Transport Use Case
$f_2(\mathbf{x})$	Total Fuel Aerial Firefight Use Case
$f_3(\mathbf{x})$	Operating Costs Passenger Transport Use Case
$f_4(\mathbf{x})$	Operating Costs Aerial Firefight Use Case
$1/f_5(\mathbf{x})$	Operational Efficiency Aerial Firefight Use Case

demonstrated that configurations achieving a 50% component commonality tend to yield both minimum fuel consumption and maximum take-off mass.

It is further observed that the shared horizontal tail volumetric coefficient induces differences in the tailplane surface area. The significant reduction identified in the optimal configuration arises from two main factors: the zero wing sweep angle, which shifts the wing aerodynamic center forward, and the enlarged vertical tail surface area and span, which permit repositioning the horizontal tail further aft. Both effects increase the tail arm, thereby enabling a smaller horizontal tail surface area while maintaining adequate control authority, enhanced by a higher chord ratio between the elevator and the local chord of the tailplane. Additionally, the higher aspect ratio of the vertical tail contributes to a reduction in its root chord length, resulting in a minor decrease in the overall fuselage length.

The main differences observed during multi-role operations arise from variations in the aircraft's mass breakdown and operating CG position. Table 5.10 summarizes the principal design masses of the optimal seaplane configuration when operating in passenger transport and aerial firefighting roles, along with the corresponding operating CG locations. It is important to note that the table reports different operating empty masses for the two cases. This variation is permissible, as the operating empty mass includes the contribution of OBS and mission-specific equipment, which differ between the two operational scenarios. Finally Figure 5.8 provides a graphical representation of the optimal seaplane, leveraging the TiGL library, similarly, Figure 5.9 describes the component breakdown of the configuration highlighting the main architectural choices and results. Performance analysis and comparison with respect the baseline configurations will be discussed in § 5.4.

5.3.3 Hull Parametric Optimization

During the conceptual design studies and initial vehicle architecture explorations, no specific assumptions or analyses were conducted to assess the hydrodynamic behaviour of the seaplane hull, which plays a crucial role in determining the take-off

Table 5.9: Architecture specification of the preliminary design solution, compared to the conceptual level passenger transport and aerial firefight variants.

Parameter	**Unit**	**Value**	**Passenger Transport**	**Aerial Firefight**
Wing				
S_w	m^2	35.17	35.17	49.73
AR_w	-	7.95	7.95	7.52
Root Chord	m	2.2	2.2	2.94
λ_w	-	0.884	0.884	0.674
Λ_w	deg	0.0	0.0	5.0
i_w	deg	1.5	1.0	1.1
c_f/c_w	-	0.30	0.25	0.4
Root Airfoil	-	NACA 43018	NACA 43018	NACA 43018
Kink Airfoil	-	NACA 23015	NACA 23015	NACA 43015
Tip Airfoil	-	NACA 23015	NACA 23015	NACA 23015
Horizontal Tail				
S_H	m^2	7.07	10.09	12.43
AR_H	-	3.7	4.9	3.6
Root Chord	m	1.39	1.92	1.86
λ_H	-	1.0	0.5	1.0
Λ_H	deg	0.0	8.5	0.0
i_H	deg	-1.0	0.0	0.0
c_e/c_{htp}	-	0.4	0.3	0.3
Airfoil	-	NACA 0012	NACA 0012	NACA 0012
Vertical Tail				
S_V	m^2	5.50	5.45	7.67
AR_V	-	1.70	1.15	1.57
Root Chord	m	2.34	2.59	3.03
λ_V	-	0.55	0.68	0.48
Λ_V	deg	33.5	35.0	30.0
c_r/c_{vtp}	-	0.4	0.3	0.3
Airfoil	-	NACA 0012	NACA 0012	NACA 0012
Fuselage				
Length	m	14.30	14.75	14.60
Max Height	m	2.00	2.05	2.05
Max Width	m	1.90	2.05	2.05
Powertrain				
Type	-	Hybrid-Turboprop	Hybrid-Turboprop	Turboprop
P_0	hp	720.5	720.0	1 200.0
E_{bat}	kWh	261.28	261.28	-
P_{EM}	kW	118.5	118.5	-

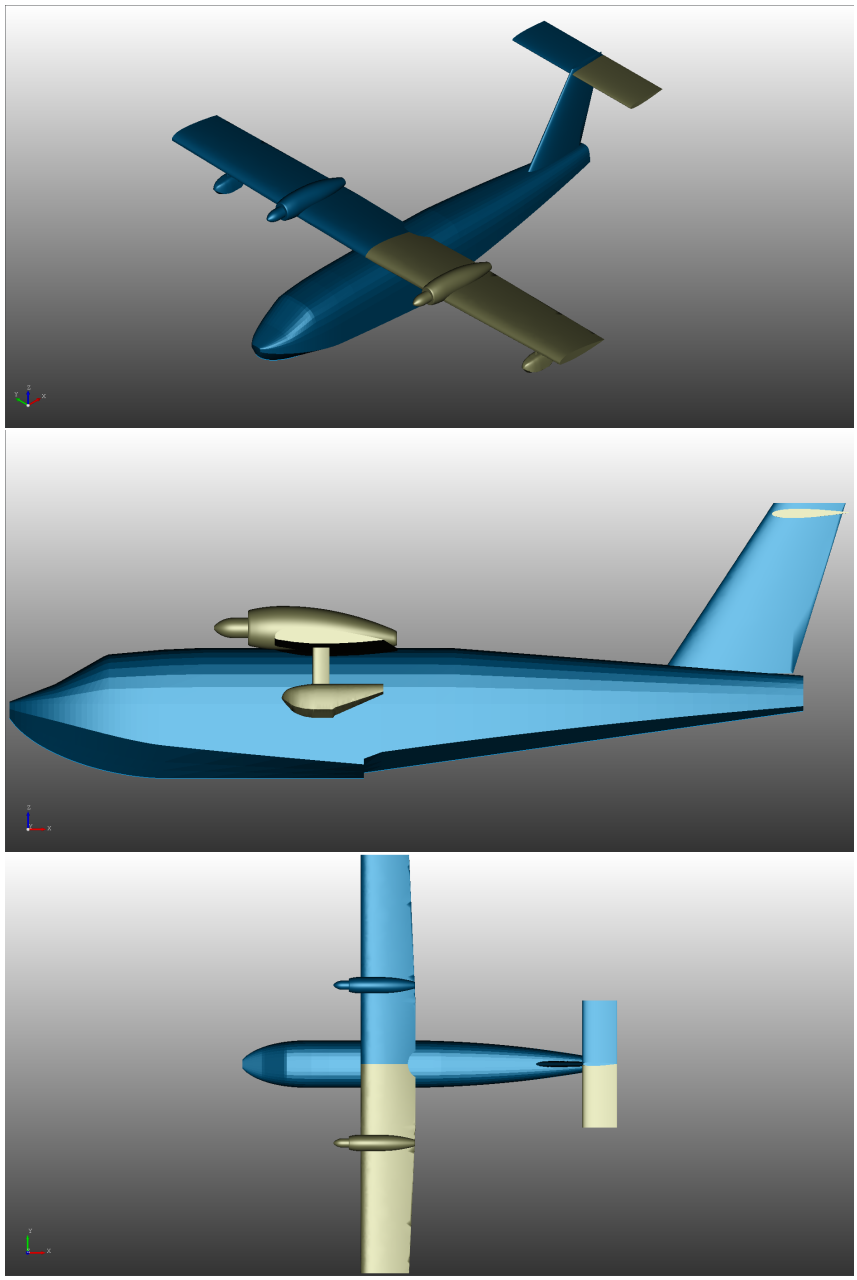

Figure 5.8: Graphical representation of the optimal seaplane using the TiGL library.

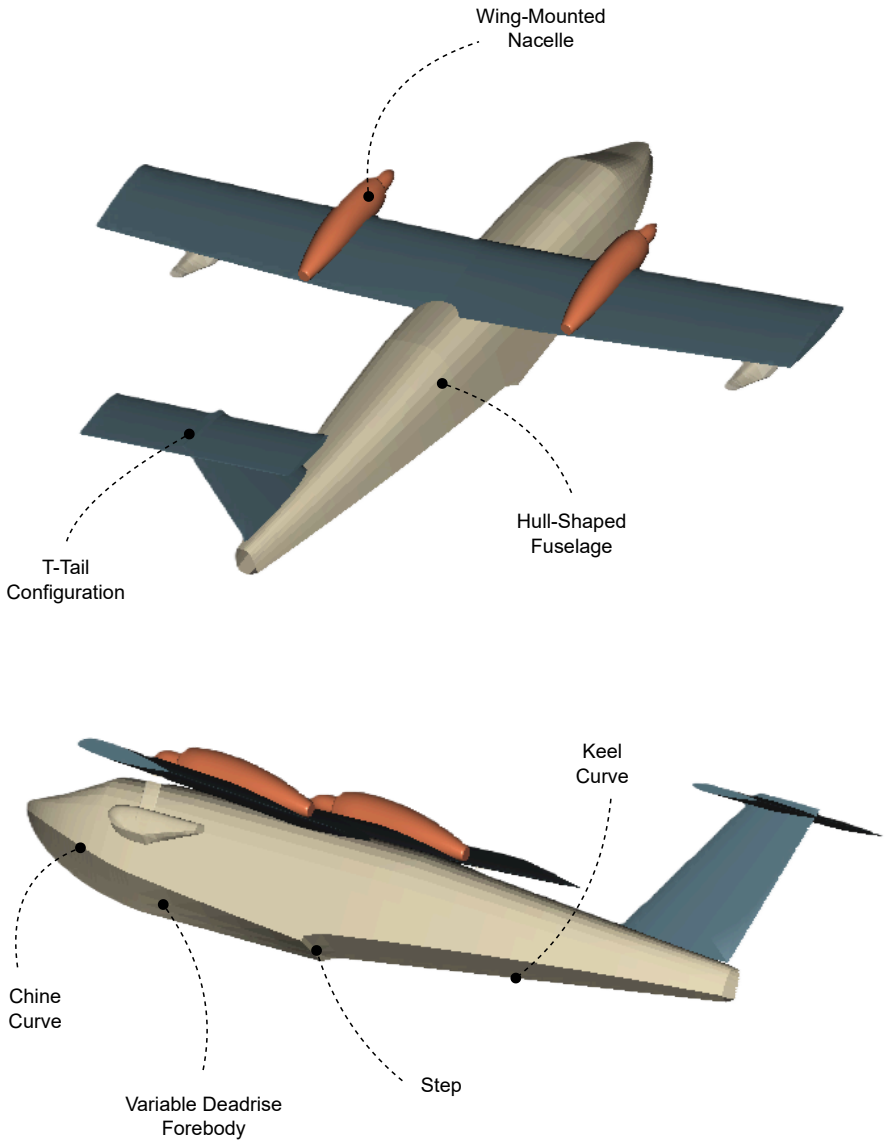

Figure 5.9: Component breakdown of the optimal seaplane configuration. Details of the hull-shaped fuselage are provided in § 5.3.3.

Table 5.10: Optimal seaplane design masses breakdown and operating CG position for both use cases.

Item	Passenger Transport	Aerial Firefight
Operating Empty Mass	10 541.7 lb	9 515.3 lb
Design Payload	3 510.0 lb	4 500.0 lb
Max Payload	3 510.0 lb	6 075.5 lb
Zero Fuel Mass	13 984.2 lb	14 015.7 lb
Jet-A1 Mass	930.5 lb	1 978.2 lb
Max Jet-A1 Mass	2 910.6 lb	2 910.6 lb
MTOM	14 986.7 lb	15 994.0 lb
Operating CG	34.5% MAC	32.0% MAC

performance from water surfaces. At the conceptual stage, the overall aircraft performance, captured through global objective functions such as operating costs and fuel consumption, had a dominant influence on the assessment of the seaplane's overall attractiveness. Consequently, a single performance metric, such as the take-off distance from water, had a comparatively minor effect on the optimization outcome. To account for this, simplified statistical correlations were employed to estimate the take-off distance as a function of two key conceptual-level drivers: wing loading and power-to-weight ratio [108]. In contrast, during the preliminary design stage, more detailed methodologies can be implemented to refine the vehicle architecture, allowing for improvements not only in global performance indicators but also in specific key performance metrics, including the take-off distance from water surfaces.

The primary parameters influencing this type of performance are predominantly associated with the geometry of the main components that provide buoyancy and hydrodynamic support to the aircraft on the water, specifically, in the case of amphibious seaplanes, the hull-shaped fuselage. These parameters include the fuselage length-to-beam ratio, the ratio between the forebody and afterbody lengths, the deadrise angles at both the planning bottom and the step, the step height, and the sternpost angle.

Given the large number of influencing parameters and the necessity of identifying suitable combinations to enhance water take-off performance, it is evident that high-fidelity methods, such as CFD, would not offer an effective compromise between result accuracy and computational cost at this stage of design. To address this limitation during the early design phase, semi-empirical approaches are typically employed. Among these, the method developed by Savitsky (1964) and Brown (1976) [188, 189] remains the most widely adopted, later refined together with Morabito [190] to mitigate some of its inherent limitations, most notably, its inability to account for the presence of a transverse step in the hull. This feature is of particular importance, as the step facilitates hull rotation during take-off and reduces the wetted surface area, thereby decreasing hydrodynamic drag and improving take-off

performance [104].

In this section, the analysis focuses exclusively on the water run segment of the take-off distance, as the airborne phase and associated procedures are largely analogous to those employed for conventional landplanes. Consequently, improving the overall take-off performance primarily involves optimizing the water run.

The determination of the water run can be performed using an approach similar to that employed for calculating the ground roll distance of landplanes operating on level runways. Assuming calm conditions, with no headwind or tailwind components, the forces acting on the seaplane along the water surface include the propulsive thrust, T, the aerodynamic drag, D, and the total hydrodynamic resistance, R_{hydro}. The corresponding longitudinal equation of motion can therefore be expressed as in Eq. (5.8), where the right-hand side represents the product of the seaplane mass and its acceleration along the water path. This formulation constitutes the foundation for estimating the water run distance and clearly illustrates how the magnitude of the hydrodynamic resistance adversely affects take-off acceleration performance.

$$T - D - R_{\text{hydro}} = \frac{W}{g}\frac{dV}{dt} \tag{5.8}$$

It is important to note that Eq. (5.8) is derived under the assumptions that the velocity vector remains aligned with the direction of motion, that the propeller thrust acts along the same direction, and that the hydrodynamic resistance is considered solely as the component parallel to the trajectory of motion.

Seaplane Hydrodynamic Behaviour

The optimization of the water run distance requires minimizing the hydrodynamic resistance throughout the entire waterborne phase. Since this force varies with the velocity along the trajectory, an ideal formulation would involve minimizing the resistance at each speed increment, from rest, where hydrostatic forces dominate, up to the lift-off velocity, with respect to the primary geometrical parameters of the hull.

A more practical approach to this minimization problem involves considering the hydrodynamic resistance coefficient, C_R, and minimizing the area under its curve. Eq. (5.9) defines the objective function used in the parametric optimization of the seaplane hull, where V_{LO} denotes the lift-off velocity. The definition of the resistance coefficient follows Gudmundsson [104], with ρ_w representing the water density and "B" the beam of the seaplane hull.

$$f_{\text{obj}} = \int_0^{V_{\text{LO}}} C_R \, dV = \int_0^{V_{\text{LO}}} \frac{R_{\text{hydro}}}{\rho_w \text{B}^3} \, dV \tag{5.9}$$

The analysis of the hydrodynamic resistance follows the methodology proposed by

Table 5.11: Lift and pitching moment coefficient and derivatives of the optimal seaplane for the passenger transport and aerial firefight use (take-off conditions).

Coefficient	Unit	Pax Transport	Aerial Firefight
$C_{L,0}$	-	0.876	0.875
$C_{L,\alpha}$	1/rad	5.045	5.085
C_{L,δ_e}	1/rad	0.964	0.971
$C_{\mathcal{M},0}$	-	0.011	0.005
$C_{\mathcal{M},\alpha}$	1/rad	-0.481	-0.545
$C_{\mathcal{M},\delta_e}$	1/rad	-2.865	-2.865

Svahn [191], which also enables the determination of the trim angle corresponding to each speed, under the condition that both vertical and rotational equilibrium are satisfied. It is important to note that the original approach considers only the forces and moments arising from the interaction between the hull and the water, completely neglecting aerodynamic effects, both in terms of forces and moments, that also contribute to achieving vertical and rotational equilibrium, thereby influencing the resulting resistance and trim angle.

To overcome this limitation, the adopted methodology has been modified to include the contributions of aerodynamic forces and moments generated by the fuselage and the lifting surfaces, specifically the wing and the horizontal tailplane, when solving the equilibrium problem. Eq. (5.10) and (5.11) describe the lift and pitching moment functions integrated into the enhanced computational model, derived during the preliminary design stage from the adopted aerodynamic model.

$$L = \mathrm{qS_w}\left(C_{L,0} \; + \; C_{L,\alpha}\,\alpha_B \; + \; C_{L,\delta_e}\,\delta_e\right) \tag{5.10}$$

$$\mathcal{M}_{\text{aero}} = \mathrm{qS_w\overline{c}}\left(C_{\mathcal{M},0} \; + \; C_{\mathcal{M},\alpha}\,\alpha_B \; + \; C_{\mathcal{M},\delta_e}\,\delta_e\right) \tag{5.11}$$

In both expressions, the primary contributions are highlighted: the term associated with the angle of attack, which depends on the trim angle, and the contribution of the horizontal tailplane, influenced by the elevator deflection. Since a CS-23 seaplane can still be classified as a general aviation aircraft, standard design practices prescribe a fixed incidence angle for the horizontal tailplane. Consequently, this contribution to the lift and aerodynamic pitching moment is incorporated into the $C_{L,0}$ and $C_{\mathcal{M},0}$ terms. Table 5.11 summarises the aerodynamic coefficients and derivatives for both uses cases in the take-off conditions.

According to the Svahn model, the geometrical characteristics of a stepped hull that influence hydrodynamic forces and moments include the deadrise angle of the forebody flat (assumed constant up to the step), the deadrise angle of the afterbody (also assumed constant), the sternpost angle, the step height, and the longitudinal distance of the step from the transom, corresponding in this context to the afterbody

Table 5.12: Hull geometrical parameters and design variables for the hydrodynamic resistance minimization problem.

Description	**Symbol**	**Type**
Step Height (as percentage of beam)	$h_{\%\mathrm{B}}$	Design Variable
Afterbody Length	L_a	Design Variable
Forebody Deadrise Angle (at the step)	β_1	Design Variable
Afterbody Deadrise Angle	β_2	Design Variable
Maximum Beam	B	Constant
Sternpost Angle	φ	Constant

length. These five design variables constitute the parameter set available for the optimization of hull geometry aimed at improving hydrodynamic resistance characteristics.

It is important to note, however, that the geometric features of a stepped hull affect not only resistance and spray formation but also stability limits, for which no simple analytical methods are applicable during the conceptual or preliminary design stages. Among these parameters, the sternpost angle requires a particularly careful trade-off between performance and stability, as no universally accepted design guideline exists. For this reason, and following the recommendations of Morabito [107], the sternpost angle has been fixed at 8 deg, representing an average value within the suggested design range.

To address the limitations associated with stability prediction, Morabito conducted an extensive survey of available experimental data and observed that Olson and Land [192] derived an empirical relationship between selected hull design variables, reported in Eq. (5.12), which can serve as a design guideline for flying boat hulls to ensure satisfactory performance and stability characteristics.

$$h_{\%\mathrm{B}} \geq 0.59 \, \frac{L_a}{\mathrm{B}} \varphi \tag{5.12}$$

Table 5.12 summarizes the geometrical parameters under consideration, providing a description of each corresponding symbol and indicating whether the parameter is treated as a constant or included in the vector of design variables for the hull optimization problem. In the table, both the sternpost angle, fixed according to the recommendations of Morabito, and the maximum hull beam are treated as constants. The latter coincides with the maximum fuselage width for the considered seaplane configuration and must therefore be preserved to maintain weight and aerodynamic consistency.

To perform the parametric analysis and optimization of the seaplane hull's hydrodynamic performance, the parametric representation proposed in the technical note of Hugli and Axt [193] was adopted. The objective of this modelling approach is to provide a geometric description suitable for small amphibious seaplanes and flying boats, employing simplified yet representative hull lines. Oversimplification was

Table 5.13: Formulation of the parametric hull optimization problem.

	Function/Variable	Nature	Quantity	Note(s)
minimize	f_{obj}	cont.	1	From Eq. (5.9)
			1	**Total Objectives**
with respect to	$h_{\%\text{B}}$	cont.	1	5% to 8% [104]
	β_1	cont.	1	-
	β_2	cont.	1	-
	L_a	cont.	1	50% to 70% of the fuselage length [107]
			4	**Total variables**
subject to	Eq. (5.12)	cont.	1	-
	$\mathcal{M}_{\text{hydro}} + \mathcal{M}_{\text{aero}} = 0$	cont.	1	-
			2	**Total constraints**

avoided by introducing a variable deadrise angle along the forebody, extending from the nose to the forebody flat station. The NACA Report also provides the parametric mathematical formulations for defining the keel line, the planform shape, and the variation laws for the deadrise angle of both the forebody and afterbody.

Table 5.13 summarizes the hull optimization problem, also outlining the rationale behind the selected ranges for key design variables. Specifically, the percentage height of the step was defined according to Gudmundsson [104], while the limits on the afterbody length were established to ensure that the step location remains approximately aligned with the centre of gravity position, as recommended by Morabito [107].

It is important to note that the adopted hydrodynamic model does not account for the pressure drag component, which depends on the trim angle and hull displacement, but only for the viscous resistance contribution. The latter is more sensitive to the geometric characteristics of the hull, increases with forward speed, and is also influenced by the hull weight. Nevertheless, the model does not include the effects of reduced water displacement resulting from the lift generated by the main lifting surfaces. Table 5.14 presents the set of hull parameters that minimize the viscous drag contribution and Figure 5.10 illustrates the keel curve obtained from the optimization problem, and its position with respect to the Fuselage Reference Line (FRL).

Figure 5.11 shows the variation of the trim angle and of both the viscous and pressure components of the hydrodynamic resistance as functions of the beam Froude number, Fr_B, whose definition is provided in Eq. (5.13) and that often indicated as speed coefficient, C_V. The results clearly highlight the contribution of the lifting surfaces in achieving pitch equilibrium, leading to a significantly narrower range of trim angle variation compared to that of a standalone hull, which, over the same range of speed coefficients, typically varies between 2 deg and 8 deg. The higher

Table 5.14: Optimal Hull Geometry.

Parameter	**Value**	**Unit**	**Note(s)**
B	1.90	m	Seaplane width.
φ	8.0	deg	Average value.
β_1	14.5	deg	-
β_2	19.0	deg	-
L_a	7.83	m	55% of the fuselage length.
h_{step}	0.1	m	5.26% of the Beam.

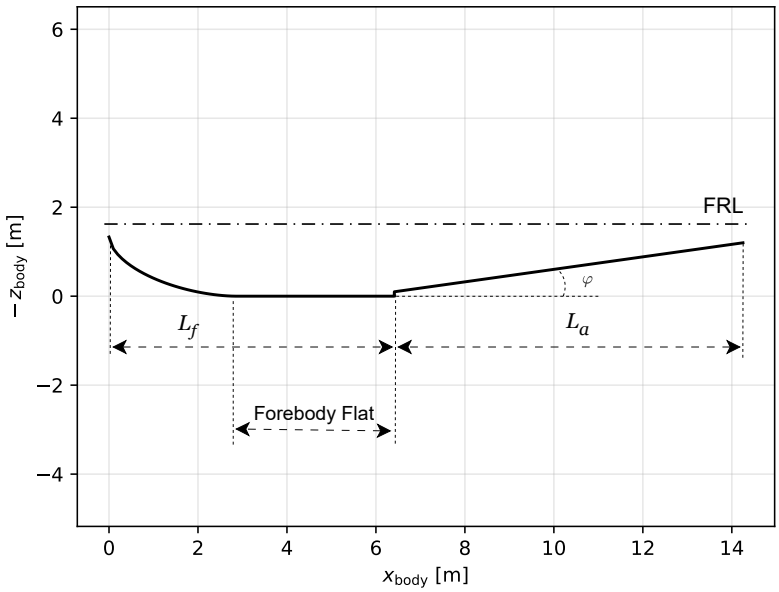

Figure 5.10: Representation of the seaplane keel curve at the end of the optimization process.

trim angles observed for the aerial firefighting configuration are attributable to the increased take-off mass associated with this operational scenario. Furthermore, the figure shows that the viscous resistance components for the passenger transport and firefighting configurations are nearly identical, indicating that the optimized set of hull geometric parameters provides an effective compromise suitable for both missions.

$$C_V \equiv \mathrm{Fr_B} = \frac{V}{\sqrt{gB}} \tag{5.13}$$

Analysis of TakeOff Water Run

The analysis of the water take-off run is conducted under simplified assumptions. Specifically, the aircraft motion is assumed to occur exclusively in the longitudinal plane, thereby neglecting lateral-directional effects in the evaluation of the take-off distance. Treating the aircraft as a rigid body, the longitudinal state variables governing its motion include the angle of attack, forward velocity, pitch attitude, and altitude. The control variables influencing longitudinal dynamics comprise the powertrain throttle setting and elevator deflection. Accordingly, a general longitudinal flight condition can be represented by the system of Ordinary Differential Equations (ODE) given in Eq. (5.14) and in Eq. (5.15).

$$\begin{cases} \dot{V} = \dfrac{g}{W}\Big[-D + X_T \cos\alpha_B + Z_T \sin\alpha_B + \\ \quad - W\left(\cos\alpha_B \sin\theta - \sin\alpha_B \cos\theta\right)\Big] \\ \\ \dot{\alpha}_B = \dfrac{g}{W\,V}\Big[-L + Z_T \cos\alpha_B - X_T \sin\alpha_B + \\ \quad + W\left(\cos\alpha_B \cos\theta + \sin\alpha_B \sin\theta\right)\Big] + q \\ \\ I_y\,\dot{q} = \mathcal{M}_{\text{aero}} + \mathcal{M}_T \end{cases} \tag{5.14}$$

$$\begin{cases} \dot{x}_{\text{CG}} = V\cos\alpha_B \cos\theta + V\sin\alpha_B \sin\theta \\ \\ \dot{z}_{\text{CG}} = -V\cos\alpha_B \sin\theta + V\sin\alpha_B \cos\theta \\ \\ \dot{\theta} = q \end{cases} \tag{5.15}$$

In this study, the primary focus is on the ground segment of the take-off run, allowing for additional assumptions that simplify the problem formulation. Specifically, during the ground (or water) run, the flight path angle can be neglected, and the velocity vector is assumed to be aligned with the aircraft's longitudinal axis. Under

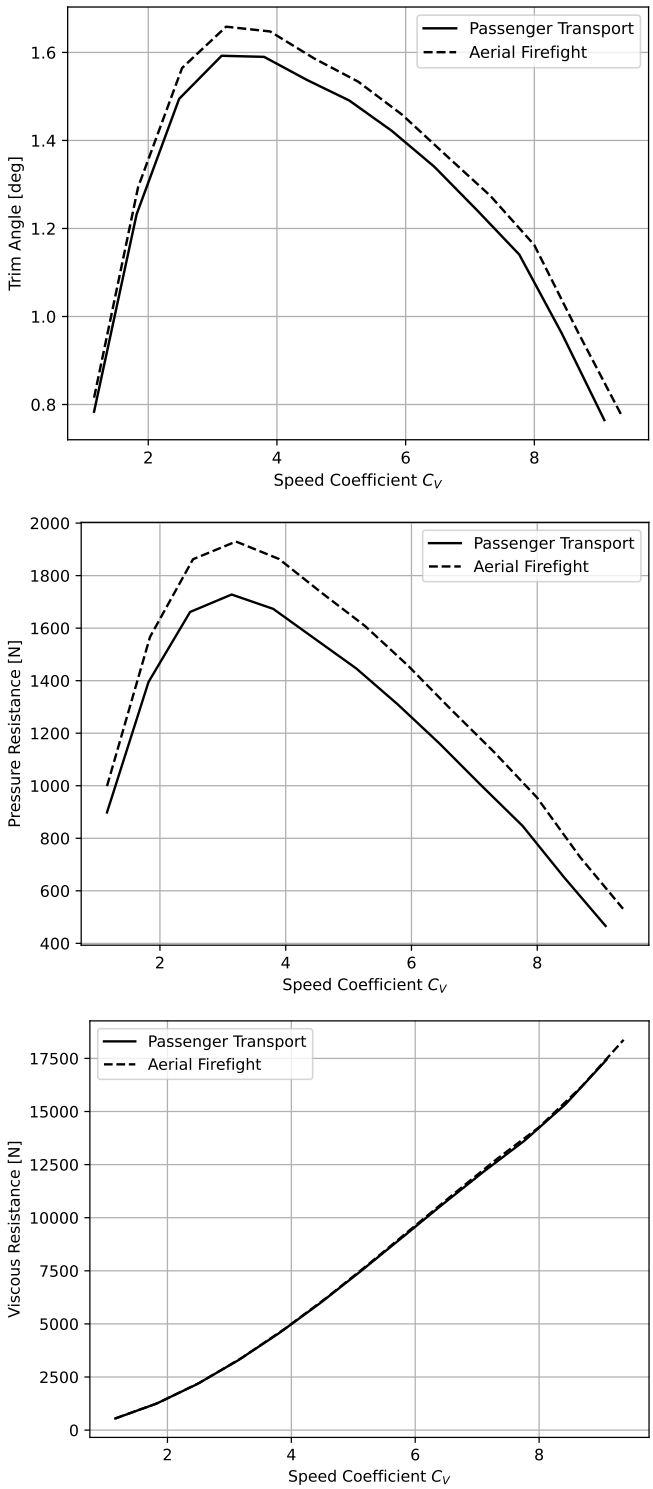

Figure 5.11: Trim angle, viscous resistance and pressure resistance for the optimal hull configuration. Analysis performed on both use cases to address weight and CG differences.

Table 5.15: State variables for the longitudinal motion of the seaplane and applicability definition in the analysis of the ground (water) run take-off segment.

Variable	Symbol	Applied	Note(s)
Speed	V	Yes	-
Angle of Attack	α_B	No	-
Pitch Rate	q	No	Pitch equilibrium always satisfied.
Longitudinal Position	x_G	Yes	-
Vertical Position	z_G	No	Constant altitude motion.
Pitch Angle	θ	No	Coincident with the angle of attack.

this assumption, the angle of attack becomes equivalent to the pitch angle. Furthermore, aerodynamic and hydrodynamic forces are derived under pitch equilibrium conditions, thereby eliminating the rotational degrees of freedom from the equations of motion. Assuming a null runway gradient, consistent with take-off from a water surface, the aircraft's centre of gravity is considered to move solely in the longitudinal direction, without any variation in altitude. Consequently, in the auxiliary kinematic equations, only the longitudinal position is retained for solving the take-off run problem. The resulting system of ODEs is described in Eq. (5.16), while Table 5.15 summarizes the original state variables, indicating which are retained in the simplified formulation and the corresponding assumptions applied.

$$\begin{cases} \dot{V} = \dfrac{g}{W}\left[-D - \dfrac{\Delta(C_V)}{W}R - N_1 \sin\tau_1 - N_2 \sin\tau_2 + T \right] \\ \\ \dot{x}_{\text{CG}} = V \end{cases} \tag{5.16}$$

The simplified equations of motion include additional resistive terms compared to the original formulation. Specifically, the viscous component R the hydrodynamic resistance is multiplied by the ratio between the displacement at a given speed coefficient and the total weight of the seaplane. This formulation, adopted from Gudmundsson [104], accounts for the reduction in viscous resistance as the seaplane rises from the water, thereby decreasing the wetted surface area, an effect not captured by the baseline hydrodynamic model. Furthermore, the first equation in Eq. 5.16 includes the pressure component of the hydrodynamic resistance, represented by the terms N_1 and N_2, which correspond to the normal forces acting on the forebody and afterbody portions of the hull, respectively, projected along the direction of motion.

The problem is therefore reduced to solving Eq. (5.8), which represents the classical flight mechanics formulation for modelling the ground (or water) run segment during take-off simulations.

Table 5.16 presents the results obtained from the simplified system of ODEs used to

Table 5.16: Take-off ground and water segments run comparison in both use cases.

Use Case	**Water Run**	**Ground Run**	Δ
Passenger Transport	338.2 m	234.9 m	+44.0%
Aerial Firefight	431.0 m	279.9 m	+54.0%

analyse the water run during take-off. The additional drag components significantly influence the achievable acceleration along the water surface, delaying the attainment of lift-off speed and consequently increasing the total water run distance. For comparison, the table also reports the ground take-off distance of the aircraft, assuming operations from a paved runway. This case was solved using the same system of ODEs, with the hydrodynamic resistance terms removed and the runway friction effects included. The percentage increase in water run distance relative to the ground run is also indicated. Finally, Figure 5.12 illustrates the individual contributions of the various forces acting on the seaplane throughout the water run.

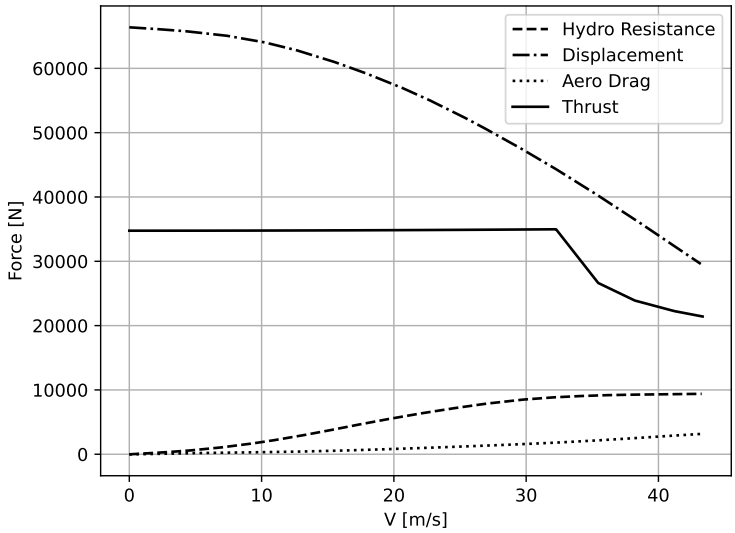

(a) Passenger Transport Use Case

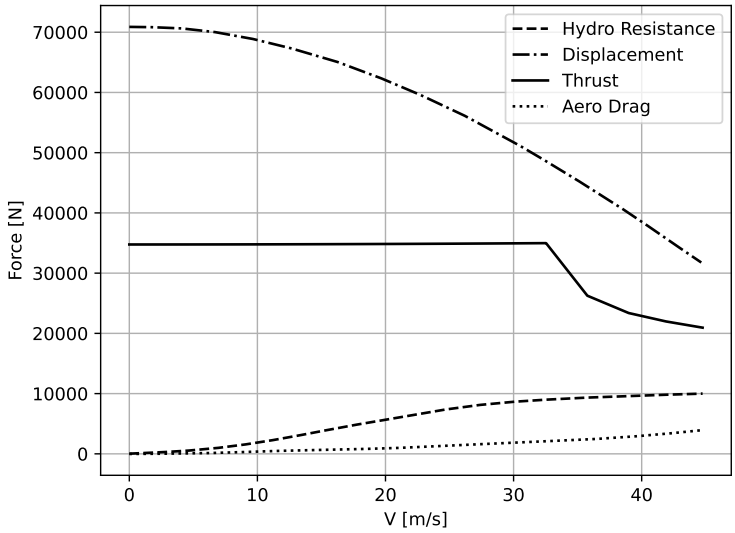

(b) Aerial Firefight Use Case

Figure 5.12: Forces acting on the seaplane during the water take-off run in both use cases. The thrust model account fo a constant contribution of the electric machine and the contribution of the turboprop engine, according to the Mattinlgy's model [194].

Related Publications

The author participated in one conference publication that explores the application of high-fidelity methodologies to determine hydrodynamic performance of hull-shaped seaplane fuselages:

> (*Accepted*) Giacomo Benedetti; **Michele Tuccillo**; Manuela Ruocco; Jan Vos. *Multidisciplinary Conceptual Design and Aero-Hydrodynamic Assessment of a Multi-Role Amphibious Seaplane in the COLOSSUS Project*. To be presented at the 2026 AIAA SciTech, Orlando, Florida.
>
> The study discuss the investigation of the hydrodynamic performance of seaplanes designed within the context of the COLOSSUS project. A CFD analysis was conducted to evaluate the effectiveness and a critical concern of integrating hydrofoils. This approach was inspired by the proven effectiveness of hydrofoils in high-speed marine vessels. Their influence on take-off performance and water handling was assessed by comparing configurations with and without hydrofoils. This was done using a two-step methodology, (1) simplified physics-based models were used to estimate the aircraft's take-off trajectory, (2) selected points along this trajectory were then validated through computational fluid dynamics simulations using a Volume of Fluid approach, enabling an accurate analysis of wave resistance, pressure distribution, and free-surface effects.

5.4 Operational Strategies Analysis

To assess the effectiveness of the proposed design approach in developing a viable multi-role seaplane, it is essential to benchmark the performance of the resulting configuration against an existing reference aircraft. Based on the validation activities conducted in § 4.3, the DHC-6 Twin Otter has been selected as the benchmark platform for this comparative analysis.

The implemented design framework, in conjunction with dedicated mission profile simulation tools [55, 56], was employed to evaluate and compare the candidate solutions from both fuel efficiency and economic performance perspectives. For the passenger transport mission, a direct performance comparison with the Twin Otter is presented. In contrast, for the aerial firefighting configuration, two alternative operational strategies are analysed with the objective of identifying potential improvements in overall operational efficiency.

Passenger Transport

Table 5.17 presents a comparison between the main characteristics and performance metrics of the optimal passenger transport seaplane obtained through the proposed framework and those of the DHC-6 Twin Otter. A key observation is the significant difference in design masses: despite the Twin Otter exhibiting a higher maximum payload capacity, the hybrid-electric seaplane features both an operational empty weight and a maximum take-off weight approximately 20% higher than those of the conventional benchmark.

The increased weight, combined with more demanding performance requirements, results in a total installed power of 1 723 hp for the hybrid-electric configuration (including gearbox efficiency between the electric motor and turboprop shafts). This corresponds to a power loading of approximately 8.55 lb/hp, which is lower than the Twin Otter's value of about 9.20 lb/hp. This power loading notably enhances both take-off and in-flight performance, yielding a 22% reduction in take-off distance and an increase in level flight performance (maximum speed) of approximately 32% compared to the conventional aircraft.

The figures of merit selected for the optimization of the passenger-transport variant of the multi-role seaplane include the range factor (directly related to the maximum range performance), fuel consumption over the design mission, and operating costs. It is noteworthy that the additional degrees of freedom introduced by the hybrid-electric powertrain not only influence the overall design process but also provide opportunities to enhance the operational performance of the aircraft.

Table 5.18 compares the fuel consumption and block time of the DHC-6 Twin Otter and the hybrid-electric seaplane over a representative 165 nm mission. The payload conditions are assumed to be equivalent for both aircraft, with 18 passengers on board, corresponding to a 95% load factor for the Twin Otter. The cruise altitude is set at 10 000 ft, with a cruise Mach number of 0.27, representing the maximum achievable value for the Twin Otter. The climb and descent profiles are defined according to the specific performance characteristics of each configuration.

In Table 5.18, the innovative hybrid-electric seaplane is evaluated under three battery throttle settings during the cruise phase: the design setting of 37.5%, an intermediate 50%, and a high setting of 90%. As expected, increasing battery utilization leads to a reduction in fuel consumption, yielding a 31.3% fuel saving under design conditions and up to 34.3% when operating at 90% battery throttle. However, at the highest throttle setting, the battery is fully discharged before the completion of the cruise segment, thereby diminishing the benefit of hybrid-electric operation and consequently reducing the maximum achievable range.

Under design conditions, maintaining a constant 37.5% battery throttle not only achieves substantial fuel savings relative to the conventional reference aircraft but also maximizes mission range, with complete battery discharge (at a residual 20% state of charge) corresponding to a total range of approximately 250 nm. In contrast,

Table 5.17: Technical comparison between the DHC-6 Twin Otter and the hybrid-electric seaplane in the passenger transport version.

	Twin Otter	**Hybrid-Electric Seaplane**	
Dimensions			
Wingspan	65.0 ft	54.85 ft	-15.6%
Wing Area	420.0 ft^2	378.57 ft^2	-9.8%
Length	51.75 ft	46.75 ft	-9.7%
Engine			
Manufacturer	Pratt & Whitney	-	-
Model	PT6A-27	-	-
Output Power	680 shp	720.5 shp	+16.2%
Battery Energy	-	261.28 kWh	-
Number of Units	2	2	-
Weights			
Max Take-Off Weight	12 500.0 lb	14 986.7.0 lb	+19.9%
Empty Weight	8 573.0 lb	10 541.7 lbb	+23.0%
Fuel Capacity	2 576.0 lb	2 910.6 lb	+13.0%
Max Passengers	19	18	-5.2%
Performance			
Take-Off Ground Roll	1 843.0 ft	1 420.0 ft	-22.9%
Take-Off Water Run	1 965.0 ft	1 539.0 ft	-21.7%
Landing Distance	1 450.0 ft	1 817.0 ft	+23.3%
Max Cruise Speed	162.0 KTAS	214.0 KTAS	+32.1%
Ferry Range	705.0 nm	750.0 nm[a]	+6.4%

[a] The ferry range of hybrid-electric aircraft depends on the approach selected to perform the mission. In this work a constant use of the battery has been assumed, equal to a 37.5% of battery usage in the cruise condition (design condition).

Table 5.18: Fuel consumption, energy consumption and block time comparison between the Twin Otter and the hybrid-electric seaplane on a 165 nm mission. FL100 and Mach number 0.27.

			Hybrid-Electric Seaplane		
Item	**Unit**	**Twin Otter**	ϕ_{BAT}**: 37.5%**	ϕ_{BAT}**: 50.0%**	ϕ_{BAT}**: 90.0%**
Jet-A1 Mass	lb	1 155.0	793.4	763.6	757.8
Battery Energy	kWh	-	145.5	186.96	199.15
Block Time	min	60.0	61.98	61.97	61.97
Take-Off Mass	lb	12 144.7	14 819.5	14 788.3	14 782.0

Table 5.19: Direct and Indirect operating costs comparison between the Twin Otter and the hybrid-electric seaplane on a 165 nm mission. FL100 and Mach number 0.27. Economic assumptions and cost model discussed in § 5.3.1 and in Appendix C.

			Hybrid-Electric Seaplane		
Item	**Unit**	**Twin Otter**	**ϕ_{BAT}: 37.5%**	**ϕ_{BAT}: 50.0%**	**ϕ_{BAT}: 90.0%**
Capital Costs					
Insurance	USD/hr	62.21	70.42	70.42	70.42
Depreciation	USD/hr	234.28	264.74	264.74	264.74
Interests	USD/hr	275.93	311.80	311.80	311.80
Operational Costs					
Jet-A1 Fuel	USD/hr	317.85	211.36	203.42	201.88
Electricity	USD/hr	-	36.62	47.06	50.12
Cockpit Crew	USD/hr	240.0	240.0	240.0	240.0
Airframe Maintenance	USD/hr	220.27	240.27	240.27	240.27
Turboprop Maintenance	USD/hr	170.44	171.90	171.90	171.90
EM Maintenance	USD/hr	-	20.38	20.38	20.38
Battery Maintenance	USD/hr	-	41.27	53.02	56.48
Charges					
Take-Off & Landing	USD/hr	28.35	32.89	32.89	32.89
Navigation	USD/hr	70.53	74.75	74.75	74.75
Ground Handling	USD/hr	307.80	297.97	297.97	297.97
CO_2 EU ETS	USD/hr	30.25	20.12	19.36	19.21
DOC	USD/hr	1 957.91	2 034.49	2 048.0	2 052.82
IOC	USD/hr	900.57	901.89	910.67	913.81
DOC	USD	1 957.91	2 101.63	2 115.57	2 120.57
IOC	USD	900.57	931.66	940.72	943.97

Table 5.20: Economic assumptions on the aircraft delivery price and turboprop engine according to Ref. [195].

Item	**Unit**	**Twin Otter**	**Hybrid-Electric Seaplane**
Aircraft Delivery Price	USD	5 530 000.0	6 260 000.0
Turboprop Engine Price	USD	411 000.0	434 000.0

at 90% battery usage, the maximum range decreases to 130 nm, providing only a 3% additional fuel saving, thereby illustrating the trade-off between fuel efficiency and range performance in hybrid-electric operation.

Table 5.19 presents a comparison of the operating costs of the hybrid-electric seaplane and the reference DHC-6 Twin Otter. For the latter, identical economic assumptions were applied, with the only differences being the aircraft acquisition cost, updated from its 1985 market value to 2024 USD 5.53 million, as discussed in the market analysis, and the turboprop engine cost, which was estimated using the methodology proposed by Roskam [195] and similarly adjusted to 2024 economic conditions. The breakdown of these costs is summarised in Table 5.20.

The results indicate that, despite the fuel consumption savings achieved by the hybrid-electric configuration, the weight-driven cost model and the inclusion of additional maintenance expenses associated with the electric components of the powertrain

Table 5.21: Fuel consumption, energy consumption and block time of the hybrid-electric seaplane on a 165 nm mission in design flight conditions. FL100 and Mach number 0.33.

Item	**Unit**	ϕ_{BAT}**: 37.5%**	ϕ_{BAT}**: 50.0%**	ϕ_{BAT}**: 90.0%**
Jet-A1 Mass	lb	837.1	817.5	788.5
Battery Energy	kWh	124.3	158.5	199.2
Block Time	min	55.9	55.9	56.2
Take-Off Mass	lb	14 865.8	14 844.9	14 814.4

limit its potential for economic competitiveness relative to the conventional counterpart. Moreover, the analysis reveals that higher utilization or stress of the electric components results in an increase in overall operating costs, thereby counteracting part of the expected economic advantage deriving from the fuel saving.

It is important to note, however, that these results assume equivalent operating environments and mission conditions for both aircraft. Specifically, the hybrid-electric seaplane's costs were estimated under off-design conditions, particularly with respect to the cruise Mach number, which was optimized to 0.33. Consequently, economic viability for a hybrid-electric aircraft may require mission and operational profiles distinct from those of conventional turboprop aircraft, as identical utilization strategies may not yield comparable cost efficiency.

Table 5.21 presents the fuel consumption, battery energy consumption, and mission duration for the representative mission executed under design conditions, corresponding to a cruise Mach number higher than that used in the comparison with the Twin Otter and consistent with the conditions at which the battery system was sized. As expected, for a fixed battery contribution to the total shaft power, an increase in cruise Mach number necessitates a higher thermal engine throttle setting, resulting in greater fuel consumption. Conversely, a reduction in battery energy consumption is observed, primarily due to a decrease in block time of approximately five minutes. This reduction in mission duration, however, affects the most demanding operational case in terms of battery utilization (i.e., the 90% throttle setting). In this configuration, the fuel saving obtained when increasing battery usage from 50% to 90% amounts to approximately 3.6%.

Table 5.22 illustrates the variation in operating costs as the cruise Mach number increases from 0.27 to the design cruise Mach number. It is noteworthy that, for the hybrid-electric seaplane, energy-dependent cost components are generally higher than those of the conventional counterpart. Consequently, to compensate for the cost penalties associated with energy usage, a reduction in block time is required, thereby lowering the time-related components of the DOCs.

An average DOC reduction of approximately 5% is observed with increasing Mach number, as shown in Figure 5.13. Under design conditions (with the battery throttle set to 37.5%), the total operating cost remains 1.5% higher than that of the DHC-6 Twin Otter, while achieving a 27.5% reduction in fuel consumption. These results emphasize the necessity of adapting operational strategies when assessing the eco-

Table 5.22: Direct and Indirect operating costs comparison of the hybrid-electric seaplane on a 165 nm mission in design flight conditions. FL100 and Mach number 0.33. Economic assumptions and cost model discussed in § 5.3.1 and in Appendix C.

Item	**Unit**	ϕ_{BAT}**: 37.5%**	ϕ_{BAT}**: 50.0%**	ϕ_{BAT}**: 90.0%**
Capital Costs				
Insurance	USD/hr	70.42	70.42	70.42
Depreciation	USD/hr	264.74	264.74	264.74
Interests	USD/hr	311.80	311.80	311.80
Operational Costs				
Jet-A1 Fuel	USD/hr	247.26	241.47	231.66
Electricity	USD/hr	34.69	44.23	55.29
Cockpit Crew	USD/hr	240.00	240.00	240.00
Airframe Maintenance	USD/hr	255.74	255.74	254.90
Turboprop Maintenance	USD/hr	175.90	175.90	175.68
EM Maintenance	USD/hr	20.38	20.38	20.38
Battery Maintenance	USD/hr	39.09	49.84	62.31
Charges				
Take-Off & Landing	USD/hr	36.47	36.47	36.28
Navigation	USD/hr	82.88	82.88	82.43
Ground Handling	USD/hr	330.38	330.38	328.61
CO_2 EU ETS	USD/hr	23.53	22.98	22.05
DOC	USD/hr	2 133.27	2 147.23	2 156.56
IOC	USD/hr	966.11	975.18	981.24
DOC	USD	1 987.50	2 000.51	2 019.97
IOC	USD	900.09	908.54	919.09

nomic viability of non-conventional aircraft architectures, where performance benefits may be offset by differences in cost structure and mission profile optimization.

Aerial Firefight

In aerial firefighting operations, both regulatory authorities and aircraft operators impose limits on the maximum allowable flight hours for safety, maintenance, and operational reliability reasons. To sustain continuous operations beyond these legal flight-hour constraints, a fleet of aircraft is therefore required, typically operating in parallel to ensure uninterrupted mission coverage. Within the available operational time window, the primary objective is to maximize the total payload, specifically, the volume of water, that the fleet can deliver over the fire area. Consequently, pilots and mission planners aim to maximize the water drop volume per sortie for each aircraft, thereby enhancing the overall firefighting effectiveness and mission efficiency [196].

At the preliminary design stage, a sufficient understanding of the aircraft's performance and operational behaviour is typically available, enabling the assessment of flight and mission performance across one or more representative mission profiles. This can be achieved using simulation models that offer higher levels of fidelity and

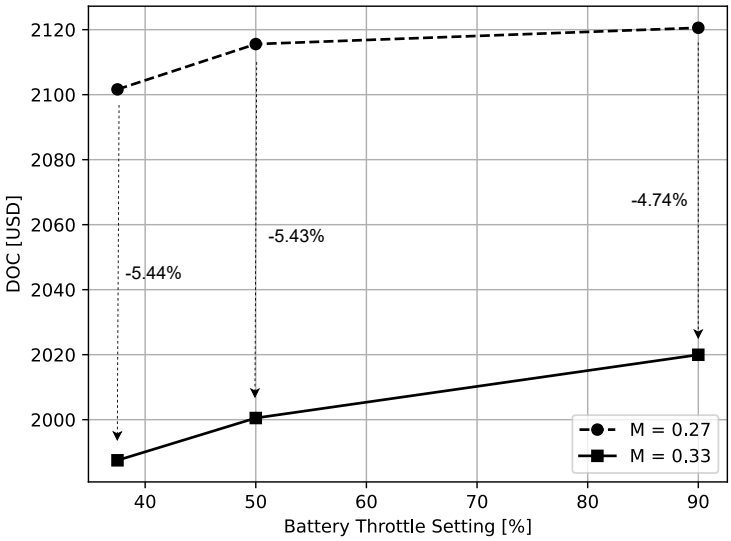

Figure 5.13: DOC saving as function of the battery throttle saving.

flexibility, such as those developed by Grazioso et al. [55], compared to the tools employed during the conceptual design phase. The ability to define a fully customized mission profile for aerial firefighting operations allows for the systematic exploration of scenarios in which the aircraft can fully exploit its operational potential, as well as those where its effectiveness may be limited. This capability supports the development strategies to maximize mission efficiency and effectiveness in real-world firefighting operations.

Unlike in the design phase, the assessment of aircraft operational efficiency and operating costs can be conducted without prescribing a fixed number of water drops per mission. Instead, the analysis can be based on the definition of specific aerial firefighting mission parameters, such as those used to establish the sizing scenarios. These include the distance between the base airport and the fire location and the distance between the fire zone and the nearest available water source. By varying these parameters, it becomes possible to evaluate the effectiveness of the aircraft in terms of its ability to maximize the cumulative payload of water delivered to the fire, thereby providing a more representative assessment of operational performance across diverse mission conditions.

To perform a preliminary evaluation of operational efficiency, two representative mission profiles were selected from Table B.2, specifically, scenarios 1 and 4. These scenarios were chosen due to their substantial differences in key mission parameters, including those previously discussed. However, to ensure a consistent and fair comparison, comparable environmental and operational conditions were defined, particularly with respect to water pick-up altitude, fire altitude, and drop altitude.

For example, in a sea-side firefighting scenario, the water pick-up altitude is set to

sea level, while the fire altitude is fixed at 1 500 ft, corresponding approximately to the average value between the two reference scenarios. The drop altitude is then defined to maintain a 150 ft vertical separation from the fire altitude, resulting in a drop altitude of 1 650 ft, enabling a consistent assessment of mission effectiveness across the two operational cases. Finally in both scenarios the cruise altitude necessary to reach the water pick-up spot from the base airport (assuming that at the beginning of the mission no water is carried on-board) is set to 6 000 ft, with a maximum operational flight time of 2 hours, a little less than the 3 hours for a CL-415 [196], that is however capable of higher payload and fuel capacity.

Table 5.23 presents, for both scenarios, the main mission performance indicators, including the total fuel required to complete a 2-hour mission, the effective firefighting time (excluding the transit segments between the base airport and the fire location), the total payload released over the fire, the operational efficiency, and the DOC. These parameters are evaluated under two operating conditions: (1) constant payload release over time, and (2) variable payload release, made possible by the progressive reduction in aircraft mass throughout the mission, as observed in operational configurations such as the AT-802 Fire Boss.

In the first scenario, the influence of the maximum allowable flight time constraint is clearly evident. The aircraft completed five drops under both operational strategies; however, the variable payload strategy resulted in a 12.4% increase in operational efficiency compared to the constant payload approach. Despite this improvement, the achieved efficiency value of 280 lt/min (73.15 US Gal./min) remains lower than the optimal value identified during the conceptual design phase, which did not account, due to the simplified performance analysis model, for the transit time between the base airport and the fire location and of the flight time constraint.

Table 5.24 illustrates the evolution of the payload across successive sorties, showing that the maximum payload was nearly reached only during the final drop. The higher total payload delivered in the variable payload configuration led, in the first scenario, to a 9.4% reduction in normalized DOC relative to the constant payload strategy, with only a 0.4% increase in total fuel consumption.

Figure 5.14 illustrates the time evolution of the aircraft mass throughout the aerial firefighting simulation for Scenario 1. It is observed that, under the constant payload strategy, the aircraft reaches its maximum mass at the beginning of the firefighting phase. Conversely, when adopting the variable payload strategy, the maximum mass occurs toward the end of the mission, primarily as a consequence of the progressive reduction in fuel mass during flight.

A notable difference between the two scenarios lies in the factors constraining mission efficiency. In Scenario 1, efficiency is primarily limited by the maximum allowable flight time, which restricts the total number of water drops that can be performed over the fire. Conversely, in Scenario 4, the shorter distances between the base airport and the fire location allow for a greater number of drops, twelve, according to the mission simulation. In this case, the operational performance is in-

Table 5.23: Mission performance indicators on the aerial firefight mission determined through preliminary mission analysis simulations according to Ref. [55].

Item	**Unit**	**Constant Payload**	**Variable Payload**
Scenario 1			
Jet-A1 Mass	lb	1 153.7	1 158.7
Battery Energy	kWh	204.35	204.35
Aircraft WTO	lb	10 730.0	10 735.1
Maximum Aircraft Mass	lb	14 848.0	15 876.0
Total Mission Time	min	112.0	112.3
Firefight Mission Time	min	41.0	41.2
Number of Drops	-	5	5
Total Mission Range	nm	310.0	310.0
Operational Effiency	lt/min	249.0	280.0
	US Gal./min	65.76	73.15
DOC	USD	5 900.0	5 953.0
	USD/hr	3 161.0	3 181.0
	USD/US Gal. hr	1.17	1.06
Scenario 4			
Jet-A1 Mass	lb	754.4	766.6
Battery Energy	kWh	131.5	131.5
Aircraft WTO	lb	10 309.5	10 322.4
Maximum Aircraft Mass	lb	14 753.8	15 225.8
Total Mission Time	min	90.2	90.5
Firefight Mission Time	min	74.7	75.0
Number of Drops	-	12	12
Total Mission Range	nm	181.5	181.5
Operational Effiency	lt/min	328.7	374.75
	US Gal./min	86.8	99.0
DOC	USD	4 730.2	4 785.9
	USD/hr	3 145.4	3 171.9
	USD/US Gal. hr	0.49	0.43

Table 5.24: Payload drop profile for both scenarios and strategies.

Drop ID	Unit	Constant Payload	Variable Payload	Note(s)
Scenario 1				
1	US Gal.	540.0	540.0	-
2	US Gal.	540.0	555.0	-
3	US Gal.	540.0	581.2	-
4	US Gal.	540.0	634.0	-
5	US Gal.	540.0	700.0	-
	US Gal.	2 160.0	3 010.2	Total Payload
Scenario 4				
1	US Gal.	540.0	540.0	-
2	US Gal.	540.0	568.0	-
3	US Gal.	540.0	594.4	-
4	US Gal.	540.0	594.4	-
5	US Gal.	540.0	620.8	-
6	US Gal.	540.0	620.8	-
7	US Gal.	540.0	634.0	-
8	US Gal.	540.0	634.0	-
9	US Gal.	540.0	647.2	-
10	US Gal.	540.0	647.2	-
11	US Gal.	540.0	660.4	-
12	US Gal.	540.0	660.4	-
	US Gal.	6 480.0	7 421.6	Total Payload

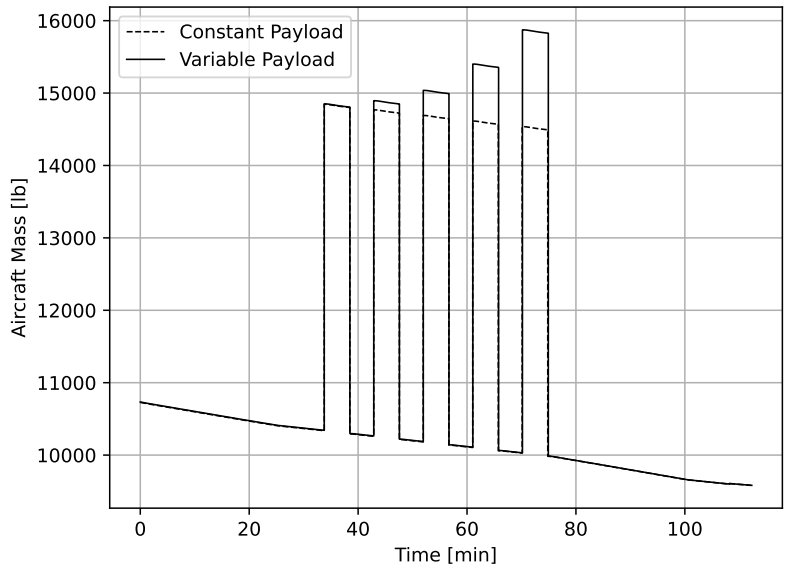

Figure 5.14: Mass Profile as function of mission time for Scenario 1.

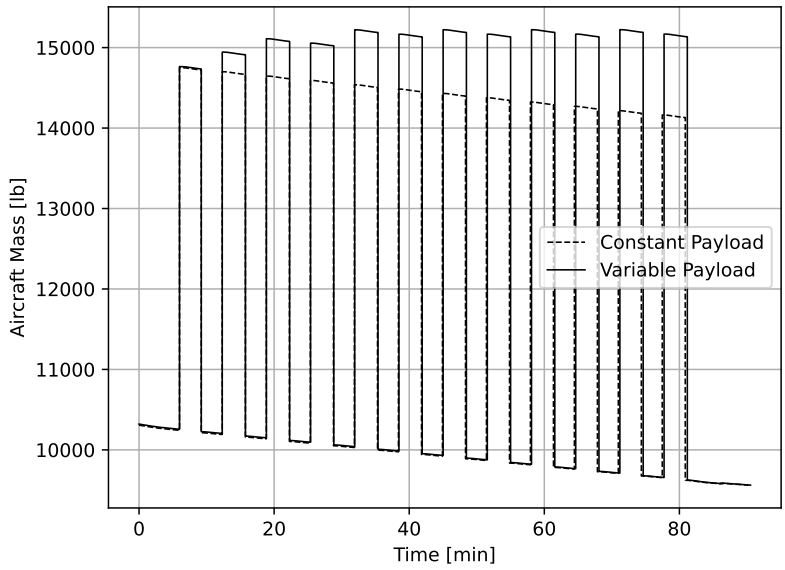

Figure 5.15: Mass Profile as function of mission time for Scenario 4.

stead constrained by weight limitations, particularly the maximum take-off mass and the instantaneous aircraft mass, both of which influence the ability to maintain prescribed flight conditions (e.g., cruise Mach number, climb and descent speeds, and rate of descent). Moreover, the higher number of drops in Scenario 4 enables a gradual increase in water payload, as illustrated in Figure 5.15, accompanied by a progressive reduction in operating costs per unit time and payload.

It can be concluded that the preliminary-level assessment of aircraft behaviour, under both design and off-design conditions, constitutes a powerful tool for verifying the consistency and coherence of design solutions developed during the conceptual stage. Furthermore, it enables the identification of refined operational strategies that enhance platform performance, particularly under off-design conditions, by delineating the boundaries of feasible operating scenarios.

Conclusions

COLLABORATIVE and multidisciplinary design frameworks have become fundamental to the development and analysis of modern aircraft. Such approaches are required to address the growing complexity of aerial systems, as well as the increasing number of design variables and performance requirements necessary to solve comprehensive conceptual and preliminary design problems. These frameworks enable consistent and effective investigations of disruptive and unconventional aircraft concepts. Furthermore, advancements in subsystem technologies have facilitated the exploration of new business models and renewed interest in historical configurations, such as seaplanes, by demonstrating the potential to enhance their performance and integrate them into a continuously evolving aviation market.

Traditionally, state-of-the-art numerical methodologies and aircraft disciplinary design and analysis tools have been incorporated into the conceptual and preliminary design stages primarily to address specific aspects of the design problem. These efforts have often focused on the implementation of high-fidelity methods or detailed subsystem-level analyses, such as those related to hybrid-electric powertrain design, analysis and management, in order to reduce uncertainty in the early development phases. However, this approach has constrained the inherent potential of conceptual design, limiting the scope of configuration exploration typically associated with this stage. This observation motivated the central research question of this work:

In what ways can conceptual and preliminary design workflows be extended and restructured to support architecture exploration and optimization of innovative amphibious aircraft, while enhancing the operational attractiveness in achieving an optimal balance between performance and cost-effectiveness ?

This research has demonstrated the potential of integrating machine learning strategies and methodologies within traditional aircraft conceptual design frameworks to improve the efficiency, adaptability, and flexibility of the early-stage design process, posing the attention of a first central topic of the main research question:

In what ways can conceptual design workflows be extended to support architecture exploration and optimization of innovative amphibious aircraft ?

The developed framework enables feasibility assessments of new programs from the earliest stages of development by establishing a seamless interface between conventional aircraft design and analysis disciplines and data-driven algorithms. This integration allows automated and iterative design space exploration for multi-role vehicles that incorporate non-conventional design variables, hybrid-electric architectures, and use-case-specific performance and operational metrics. Ultimately, the proposed methodology enhances design flexibility and supports more informed, data-driven decision-making throughout the aircraft concept exploration and evaluation process.

By embedding machine learning strategies within the multidisciplinary design analysis and optimization workflow, this research has demonstrated that complex concepts exploration activities, particularly those involving novel aircraft configurations and non-conventional energy systems operating under multiple mission scenarios, can be effectively addressed through predictive and adaptive modelling techniques. The integration of ML-based approaches enabled the continuous refinement of surrogate-based fast-predictive disciplinary models, thereby enhancing the quality of information available for decision-making during the conceptual design phase. As a result, the design process achieved faster convergence toward families of optimal configurations while maintaining analytical rigor and computational efficiency.

A key contribution of this work lies in the implementation of Active Learning and surrogate-based optimization methodologies for the systematic exploration of multiple seaplane architectures. The proposed framework employed an iterative data-generation process to train surrogate models capable of accurately approximating the behaviour of complex disciplinary analyses workflows across broad and multi-dimensional design spaces. This approach significantly reduced the computational burden typically associated with training machine learning models, while preserving model accuracy and reliability. Active Learning strategies were specifically applied to identify the most informative data samples, further improving computational efficiency.

The resulting methodology enabled a comprehensive comparison among alternative seaplane configurations by evaluating multiple performance metrics, including operational efficiency, aerodynamic performance, operating costs, and energy consumption, across representative mission profiles and operational scenarios, the latter specifically derived to address the variety of aerial firefighting operating conditions. The findings underscored the effectiveness of surrogate-assisted exploration in identifying feasible design trends and in supporting informed early-stage architectural decisions.

The exploration of families of seaplane configurations satisfying given design requirements represented only the initial step toward enhancing the potential of this aircraft category. The inherent versatility of seaplanes can be further optimized by considering their capability to perform multiple roles, not as independent functions,

but as integrated mission profiles within a single, multi-role platform. To this end, two promising configurations were extracted from the families of optimal concepts identified during the conceptual phase and further developed in the preliminary design stage. The objective was to achieve an optimal trade-off between performance and cost, while accounting for the potential advantages and limitations associated with non-conventional powertrain architectures observed in the passenger transport variant. This progression naturally shifted the focus to the second component of the main research question:

How can preliminary design methodologies be restructured to enhance operational attractiveness by integrating multi-role capabilities, achieving an optimal balance between performance and cost-effectiveness in innovative seaplanes ?

The preliminary design investigations, conducted on the most promising aircraft derived from the surrogate-based optimization, confirmed the feasibility of multi-role seaplane operations, addressing both passenger transport and aerial firefighting missions. The adoption of modular architectures and adaptable subsystem layouts enabled the optimization of key performance indicators, such as take-off distance, fuel consumption, and payload capacity, without compromising the overall configuration or operational cost targets. The findings demonstrated that hybrid-electric powertrain solutions, when integrated with optimized hull geometries, can substantially improve both environmental sustainability and mission performance, even under the demanding conditions of aerial firefighting operations.

These results establish a solid foundation for future developments in flexible and sustainable amphibious aircraft, reinforcing their potential competitiveness within emerging aviation markets and contributing to the broader goals of next-generation green aviation.

Appendix A

Seaplane Statistical Design Point

Contents

THIS appendix outlines the statistical sizing process employed to generate initial configurations of both a passenger transport seaplane and an aerial firefighting seaplane, which serve as starting points for the subsequent conceptual design stage. The relatively low level of detail characterizing this phase enables the adoption of classical textbook methodologies. In this context, the preliminary sizing approaches proposed by Roskam [23] are applied to estimate the weight breakdown and identify the sizing point. Furthermore, statistical relationships derived from an extensive dataset of amphibious seaplanes are integrated with these results to size the principal vehicle components.

A.1 Estimating Weight Breakdown

Regardless of the intended scope of an aircraft, whether for passenger transport or emergency response, such platforms are generally required to satisfy stringent specifications defined in terms of range, speed, and endurance, which are typically reported in the TLAR table. At this early stage of the design process, the ability to predict the principal aircraft design masses is critical, particularly the Maximum Take-Off Mass (MTOM), the Operating Empty Mass (OEM), and the fuel mass required to

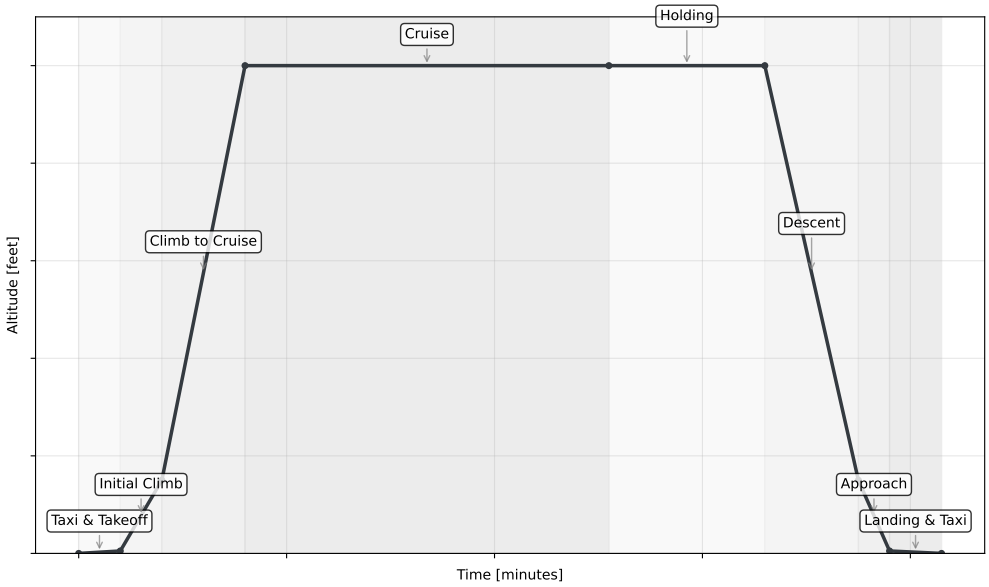

Figure A.1: Qualitative representation of a passenger transport aircraft mission profile.

complete the assigned mission. The mission is generally expressed as a sequence of phases within a mission-profile diagram. Figure A.1 and Figure A.2 provide a qualitative representation of a typical operational mission profile for a passenger transport aircraft (also applicable to seaplanes) and for an aerial firefighting seaplane, respectively.

According to Roskam [23], the three weight components are related through the expression reported in Eq. A.1. In this relation, W_{TO} denotes the MTOM, W_{OE} the OEM, W_F the required fuel mass, and W_{PL} the assigned payload mass. To solve this equation, which involves three unknowns, it is necessary to express one variable as a function of another and to introduce a second independent relation. This allows the formulation of a linear system of equations admitting a unique solution.

$$W_{TO} = W_{OE} + W_F + W_{PL} \tag{A.1}$$

The required mission fuel is generally expressed as the sum of the usable fuel for the mission and the reserve fuel necessary to meet regulatory or operational requirements. The reserve fuel is typically specified as a percentage of the usable fuel, or alternatively as an additional requirement to ensure the capability to reach an alternate airport (if applicable) or to loiter over the destination airport for a prescribed duration.

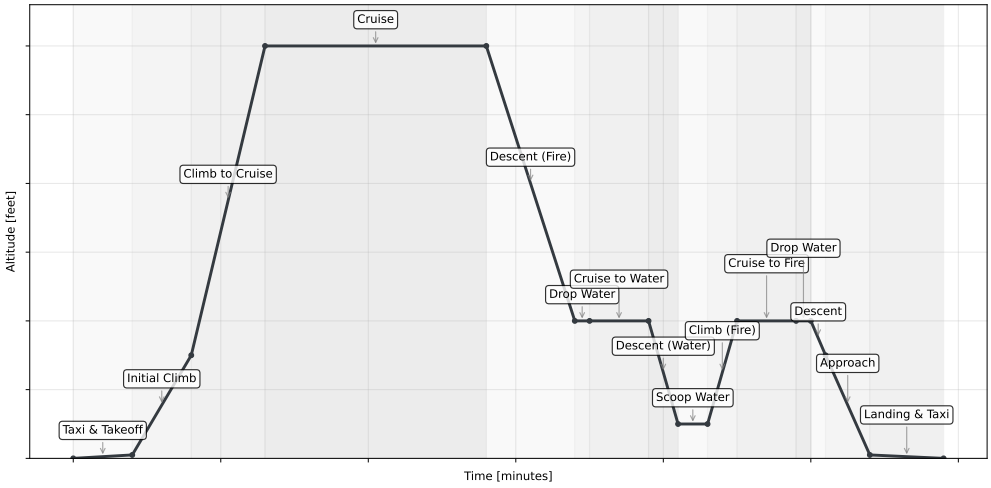

Figure A.2: Qualitative representation of a scooper firefighter aircraft mission profile. The number of active firefighting phases has been reduced to one to ease the visualization of typical operating phases.

A.1.1 The Fuel-Fraction Method

The usable fuel is commonly estimated through the fuel-fraction method. In this approach, the mission profile is decomposed into its characteristic phases, as illustrated in Figure A.1 and Figure A.2. The fuel consumption associated with each phase can then be determined either from statistical correlations or by applying simplified flight mechanics relations.

Considering an aircraft with an initial weight at the beginning of the i-th mission phase, denoted as W_i, and a reduced weight at the end of that phase, W_{i+1}, the corresponding fuel fraction for the phase can be expressed as shown in Eq. A.2. By multiplying the fuel fractions across all phases of the mission profile, it is possible to obtain the ratio between the final aircraft weight at the end of the mission and the MTOM. This ratio defines the mission fuel fraction, M_{FF}, as presented in Eq. A.3, that help posing the fuel mass as a function of the aircraft MTOM, as depicted in Eq. A.4.

$$FF_i = \frac{W_i}{W_{i+1}} \tag{A.2}$$

$$M_{FF} = \frac{W_N}{W_{TO}} = \prod_{i=1}^{N-1} \frac{W_i}{W_{i+1}} \tag{A.3}$$

$$W_F = W_{TO} - W_N = (1 - M_{FF})\, W_{TO} \tag{A.4}$$

Table A.1 summarises the contribution of each flight phase to the mission fuel fraction, with the indication of the flight mechanic equation to be used where no sug-

Table A.1: Fuel-fraction by phase for both passenger transport and aerial firefighting missions (derived from [23]).

Phase	Pax Transport	Aerial Firefight	Note(s)
Taxi	0.990	0.990	-
TakeOff	0.996	0.996	-
Climb	0.985	0.985	Including also to the Initial Climb phase
Cruise	-	-	Derived from the Breguet range equation
Holding	-	-	Derived from the Breguent endurance equation
Descent	0.990	0.990	Including also the Approach phase
Drop Water	N/A	1.000	Assumed to occur in a negligible amount of time
Cruise to Water	N/A	-	Derived from the Breguet range equation
Descent (Water)	N/A	0.998	-
Scoop Water	N/A	1.000	Assumed to occur in a negligible amount of time
Climb (Fire)	N/A	0.996	Contributing as a TakeOff phase
Cruise to Fire	N/A	-	Derived from the Breguet range equation
Landing & Taxi	0.990	0.990	-

gestions are provided.

A.1.2 The Statistical Closing Equation

The fuel-fraction method facilitates the solution of Eq. A.1 by expressing one of the unknown terms as a function of another, thereby reducing the problem to a single equation with two unknowns: the aircraft MTOM and the operating empty weight.

To close the system and obtain a solvable set of equations, an additional independent relationship must be introduced. This auxiliary equation is typically derived from statistical correlations observed in a representative sample of aircraft. In particular, Roskam demonstrated that a linear dependence, in a regression sense, exists between $\log_{10}(\mathrm{W_{TO}})$ and $\log_{10}(\mathrm{W_{OE}})$ for aircraft within the same category. This relationship is generally expressed in the form shown in Eq. A.5.

$$\log_{10}(\mathrm{W_{TO}}) = A + B\,\log_{10}(\mathrm{W_{OE}}) \tag{A.5}$$

Coefficients A and B depend on the specifc aircraft cateogry, the sample of aircraft collected in the class of seaplanes shows, $A = 0.1703$ and $B = 1.0083$.

A.2 The Sizing Diagram

In addition to satisfying range, endurance, and cruise requirements, aircraft are typically sized to meet a set of specific performance criteria. These include stall speed limits (in both clean and high-lift configurations), take-off and landing distance requirements, maximum or nominal cruise speed, and climb performance or service ceiling requirements, generally defined under the most adverse operating conditions prescribed by regulatory authorities.

A sizing diagram, or sizing plot, is a well-established tool for determining admissible combinations of wing loading and weight-to-power ratio, for propeller-driven aircraft, ensuring compliance with these requirements. For each performance metric, a mathematical relation of the form $W/P = f(W/S)$ can be formulated, where, for any assigned wing loading, the expression provides the maximum required weight-to-power ratio (i.e. the minimum required installed power) to meet the performance requirement under consideration. The superposition of all such relations defines a feasible design region within the sizing plot, where all regulatory and operational performance constraints are simultaneously satisfied.

A.3 Results of the Statistical Design

The application of the fuel-fraction method requires, for those flight phases governed by the Breguet range and endurance equations, initial assumptions regarding the parameters that define the so-called Range Factor and Endurance Factor. These parameters include the lift-to-drag ratio in the relevant flight segments and the engine specific fuel consumption for the same operating conditions.

When addressing the design of non-conventional configurations, the selection of these assumptions should account for recent advancements in the design and operation of such platforms. However, it must be emphasized that achievable performance strongly depends on the specific powertrain architecture and its operational strategy within the representative mission scenario. To avoid bias in the preliminary estimation, it is therefore appropriate to establish a reference baseline based on conventional aircraft. According to Roskam [23], typical lift-to-drag ratios for seaplanes in cruise conditions range between 10 and 12, while values of 13 to 15 are generally achieved during loiter, a flight segment characterized by reduced speed aimed at minimizing fuel consumption.

Similarly, representative values of specific fuel consumption (SFC) for propeller-driven seaplanes, predominantly equipped with turboprop engines, typically fall within the range of 0.5 to 0.7 lb/hp/hr. The ranges adopted in this work, together with the selected target values for subsequent analyses, are summarized in Table A.2.

Table A.2 reports how the selected lift-to-drag ratios, for the aerial firefighting configuration, positioned at the lower bound of the suggested variation ranges, or in

Table A.2: Assumed aerodynamic and propulsion parameters for the application of the fuel-fraction method in seaplane preliminary sizing.

Parameter	Range	Pax Transport	Aerial Firefight
Lift-to-Drag (cruise)	[10 - 12]	10	9
Lift-to-Drag (loiter)	[13 - 15]	14	13
SFC [lb/hp hr]	[0.5 - 0.7]	0.6	0.6

Table A.3: Fuel-fraction method results.

Weight Item	Pax Transport	Aerial Firefight	Note(s)
Payload [lb]	3 860.0	4 850.0	Including Pilots
Fuel [lb]	1 484.7	1 679.8	Including Reserve
OEM [lb]	8 996.4	10 903.7	-
MTOM [lb]	14 361.1	17 433.5	-

some cases slightly below. This choice is motivated by the figures of merit typically optimized for this class of aircraft, where operational efficiency, defined in terms of the maximum volume of fire suppressant delivered per unit time, represents one of the most critical performance metrics. Such requirements directly influence the operating speeds, which are generally higher than those of an equivalent passenger transport variant. Table A.3 summarizes the principal weight components as defined by the fuel-fraction method.

Finally, Figure A.3 presents the sizing diagram, which is applicable to both seaplane configurations, passenger transport and aerial firefighting, since all performances are generally normalized with respect to the aircraft MTOM. The primary objective of the plot is to identify, within the feasible region, the design point that provides an initial estimate of the required installed power and the wing reference area. It is noteworthy that, for low wing loading conditions, the most influential constraints are the climb requirements prescribed by certification authorities, specifically under All Engines Operating (AEO) conditions, CS-23.65(b) and CS-23.67(b)(2), as well as under One Engine Inoperative (OEI) conditions, represented by the curve labelled CS-23.77(b). These requirements are primarily driven by the large wing surface area, which limits the maximum achievable rate of climb and consequently increases the required installed power to satisfy imposed regulation constraints. At higher wing loading conditions, the feasible region is bounded by cruise speed, landing distance, and take-off distance requirements. A balanced trade-off between installed power and wing surface area can be achieved by selecting a design point that lies between the maximum weight-to-power ratio and the maximum wing loading limits. Table A.4 summarizes the selected design point together with the corresponding installed power and wing reference area.

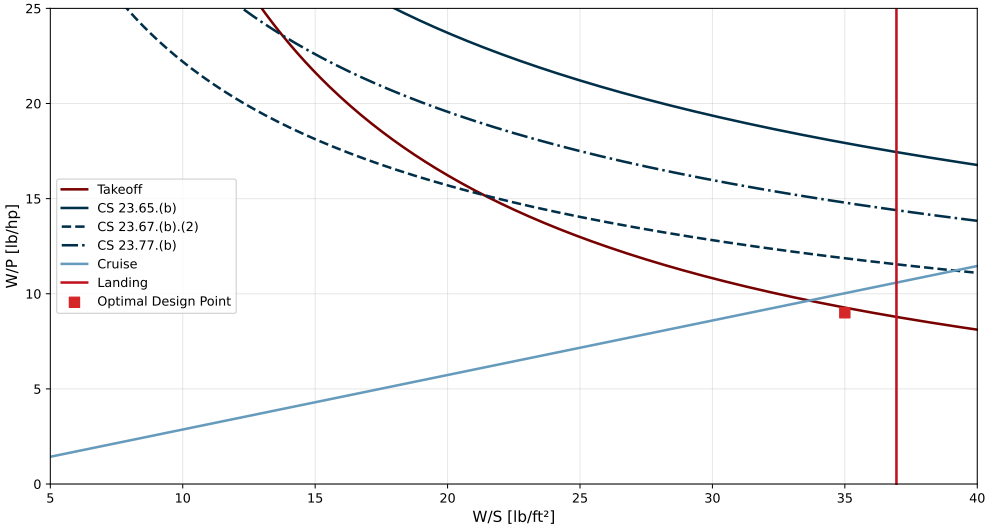

Figure A.3: Seaplane sizing diagram and selected design point.

Table A.4: Sizing diagram results and main geometrical features derived from a statistics of seaplanes from Ref. [23] and Ref. [108].

	Pax Transport	**Aerial Firefight**	**Note(s)**
W/P [lb/hp]	9.0	9.0	-
W/S [lb/ft^2]	35.0	35.0	-
P [hp]	797.0	970.0	Single Engine
S_w [ft^2]	410.0	500.0	-
AR_w	8.04	8.25	-
Λ_w	1.5	0.0	At quarter chord
λ_w	0.63	0.75	-
AR_H	4.55	4.20	-
Λ_H	4.0	6.5	At quarter chord
λ_H	0.61	0.55	-
S_H [ft^2]	82.30	100.0	-
AR_V	1.25	1.5	-
Λ_V	32.0	35.0	At leading edge
λ_V	0.55	0.45	-
S_V [ft^2]	64.5	75.0	-
Fuselage Length [ft]	48.72	46.53	-

Appendix B

Aerial Firefight Scenario Analysis

Contents

THE primary objective of this appendix is to provide a concise overview of the rationale underlying the construction of the aerial firefighting table of scenarios presented in § 4.5.1. The analysis of representative scenarios begins with the identification of a reference aerial firefighting operator and a geographical region in which multiple independent missions have been conducted. Operational data from real missions are then collected and systematically compared. This comparison includes both the temporal evolution of the mission profiles and their key characteristic parameters, namely the number of drops, fire ground altitude, water source altitude, number of consecutive operating days, distance between the fire location and the nearest water source, and distance between the base airport and the fire location.

B.1 Reference Geographical Region

In 2024, the European Forest Fire Information System (EFFIS)[1] conducted an assessment to identify the regions in Europe (EU27) most critically exposed to wildfire risk, based on the Fire Weather Index (FWI). The FWI is a widely adopted indicator that quantifies the influence of meteorological conditions on fuel flammability and is commonly used to evaluate both the potential spread and intensity of wildfires.

[1] Wildfire Copernicus website: `https://climate.copernicus.eu/esotc/2024/wildfires`

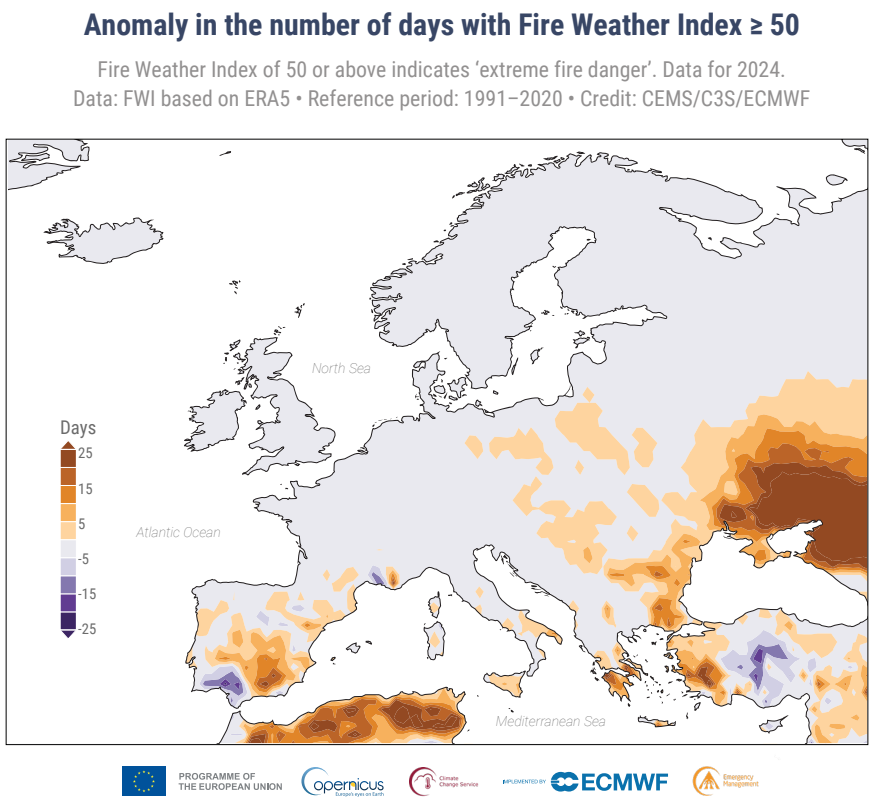

Figure B.1: Anomalies in the number of days with a Fire Weather Index of 50 or above (indicating 'extreme' fire danger) in Europe in 2024, relative to the average for the 1991–2020 reference period. These conditions are when 'critical' fires, those above 10,000 ha, can develop. Data: FWI based on ERA5. Credit: CEMS/C3S/ECMWF.

Figure B.1 presents the spatial distribution of the FWI during the summer of 2024, expressed in terms of the number of days classified under "extreme" fire danger conditions. The results clearly indicate that southern European regions exhibit disproportionately high wildfire risk, despite the relatively short temporal window of the analysis, which was restricted to the summer period.

The FWI alone, however, does not constitute a sufficient indicator for selecting a reference region from which to extract aerial firefighting operational data, as it reflects only the potential risk of wildfires rather than their actual occurrence. To complement this measure, EFFIS recorded all wildfire events during the summer of 2024, specifically from June to September, and summarized the results in Figure B.2. The analysis highlights three macro-regions characterized simultaneously by high wildfire potential, as indicated by the FWI, and by a significant number of large-scale wildfires exceeding 500 ha in burned area: Greece, southern Italy and southern Spain.

In this work, southern Italy was selected as the reference region for scenario deriva-

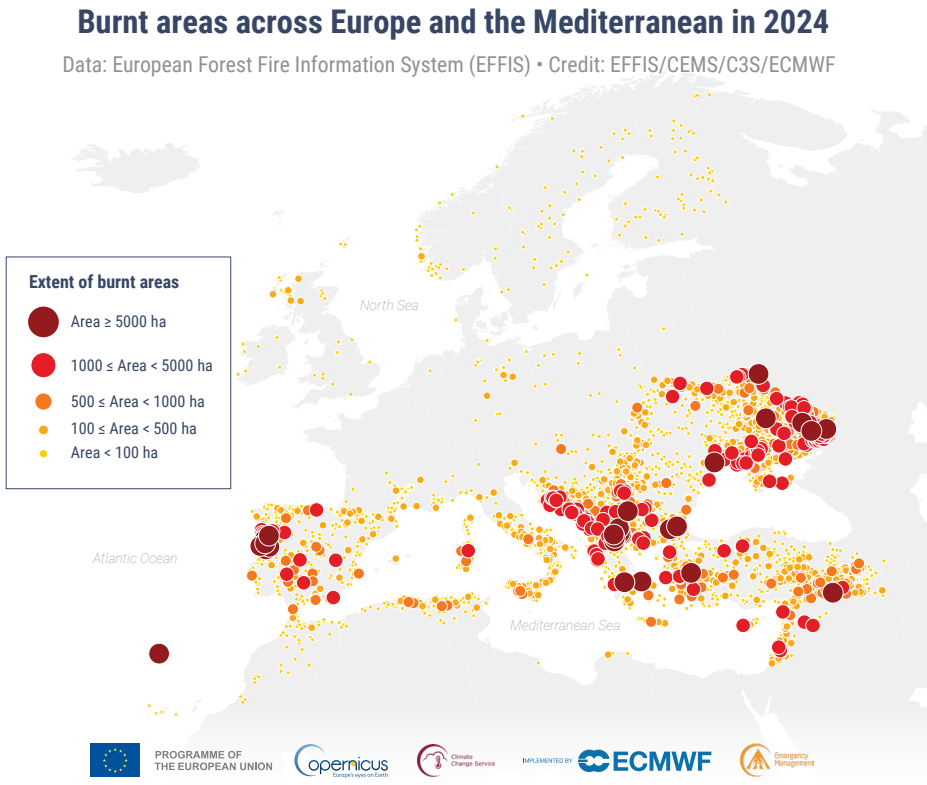

Figure B.2: Distribution and extent of burnt areas across Europe and the Mediterranean in 2024. Data: European Forest Fire Information System (EFFIS). Credit: EFFIS/CEMS/C3S/ECMWF.

tion, owing to both the high frequency and severity of wildfires observed in 2024 and the availability of detailed operational flight data from the Italian firefighting department. This choice ensures that the constructed mission scenarios are grounded in realistic operational conditions while remaining representative of the broader Mediterranean context.

B.2 Mission Profiles Data Collection

The Italian firefighting department currently operates a fleet of 18 Canadair CL-415 aircraft[2], each with a maximum water payload capacity of 6 137.0 L. For the present study, the mission profile analysis has been restricted to operations conducted in southern Italy, identified by the EFFIS analysis as one of the regions at highest wildfire risk, specifically focusing on the areas of Sicily and Calabria. Operational data

[2]Italian Firefight Department Website: `https://www.vigilfuoco.it/chi-siamo/il-soccorso/mezzi-aria/canadair`

Table B.1: Flight parameters of the active firefight segments.

Scenario ID	Number of Drops	Fire Ground Altitude	Water Ground Altitude	Region
1	5	1 000 ft	SL	Sicily
2	13	500 ft	50 ft	Sicily
3A[a]	6	2 000 ft	50 ft	Sicily
3B[a]	10	1 800 ft	SL	Sicily
4	11	2 350 ft	100 ft	Calabria

[a] Two-days operation. Both table entries belong to the same scenario partitioned in two days.

Table B.2: Base airport operational parameters and operating distances.

Scenario ID	Base (ICAO Code)	Base-Fire Distance	Fire-Water Distance
1	LICT	110.0 nm	10.0 nm
2	LICT	59.5 nm	7.5 nm
3	LICT	45.0 nm	14.0 nm
4	LICA	16.6 nm	6.4 nm

for these missions were obtained from publicly accessible Flightradar24 records.

A total of five missions were selected for detailed analysis: four in southern Sicily and one, the most recent at the time of this study, in Calabria. To facilitate the integration of real-world data into the conceptual design framework, operational parameters have been summarized in two dedicated tables: Table B.1 reports the characteristics of the active firefighting segments, including the number of drops, the fire ground altitude, and the altitude of the nearest accessible water source, while Table B.2 provides baseline operational data, including the departure airport, the distance from the base to the fire location, and the distance between the fire site and the nearest water source.

It is important to note that the operational data collected from Flightradar24 may be affected by measurement uncertainties, particularly regarding altitude information, which is derived from the Automatic Dependent Surveillance–Broadcast (ADS-B) system. Reported altitudes are discretized with a resolution of 25.0 ft, implying that the altitude values provided in Table B.1 should be interpreted within an uncertainty band of ± 25.0 ft. This level of accuracy is deemed acceptable, since in all analysed missions the nearest accessible water source was either the Mediterranean Sea or the Tyrrhenian Sea, both of which have a reference altitude effectively at sea level (SL).

B.2.1 Data Analysis and Sampling Strategy

A preliminary examination of the flight parameters reported in Table B.1 reveals a significant variability in the number of water drops performed during individual

Table B.3: Parameters for the full-factorial sampling of operational scenarios for the surrogate-based design and optimization of the aerial firefight seaplane variant.

Parameter	**Level 1**	**Level 2**
Number of Drops	5	13
Fire Ground Altitude	500.0 ft	2 000.0 ft
Altitude Differential	100.0 ft	500.0 ft

missions. Notably, this variability does not appear to be directly correlated with the altitude differential between the fire location and the nearest water source. The collected data show altitude differences ranging from a few hundred feet to more than 2 000.0 ft, yet in both cases no consistent relationship with the number of drops is observed. To ensure that the surrogate-based concept exploration activity remains sufficiently general, two representative altitude differential scenarios are considered: (i) a low-differential case, with a fire-to-water altitude difference of approximately 100.0 ft, and (ii) a higher-differential case, with a difference of approximately 500.0 ft.

These altitude differentials are applied to two reference fire ground altitudes, set at 500.0 ft and 2 000.0 ft, which are representative of less demanding and more demanding climb conditions, respectively. A weak correlation can also be observed between the number of drops and the distances separating the fire location from the water source, as well as the distance between the fire location and the base airport. Specifically, greater distances generally reduce the number of drops achievable within a single mission. However, given the limited dataset available, the statistical significance of such correlations cannot be established with confidence.

To ensure that the aircraft conceptual design process retains an adequate level of operational flexibility, two representative levels for the number of drops are introduced: 5, corresponding to a less demanding mission scenario, and 13, representative of a more demanding scenario. On this basis, a three-parameter sampling framework is constructed, comprising:

- the number of drops,
- the fire ground altitude, and
- the altitude differential between the fire location and the water source.

By defining two levels for each parameter, a full factorial sampling strategy is established. This approach ensures adequate coverage of several operating conditions, thereby enabling the surrogate-based optimization framework to capture a representative spectrum of operational scenarios. The adopted parameters and their associated levels are summarized in Table B.3.

Appendix C

Aircraft Operating Costs Assumptions

Contents

THE application of operating cost estimation methodologies, whether based on classical state-of-the-art approaches or specifically developed for innovative aircraft architectures such as hybrid-electric vehicles or seaplanes, requires the definition of suitable assumptions and constants that accurately reflect the economic context in which the analysis is conducted.

These economic assumptions generally encompass unit prices, used to estimate cumulative fuel and energy consumption costs, and unit rates, associated with navigation and airport service charges. They also include parameters related to crew compensation, such as pilot and flight crew salaries and associated benefits. A further category pertains to aircraft procurement and financing, encompassing interest rates for loans or leases, as well as insurance premiums, with hull insurance, passenger liability, and third-party liability representing the principal components.

Finally, a distinct set of assumptions addresses operational parameters, including the aircraft's expected service life and annual utilization hours. These factors govern the scheduling of maintenance activities and directly influence assessments of aircraft profitability and life-cycle economic performance.

C.1 Passenger Transport Assumptions

The economic assumptions required to support the analysis of operating costs for passenger transport operations are summarized in Table C.1, along with a brief rationale describing the origin and justification of each parameter.

During passenger and freight transport operations, certain cost items exhibit a strong dependency on the specific route and, in particular, on the characteristics of the origin and destination airports. Among these, the ground handling charge, which aggregates the costs of various airport-provided services required for passenger and aircraft handling, and the take-off and landing fees are the most significant. In Table C.1, these items are presented as average values, derived from the official airport cost documentation of four European regions suitable for seaplane operations, namely Sweden, Italy, Spain, and Greece. It is important to note that the reported values correspond to operations conducted from conventional airports and paved runways rather than waterways, thereby representing the most conservative, or critical, cost scenario.

Tables C.2 to C.5 detail the principal cost components constituting the ground handling charges and the take-off and landing fees for selected representative airports within these regions.

C.2 Aerial Firefight Assumptions

Aircraft belonging to the same category, such as fixed-wing configurations, typically share a common set of parameters when defining economic assumptions. However, significant differences arise in the relative values of these parameters depending on the aircraft's operational role and mission profile.

In the case of aerial firefighting operations, key economic parameters that diverge from those of conventional transport aircraft include the expected service life, depreciation period, annual utilization rate, loan interest rate, total annual insurance rate, crew annual salary or hourly wage, and navigation charges imposed by national and international regulatory bodies.

Table C.6 reports the main economic assumptions that differ from those applied to passenger transport aircraft discussed previously. The most significant variations concern the annual utilization rate and the navigation charges established by EUROCONTROL.

To estimate the annual utilization for aerial firefighting operations, data were collected from the Italian operator Avincis[1]. According to press releases by AirMed &

[1] Avincis website: `https://www.avincis.com/it/casa/`

Table C.1: Economic assumptions to conduct the cost estimation analysis for passenger transport operations.

Item	**Value**	**Note(s)**
Capital Costs Assumptions		
Interest Rate	5.0%	Annual.
Insurance Rate	1.35%	Annual. 1.35% of the aircraft delivery price.
Lifespan	20.0 years	-
Depreciation Period	20.0 years	-
Residual Value	0.10	10.0% of the initial aircraft price.
Thermal Engine Spares	0.10	10.0% of the thermal engine price. Assumed from Roskam.
Airframe Spares	0.30	30.0% of the airframe cost. Assumed from Roskam.
Utilization	1 200.0 hr	Annual. Assumed from similar commuter aircraft in the passenger transport segment.
Energy Assumptions		
Jet-A1 Unit Price	1.85 USD/US. Gal.	IATA Jet Fuel Price Monitor.
Electricity Unit Price	0.26 USD/kWh	Assumed from short-term horizon of Ref. [112].
Maintenance Assumptions		
Labor Rate	127.0 USD/MMH	Two operators assuming 76 260 USD/year[a] each and 1 200.0 hr of utilization per year.
Battery Unit Price	250.0 USD/kWh	-
Battery Lifespan	800.0 cycles	-
Battery Residual Value	0.22	22.0% of the initial price. Assumed from Ref. [112]
EM Spares (Line)	125.0 USD	Suggestion of Cusati et al. [121]
EM Spares (Base)	1 190.0 USD	Suggestion of Cusati et al. [121]
EM Labor Rate	21.50 USD/MMH	Suggestion of Cusati et al. [121]
Crew Assumptions		
Pilot Hourly Wage	120.0 USD/hr	Considering a 2020 gross salary of 74 730.0 USD assumed from Ref. [112].
Pilots Number	2	-
Crew Hourly Wage	76.35 USD/hr	Considering a 2020 gross salary of 47 730.0 USD assumed from Ref. [112].
Crew Numbers	0	Roskam suggestion is 1 crew member per 35 passengers.
Charges		
ENR Unit Rate	68.5 USD	2024 average for all EUROCONTROL countries.
Ground Handling	180.0 USD/tonn	Per tonn. of payload. Average value from collected airports data assuming maximum payload conditions.
Take-Off & Land	5.0 USD/tonn	As function of the aircraft MTOM (in tonn.). Average value from collected airports data.
CO_2 Allowance	21.70 USD/tonn	Per tonn. of CO_2. Actualized from Ref. [184]
Free Allocated Portion CO_2	0.15	Assumed from Ref. [184]

[a] Annual gross salary assumed from the U.S Bureau of Labor Statistics: `https://www.bls.gov/oes/2023/may/oes493011.htm`

Table C.2: Ground handling charges and take-off and landing fees for Sweden.

Item	Bromma-Stockholm	Visby	Arlanda
Parking Charge	1.39 EUR/tonn day	1.35 EUR/tonn day	-
Security Charge	4.0 EUR/pax	4.0 EUR/pax	4.0 EUR/pax
Pax Handling	-	-	2.68 EUR/pax
Pax Departing Charge	10.27 EUR/pax	5.66 EUR/pax	7.92 EUR/pax
Take-Off & Land	4.18 EUR/tonn	1.83 EUR/tonn	5.66 EUR/tonn
Ground Handling ToT.	14.27 EUR/pax	9.66 EUR/pax	14.60 EUR/pax

Table C.3: Ground handling charges and take-off and landing fees for Italy.

Item	Napoli	Palermo	Aeroporti Puglia
Pax Departing Charge	10.44 EUR/pax	9.02 EUR/pax	4.55 EUR/pax
Security Charge	5.15 EUR/pax	2.74 EUR/pax	1.94 EUR/pax
Regional Fee	8.50 EUR/pax	6.50 EUR/pax	6.50 EUR/pax
Take-Off & Land	2.34 EUR/tonn	3.40 EUR/tonn	3.54 EUR/tonn
Ground Handling ToT.	24.09 EUR/pax	18.26 EUR/pax	12.99 EUR/pax

Table C.4: Ground handling charges and take-off and landing fees for Spain.

Item	Barcelona	Palma de Mallorca	Valencia
Pax Departing Charge	12.92 EUR/pax	5.77 EUR/pax	4.9 EUR/pax
Security Charge	0.63 EUR/pax	0.63 EUR/pax	0.63 EUR/pax
Ground Services	16.97 EUR/trip	16.79 EUR/trip	16.23 EUR/trip
Meteo Service	0.19 EUR/tonn	0.19 EUR/tonn	0.19 EUR/tonn
Take-Off & Land	7.62 EUR/tonn	7.23 EUR/tonn	6.07 EUR/tonn
Ground Handling ToT.	13.55 EUR/pax	6.40 EUR/pax	5.54 EUR/pax

Table C.5: Ground handling charges and take-off and landing fees for Greece.

Item	Cyprus	Mykonos
Pax Departing Charge	22.34 EUR/pax	18.50 EUR/pax
Security Charge	4.08 EUR/pax	2.80 EUR/pax
Fire Services	0.70 EUR/pax	-
CUTE Charge	-	0.30 EUR/pax
Take-Off & Land	5.53 EUR/tonn	200.0 EUR
Ground Handling ToT.	27.12 EUR/pax	21.60 EUR/pax

Table C.6: Economic assumptions for the aerial firefight operations. Missing items are assumed to be equal to those applicable to passenger transport aircraft

Item	**Value**	**Note(s)**
Capital Costs Assumptions		
Lifespan	30 years	Average from Ref. [101]
Depreciation Period	15 years	From Ref. [197]
Interests Rate	5.62%	Annual. From Ref. [197]
Insurance Rate	3.0%	Annual. From Ref. [197]
Utilization	450.0 hr	Annual.
Crew Assumptions		
Pilot Hourly Wage	150.0 USD/hr	Single pilot. Actualized from Ref. [197]
Charges		
ENR Unit Rate	0.0 USD	From EUROCONTROL.
Ground Handling	85.0 USD/tonn hr	Average, actualized from Ref. [197]

Rescue[2] and Aerospace Global News[3], Avincis recorded approximately 4 000 flight hours over a 62-day period with a fleet of 15 aircraft, corresponding to an average of 267 flight hours per aircraft over that timeframe. Scaling this utilization to a typical 120-day summer firefighting campaign results in an estimated 515 flight hours per aircraft per year. A previous Italian operator, Inaer Aviation Italia, later incorporated into Avincis, held a contract with the Italian *Protezione Civile* that required a minimum of 360 block flight hours per year per aircraft, including technical and training operations[4]. Based on these data, an average annual utilization of approximately 450 flight hours per aircraft has been adopted for the present analysis.

According to the EUROCONTROL Customer Guide to Charges, certain exemptions apply to both en-route and terminal navigation charges, depending on the nature of the operation. As stated in Article 8 of the Conditions of Application of the Route Charges System, the following categories of flights are exempt: (i) military flights operated by State aircraft; (ii) circular flights terminating at the aerodrome of departure without intermediate landings; and (iii) search and rescue (SAR) flights authorized by the competent authority. Consequently, depending on the national agency responsible for aerial firefighting operations, such flights may be exempt from navigation charges. The list of European countries applying these exemptions is available on the EUROCONTROL website.

[2] https://www.airmedandrescue.com/latest/news/avincis-wins-contract-biggest-firefighting-operation-europe

[3] https://aerospaceglobalnews.com/news/avincis-awarded-largest-aerial-firefighting-contract-in-europe/#:~:text=During%202024's%20summer%20season%2C%20the,Avincis%20Canadair%20CL%2D415%20RescEU

[4] https://www.camera.it/leg17/410?idSeduta=0894&tipo=atti_indirizzo_controllo

Bibliography

[1] "Overview of the Design Process". In: *Aircraft Design: A Conceptual Approach, Seventh Edition*. Chap. Chapter 2, pp. 12–28. DOI: 10.2514/5.9781624107290.0012.0028. eprint: https://arc.aiaa.org/doi/pdf/10.2514/5.9781624107290.0012.0028. URL: https://arc.aiaa.org/doi/abs/10.2514/5.9781624107290.0012.0028.

[2] I. van Gent. "Agile MDAO Systems: A Graph-based Methodology to Enhance Collaborative Multidisciplinary Design". Dissertation. Delft University of Technology, 2019. DOI: 10.4233/uuid:c42b30ba-2ba7-4fff-bf1c-f81f85e890af. URL: https://doi.org/10.4233/uuid:c42b30ba-2ba7-4fff-bf1c-f81f85e890af.

[3] M. Sadraey. "Aircraft Weight Distribution". In: *Aircraft Design*. John Wiley & Sons, Ltd, 2012. Chap. 11, pp. 575–630. DOI: https://doi.org/10.1002/9781118352700.ch11. eprint: https://onlinelibrary.wiley.com/doi/pdf/10.1002/9781118352700.ch11. URL: https://onlinelibrary.wiley.com/doi/abs/10.1002/9781118352700.ch11.

[4] F. Sanchez, S. Liscouët-Hanke, and A. Tfaily. "Improving aircraft conceptual design through parametric CAD modellers – A case study for thermal analysis of aircraft systems". In: *Computers in Industry* 130 (2021), p. 103467. DOI: https://doi.org/10.1016/j.compind.2021.103467. URL: https://www.sciencedirect.com/science/article/pii/S0166361521000749.

[5] S. Hosseini, M. A. Vaziry-Zanjany, and H. R. Ovesy. "A Framework for Aircraft Conceptual Design and Multidisciplinary Optimization". In: *Aerospace* 11.4 (2024). DOI: 10.3390/aerospace11040273. URL: https://www.mdpi.com/2226-4310/11/4/273.

[6] S. Corcione, M. Mandorino, and V. Cusati. "Beyond conventional: An integrated aerostructural optimization approach for innovative tailplane configurations". In: *Aerospace Science and Technology* 150 (2024), p. 109242. DOI: https://doi.org/10.1016/j.ast.2024.109242. URL: https://www.sciencedirect.com/science/article/pii/S1270963824003730.

[7] European Commission, Directorate-General for Research and Innovation, and Directorate-General for Mobility and Transport. *Flightpath 2050 : Europe's vi-*

sion for aviation : maintaining global leadership and serving society's needs. Publications Office, 2011. DOI: doi/10.2777/50266.

[8] K. Abu Salem, G. Palaia, and A. A. Quarta. "Review of hybrid-electric aircraft technologies and designs: Critical analysis and novel solutions". In: *Progress in Aerospace Sciences* 141 (2023). Special Issue on Green Aviation, p. 100924. DOI: https://doi.org/10.1016/j.paerosci.2023.100924.

[9] B. J. Brelje and J. R. Martins. "Electric, hybrid, and turboelectric fixed-wing aircraft: A review of concepts, models, and design approaches". In: *Progress in Aerospace Sciences* 104 (2019), pp. 1–19. DOI: https://doi.org/10.1016/j.paerosci.2018.06.004. URL: https://www.sciencedirect.com/science/article/pii/S0376042118300356.

[10] F. Orefice, P. Della Vecchia, D. Ciliberti, F. Nicolosi, et al. "Preliminary design to fulfil future market demand of electric aircraft". In: *International Review of Aerospace Engineering* 14.6 (2021), pp. 294–308.

[11] R. de Vries, M. T. Brown, and R. Vos. "A Preliminary Sizing Method for Hybrid-Electric Aircraft Including Aero-Propulsive Interaction Effects". In: *2018 Aviation Technology, Integration, and Operations Conference*. 2018. DOI: 10.2514/6.2018-4228. URL: https://arc.aiaa.org/doi/abs/10.2514/6.2018-4228.

[12] C. Nasoulis, V. Gkoutzamanis, and A. Kalfas. "Multidisciplinary conceptual design for a hybrid-electric commuter aircraft". In: *The Aeronautical Journal* 126.1302 (2022), pp. 1242–1264. DOI: 10.1017/aer.2022.32.

[13] L. R. Jenkinson, P. Simpkin, D. Rhodes, and L. R. Jenkison. *Civil jet aircraft design*. Vol. 338. Arnold London, 1999.

[14] J. E.R. *American Flying Boats and Amphibious Aircraft: An Illustrated History*. McFarland & Co Inc, 2009.

[15] M. Tuccillo and P. Della Vecchia. "Multidisciplinary Preliminary Design Process of Hybrid-Electric Seaplane". In: *Proceedings of the 34th Congress of the International Council of the Aeronautical Sciences (ICAS 2024)*. International Council of the Aeronautical Sciences. Florence, Italy, 2024.

[16] Bryan Bender. Aerospace America. *Are Seaplanes Making a Comeback? It May Be Just Beyond the Horizon*. 2025. URL: https://aerospaceamerica.aiaa.org/institute/are-seaplanes-making-a-comeback-it-may-be-just-beyond-the-horizon/ (visited on 09/22/2025).

[17] M. Spieck, L. K. Franzén, K. Amadori, P. S. Prakasha, and N. Naeem. "A Capability-Focused Approach To Model Complex, Multi-Layered Systems-of-Systems". In: *AIAA AVIATION FORUM AND ASCEND 2024*. 2024. DOI: 10.2514/6.2024-3559. eprint: https://arc.aiaa.org/doi/pdf/10.2514/6.2024-3559. URL: https://arc.aiaa.org/doi/abs/10.2514/6.2024-3559.

[18] P. Shiva Prakasha, N. Naeem, K. Amadori, G. Donelli, J. Akbari, F. Nicolosi, L. Knöös Franzén, M. Ruocco, T. Lefebvre, and B. Nagel. “COLOSSUS EU Project – Collaborative SoS Exploration of Aviation Products, Services and Business Models: Overview and Approach”. In: *ICAS 2024*. Florence, Italy, Sept. 2024. URL: https://hal.science/hal-05021611.

[19] M. Tuccillo and M. Ruocco. “Aircraft Design Capabilities for a System-of-Systems Approach (eVTOL and Seaplane Design)”. In: *Engineering Proceedings* 90.1 (2025). DOI: 10.3390/engproc2025090021. URL: https://www.mdpi.com/2673-4591/90/1/21.

[20] S. Gudmundsson. “Chapter 1 - The Aircraft Design Process”. In: *General Aviation Aircraft Design*. Ed. by S. Gudmundsson. Boston: Butterworth-Heinemann, 2014, pp. 1–32. DOI: https://doi.org/10.1016/B978-0-12-397308-5.00001-5. URL: https://www.sciencedirect.com/science/article/pii/B9780123973085000015.

[21] E. Torenbeek. “Design of the Well-Tempered Aircraft”. In: *Advanced Aircraft Design*. John Wiley & Sons, Ltd, 2013. Chap. 1, pp. 1–30. DOI: https://doi.org/10.1002/9781118568101.ch1. eprint: https://onlinelibrary.wiley.com/doi/pdf/10.1002/9781118568101.ch1. URL: https://onlinelibrary.wiley.com/doi/abs/10.1002/9781118568101.ch1.

[22] D. Raymer. *Aircraft design: a conceptual approach*. American Institute of Aeronautics and Astronautics, Inc., 2012.

[23] J. Roskam. *Airplane Design. Part I: Preliminary Sizing of Airplanes*. 1990.

[24] A. Sgueglia. “Methodology for sizing and optimising a Blended Wing-Body with distributed electric ducted fans”. Theses. ISAE - Institut Supérieur de l’Aéronautique et de l’Espace, Dec. 2019. URL: https://hal.science/tel-02487044.

[25] L. M. Nicolai and G. E. Carichner. *Fundamentals of aircraft and airship design: Volume I–aircraft design*. American Institute of Aeronautics and Astronautics, Inc., 2010.

[26] C. Österheld, W. Heinze, and P. Horst. “Preliminary Design of a Blended Wing Body Configuration using the Design Tool PrADO”. In: *CEAS Conference on Multidisciplinary Aircraft Design and Optimisation*. 2001. URL: https://api.semanticscholar.org/CorpusID:7546001.

[27] Lissys Limited and Simos, D. *Piano*. https://www.lissys.uk/index2.html. Accessed: 2025-08-24. 2010.

[28] DARcorporation. *Advanced aircraft analysis (AAA)*. https://www.darcorp.com/advanced-aircraft-analysis-software/. Accessed: 2025-08-24. 2022.

[29] C. Werner-Westphal, W. Heinze, and P. Horst. “Multidisciplinary Integrated Preliminary Design Applied to Unconventional Aircraft Configurations”. In: *Journal of Aircraft* 45.2 (2008), pp. 581–590. DOI: 10.2514/1.32138. eprint: https://doi.org/10.2514/1.32138. URL: https://doi.org/10.2514/1.32138.

[30] J. Roskam. *Airplane design*. DARcorporation, 1997.

[31] B. Aigner, P. Strathoff, and E. Stumpf. "MICADO: Recent Developments of Models for Design and Evaluation of Electric Aircraft Propulsion Systems". In: *Deutsche Gesellschaft für Luft- und Raumfahrt - Lilienthal-Oberth e.V.* (2021). DOI: 10.25967/530051. URL: https://doi.org/10.25967/530051 (visited on 01/29/2021).

[32] A. Wendorff, A. Variyar, C. Ilario, E. Botero, F. Capristan, J. Smart, J. Alonso, L. Kulik, M. Clarke, M. Colonno, M. Kruger, J. M. Vegh, P. Goncalves, R. Erhard, R. Fenrich, T. Orra, T. St. Francis, T. MacDonald, T. Momose, T. Economon, T. Lukaczyk, and W. Maier. *SUAVE: An Aerospace Vehicle Environment for Designing Future Aircraft*. Version 2.1. 2020. URL: https://github.com/suavecode/SUAVE.

[33] V. Trifari. "Development of a Multi-Disciplinary Analysis and Optimization framework and applications for innovative efficient regional aircraft". Doctoral Thesis. Università degli Studi di Napoli Federico II, 2020. URL: http://www.fedoa.unina.it/13096/.

[34] T. MacDonald, M. Clarke, E. M. Botero, J. M. Vegh, and J. J. Alonso. "SUAVE: An Open-Source Environment Enabling Multi-Fidelity Vehicle Optimization". In: *18th AIAA/ISSMO Multidisciplinary Analysis and Optimization Conference*. 2017. DOI: 10.2514/6.2017-4437. eprint: https://arc.aiaa.org/doi/pdf/10.2514/6.2017-4437. URL: https://arc.aiaa.org/doi/abs/10.2514/6.2017-4437.

[35] T. D. Economon, F. Palacios, S. R. Copeland, T. W. Lukaczyk, and J. J. Alonso. "SU2: An Open-Source Suite for Multiphysics Simulation and Design". In: *AIAA Journal* 54.3 (2016), pp. 828–846. DOI: 10.2514/1.J053813. eprint: https://doi.org/10.2514/1.J053813. URL: https://doi.org/10.2514/1.J053813.

[36] B. Boden, J. Flink, N. Först, R. Mischke, K. Schaffert, A. Weinert, A. Wohlan, and A. Schreiber. "RCE: An Integration Environment for Engineering and Science". In: *SoftwareX* 15 (2021), p. 100759. DOI: https://doi.org/10.1016/j.softx.2021.100759. URL: https://www.sciencedirect.com/science/article/pii/S2352711021000820.

[37] F. Gallard, C. Vanaret, D. Guénot, V. Gachelin, R. Lafage, B. Pauwels, P.-J. Barjhoux, and A. Gazaix. "GEMS: A Python Library for Automation of Multidisciplinary Design Optimization Process Generation". In: *2018 AIAA/ASCE/AHS/ASC Structures, Structural Dynamics, and Materials Conference*. 2018.

[38] J. S. Gray, J. T. Hwang, J. R. R. A. Martins, K. T. Moore, and B. A. Naylor. "OpenMDAO: An open-source framework for multidisciplinary design, analysis, and optimization". In: *Structural and Multidisciplinary Optimization* 59.4 (Apr. 2019), pp. 1075–1104. DOI: 10.1007/s00158-019-02211-z.

[39] J. Anibal, C. A. Mader, and J. R. R. A. Martins. “Aerodynamic shape optimization of an electric aircraft motor surface heat exchanger with conjugate heat transfer constraint”. In: *International Journal of Heat and Mass Transfer* 189 (June 2022), p. 122689. DOI: 10.1016/j.ijheatmasstransfer.2022.122689.

[40] E. J. Adler, B. J. Brelje, and J. R. R. A. Martins. “Thermal Management System Optimization for a Parallel Hybrid Aircraft Considering Mission Fuel Burn”. In: *Aerospace* 9.5 (Apr. 2022). DOI: 10.3390/aerospace9050243. URL: https://www.mdpi.com/2226-4310/9/5/243.

[41] A. B. Lambe and J. R. Martins. “Extensions to the design structure matrix for the description of multidisciplinary design, analysis, and optimization processes”. In: *Structural and Multidisciplinary Optimization* 46.2 (2012), pp. 273–284.

[42] B. Nagel, D. Böhnke, V. Gollnick, P. Schmollgruber, A. Rizzi, G. La Roccax, and J. J. Alonso. “Communication in aircraft design : Can we establish a common language?” In: *28th Congress of the International Council of the Aeronautical Sciences 2012, ICAS 2012 : Volume 1*. QC 20131008. 2012, pp. 443–455.

[43] M. Alder, E. Moerland, J. Jepsen, and B. Nagel. “Recent Advances in Establishing a Common Language for Aircraft Design with CPACS”. In: *Aerospace Europe Conference 2020*. 2020. URL: https://elib.dlr.de/134341/.

[44] C. David, S. Delbecq, S. Defoort, P. Schmollgruber, E. Benard, and V. Pommier-Budinger. “From FAST to FAST-OAD: An open source framework for rapid Overall Aircraft Design”. In: *IOP Conference Series: Materials Science and Engineering* 1024.1 (Jan. 2021), p. 012062. DOI: 10.1088/1757-899X/1024/1/012062. URL: https://doi.org/10.1088/1757-899X/1024/1/012062.

[45] Carl Recine, ARC, Aviary Co-Lead, Jason Kirk, LaRC, Aviary Lead and Eliot Aretskin-Hariton, Aviary Feature Developer. *Aviary: A Transformational Tool For Aircraft Design*. 2024. URL: https://ntrs.nasa.gov/api/citations/20240013426/downloads/24_10_24_Industry_Day-CR.pdf (visited on 09/02/2025).

[46] G. Corrado, G. Ntourmas, M. Sferza, N. Traiforos, A. Arteiro, L. Brown, D. Chronopoulos, F. Daoud, F. Glock, J. Ninic, E. Ozcan, J. Reinoso, G. Schuhmacher, and T. Turner. “Recent progress, challenges and outlook for multidisciplinary structural optimization of aircraft and aerial vehicles”. In: *Progress in Aerospace Sciences* 135 (2022), p. 100861. DOI: https://doi.org/10.1016/j.paerosci.2022.100861. URL: https://www.sciencedirect.com/science/article/pii/S0376042122000537.

[47] M. Saporito, A. Da Ronch, N. Bartoli, and S. Defoort. “Robust multidisciplinary analysis and optimization for conceptual design of flexible aircraft under dynamic aeroelastic constraints”. In: *Aerospace Science and Technology* 138 (2023), p. 108349. DOI: https://doi.org/10.1016/j.ast.2023.108349. URL: https://www.sciencedirect.com/science/article/pii/S1270963823002468.

[48] D. Quinn, S. Colbert, D. C. Nolan, R. Fox, and J. Gaskell. “Propulsion system integration on truss-braced aircraft: structural performance sensitivity to architectural design parameters”. In: *Aerospace Science and Technology* 159 (2025), p. 109987. DOI: https://doi.org/10.1016/j.ast.2025.109987. URL: https://www.sciencedirect.com/science/article/pii/S1270963825000598.

[49] J. R. Martins. “Aerodynamic design optimization: Challenges and perspectives”. In: *Computers & Fluids* 239 (2022), p. 105391. DOI: https://doi.org/10.1016/j.compfluid.2022.105391. URL: https://www.sciencedirect.com/science/article/pii/S0045793022000615.

[50] L. Li, J. Bai, and F. Qu. “Multipoint Aerodynamic Shape Optimization of a Truss-Braced-Wing Aircraft”. In: *Journal of Aircraft* 59.5 (2022), pp. 1179–1194. DOI: 10.2514/1.C036413. eprint: https://doi.org/10.2514/1.C036413. URL: https://doi.org/10.2514/1.C036413.

[51] G. M. Streuber and D. W. Zingg. “Evaluating the Risk of Local Optima in Aerodynamic Shape Optimization”. In: *AIAA Journal* 59.1 (2021), pp. 75–87. DOI: 10.2514/1.J059826. eprint: https://doi.org/10.2514/1.J059826. URL: https://doi.org/10.2514/1.J059826.

[52] C. You, M. Yasaee, S. He, D. Yang, Y. Xu, I. Dayyani, H. Ghasemnejad, S. Guo, P. Webb, J. Jennings, and G. Federico. “Identification of the key design inputs for the FEM-based preliminary sizing and mass estimation of a civil aircraft wing box structure”. In: *Aerospace Science and Technology* 121 (2022), p. 107284. DOI: https://doi.org/10.1016/j.ast.2021.107284. URL: https://www.sciencedirect.com/science/article/pii/S127096382100794X.

[53] M. Belardo, A. D. Marano, J. Beretta, G. Diodati, M. Graziano, M. Capasso, P. Ariola, S. Orlando, F. Di Caprio, N. Paletta, and L. Di Palma. “Wing Structure of the Next-Generation Civil Tiltrotor: From Concept to Preliminary Design”. In: *Aerospace* 8.4 (2021). DOI: 10.3390/aerospace8040102. URL: https://www.mdpi.com/2226-4310/8/4/102.

[54] V. PALLADINO, N. BARTOLI, V. POMMIER-BUDINGER, E. BENARD, P. SCHMOLLGRUBER, and A. JORDAN. “Optimization of a hydrogen-based hybrid propulsion system under aircraft performance constraints”. In: *Chinese Journal of Aeronautics* 36.5 (2023), pp. 41–56. DOI: https://doi.org/10.1016/j.cja.2023.02.019. URL: https://www.sciencedirect.com/science/article/pii/S1000936123000407.

[55] G. Grazioso, A. De Marco, P. Della Vecchia, M. Di Stasio, V. Trifari, and F. Nicolosi. “A simulation-based mission optimization approach for regional transport hybrid-electric aircraft”. In: *Applied Energy* 402 (2025), p. 126869. DOI: https://doi.org/10.1016/j.apenergy.2025.126869. URL: https://www.sciencedirect.com/science/article/pii/S0306261925015995.

[56] G. Grazioso, M. Di Stasio, F. Nicolosi, and S. Trepiccione. “A mathematical model for hybrid-electric propulsion system for regional propeller-driven aircraft”. In: *Energy Conversion and Management: X* 26 (2025), p. 100957. DOI: https://doi.org/10.1016/j.ecmx.2025.100957. URL: https://www.sciencedirect.com/science/article/pii/S2590174525000893.

[57] F. Orefice, F. Nicolosi, P. D. Vecchia, and D. Ciliberti. “Aircraft Conceptual Design of Commuter Aircraft including Distributed Electric Propulsion”. In: *AIAA AVIATION 2020 FORUM*. 2020. DOI: 10.2514/6.2020-2627. eprint: https://arc.aiaa.org/doi/pdf/10.2514/6.2020-2627. URL: https://arc.aiaa.org/doi/abs/10.2514/6.2020-2627.

[58] V. MARCIELLO, F. OREFICE, F. NICOLOSI, D. CILIBERTI, and P. DELLA VECCHIA. “Design of hybrid-electric aircraft with fault-tolerance considerations”. In: *Chinese Journal of Aeronautics* 36.2 (2023), pp. 160–178. DOI: https://doi.org/10.1016/j.cja.2022.05.014. URL: https://www.sciencedirect.com/science/article/pii/S1000936122001066.

[59] P. Jiang, Q. Zhou, and X. Shao. “Surrogate-Model-Based Design and Optimization”. In: *Surrogate Model-Based Engineering Design and Optimization*. Singapore: Springer Singapore, 2020, pp. 135–236. DOI: 10.1007/978-981-15-0731-1\textunderscore7. URL: https://doi.org/10.1007/978-981-15-0731-1%5Ctextunderscore7.

[60] N. V. Queipo, R. T. Haftka, W. Shyy, T. Goel, R. Vaidyanathan, and P. Kevin Tucker. “Surrogate-based analysis and optimization”. In: *Progress in Aerospace Sciences* 41.1 (2005), pp. 1–28. DOI: https://doi.org/10.1016/j.paerosci.2005.02.001. URL: https://www.sciencedirect.com/science/article/pii/S0376042105000102.

[61] C. M. Bishop and N. M. Nasrabadi. *Pattern recognition and machine learning*. Vol. 4. 4. Springer, 2006.

[62] J. Li, X. Du, and J. R. Martins. “Machine learning in aerodynamic shape optimization”. In: *Progress in Aerospace Sciences* 134 (2022), p. 100849. DOI: https://doi.org/10.1016/j.paerosci.2022.100849. URL: https://www.sciencedirect.com/science/article/pii/S0376042122000410.

[63] M. T. Tong. *Machine learning-based predictive analytics for aircraft engine conceptual design*. Tech. rep. Glenn Research Center, Cleveland, Ohio, 2020.

[64] R. Macit, H. A. Özkan, and T. Baklacioglu. “Machine learning-based fuel flow rate prediction for Boeing 737-800 aircraft: A comprehensive approach across climb, cruise and descent flight phases”. In: *Energy* 337 (2025), p. 138576. DOI: https://doi.org/10.1016/j.energy.2025.138576. URL: https://www.sciencedirect.com/science/article/pii/S0360544225042185.

[65] A. De Marco, P. M. D’Onza, and S. Manfredi. “A Deep Reinforcement Learning Control Approach for High-Performance Aircraft”. In: *Nonlinear Dynamics* 111 (2023), pp. 17037–17077. DOI: 10.1007/s11071-023-08725-y. URL: https://doi.org/10.1007/s11071-023-08725-y.

[66] K. C. Wu and J. S. Litt. *Reinforcement Learning Approach to Flight Control Allocation with Distributed Electric Propulsion*. Tech. rep. Glenn Research Center, Cleveland, Ohio, 2023.

[67] K. Hassan, A. K. Thakur, G. Singh, J. Singh, L. R. Gupta, and R. Singh. "Application of artificial intelligence in aerospace engineering and its future directions: A systematic quantitative literature review". In: *Archives of Computational Methods in Engineering* 31.7 (2024), pp. 4031–4086.

[68] S. L. Brunton, J. Nathan Kutz, K. Manohar, A. Y. Aravkin, K. Morgansen, J. Klemisch, N. Goebel, J. Buttrick, J. Poskin, A. W. Blom-Schieber, T. Hogan, and D. McDonald. "Data-Driven Aerospace Engineering: Reframing the Industry with Machine Learning". In: *AIAA Journal* 59.8 (2021), pp. 2820–2847. DOI: 10.2514/1.J060131. eprint: https://doi.org/10.2514/1.J060131. URL: https://doi.org/10.2514/1.J060131.

[69] H. Karali, G. Inalhan, and A. Tsourdos. "Advanced UAV Design Optimization Through Deep Learning-Based Surrogate Models". In: *Aerospace* 11.8 (2024). DOI: 10.3390/aerospace11080669. URL: https://www.mdpi.com/2226-4310/11/8/669.

[70] J. R. R. A. Martins and A. Ning. *Engineering Design Optimization*. Cambridge, UK: Cambridge University Press, Jan. 2022. DOI: 10.1017/9781108980647. URL: https://mdobook.github.io.

[71] J. L. J. Pereira, G. A. Oliver, M. B. Francisco, S. S. Cunha Jr, and G. F. Gomes. "A review of multi-objective optimization: methods and algorithms in mechanical engineering problems". In: *Archives of Computational Methods in Engineering* 29.4 (2022), pp. 2285–2308.

[72] E. Nikolaou, S. Kilimtzidis, and V. Kostopoulos. "Multi-Fidelity Surrogate-Assisted Aerodynamic Optimization of Aircraft Wings". In: *Aerospace* 12.4 (2025). DOI: 10.3390/aerospace12040359. URL: https://www.mdpi.com/2226-4310/12/4/359.

[73] D. G. Krige. "A statistical approach to some basic mine valuation problems on the Witwatersrand". In: *Journal of the Southern African Institute of Mining and Metallurgy* 52.6 (1951), pp. 119–139.

[74] T. Jesus, M. Sohst, J. L. d. Vale, and A. Suleman. "Surrogate based MDO of a canard configuration aircraft". In: *Structural and Multidisciplinary Optimization* 64.6 (2021), pp. 3747–3771.

[75] J. Zhang, I. Roumeliotis, X. Zhang, and A. Zolotas. "Techno-economic-environmental evaluation of aircraft propulsion electrification: Surrogate-based multi-mission optimal design approach". In: *Renewable and Sustainable Energy Reviews* 175 (2023), p. 113168. DOI: https://doi.org/10.1016/j.rser.2023.113168. URL: https://www.sciencedirect.com/science/article/pii/S1364032123000242.

[76] EUROCONTROL. Performance Review Commission (PRC). *Performance Review Report. An Assessment of Air Traffic Management in Europe*. 2025. URL: https://www.eurocontrol.int/sites/default/files/2025-03/eurocontrol-performance-review-report-2024.pdf (visited on 08/28/2025).

[77] D. V. Siskos, A. Maravas, and R. Mau. "PESTLE Analysis of a Seaplane Transport Network in Greece". In: *Aerospace* 12.1 (2025). DOI: 10.3390/aerospace12010028. URL: https://www.mdpi.com/2226-4310/12/1/28.

[78] I. Manole and A. Majumdar. "When Maritime Meets Aviation: The Safety of Seaplanes on the Water". In: *Applied Sciences* 15.11 (2025). DOI: 10.3390/app15115808. URL: https://www.mdpi.com/2076-3417/15/11/5808.

[79] J. F. Andrade, S. Kalakou, and R. L. da Costa. "Exploratory analysis of seaplane operations in Greece: insights of a survey and SWOT analysis". In: *European Planning Studies* 31.4 (2023), pp. 679–699. DOI: 10.1080/09654313.2022.2057187. eprint: https://doi.org/10.1080/09654313.2022.2057187. URL: https://doi.org/10.1080/09654313.2022.2057187.

[80] S. Wakayama. "Subsonic Multi-Role Aircraft". In: *44th AIAA Aerospace Sciences Meeting and Exhibit*. DOI: 10.2514/6.2006-1513. eprint: https://arc.aiaa.org/doi/pdf/10.2514/6.2006-1513. URL: https://arc.aiaa.org/doi/abs/10.2514/6.2006-1513.

[81] I. Mattmann. *Modellintegrierte Produkt- und Prozessentwicklung*. Jan. 2017. DOI: 10.1007/978-3-658-19409-3.

[82] B. Carey. *20/Twenty: The DHC-6, Enduring Versatility*. 2024. URL: https://aviationweek.com/business-aviation/aircraft-propulsion/20twenty-dhc-6-enduring-versatility (visited on 08/24/2025).

[83] Conklin & De Decker. *Aircraft Operating Cost and Performance Guide: Viking Air DHC 6-400 Twin Otter*. 2025. URL: https://conklindedecker.jetsupport.com/details/Viking%20Air%20DHC%206-400%20Twin%20Otter (visited on 08/24/2025).

[84] Alton K. Marsh. Aircraft Owners and Pilots Association (AOPA). *Operating costs for jets, turboprops detailed*. 2016. URL: https://www.aopa.org/news-and-media/all-news/2016/october/31/hourly-operating-costs (visited on 08/26/2025).

[85] ZeroAvia. *The Hydrogen-Electric Cessna Grand Caravan. Zero-Emission, Lower Cost Flight Operations in the Decade Ahead*. 2023. URL: https://zeroavia.com/wp-content/uploads/2023/07/ZeroAvia-ZA600-Caravan-Whitepaper-2023.pdf (visited on 08/26/2025).

[86] General Aviation News. *A milestone for the Caravan*. 2023. URL: https://generalaviationnews.com/2023/01/16/a-milestone-for-the-caravan/ (visited on 08/26/2025).

[87] Molly McMillin. Aviation Week. *Textron Aviation Delivers 500th Cessna Grand Caravan EX*. 2019. URL: https://aviationweek.com/business-aviation/textron-aviation-delivers-500th-cessna-grand-caravan-ex (visited on 08/26/2025).

[88] CoinNews. *US Inflation Calculator*. 2025. URL: https://www.usinflationcalculator.com/ (visited on 08/26/2025).

[89] D. H. A. of Canada Limited. *DHC-6 TWIN OTTER CLASSIC 300-G – FLOATS*. Brochure. 2025. URL: https://dehavilland.com/wp-content/uploads/2025/03/DHC_Twin_Otter_300-G_FLOATS_Spec_Sheet_v1_DIGITAL.pdf.

[90] M. Kühlen, K. Kölker, F. Linke, K. Dahlmann, V. Gollnick, and K. Lütjens. "From passenger itineraries to climate impact: Analyzing the implications of a new mid-range aircraft on the global air transportation system". In: *Journal of Air Transport Management* 113 (2023), p. 102474. DOI: https://doi.org/10.1016/j.jairtraman.2023.102474. URL: https://www.sciencedirect.com/science/article/pii/S0969699723001175.

[91] J. Zuidberg. "Identifying airline cost economies: An econometric analysis of the factors affecting aircraft operating costs". In: *Journal of Air Transport Management* 40 (2014), pp. 86–95. DOI: https://doi.org/10.1016/j.jairtraman.2014.06.007. URL: https://www.sciencedirect.com/science/article/pii/S0969699714000817.

[92] N. Avogadro and R. Redondi. "Demystifying electric aircraft's role in aviation decarbonization: Are first-generation electric aircraft cost-effective?" In: *Transportation Research Part D: Transport and Environment* 130 (2024), p. 104191. DOI: https://doi.org/10.1016/j.trd.2024.104191. URL: https://www.sciencedirect.com/science/article/pii/S1361920924001482.

[93] A. K. Kundu. "Aircraft Weight and Center of Gravity Estimation". In: *Aircraft Design*. Cambridge Aerospace Series. Cambridge University Press, 2010, pp. 223–257.

[94] M. H. Sadraey. *Aircraft design: A systems engineering approach*. John Wiley & Sons, 2024.

[95] J. He, R. Pan, W. Cheng, C. Guo, and Z. Meng. "Competitiveness Evaluation Method of Supersonic Civil Aircraft Based on Analytic Hierarchy Process". In: *Aerospace* 12.1 (2025). DOI: 10.3390/aerospace12010037. URL: https://www.mdpi.com/2226-4310/12/1/37.

[96] S. Coy. "A global model for estimating the block time of commercial passenger aircraft". In: *Journal of Air Transport Management* 12.6 (2006), pp. 300–305. DOI: https://doi.org/10.1016/j.jairtraman.2006.07.005. URL: https://www.sciencedirect.com/science/article/pii/S0969699706000561.

[97] Peter A. Bedell. Aircraft Owners and Pilots Association (AOPA). *Quick Look: Cessna 208 Caravan*. 2017. URL: https://www.aopa.org/news-and-media/all-news/2017/october/pilot/turbine-quick-look-cessna-208#:~:text=The%5C%20Caravan%5C%20offers%5C%20excellent%5C%20cockpit,slower%5C%20while%5C%20using%5C%20more%5C%20fuel. (visited on 08/26/2025).

[98] A. Struminska and A. Filippone. "Flight performance analysis of aerial fire fighting". In: *The Aeronautical Journal* 128.1327 (2024), pp. 1895–1923. DOI: 10.1017/aer.2024.29.

[99] William Garvey. Aviation Week. *Fire Country First Responders Appreciate A Wildfire Walloper*. 2023. URL: https://aviationweek.com/business-aviation/aircraft-propulsion/fire-country-first-responders-appreciate-wildfire-walloper#:~:text=Moreover%5C%2C%5C%20the%5C%20AT%5C%2D802F's%5C%20relatively,douse%5C%20flames%20in%5C%20steady%5C%20sequence. (visited on 09/02/2025).

[100] International Air Transport Association. *The Global Commercial Aircraft Fleet: Shortages Cap Growth*. Report. All Rights Reserved. Available on IATA Economics page. International Air Transport Association (IATA), Aug. 2025. URL: https://www.iata.org/en/publications/economics/reports/the-global-commercial-aircraft-fleet/.

[101] L. Sherry and M. Chaudhari. "Aerial Fire Fighting Operational Statistics (2024): Very Large/Large Air Tankers". In: *Fire* 8.4 (2025). DOI: 10.3390/fire8040160. URL: https://www.mdpi.com/2571-6255/8/4/160.

[102] Edward G. Keating, Andrew R. Morral, Daniel M. Norton and Dulani Woods. RAND. *Investing in Firefighting*. 2013. URL: https://www.rand.org/pubs/commentary/2013/12/investing-in-firefighting.html (visited on 09/03/2025).

[103] Hayden Biggs. Forest Fire Management Victoria. *Fire Boss amphibious single engine air tanker: Final Report*. 2008. URL: https://www.ffm.vic.gov.au/__data/assets/pdf_file/0013/21109/Report-81-Fire-Boss-Amphibian-Single-Engine-Tanker.pdf (visited on 09/03/2025).

[104] S. Gudmundsson. "Appendix C - Design of Biplanes and Seaplanes". In: *General Aviation Aircraft Design (Second Edition)*. Second Edition. Butterworth-Heinemann, 2022, pp. 1049–1074. DOI: https://doi.org/10.1016/B978-0-12-818465-3.09995-X. URL: https://www.sciencedirect.com/science/article/pii/B978012818465309995X.

[105] C. Kalogeri, T. I. Lekas, and G. Kallos. "Assessing the Availability of Seaplane Operations in the Aegean Sea". In: *Aeronautics and Aerospace Open Access Journal* 3.2 (2019), pp. 76–82. DOI: 10.15406/aaoaj.2019.03.00083.

[106] D. Thurston. *Design for Flying*. Design for Flying. TAB Books, 1995.

[107] M. G. Morabito. “A Review of Hydrodynamic Design Methods for Seaplanes”. In: *Journal of Ship Production and Design* 37.03 (Aug. 2021), pp. 159–180. DOI: 10.5957/JSPD.11180039. eprint: https://onepetro.org/JSPD/article-pdf/37/03/159/2478035/sname-jspd-11180039.pdf. URL: https://doi.org/10.5957/JSPD.11180039.

[108] S. H. Chicken. “Conceptual design methodologies for waterborne and amphibious aircraft”. Dissertation. Cranfield University, 1999. URL: http://dspace.lib.cranfield.ac.uk/handle/1826/9945.

[109] I. DATHE and M. DELEO. “Hydrodynamic characteristics of seaplanes as affected by hull shape parameters”. In: *Advanced Marine Vehicles Conference*. 2012. DOI: 10.2514/6.1989-1540. eprint: https://arc.aiaa.org/doi/pdf/10.2514/6.1989-1540. URL: https://arc.aiaa.org/doi/abs/10.2514/6.1989-1540.

[110] Y. Deng, A. Kryuchkov, P. Mokotoff, E. Smith, J. Patel, S. Garcia Lavanchy, M. Z. Li, and G. Cinar. “Operational Analysis for Hybrid Electric Aircraft Fleets: A feasibility study for the short- and medium-haul markets”. en. In: *AIAA AVIATION 2023 Forum*. San Diego, CA and Online: American Institute of Aeronautics and Astronautics, June 2023. DOI: 10.2514/6.2023-3868. URL: https://arc.aiaa.org/doi/10.2514/6.2023-3868 (visited on 07/13/2023).

[111] V. Marciello, M. Di Stasio, M. Ruocco, V. Trifari, F. Nicolosi, M. Meindl, B. Lemoine, and P. Caliandro. “Design Exploration for Sustainable Regional Hybrid-Electric Aircraft: A Study Based on Technology Forecasts”. In: *Aerospace* 10.2 (2023). URL: https://www.mdpi.com/2226-4310/10/2/165.

[112] V. Marciello, V. Cusati, F. Nicolosi, K. Saavedra-Rubio, E. Pierrat, N. Thonemann, and A. Laurent. “Evaluating the economic landscape of hybrid-electric regional aircraft: A cost analysis across three time horizons”. In: *Energy Conversion and Management* 312 (2024), p. 118517. DOI: https://doi.org/10.1016/j.enconman.2024.118517. URL: https://www.sciencedirect.com/science/article/pii/S0196890424004588.

[113] J. Hoelzen, D. Silberhorn, T. Zill, B. Bensmann, and R. Hanke-Rauschenbach. “Hydrogen-powered aviation and its reliance on green hydrogen infrastructure – Review and research gaps”. In: *International Journal of Hydrogen Energy* 47.5 (2022). Hydrogen Energy and Fuel Cells, pp. 3108–3130. DOI: https://doi.org/10.1016/j.ijhydene.2021.10.239.

[114] M. Sparano, M. Sorrentino, G. Troiano, G. Cerino, G. Piscopo, M. Basaglia, and C. Pianese. “The future technological potential of hydrogen fuel cell systems for aviation and preliminary co-design of a hybrid regional aircraft powertrain through a mathematical tool”. In: *Energy Conversion and Management* 281 (2023), p. 116822. DOI: https://doi.org/10.1016/j.enconman.2023.116822. URL: https://www.sciencedirect.com/science/article/pii/S0196890423001681.

[115] J. Eaton, M. Naraghi, and J. G. Boyd. “Regional pathways for all-electric aircraft to reduce aviation sector greenhouse gas emissions”. In: *Applied Energy* 373 (2024), p. 123831. DOI: https://doi.org/10.1016/j.apenergy.2024.123831. URL: https://www.sciencedirect.com/science/article/pii/S0306261924012145.

[116] A. Farsi and M. A. Rosen. “Performance analysis of a hybrid aircraft propulsion system using solid oxide fuel cell, lithium ion battery and gas turbine”. In: *Applied Energy* 329 (2023), p. 120280. DOI: https://doi.org/10.1016/j.apenergy.2022.120280. URL: https://www.sciencedirect.com/science/article/pii/S0306261922015379.

[117] F. Morawska, P. Kurzawska-Pietrowicz, R. Jasiński, and A. Ziółkowski. “Alternative Fuels for General Aviation Piston Engines: A Comprehensive Review”. In: *Energies* 18.19 (2025). DOI: 10.3390/en18195299. URL: https://www.mdpi.com/1996-1073/18/19/5299.

[118] Pratt & Whitney. *PT6A Engine*. 2025. URL: https://www.prattwhitney.com/en/products/general-aviation-engines/pt6a (visited on 08/24/2025).

[119] Wikipedia Contribution. *Pratt & Whitney Canada PT6*. 2025. URL: https://en.wikipedia.org/wiki/Pratt_%26_Whitney_Canada_PT6 (visited on 08/24/2025).

[120] RED Aircraft GmbH. *Ampaire Had the Maiden Flight with the RED A03 Powered ECO-Caravan*. https://red-aircraft.com/ampaired-had-the-maidenflight-with-the-red-a03-powered-eco-caravan/. Accessed: 2025-10-09. 2022.

[121] V. Cusati, M. Di Stasio, G. Lucci, and Q. Zhang. “Evaluating hybrid-electric aircraft viability: The Ampaire Eco Caravan cost analysis”. In: *Transportation Research Part D: Transport and Environment* 144 (2025), p. 104759. DOI: https://doi.org/10.1016/j.trd.2025.104759. URL: https://www.sciencedirect.com/science/article/pii/S1361920925001695.

[122] *P&WC Engines & APUs for Sale*. 2024. URL: https://www.prattwhitney.com/en/services/pwc-engine-services/engine-sales?gad_campaignid=13345101347#/details (visited on 09/03/2025).

[123] *500 Horsepower V-12 Turbo Diesel Engine From Germany*. 2012. URL: https://avweb.com/news/500-horsepower-v-12-turbo-diesel-engine-from-germany/ (visited on 09/03/2025).

[124] T. Kim, W. Song, D.-Y. Son, L. K. Ono, and Y. Qi. “Lithium-ion batteries: outlook on present, future, and hybridized technologies”. In: *J. Mater. Chem. A* 7 (7 2019), pp. 2942–2964. DOI: 10.1039/C8TA10513H. URL: http://dx.doi.org/10.1039/C8TA10513H.

[125] E. J. Adler and J. R. Martins. “Hydrogen-powered aircraft: Fundamental concepts, key technologies, and environmental impacts”. In: *Progress in Aerospace Sciences* 141 (2023). Special Issue on Green Aviation, p. 100922. DOI: https://doi.org/10.1016/j.paerosci.2023.100922. URL: https://www.sciencedirect.com/science/article/pii/S0376042123000386.

[126] L. Kang, S. Lin, S. Bao, and J. Mao. “Modeling and analysis of performance degradation in proton exchange membrane fuel cell system for aviation applications”. In: *Aerospace Science and Technology* 162 (2025), p. 110236. DOI: https://doi.org/10.1016/j.ast.2025.110236. URL: https://www.sciencedirect.com/science/article/pii/S1270963825003074.

[127] M. Ayar and T. H. Karakoc. “Decision mechanism between fuel cell types: A case study for small aircraft”. In: *International Journal of Hydrogen Energy* 48.60 (2023). The 6th International Hydrogen Technologies Congress (IHTEC-2022), pp. 23156–23167. DOI: https://doi.org/10.1016/j.ijhydene.2022.12.020. URL: https://www.sciencedirect.com/science/article/pii/S0360319922057378.

[128] J. Huete and P. Pilidis. “Parametric study on tank integration for hydrogen civil aviation propulsion”. In: *International Journal of Hydrogen Energy* 46.74 (2021), pp. 37049–37062. DOI: https://doi.org/10.1016/j.ijhydene.2021.08.194. URL: https://www.sciencedirect.com/science/article/pii/S0360319921034418.

[129] S. Nicolay, S. Karpuk, and A. Elham. “Conceptual design and optimization of a general aviation aircraft with fuel cells and hydrogen as propulsion system”. In: Feb. 2020.

[130] M. Santin, A. Traverso, and A. Massardo. “Technological aspects of gas turbine and fuel cell hybrid systems for aircraft: a review”. In: *The Aeronautical Journal* 112.1134 (2008), pp. 459–467. DOI: 10.1017/S0001924000002426.

[131] M. Meindl, B. Lemoine, P. Caliandro, T. Wannemacher, N. Baumann, A. Guiguemde, Z. Wang, M. Di Stasio, M. Ruocco, E. Akay, S. Turteltaub, F. Nicolosi, A. De Marco, and P. Della Vecchia. *Deliverable 2.1 – Short-term Technology Analysis Covering All Main Technologies*. Technical Report. Accessed on 2025-09-30. Clean Sky 2 GENESIS Project, 2021. URL: https://www.genesis-cleansky.eu/deliverables/.

[132] M. H. Sadraey. “Systems Engineering Approach”. In: *Aircraft Design*. John Wiley & Sons, Ltd, 2012. Chap. 2, pp. 19–48. DOI: https://doi.org/10.1002/9781118352700.ch2. eprint: https://onlinelibrary.wiley.com/doi/pdf/10.1002/9781118352700.ch2. URL: https://onlinelibrary.wiley.com/doi/abs/10.1002/9781118352700.ch2.

[133] C. E. Riboldi. “Energy-optimal off-design power management for hybrid-electric aircraft”. In: *Aerospace Science and Technology* 95 (2019), p. 105507. DOI: https://doi.org/10.1016/j.ast.2019.105507. URL: https://www.sciencedirect.com/science/article/pii/S1270963819308946.

[134] L. He, F. Chen, P. Tian, and H. Gou. “An improved energy management strategy for hybrid electric powered aircraft based on deep reinforcement learning”. In: *Aerospace Science and Technology* 149 (2024), p. 109137. DOI: https://doi.org/10.1016/j.ast.2024.109137. URL: https://www.sciencedirect.com/science/article/pii/S1270963824002700.

[135] J. Yang, Z. Wu, W. Wang, W. Zhang, H. Zhao, and J. Sun. “A surrogate-based optimization method for mixed-variable aircraft design”. In: *Engineering Optimization* 54.1 (2022), pp. 113–133. DOI: 10.1080/0305215X.2020.1855156. eprint: https://doi.org/10.1080/0305215X.2020.1855156. URL: https://doi.org/10.1080/0305215X.2020.1855156.

[136] J.-Y. Choi, J. Park, S. Yi, Y. Jo, and S. Choi. “Design by adaptive infill sampling with multi-objective optimization for exploitation and exploration”. In: *Probabilistic Engineering Mechanics* 67 (2022), p. 103175. DOI: https://doi.org/10.1016/j.probengmech.2021.103175. URL: https://www.sciencedirect.com/science/article/pii/S026689202100059X.

[137] T. Long, X. Li, R. Shi, J. Liu, X. Guo, and L. Liu. “Gradient-Free Trust-Region-Based Adaptive Response Surface Method for Expensive Aircraft Optimization”. In: *AIAA Journal* 56.2 (2018), pp. 862–873. DOI: 10.2514/1.J054779. eprint: https://doi.org/10.2514/1.J054779. URL: https://doi.org/10.2514/1.J054779.

[138] M. D. Stasio, V. Trifari, F. Nicolosi, A. D. Marco, and R. Schaber. “Bypass Ratio Parametric Analyses on a Narrow-Body Aircraft Using a New Tool for Turbofan Rubberization”. In: *AIAA AVIATION 2022 Forum*. 2022. DOI: 10.2514/6.2022-3289. eprint: https://arc.aiaa.org/doi/pdf/10.2514/6.2022-3289. URL: https://arc.aiaa.org/doi/abs/10.2514/6.2022-3289.

[139] D. Raymer. “Enhancing aircraft conceptual design using multidisciplinary optimization”. PhD thesis. Institutionen för flygteknik, 2002.

[140] P. Borisut and A. Nuchitprasittichai. “Adaptive Latin Hypercube Sampling for a Surrogate-Based Optimization with Artificial Neural Network”. In: *Processes* 11.11 (2023). DOI: 10.3390/pr11113232. URL: https://www.mdpi.com/2227-9717/11/11/3232.

[141] K. Abu Salem, G. Palaia, and A. A. Quarta. “Impact of Figures of Merit Selection on Hybrid–Electric Regional Aircraft Design and Performance Analysis”. In: *Energies* 16.23 (2023). DOI: 10.3390/en16237881. URL: https://www.mdpi.com/1996-1073/16/23/7881.

[142] M. A. Rendón, C. D. R. Sánchez, J. M. Gallo, et al. “Aircraft Hybrid-Electric Propulsion: Development Trends, Challenges and Opportunities”. In: *Journal of Control, Automation and Electrical Systems* 32 (2021), pp. 1244–1268. DOI: 10.1007/s40313-021-00740-x. URL: https://doi.org/10.1007/s40313-021-00740-x.

[143] J. H. Bussemaker. “System Architecture Optimization: Function-Based Modeling, Optimization Algorithms, and Multidisciplinary Evaluation”. Dissertation (TU Delft, preparation external). Delft University of Technology and ISAE-SUPAERO, 2025. DOI: 10.4233/uuid:246b18f9-1f8c-4ff7-b824-2b1786cf9d14. URL: https://doi.org/10.4233/uuid:246b18f9-1f8c-4ff7-b824-2b1786cf9d14.

[144] P. Saves, R. Lafage, N. Bartoli, Y. Diouane, J. Bussemaker, T. Lefebvre, J. T. Hwang, J. Morlier, and J. R. R. A. Martins. “SMT 2.0: A Surrogate Modeling Toolbox with a focus on Hierarchical and Mixed Variables Gaussian Processes”. In: *Advances in Engineering Sofware* 188 (2024), p. 103571. DOI: https://doi.org/10.1016/j.advengsoft.2023.103571.

[145] H. Ritchie, P. Rosado, and V. Samborska. *Data Page: Annual CO_2 emissions from wildfires*. https://archive.ourworldindata.org/20250802-153412/grapher/annual-carbon-dioxide-emissions.html. Part of: *Climate Change*. Data adapted from Global Wildfire Information System. Archived on August 2, 2025. Online resource. 2024.

[146] B. Herre and V. Samborska. *Data Page: Annual CO_2 emissions from aviation*. https://archive.ourworldindata.org/20250624-125417/grapher/annual-co-emissions-from-aviation.html. Part of: *Tourism*. Data adapted from OECD. Archived on June 24, 2025. Online resource. 2023.

[147] J. Gao, L. Wang, W. Zhang, J. Ning, W. Li, T. Hu, and G. Yang. “Advances and Environmental Impact Assessment of Forest Fire Extinguishing Agents”. In: *Fire* 8.11 (2025). DOI: 10.3390/fire8110411. URL: https://www.mdpi.com/2571-6255/8/11/411.

[148] M. Tuccillo, S. Wang, F. Nicolosi, T. Lima Pereira, P. Della Vecchia, F. Di Verniere, and L. Zutta. *Deliverable D4.3 – Seaplane & UAM aircraft design (design loop 2)*. Technical Report. Accessed on 2025-09-30. COLOSSUS Project, 2025.

[149] M. Mandorino, P. D. Vecchia, S. Corcione, F. Nicolosi, V. Trifari, G. Cerino, M. Fioriti, C. Cabaleiro, T. Lefebvre, D. Charbonnier, Z. Wang, and D. Peeters. “Multidisciplinary Design and Optimization of Regional Jet Retrofitting Activity”. In: AIAA Aviation , Chicago, June 30, 2022. DOI: 10.2514/6.2022-3933. URL: https://www.zenodo.org/record/6801191 (visited on 06/30/2022). published.

[150] D. Ciliberti, P. Della Vecchia, F. Nicolosi, and A. De Marco. “Aircraft directional stability and vertical tail design: A review of semi-empirical methods”. In: *Progress in Aerospace Sciences* 95 (2017), pp. 140–172. DOI: https://doi.org/10.1016/j.paerosci.2017.11.001. URL: https://www.sciencedirect.com/science/article/pii/S0376042117301598.

[151] F. Nicolosi, P. Della Vecchia, D. Ciliberti, and V. Cusati. “Fuselage aerodynamic prediction methods”. In: *Aerospace Science and Technology* 55 (2016), pp. 332–343. DOI: https://doi.org/10.1016/j.ast.2016.06.012. URL: https://www.sciencedirect.com/science/article/pii/S1270963816302218.

[152] L. Stingo, P. Della Vecchia, G. Cerino, F. Nicolosi, A. De Marco, et al. “MDO applications to conventional and novel turboprop aircraft within agile European project”. In: *Belo Horizonte, Brazil* (2018).

[153] V. Cusati, S. Corcione, F. Nicolosi, and Q. Zhang. “Improvement of Take-Off Performance for an Electric Commuter Aircraft Due to Distributed Electric Propulsion”. In: *Aerospace* 10.3 (2023). DOI: 10.3390/aerospace10030276. URL: https://www.mdpi.com/2226-4310/10/3/276.

[154] F. Orefice, P. D. Vecchia, D. Ciliberti, and F. Nicolosi. “Aircraft Conceptual Design Including Powertrain System Architecture and Distributed Propulsion”. In: *2019 AIAA/IEEE Electric Aircraft Technologies Symposium (EATS)*. 2019, pp. 1–20. DOI: 10.2514/6.2019-4465.

[155] F. Nicolosi, V. Marciello, and F. Orefice. “Conceptual Design of a Hydrogen-Propelled Aircraft with Distributed Electric Propulsion”. In: *AIAA AVIATION 2022 Forum*. 2022. DOI: 10.2514/6.2022-3205. eprint: https://arc.aiaa.org/doi/pdf/10.2514/6.2022-3205. URL: https://arc.aiaa.org/doi/abs/10.2514/6.2022-3205.

[156] M. Siggel, J. Kleinert, T. Stollenwerk, and R. Maierl. “TiGL: an open source computational geometry library for parametric aircraft design”. In: *Mathematics in Computer Science* 13.3 (2019), pp. 367–389.

[157] J. Roskam. *Airplane Design Part V: Component Weight Estimation*. 1990.

[158] X.-H. Le, D. Van Binh, and G. Lee. “Performance and uncertainty analysis in deep learning frameworks for streamflow forecasting via Monte Carlo dropout technique”. In: *Journal of Hydrology: Regional Studies* 61 (2025), p. 102668. DOI: https://doi.org/10.1016/j.ejrh.2025.102668. URL: https://www.sciencedirect.com/science/article/pii/S2214581825004975.

[159] A. D. Jagtap and G. E. Karniadakis. *How important are activation functions in regression and classification? A survey, performance comparison, and future directions*. 2022. arXiv: 2209.02681 [cs.LG]. URL: https://arxiv.org/abs/2209.02681.

[160] D. P. Kingma and J. Ba. *Adam: A Method for Stochastic Optimization*. 2017. arXiv: 1412.6980 [cs.LG]. URL: https://arxiv.org/abs/1412.6980.

[161] J. Duchi, E. Hazan, and Y. Singer. “Adaptive Subgradient Methods for Online Learning and Stochastic Optimization”. In: *Journal of Machine Learning Research* 12.61 (2011), pp. 2121–2159. URL: http://jmlr.org/papers/v12/duchi11a.html.

[162] “Lecture 6.5-rmsprop: Divide the gradient by a running average of its recent magnitude”. In: *COURSERA: Neural networks for machine learning* 4.2 (2012), p. 26.

[163] R. Fontana, A. Molena, L. Pegoraro, and L. Salmaso. “Design of experiments and machine learning with application to industrial experiments”. In: *Statistical Papers* 64 (Mar. 2023), pp. 1–24. DOI: 10.1007/s00362-023-01437-w.

[164] Y. Gal and Z. Ghahramani. *Dropout as a Bayesian Approximation: Representing Model Uncertainty in Deep Learning*. 2016. arXiv: 1506.02142 [stat.ML]. URL: https://arxiv.org/abs/1506.02142.

[165] K. Deb and H. Jain. "An Evolutionary Many-Objective Optimization Algorithm Using Reference-Point-Based Nondominated Sorting Approach, Part I: Solving Problems With Box Constraints". In: *IEEE Transactions on Evolutionary Computation* 18.4 (2014), pp. 577–601. DOI: 10.1109/TEVC.2013.2281535.

[166] J. H. Bussemaker, N. Bartoli, T. Lefebvre, P. D. Ciampa, and B. Nagel. "Effectiveness of Surrogate-Based Optimization Algorithms for System Architecture Optimization". In: *AIAA AVIATION 2021 FORUM*. 2021. DOI: 10.2514/6.2021-3095. eprint: https://arc.aiaa.org/doi/pdf/10.2514/6.2021-3095. URL: https://arc.aiaa.org/doi/abs/10.2514/6.2021-3095.

[167] R. De Vries, M. F. Hoogreef, and R. Vos. "Range equation for hybrid-electric aircraft with constant power split". In: *Journal of Aircraft* 57.3 (2020), pp. 552–557. DOI: https://doi.org/10.2514/1.C035734.

[168] J. Blank and K. Deb. "pymoo: Multi-Objective Optimization in Python". In: *IEEE Access* 8 (2020), pp. 89497–89509.

[169] J. H. Bussemaker, P. Saves, N. Bartoli, T. Lefebvre, and B. Nagel. "Surrogate-Based Optimization of System Architectures Subject to Hidden Constraints". In: *AIAA AVIATION FORUM AND ASCEND 2024*. 2024. DOI: 10.2514/6.2024-4401. eprint: https://arc.aiaa.org/doi/pdf/10.2514/6.2024-4401. URL: https://arc.aiaa.org/doi/abs/10.2514/6.2024-4401.

[170] J. H. Bussemaker. "SBArchOpt: Surrogate-Based Architecture Optimization". In: *Journal of Open Source Software* 8.89 (2023), p. 5564. DOI: 10.21105/joss.05564. URL: https://doi.org/10.21105/joss.05564.

[171] H. Jain and K. Deb. "An Evolutionary Many-Objective Optimization Algorithm Using Reference-Point Based Nondominated Sorting Approach, Part II: Handling Constraints and Extending to an Adaptive Approach". In: *IEEE Transactions on Evolutionary Computation* 18.4 (2014), pp. 602–622. DOI: 10.1109/TEVC.2013.2281534.

[172] K. Deb, K. Sindhya, and T. Okabe. "Self-adaptive simulated binary crossover for real-parameter optimization". In: *Proceedings of the 9th Annual Conference on Genetic and Evolutionary Computation*. GECCO '07. London, England: Association for Computing Machinery, 2007, pp. 1187–1194. DOI: 10.1145/1276958.1277190. URL: https://doi.org/10.1145/1276958.1277190.

[173] I. Das and J. E. Dennis. "Normal-Boundary Intersection: A New Method for Generating the Pareto Surface in Nonlinear Multicriteria Optimization Problems". In: *SIAM Journal on Optimization* 8.3 (1998), pp. 631–657. DOI: 10.1137/S1052623496307510. URL: https://doi.org/10.1137/S1052623496307510.

[174] M. Keshavarz-Ghorabaee, M. Amiri, E. K. Zavadskas, Z. Turskis, and J. Antucheviciene. "Determination of Objective Weights Using a New Method Based on the Removal Effects of Criteria (MEREC)". In: *Symmetry* 13.4 (2021). DOI: 10.3390/sym13040525. URL: https://www.mdpi.com/2073-8994/13/4/525.

[175] A. Guitouni and J.-M. Martel. "Tentative guidelines to help choosing an appropriate MCDA method". In: *European Journal of Operational Research* 109.2 (1998), pp. 501–521. DOI: https://doi.org/10.1016/S0377-2217(98)00073-3. URL: https://www.sciencedirect.com/science/article/pii/S0377221798000733.

[176] J. Dezert, A. Tchamova, D. Han, and J.-M. Tacnet. "The SPOTIS Rank Reversal Free Method for Multi-Criteria Decision-Making Support". In: *2020 IEEE 23rd International Conference on Information Fusion (FUSION)*. Sun City, South Africa: IEEE, July 2020, pp. 1–8. DOI: 10.23919/FUSION45008.2020.9190347. URL: https://hal.science/hal-03007675.

[177] G.-H. Tzeng and J.-J. Huang. *Multiple attribute decision making: methods and applications*. CRC press, 2011.

[178] W. Sałabun, J. Wątróbski, and A. Shekhovtsov. "Are MCDA Methods Benchmarkable? A Comparative Study of TOPSIS, VIKOR, COPRAS, and PROMETHEE II Methods". In: *Symmetry* 12.9 (2020). DOI: 10.3390/sym12091549. URL: https://www.mdpi.com/2073-8994/12/9/1549.

[179] B. Kizielewicz, A. Shekhovtsov, and W. Sałabun. "pymcdm—The universal library for solving multi-criteria decision-making problems". In: *SoftwareX* 22 (2023), p. 101368.

[180] J. H. Bussemaker, P. D. Ciampa, J. Singh, M. Fioriti, C. C. D. L. Hoz, Z. Wang, D. Peeters, P. Hansmann, P. D. Vecchia, and M. Mandorino. "Collaborative Design of a Business Jet Family Using the AGILE 4.0 MBSE Environment". In: *AIAA AVIATION 2022 Forum*. 2022. DOI: 10.2514/6.2022-3934. eprint: https://arc.aiaa.org/doi/pdf/10.2514/6.2022-3934. URL: https://arc.aiaa.org/doi/abs/10.2514/6.2022-3934.

[181] *Air Transport Association of America. Standard Method of Estimating Comparative Direct Operating Costs of Turbine Powered Transport Airplanes*. The Association, 1967.

[182] AEA. *Short medium range aircraft: AEA requirements*. 1989. URL: https://books.google.it/books?id=6dz0jgEACAAJ.

[183] *EU emissions trading system (EU ETS)*. 2023. URL: https://climate.ec.europa.eu/eu-action/eu-emissions-trading-system-eu-ets_en.

[184] A. E. Scholz, D. Trifonov, and M. Hornung. "Environmental life cycle assessment and operating cost analysis of a conceptual battery hybrid-electric transport aircraft". In: *CEAS Aeronautical Journal* 13.1 (2022), pp. 215–235.

[185] J. Roskam. "Airplane Design: Part II". In: *Preliminary Configuration Design and Integration of the Propulsion System* (1989).

[186] C. Niu and M. Niu. *Airframe Structural Design: Practical Design Information and Data on Aircraft Structures*. Airframe book series. Adaso Adastra Engineering Center, 1999.

[187] M. Fioriti, P. Della Vecchia, and G. Donelli. “Effect of Progressive Integration of On-Board Systems Design Discipline in an MDA Framework for Aircraft Design with Different Level of Systems Electrification”. In: *Aerospace* 9.3 (2022). DOI: 10.3390/aerospace9030161. URL: https://www.mdpi.com/2226-4310/9/3/161.

[188] D. Savitsky. “Hydrodynamic design of planing hulls”. In: *Marine Technology and SNAME News* 1.04 (1964), pp. 71–95.

[189] D. Savitsky and P. W. Brown. “Procedures for hydrodynamic evaluation of planing hulls in smooth and rough water”. In: *Marine Technology and SNAME News* 13.04 (1976), pp. 381–400.

[190] D. Savistky and M. Morabito. “Surface Wave Contours Associated with the Forebody Wake of Stepped Planing Hulls”. In: *Marine Technology and SNAME News* 47.01 (Jan. 2010), pp. 1–16. DOI: 10.5957/mtsn.2010.47.1.1. URL: https://doi.org/10.5957/mtsn.2010.47.1.1.

[191] D. Svahn. “Performance prediction of hulls with transverse steps”. In: *A Report of Masters Thesis, The Royal Institute of Technology, KTH, Centre for Naval Architecture* (2009).

[192] R. E. Olson and N. S. Land. *Effect of Afterbody Length and Keel Angle on Minimum Depth of Step for Landing Stability and on Take-Off Stability of a Flying Boat*. Technical Note 1571. Langley Aeronautical Laboratory, Langley Field, Va.: National Advisory Committee for Aeronautics, Sept. 1948.

[193] J. Hugli W. C. and W. C. Axt. *Hydrodynamic Investigation of a Series of Hull Models Suitable for Small Flying Boats and Amphibians*. Technical Note 2503. Stevens Institute of Technology. Washington, D.C.: National Advisory Committee for Aeronautics, Nov. 1951.

[194] J. D. Mattingly, W. H. Heiser, and D. T. Pratt. *Aircraft Engine Design*. 2nd. eISBN: 978-1-60086-144-4. AIAA Education Series, 2002.

[195] J. Roskam. *Airplane Design. Part VIII: Airplane Cost Estimation: Design, Development, Manufacturing and Operating*. 1990.

[196] A. Pupillo and F. Majerna. *AVINCIS Presentation and Aerial Firefight Operations*. Personal communication in the context of the COLOSSUS Project. First Officer Andrea Pupillo and Safety Manager Fabrizio Majerna. Oct. 2025.

[197] *National Study of (Large) Airtankers to Support Initial Attack and Large Fire Suppression: Final Report, Phase 2*. Technical Report. Final Report, Phase 2. Washington, D.C.: USDA Forest Service, Department of the Interior, Nov. 1996.